National Library of Canada
Acquisitions and Bibliographic Services Branch
395 Wellington Street
Ottawa, Ontario
K1A 0N4

Bibliothèque nationale du Canada
Direction des acquisitions et des services bibliographiques
395, rue Wellington
Ottawa (Ontario)
K1A 0N4

Your file Votre référence

Our file Notre référence

NOTICE

The quality of this microform is heavily dependent upon the quality of the original thesis submitted for microfilming. Every effort has been made to ensure the highest quality of reproduction possible.

If pages are missing, contact the university which granted the degree.

Some pages may have indistinct print especially if the original pages were typed with a poor typewriter ribbon or if the university sent us an inferior photocopy.

Reproduction in full or in part of this microform is governed by the Canadian Copyright Act, R.S.C. 1970, c. C-30, and subsequent amendments.

AVIS

La qualité de cette microforme dépend grandement de la qualité de la thèse soumise au microfilmage. Nous avons tout fait pour assurer une qualité supérieure de reproduction.

S'il manque des pages, veuillez communiquer avec l'université qui a conféré le grade.

La qualité d'impression de certaines pages peut laisser à désirer, surtout si les pages originales ont été dactylographiées à l'aide d'un ruban usé ou si l'université nous a fait parvenir une photocopie de qualité inférieure.

La reproduction, même partielle, de cette microforme est soumise à la Loi canadienne sur le droit d'auteur, SRC 1970, c. C-30, et ses amendements subséquents.

Canada

UNIVERSITY OF ALBERTA

MULTIPLE QUANTUM COHERENCE EFFECTS IN *IN VIVO* PROTON MAGNETIC RESONANCE SPECTROSCOPY

BY

© ALAN HOWARD WILMAN

A thesis submitted to the Faculty of Graduate Studies and Research
in partial fulfillment of the requirements for the degree of
DOCTOR OF PHILOSOPHY
in
Medical Physics.

DEPARTMENT OF PHYSICS

Edmonton, Alberta
FALL 1994

National Library of Canada

Acquisitions and Bibliographic Services Branch

395 Wellington Street
Ottawa, Ontario
K1A 0N4

Bibliothèque nationale du Canada

Direction des acquisitions et des services bibliographiques

395, rue Wellington
Ottawa (Ontario)
K1A 0N4

Your file Votre référence

Our file Notre référence

The author has granted an irrevocable non-exclusive licence allowing the National Library of Canada to reproduce, loan, distribute or sell copies of his/her thesis by any means and in any form or format, making this thesis available to interested persons.

L'auteur a accordé une licence irrévocable et non exclusive permettant à la Bibliothèque nationale du Canada de reproduire, prêter, distribuer ou vendre des copies de sa thèse de quelque manière et sous quelque forme que ce soit pour mettre des exemplaires de cette thèse à la disposition des personnes intéressées.

The author retains ownership of the copyright in his/her thesis. Neither the thesis nor substantial extracts from it may be printed or otherwise reproduced without his/her permission.

L'auteur conserve la propriété du droit d'auteur qui protège sa thèse. Ni la thèse ni des extraits substantiels de celle-ci ne doivent être imprimés ou autrement reproduits sans son autorisation.

ISBN 0-315-95286-5

Canada

THE UNIVERSITY OF ALBERTA
RELEASE FORM

NAME OF AUTHOR: Alan Howard Wilman

TITLE OF THESIS: Multiple Quantum Coherence Effects in *In vivo* Proton Magnetic Resonance Spectroscopy

DEGREE: Ph. D. in Medical Physics

YEAR THIS DEGREE GRANTED: 1994

Permission is hereby granted to the University of Alberta Library to reproduce single copies of this thesis and to lend or sell such copies for private, scholarly or scientific research purposes only.

The author reserves all other publication and other rights in association with the copyright in the thesis, and except as hereinbefore provided neither the thesis nor any substantial portion thereof may be printed or otherwise reproduced in any material form whatever without the author's prior written permission.

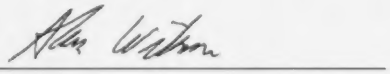

Alan H. Wilman
#1401, 10101 Saskatchewan Avenue
Edmonton, Alberta
T6R 2E6

Date: July 21, 1994

UNIVERSITY OF ALBERTA

FACULTY OF GRADUATE STUDIES AND RESEARCH

The undersigned certify that they have read, and recommend to the Faculty of Graduate Studies and Research for acceptance, a thesis entitled MULTIPLE QUANTUM COHERENCE EFFECTS IN *IN VIVO* PROTON MAGNETIC RESONANCE SPECTROSCOPY submitted by ALAN HOWARD WILMAN in partial fulfillment of the requirements of the degree of DOCTOR OF PHILOSOPHY in MEDICAL PHYSICS.

Dr. P. S. Allen (co-supervisor)

Dr. Z.W. Gortel (co-supervisor)

Dr. R. E. D. McClung

Dr. B.D. Sykes

Dr. M. Razavy

Dr. A. Penn

Dr. J.J.H. Ackerman

Date: July 21, 1994

To my father,

may his wit and wisdom live on in me.

ABSTRACT

In *in vivo* proton magnetic resonance (MR) spectroscopy, multiple quantum coherence (MQC) effects can give rise to unexpected modulations in the signal arising from J-coupled spin systems. When performing an *in vivo* MR spectroscopic exam, the consequences of these modulations can be disastrous since improper pulse sequence timings can lead to the total disappearance of the signal of interest. The goal of this thesis was to evaluate both analytically and experimentally, the effects of MQCs on four clinically important J-coupled metabolites: lactate, an indicator of anaerobic respiration; citrate, a potential marker of adenocarcinoma in the prostate gland; γ-aminobutyric acid (GABA), the most prevalent neurotransmitter in the brain; and N-acetylaspartate (NAA), a measure of neuronal population in the adult brain.

When the resonance of interest exhibited minimal spectral overlap the analysis centred on the response of the metabolite to the commonly used STEAM and PRESS localization sequences. Equations were obtained that describe the response of the lactate doublet, the citrate multiplet and the aspartyl resonances of NAA to both of these sequences. In particular, the responses of both the citrate and NAA multiplets exhibited a strong magnetic field dependence arising from the effects of strong J-coupling.

In the case of GABA, a high degree of spectral overlap makes both the STEAM and PRESS sequences ineffective at typical *in vivo* field strengths. To observe GABA, selective MQC filtering sequences were designed that used static magnetic field gradient pulses to dephase unwanted coherences. The most effective editing of GABA was accomplished using reduced-duration, selective double quantum filters that gave excellent suppression of unwanted resonances while retaining a significant portion of the GABA triplet signal.

In all cases, the theoretical equations were derived by expanding the spin density operator for each spin system in terms of products of spin angular momentum operators, then following its evolution under a succession of time-independent Hamiltonians. The concise analytical expressions derived by this approach were in agreement with experiments performed on phantoms, rat brain extracts and *in vivo* human brain. The results may be used to predict the optimal pulse sequences and timings for the observation of each of the targetted metabolites.

ACKNOWLEDGEMENT

I would like to thank my supervisor, Dr. Peter S. Allen for his continual support and advice throughout this project. In addition, my advisory committee of Dr. D. Gwynn Hughes, Dr. Brian D. Sykes and Dr. R.E.D. McClung have provided much useful feedback. Dr. R.E.D. McClung, in particular, has been an excellent source of knowledge and has often provided me with clear answers to confusing questions. As well, I would like to thank Dr. Gortel for his very helpful feedback and involvement in the final stages of this work. I would also like to thank Dr. Razavy, not only for serving as Chairman, but also for enlightening me on the finer points of Quantum Mechanics through both his teachings and his enthusiastic responses to my persistent questioning.

In the magnetic resonance laboratory, I have had the great fortune of being associated with coworkers of infinite patience. Initially, through the tutelage of Dr. Laird Trimble, Dan Doran and Al-Karim Damji, I became knowledgeable of experimental Magnetic Resonance. On countless occasions all three were asked what now seem like simple, silly questions, but without exception these questions were answered with friendliness and sincerity. My theoretical knowledge was also significantly increased through association with Dr. Jiefeng Shen, Dr. Chris Hanstock and Dan Gheorghiu.

The collaboration of Dr. Glen B. Baker in providing rat brain extracts for the experiments on GABA editing is greatly appreciated. Lastly, I thank the Department of Physics, and Dr. Peter Allen for supporting me financially throughout most of my studies.

TABLE OF CONTENTS

Chapter			Page
1 Introduction			1
1.1 Introduction to the Thesis			1
1.2 The Spin States of a Proton			4
1.3 Interaction of a Proton Spin with a Magnetic Field			7
1.3.1 Longitudinal Static Magnetic Field Interaction			8
1.3.2 Interaction with Both a Static and a Rotating Magnetic Field			11
1.4 Magnetic Shielding and the Chemical Shift			15
1.5 Indirect Scalar or J Coupling Interaction			16
1.5.1.	Weak Coupling		18
1.5.2.	Strongly Coupled Two Spin System		23
1.5.3	Classification of Spin Systems		27
1.6 Density Operator Formalism			31
1.6.1 General Equations			31
1.6.1.1 Equations for an Idealized Pure State			32
1.6.1.2 Equations for a Statistical Mixture of States			33
1.6.2	Bases for an Ensemble of Single Spin Systems		34
1.6.3	Bases for an Ensemble of Two Spin Systems		35
1.7 Transformational Equations of the Density Operator			39
1.7.1 Transformations Under a Radiofrequency Pulse			39
1.7.2 Transformations Under Chemical Shift Precession			42
1.7.3 Transformations Under Two-spin Weak J Coupling			43
1.7.4 Transformations Under Two-spin Strong J Coupling			44
1.8 Multiple Quantum Coherences			46
1.8.1 Creation of Multiple Quantum Coherences			47
1.8.2 Detection of Multiple Quantum Coherences		48	
1.8.3 Gradient Dephasing of Coherences			50
1.8.4 Multiple Quantum Filtering			53
1.9 Introduction to *In vivo* Magnetic Resonance Spectroscopy			56
1.9.1 Metabolite Concentrations			56
1.9.2 Spectral Overlap			57
1.9.3 Localization			60

1.10 Clinical Relevance of the Targetted Metabolites 64
1.10.1 Lactate 64
1.10.2 GABA 64
1.10.3 Citrate 65
1.10.4 N-Acetylaspartate 65
1.11 References and Selected Bibliography 66
2 *In Vivo* NMR Detection Strategies for γ-Aminobutyric Acid Utilizing Proton Spectroscopy and Coherence Pathway Filtering with Gradients 70
2.1 Introduction 70
2.2 Analysis 72
2.2.1 Even Ordered Filters 74
2.2.2 Odd Oredered Filters 76
2.2.3 Correlated Z Order 79
2.3 Methods and Results 80
2.4 Discussion and Conclusions 83
2.5 References 84
3 Shortened Double-Quantum Filtering with In-phase or Two-Spin Antiphase Detection, for γ-Aminobutyric Acid Editing in Proton Spectroscopy of Brain 85
3.1 Introduction 85
3.2 Theory 86
3.2.1 Detection of Antiphase Multiplets 91
3.3 Methods 94
3.4 Results and Discussion 95
3.5 Conclusions 100
3.3 References 101
4 An Analytical and Experimental Evaluation of PRESS versus STEAM for the Observation of the Lactate Doublet 102
4.1 References 111
5 The Response of the Strongly Coupled AB System of Citrate to Typical Proton MRS Localization Sequences 112
5.1 Introduction 112
5.2 Analysis 113
5.2.1 PRESS 116
5.2.2 STEAM 118

5.2.3 Signal to Noise Comparison with Uncoupled Spins 120
5.3 Experimental Methods 121
5.4 Results 122
5.5 Discussion and Conclusions 131
5.6 References 132
6 Double Quantum Filtering for the *In* Vivo Observation of Citrate 134
6.1 References 140
7 Observing N-Acetylaspartate via Both Its Aspartyl and N-Acetyl Groups in *In Vivo* Proton Magnetic Resonance Spectroscopy 141
7.1 Introduction 141
7.2 Theory 143
7.2.1 Spin Echo 146
7.2.2 STEAM 148
7.2.3 PRESS 150
7.3 Methods and Results 152
7.4 Discussion and Conclusions 161
7.5 References 163
8 Conclusions 164
8.1 The Measurement of the Intensity of the Spin Response 164
8.2 Spectral Editing of GABA 166
8.3 Localization Sequence Effects 167
8.3.1 Lactate 167
8.3.2 Citrate and N-Acetylaspartate 167
8.4 The Value of the Analytical Product Operator Approach 168
8.5 Future Directions 169
8.7 References 170

Appendix A: Product Operator Transformation Equations for a Weakly Coupled Two Spin System 171

Appendix B: Product Operator Transformation Equations for a Strongly Coupled Two Spin System 175

LIST OF TABLES

Table		Page
1.1	Chemical Shifts and J Couplings of the Targetted Metabolites	30
1.2	Concentrations of MR Visible Metabolite in Human Brain	57
2.1	The Percentage of A_2 Triplet Signal Intensity from GABA and the Creatine Suppression Factors for Various Editing Sequences	75
6.1	The Relative Citrate Signal Intensity Obtained with the DQF Sequence of Figure 6.1	139

LIST OF FIGURES

Figure		Page
1.1	Energy Levels of a Weakly Coupled System of Proton Spins	19
1.2	A Vector Model of Antiphase Magnetization	21
1.3	The Spectrum for an AB System	27
1.4	Molecular Orientations of a Chiral Carbon	28
1.5	Spin Systems and Chemical Formuli of the Targetted Metabolites	29
1.6	An Illustration of Gradient Dephasing Effects	51
1.7	An R.F. Pulse Surrounded by Gradient Pulses	52
1.8	A Multiple Quantum Filter	54
1.9	Proton Spectrum of a Perchloric Acid Extract of Rat Brain, and Corresponding Stick Spectru	59
1.10	The PRESS Localization Sequence	62
1.11	The STEAM Localization Sequence	63
2.1	The Pulse Sequences That Were Evaluated for GABA Editing	73
2.2	The RF Pulse Angle Dependence of the GABA Triplet	77
2.3(a)	Proton Spectra Corresponding to Unsucessful Editing of GABA	81
2.3(b)	Proton Spectra Corresponding to Sucessful Editing of GABA	82
2.4	Triple Quantum Filtered Rat Brain Spectrum	83
3.1	Shortened DQ Filters for GABA Editing	87
3.2	Possible Magnetization Signals Arising from the GABA Triplet	91
3.3	The Evolution Time Dependence of the GABA Triplet in Response to a DQC Filter	93
3.4	Changes in the Spectral Shape of GABA with Varying Evolution Time	96
3.5	A Comparison of the GABA Signal Intensity in Response to DQ Filtering and Difference Spectroscopy	97
3.6	A Comparison of the GABA Editing Efficiency of DQ Filtering and Difference Spectroscopy in a Rat Brain Extract	98
4.1	Approximations of the STEAM and PRESS Sequences	103
4.2	A Comparison of STEAM Versus PRESS for the Lactate Doublet	107
4.3	The TE Dependencies of the Lactate Doublet in Response to the STEAM Sequence	108
4.4	The TM Dependencies of the Lactate Doublet in Response	109

	to the STEAM Sequence	
5.1	Approximations of the STEAM and PRESS Sequences	115
5.2	A Schematic AB Stick Spectrum	121
5.3	The TE Dependence of the AB response to a Spin Echo and PRESS	123
5.4	100 MHz Proton Spectra of Citrate in Response to PRESS	124
5.5	The TE Dependence of the AB Response to STEAM	125
5.6	100 MHz Proton Spectra of Citrate in Response to STEAM	126
5.7	The TM dependence of the AB response to STEAM	127
5.8	The Magnetic Field Dependence of the TE Modulations of Citrate in Response to the PRESS Sequence	128
5.9	The Magnetic Field Dependence of the TE Modulations of Citrate in Response to the STEAM Sequence	129
5.10	The Signal to Noise Ratio of Citrate Versus that of Uncoupled Spins	130
6.1	A DQF Filtering Sequence	135
6.2	The τ Dependence of the Response of Citrate to the DQF of Fig. 6.1	137
6.3	100 MHz Proton Spectra of Citrate in Response to the DQF	138
7.1	Stick Spectra of the AB Part of an ABX System	143
7.2	The PRESS and the STEAM sequences	146
7.3	The TE Dependence of the AB Part of the NAA ABX System in Response to a Spin Echo and PRESS	153
7.4	100 MHz Proton Spectra of the NAA 2.6 ppm Multiplet in Response to the PRESS Sequence	154
7.5	The TE Dependence of the NAA Multiplet Response to STEAM	155
7.6	Proton Spectra of the NAA Multiplet in Response to STEAM	156
7.7	The Magnetic Field Dependence of the TE Modulations of 2.6 ppm NAA Multiplet in Response to the Spin Echo Sequence	157
7.8	The Magnetic Field Dependence of the TE Modulations of 2.6 ppm NAA Multiplet in Response to the PRESS Sequence	158
7.9	The Magnetic Field Dependence of the TE Modulations of 2.6 ppm NAA Multiplet in Response to the STEAM Sequence	159
7.10	63 MHz (1.5 T) Proton Spectra of *In Vivo* Human Brain Acquired With the PRESS Localization Sequence	160
8.1	Selected Spectra of the Lactate Doublet Response to the STEAM and the PRESS Sequnces	165

LIST OF SYMBOLS AND ABBREVIATIONS

aq	signal acquisition time
arg	argument of a complex number
Asp	aspartic acid
$A_{x,y,z}$	Cartesian spin angular momentum operators
$A_{\pm}$	spherical spin angular momentum operators
$B_{x,y,z}$	Cartesian spin angular momentum operators
$B_{\pm}$	spherical spin angular momentum operators
B_{eff}	effective magnetic field
B_{elec}	local magnetic field due to an electron
B_o	static magnetic field
B_1	rf magnetic field
Cr	creatine
DANTE	delays alternating with nutation for tailored excitation
DQC	double quantum coherence
DQF	double quantum filtering
$\delta\omega$	chemical shift difference
E	energy
FWHM	full width at half maximum
G	static magnetic field gradient
GABA	gamma-aminobutytric acid
gln	glutamine
glu	glutamate
γ	proton magnetogyric ratio
$\mathcal{H}$	Hamiltonian
$\hbar$	Planck's constant divided by 2π
Ins	myo-inositol
ISIS	image selected *in vivo* spectroscopy
I	spin angular momentum operator
I_z, I_y, I_x	Cartesian spin operators
$I_{\pm}$	raising and lowering spin operators
$I_{\pm}$	spherical spin angular momentum operators
J	indirect scalar coupling constant between two nuclear spins

k	Boltzmann's constant
Λ	strong coupling frequency
m	magnetic quantum number
MR	magnetic resonance
MRI	magnetic resonance imaging
MRS	magnetic resonance spectroscopy
MQC	multiple quantum coherence
MQF	multiple quantum filtering
M_o	equilibrium magnetization
$M_{x,y,z}$	magnetization components
NAA	N-Acetylaspartate
NAAG	N-acetylaspartylglutamate
NMR	nuclear magnetic resonance
PCr	phosphocreatine
PLZ	phenelzine
PRESS	point resolved spectroscopy
r	radial distance
r.f.	radio frequency
ρ	spin density operator
S	signal intensity
$\mathbf{S}$	spin angular momentum operator
$S_{z,y,x}$	Cartesian spin operators
$S_{\pm}$	raising and lowering spin operators
S/N	signal-to-noise ratio
STEAM	stimulated echo acquisition mode
SQC	single quantum coherence
σ	reduced spin density operator
t_1	multiple quantum evolution time
T	absolute temperature
T_1	longitudinal relaxation time
T_2	transverse relaxation time
TE	echo time of a spin-echo PRESS or STEAM sequence
TM	modulation time in the STEAM sequence
TQC	triple quantum coherence
TQF	triple quantum filtering

τ	evolution time
μ	nuclear magnetic moment
$\mu_{x,y,z}$	Cartesian components of the nuclear magnetic moment
ω	angular frequency
ω_0	Larmor frequency
$\omega_{r.f.}$	Frequency of oscillation of the radiofrequency magnetic field
ω_1	Magnitude of the radiofrequency field in angular frequency units
$\bar{\omega}$	average chemical shift
$X_{z,y,x}$	Cartesian spin operators
$X_{\pm}$	raising and lowering spin operators
Ψ	Schrodinger spin wavefunction
ZQC	zero quantum coherence
ζ	magnetic shielding constant

CHAPTER 1

Introduction

1.1 Introduction to the Thesis

The information obtained from *in vivo* proton magnetic resonance (MR) experiments is typically based solely on the water proton, and occasionally on the protons of fat. In human tissues such as brain or muscle, water and fat account for over 99.9% of the visible *in vivo* proton MR signal. Information from this portion of the MR signal allows for structural identification of tissues, as well as functional information based on diffusion and relaxation. The remaining 0.1% of the MR signal is partially from metabolites that are involved in some of the detailed biochemical processes in tissue. By performing *in vivo* proton magnetic resonance spectroscopy (MRS), some of these small metabolic signals may become visible, because each molecule will present a specific resonance pattern in the MR spectrum. Since biochemical changes often precede structural changes, observation of these metabolites by proton MRS may lead to earlier diagnosis of disease and subsequent earlier clinical intervention than that possible by observing solely the water signal.

At present proton MRS has exhibited some success in confirming clinical diagnoses (1-5), however, its use is not widespread because of the complexities involved both in acquiring and interpreting the MR spectroscopic signal. For example, in human brain, the metabolites of interest are normally present at concentrations of less than 10 mM, thus in order to acquire the metabolite signals with sufficient signal-to-noise ratio (S/N), a voxel size of at least 2 mL is often necessary, along with a scanning time on the order of 10 min (6-9). Moreover, *in vivo* proton MRS suffers not only from a low S/N, but also from a high degree of spectral overlap in the resulting spectrum which confounds easy identification of many of its spectral constituents. In addition, many of the metabolites in the *in vivo* proton spectrum exhibit a far greater degree of complexity in their spectral response than water due to scalar, or J, coupling between spins. Because of this complexity, the visibility of these J-coupled metabolites depends critically not only on the type of MR spectroscopic experiment, but also on its associated timing parameters.

While the problems of low metabolite concentration and spectral overlap can be easily explained, the effects of J-coupling often defy an intuitive explanation. For example, the J-coupling interaction can lead to the unexpected disappearance of all of the magnetization followed by its reappearance at a later time in the MR spectroscopic sequence. From a classical point of view, such feats can only inspire wonder, since from that perspective they cannot be adequately explained. However, from a quantum mechanical viewpoint, such occurrences are completely logical and expected: the disappearing magnetization is converted into multiple quantum coherence (MQC) that cannot be directly detected, but may be detectable following a further radiofrequency pulse.

The J-coupling interaction is the underlying mechanism that produces the MQCs to be discussed in this thesis. A limited number of studies have been done that deal quantitatively with single scan MQC applications to *in vivo* MRS (10-34), with the vast majority being in relation to the observation of the lactate doublet. Of course, the effects of J-coupling on the coupled spin response have been extensively discussed in high resolution MR; however, detailed analyses of MQCs are often limited to systems composed of just two or three weakly-coupled spins, and these analyses do not typically deal with methods that can be applied to an *in vivo* environment.

In this study, we analyze weakly coupled four (AX_3) and six ($A_2M_2X_2$) spin systems, as well as strongly coupled two (AB) and three (ABX) spin systems. These four types of spin system were not chosen merely to illustrate quantum mechanical gymnastics; instead they were chosen because they represent the spin systems of four clinically important metabolites that are visible in certain *in vivo* proton MRS experiments. The targetted J-coupled metabolites were: lactate, AX_3, an indicator of anaerobic respiration; the aspartyl resonances of N-acetylaspartate, ABX, a potential measure of neuronal population; γ-aminobutyric acid (GABA), $A_2M_2X_2$, the most prevalent inhibitory neurotransmitter; and citrate, AB, a potential marker of cancer in the prostate gland.

The overall aim of this study was to determine the optimal method, and timing parameters, for the observation of each of these coupled metabolites using

sequences that could be adapted to *in vivo* proton MRS. For each metabolite, a detailed quantum mechanical analysis was performed to determine the appropriate MR pulse sequence and timing for that metabolite. When the resonance of interest exhibited minimal spectral overlap, the MR pulse sequences used were approximations of the STEAM (35) and the PRESS (36-38) sequences which are the most commonly used localization sequences in *in vivo* proton MRS. In the cases of extreme spectral overlap, more complicated spectral editing schemes were necessary. In such cases single-scan multiple quantum filtering (MQF) methods were introduced that relied on the dephasing of unwanted coherences by static magnetic field gradient pulses. In every case, the results of the quantum mechanical calculations are verified experimentally on metabolite solutions, or rat brain extracts, at 100 MHz. For N-Acetylaspartate (NAA), additional work was also done at 63.8 MHz on human brain *in vivo* .

The next few sections of this chapter are devoted to an understanding of the concept of an MQC. Following an introduction to the quantum mechanical spin of a proton, the concept of single quantum coherence is developed from basic Schrödinger wave mechanics applied to a single spin system. In the next sections, the J-coupling interaction is introduced and applied to a two spin system, again with basic Schrödinger wave mechanics. From this two spin system, MQC is introduced.

To follow the creation, evolution and indirect detection of MQC, the quantum mechanical density operator formalism is used throughout this work. This formalism is developed in Section 1.6, from the basic Schrödinger quantum mechanics groundwork introduced in the earlier sections. Once the general formalism has been introduced, it is applied to an ensemble of single or two spin systems. Using the density operator, the creation and detection of MQC's in a two spin system are then discussed in Section 1.8 Within this section, the concept of gradient dephasing of coherences and of MQC filtering are introduced.

Section 1.9 serves as an introduction to MRS in an *in vivo* environment where the obstacles of low metabolite concentration, spectral overlap and the need for localization are discussed. The introductory chapter concludes with a brief review of the clinical relevance of the four targetted metabolites.

In the subsequent Chapters 2 to 7, each of the four targetted metabolites is analyzed in order to determine the optimal *in vivo* proton MRS sequence to maximize its observability. All of these chapters are versions of published or submitted journal manuscripts. Each chapter is devoted to a particular metabolite beginning with GABA in Chapters 2 and 3, then lactate in Chapter 4, citrate in Chapters 5 and 6, and NAA in Chapter 7. In the concluding Chapter 8, the main results of Chapters 2 to 7 are summarized and suggestions of various directions for further studies are made.

1.2 The Spin States of a Proton

In 1924, Stern and Gerlach showed that a beam of silver atoms, which have one unpaired electron, could be split into two by passing the beam through a magnetic field gradient (39,40). Within a few years, and using a similar apparatus, Estermann and Stern showed the same result for a proton (41). The immediate result of both experiments was that the magnetic moment of the electron and the proton are quantized along the direction of the magnetic field into two possible states of opposing sign. However, since both particles were in a zero *orbital* angular momentum state, it became necessary to postulate the existence of an intrinsic spin angular momentum that would account for the observed magnetic moment. From orbital angular momentum theory, it was known that the possible states of quantization along a specified z-axis varied from -L to +L in integral steps, where L is the orbital angular momentum quantum number. In an analogous manner, it was thus postulated that the electron, and later the proton, had spin 1/2, since for a spin 1/2 particle there would be only two allowable states ($\pm 1/2$) along the magnetic field axis. From other experiments, this postulate of spin 1/2 has been proven true.

The most natural description of these spin 1/2 particles is accomplished with the help of relativistic quantum mechanics. Nevertheless, by using further analogies to orbital angular momentum, which can be fully explained by nonrelativistic Schrödinger quantum mechanics, an accurate nonrelativistic description can be developed. The spin angular momentum of the proton will be denoted by $\hbar\mathbf{I}$, where $\hbar$ is Planck's constant divided by 2π and $\mathbf{I}$ is the spin angular momentum operator. As we have discussed, the component of the spin angular momentum vector along a

given magnetic field z-axis can only take on two distinct values $I_z=\pm 1/2$. By measuring the observable I_z, we expect to obtain an eigenvalue of either $\pm 1/2$, which corresponds to the spin being in either of its two possible eigenstates $|+\rangle$ and $|-\rangle$ which are defined as follows

$$I_z |+\rangle = +1/2 |+\rangle \quad \text{and} \quad I_z |-\rangle = -1/2 |-\rangle .$$
$$\langle +|+\rangle = \langle - |-\rangle = 1 \quad ; \quad \langle + |-\rangle = 0 \tag{1.1}$$

Since there are only two possible states of the system these eigenstates may be represented by two entry matrices

$$|+\rangle = \begin{pmatrix} 1 \\ 0 \end{pmatrix}, \quad |-\rangle = \begin{pmatrix} 0 \\ 1 \end{pmatrix}, \quad \langle +| = (1 \quad 0), \quad \langle - | = (0 \quad 1) \quad . \tag{1.2.}$$

In this $\{ |+\rangle, |-\rangle \}$ basis, the matrix representing I_z may be written as

$$(I_z) = \begin{pmatrix} \langle + | I_z | + \rangle & \langle + | I_z | - \rangle \\ \langle - | I_z | + \rangle & \langle - | I_z | - \rangle \end{pmatrix} = 1/2 \begin{pmatrix} 1 & 0 \\ 0 & -1 \end{pmatrix} \tag{1.3}$$

Based on Eq. (1.1), we may also define the operator I_z as

$$I_z = 1/2 \{ |+\rangle\langle +| - |-\rangle\langle -| \} \tag{1.4}$$

Even though our basis is defined along the z-axis, it must be possible to represent both the I_y and I_x components by the same basis since this basis forms a complete set. However, to do so we require knowledge of the fundamental commutation relations of spin angular momentum which are

$$[I_x, I_y] = iI_z \qquad [I_y, I_z] = iI_x \qquad [I_z, I_x] = iI_y \tag{1.5}$$

where i is $\sqrt{-1}$ and where the commutator notation is defined by $[A, B] = AB - BA$. These commutator relationships are exactly analogous to those of the orbital angular momentum which may be derived by considering an infinitely small rotation about an axis (42,43). Using Eq. (1.3) and Eq. (1.5), algebraic manipulation leads to the following matrix representations of I_x and I_y.

$$(I_x) = 1/2\begin{pmatrix} 0 & 1 \\ 1 & 0 \end{pmatrix} \quad , \quad (I_y) = 1/2\begin{pmatrix} 0 & -i \\ i & 0 \end{pmatrix} \tag{1.6}$$

In terms of the eigenvalue equations Eq. (1.6) yields

$$\begin{aligned} I_x\,|+\rangle &= +1/2\,|-\rangle \quad \text{and} \quad I_x\,|-\rangle = +1/2\,|+\rangle \\ I_y\,|+\rangle &= +i/2\,|-\rangle \quad \text{and} \quad I_y\,|-\rangle = -i/2\,|+\rangle \end{aligned} \tag{1.7}$$

Similarly to Eqs. (1.4), we may construct the operators I_x and I_y from products of the kets and bras using Eq. (1.7).

$$I_x = 1/2\ \{\ (|+\rangle\langle -|) + (|-\rangle\langle +|)\ \} \tag{1.8}$$

$$I_y = i/2\ \{\ (|-\rangle\langle +|) - (|+\rangle\langle -|)\ \} \tag{1.9}$$

It shall also be useful to introduce the spin angular momentum raising and lowering operators, I_+ and I_- respectively, defined by $I_\pm = I_x \pm iI_y$, where

$$(I_+) = \begin{pmatrix} 0 & 1 \\ 0 & 0 \end{pmatrix}, \quad (I_-) = \begin{pmatrix} 0 & 0 \\ 1 & 0 \end{pmatrix} \quad \text{and} \quad I_+ = |+\rangle\langle -| \ , \quad I_- = |-\rangle\langle +| \ . \tag{1.10}$$

It is important to realize that the resulting eigenvalues of $\pm 1/2$ are independent of the direction of quantization. For example, if the static magnetic field was rotated to be along the x direction, a measurement of I_x would yield $\pm 1/2$. Denoting the eigenvectors of I_x by ${}_x\langle \pm |$ and $|\pm\rangle_x$, we may write

$${}_x\langle +|\, I_x\, |+\rangle_x = 1/2 \quad \text{and} \quad {}_x\langle -|\, I_x\, |-\rangle_x = -1/2\ . \tag{1.11}$$

Let us now suppose that $|+\rangle_x$ can be derived from a linear combination of $|+\rangle_z$ and $|-\rangle_z$, (and similarly for $|-\rangle_x$) where the z subscript denotes the eigenvectors of I_z. By substituting this linear combination into Eq. (1.11), and using Eq. (1.7), one obtains

$$|+\rangle_x = (1/\sqrt{2})\,(\,|+\rangle_z + |-\rangle_z\,) \quad , \quad |-\rangle_x = (1/\sqrt{2})\,(\,|+\rangle_z - |-\rangle_z\,) \ . \tag{1.12}$$

Suppose, for example, that I_x has been measured and yields $|+>_x$, then from Eq. (1.12) it can be seen that when this state exists there is an equal chance of the spin being in either of the I_z states. We shall make use of Eq. (1.12) in Section 1.3.2, where the introduction of a radiofrequency magnetic field changes the effective direction of quantization.

Let us now consider the most general state of a spin wavefunction Ψ

$$|\Psi> = c_1|+> + c_2|-> \tag{1.13}$$

where we shall assume that the absence of subscripts implies quantization along the z axis, and where c_1 and c_2 are complex coefficients, defined such that the probabilities of finding the spin in the states $|+>$ and $|->$ are $|c_1|^2$ and $|c_2|^2$ respectively and hence $|c_1|^2 + |c_2|^2=1$. The arguments of c_1 and c_2 can always be specified in terms of two phase angles, ϕ and κ, where

$$\arg(c_1) =(1/2)\,(\phi +\kappa) \qquad \arg(c_2) =(1/2)\,(-\phi +\kappa)\,. \tag{1.14}$$

The most general $|\Psi>$ may thus be written as

$$|\Psi> = \{|c_1|\, e^{i\phi/2}\,|+> + |c_2|\, e^{-i\phi/2}\,|->\}\; e^{i\kappa/2}. \tag{1.15}$$

Since the measurement of any observable **O** is determined by $<\Psi|\mathbf{O}|\Psi>$, the global phase factor κ will be of no physical consequence.

1.3 Interaction of Proton Spins With a Magnetic Field

The interaction of a single proton with a magnetic field will occur via a coupling between the magnetic field **B** and the proton magnetic moment $\boldsymbol{\mu}$. This magnetic moment $\boldsymbol{\mu}$ is collinear to the spin vector and defined as

$$\boldsymbol{\mu} = \gamma \hbar \mathbf{I} \quad , \tag{1.16}$$

where γ is the proton gyromagnetic ratio. The coupling between $\boldsymbol{\mu}$ and **B** gives rise

to a Hamiltonian $\mathcal{H}$ of the form

$$\begin{aligned} \mathcal{H} &= -\boldsymbol{\mu} \cdot \mathbf{B} \\ &= -\gamma \hbar \mathbf{I} \cdot \mathbf{B} \end{aligned} \quad . \tag{1.17}$$

1.3.1 Longitudinal Static Magnetic Field Interaction

Consider a single proton in a static magnetic field $\mathbf{B_0}$ directed along the longitudinal or z-axis. From Eq. (1.17) we obtain,

$$\mathcal{H} = -\gamma \hbar \, I_Z B_0 \tag{1.18}$$

By defining the proton Larmor frequency, ω_0, as

$$\omega_0 = \gamma \, B_0, \tag{1.19}$$

the eigenvalues of this Hamiltonian in Eq. (1.18) are simply the eigenvalues of the I_Z spin operator multiplied by $(\hbar\omega_0)$, and therefore the energy eigenvalues are

$$E_{\pm} = \pm \, (1/2)\hbar\omega_0 \, . \tag{1.20}$$

where, clearly, the $|+>$, or $I_Z=+1/2$ state corresponds to the lower proton energy. The net effect of placing the proton in a static magnetic field is thus to split the energy of the two eigenstates by $\hbar\omega_0$, which at a magnetic field strength of 2 Tesla, leads to an energy difference of $\sim 10^{-7}$ eV, equivalent to a thermal energy of 10^{-3} ^{o}K. Nevertheless without this minute energy difference there would be no magnetic resonance phenomena.

We now consider the effect on a proton spin wavefunction of evolution under the Hamiltonian arising from a static magnetic field as described in Eq. (1.18) . Suppose that at a time t=0 the proton wavefunction Ψ, is defined by the most general state Eq. (1.15). The time evolution of this wavefunction is governed by the Schrödinger equation:

$$i\hbar \, (d/dt)| \Psi(t) > = \mathcal{H}(t) \, | \Psi(t) > \, . \tag{1.21}$$

For a time independent Hamiltonian of the form of Eq.(1.17), the result of evolution for a time t is

$$|\Psi(t)> = \exp(-i\,\mathcal{H}t/\hbar)\,|\Psi(0)> = \exp(i\gamma\,\mathbf{I}\cdot\mathbf{B}\,t)\,|\Psi(0)> \quad , \qquad (1.22)$$

Evolution of the wavefunction of Eq. (1.15) under the Hamiltonian of a static longitudinal $\mathbf{B_0}$ field given by Eq. (1.18), yields

$$|\Psi(t)> = \{|c_1|\exp[i(\phi+\omega_0 t)/2)]\,|+> + |c_2|\exp[-i(\phi+\omega_0 t)/2\,]\,|->\}e^{-i\kappa/2}. \qquad (1.23)$$

The presence of the $\mathbf{B_0}$ field therefore introduces a phase shift, proportional to the time, between the coefficients of |+> and |->.

Utilizing Eq. (1.23), we now determine the mean, or expectation, values for the Cartesian components of the magnetic moment.

$$\begin{aligned} &<\Psi(t)\,|\,\mu_z\,|\Psi(t)> = \gamma\hbar(1/2)(\,|c_1|^2 - |c_2|^2) \\ &<\Psi(t)\,|\,\mu_x\,|\Psi(t)> = \gamma\hbar\,|c_1|\,|c_2|\cos(\phi+\omega_0 t) \\ &<\Psi(t)\,|\,\mu_y\,|\Psi(t)> = -\gamma\hbar|c_1|\,|c_2|\sin(\phi+\omega_0 t) \end{aligned} \qquad (1.24)$$

From these expressions, we see that the three components of the mean value of μ imply classical precession at the angular frequency of $-\omega_0$ about the z axis. These mean values depend on the initial phase *difference* ϕ between the |+> and |-> states.

If the mean value of μ_x or μ_y is now summed over a large number of spins, the resulting sum would depend critically on the individual phase differences ϕ^i between the |+> and |-> states of each spin. For example, an arbitrary distribution of ϕ^i would lead to the mean values precessing with arbitrary phases, while a constant phase difference, across the sample would lead to the mean values all precessing at the same phase. Clearly, such a constant phase difference, or coherence, is desirable in order to maximize the sum of these precessing mean values. In general, we shall refer to this sum of the mean values of all $\boldsymbol{\mu}^i$ as the magnetization $\mathbf{M}$, where $\mathbf{M}=\Sigma_i <\boldsymbol{\mu}^i>$. It is an empirical fact that both M_x and M_y are zero at thermal equilibrium, and hence the distribution of ϕ^i is random.

From Eq. (1.24) we note that the mean value of μ_z depends on the difference in the probabilities of the spin being in the |+> and |-> states. For an ensemble of spins at thermal equilibrium in the presence of the static magnetic field $\mathbf{B_0}$, an excess will occupy the lower energy state |+>, which will lead to a net observable magnetization M_0. The excess of spins in the lower energy state arises from the equilibration of thermal energy between the spins and the surrounding lattice which is made up of mainly rotational and vibrational energy states. Furthermore, the lattice acts as a heat reservoir, because the thermal capacity of the spin system is insignificant in comparison to that of the lattice, and the spin system will thus equilibrate to the lattice temperature T. From statistical mechanics, it is known that for such a canonical ensemble, the probability of a spin having energy E, is proportional to the Boltzmann factor $\exp[-E/(kT)]$ (44). For our two state spin system, this factor leads to the following ratio between the probability P_+ of the spin being in the lower energy |+> state, and the probability P_- of the spin being in the higher energy |-> state,

$$P_+/P_- = \exp[\hbar\omega_0/(kT)] \tag{1.25}$$

It is interesting to note that at room temperature (T=293^{o}K) in a static magnetic field strength of 2 Tesla, this probability ratio would be 1.000014. This minute difference in probabilities is sufficient to give rise to an observable magnetization.

As we have seen, the initial equilibrium conditions of an MR experiment produce a random distribution of ϕ. The question now arises as to how one can create a coherence between all of the spins in a sample in order to get a net precessing magnetization. The answer lies in the fact that the mean values of μ_z are independent of the phase difference ϕ. If it were somehow possible to simultaneously convert μ_z of each spin into a transverse component, say μ_y, the mean value of μ_y for all of the spins in the sample would then begin precession with the same phase thus creating a net magnetization. We describe such a process as the creation of phase coherence across the sample and discuss it further in the next section.

1.3.2 Interaction with Both a Static and a Rotating Magnetic Field

We now consider the case of a single proton interacting with an oscillating, transverse magnetic field $\mathbf{B_1}$ and the longitudinal field $\mathbf{B_0}$. This $\mathbf{B_1}$ is usually brought about by applying a field along the x-axis with the magnitude of $2B_1\cos(\omega_{rf}t)$. This field does not rotate, but it may be decomposed into two counter-rotating components, one of which is

$$\mathbf{B_1}=B_1\,[\,\mathbf{i}\cos(\omega_{rf}t)-\mathbf{j}\sin(\omega_{rf}t)] \quad . \tag{1.26}$$

The applied $\mathbf{B_1}$ field will rotate in the transverse plane with a magnitude of B_1 and an angular radiofrequency (rf) of $-\omega_{rf}$. The direct creation of this circularly polarized $\mathbf{B_1}$ rotating field may be produced directly by using two orthogonally mounted solennoids or a birdcage coil (45). By introducing an angular frequency $\omega_1=\gamma B_1$, the total Hamiltonian that affects the spin may be written as

$$\mathcal{H} = -\hbar\omega_0 I_z - \hbar\omega_1\,[I_x\cos(\omega_{rf}t) - I_y\sin(\omega_{rf}t)] \quad . \tag{1.27}$$

Because a time-independent Hamiltonian will be much simpler to deal with, we introduce a rotating reference frame defined by $I'_x= I_x\cos(\omega_{rf}t) - I_y\sin(\omega_{rf}t)$, $I'_y= I_y\cos(\omega_{rf}t) + I_x\sin(\omega_{rf}t)$, and $I'_z= I_z$, where I' denotes a rotating frame spin angular momentum operator. The Hamiltonian in this rotating frame is $\mathcal{H}_{rot.}= -\hbar\omega_0 I'_z - \hbar\omega_1 I'_x$.

Transformation to this rotating frame will also affect the spin wavefunction. In Section 1.3.1, we found that evolution under only a $\mathbf{B_0}$ field for a time t introduced a phase factor in the spin wavefunction,

$$|\,\Psi(t)\rangle = \exp(i\omega_0 I_z t)\,|\,\Psi(0)\rangle \quad , \tag{1.28}$$

which was later related, in Eq. (1.24), to a precession at $-\omega_0$ for the transverse components of $\langle\mu\rangle$. By analogy to that case (46), we expect that the net effect of the $-\omega_{rf}$ rotation will lead to a rotating frame wavefunction $\Psi_{rot.}$ defined as follows

$$|\,\Psi(t)\rangle=\exp(i\omega_{rf}I_z t)\,|\,\Psi_{rot.}(t)\rangle \;, \quad |\Psi_{rot.}(t)\rangle=\exp(-i\omega_{rf}I_z t)\,|\,\Psi(t)\rangle \;. \tag{1.29}$$

We may now proceed to determine the evolution of $\Psi_{rot.}$ under the Hamiltonian $\mathcal{H}_{rot.} = -\hbar\omega_0 I'_z - \hbar\omega_1 I'_x$ beginning with Eq. (1.22) for the evolution under a time-independent Hamiltonian.

$$|\Psi(t)\rangle = \exp(-i\,\mathcal{H}t/\hbar)\,|\Psi(0)\rangle$$
$$\exp(i\omega_{rf}I_z t)\,|\Psi_{rot.}(t)\rangle = \exp(i\omega_0 I'_z t + \omega_1 I'_x t)\,|\Psi_{rot.}(0)\rangle \quad , \qquad (1.30)$$

By multiplying both sides by the operator by $\exp(-i\omega_{rf}I_z t)$, we obtain

$$|\Psi_{rot.}(t)\rangle = \exp\{i\,(\omega_0 - \omega_{rf})I'_z t + i\omega_1 I'_x t\}\,|\Psi_{rot.}(0)\rangle \quad . \qquad (1.31)$$

By comparison to Eq. (1.22), we see that the effective magnetic field in the rotating frame, $\mathbf{B_{eff}}$ is

$$\mathbf{B_{eff}} = \hat{\mathbf{z}}\,[B_0 - (1/\gamma)\omega_{rf}] + \hat{\mathbf{x}}_{rot.}\,B_1 \qquad (1.32)$$

where $\hat{\mathbf{x}}_{rot.}$ and $\hat{\mathbf{z}}$ are unit vectors along the $x_{rot.}$ and z axes respectively of the rotating frame (since the z axis is shared with the laboratory frame it has no *rot.* subscript). From our experience with the precessing mean values of $\boldsymbol{\mu}$ in the presence of only $\mathbf{B_0}$, we would expect that the resulting rotating frame magnetization will precess about $\mathbf{B_{eff}}$. Normally, the magnitude of B_0 will exceed that of B_1 by a factor of at least a factor of 3000. In order to achieve our goal of tipping the magnetization into the transverse plane, it will be necessary to neutralize the z-axis contribution to $\mathbf{B_{eff}}$, otherwise the magnetization will merely precess about this overwhelming z-axis field and never even reach the transverse plane. This can be most effectively done when $\omega_{rf}=\gamma B_0=\omega_0$. By neutralizing the z-axis field, the precession of the magnetization will now be about the transverse $x_{rot.}$ axis. Of course, some of the magnetization M_z may still be converted to transverse magnetization when $\omega_{rf} \sim \gamma B_0$, however, complete inversion to the $-$z-axis will only be possible at the exact resonant frequency. On resonance, when $\omega_{rf}=\omega_0$, the precession of the magnetization is around the x axis of the rotating frame, leading to an effective Hamiltonian in the rotating frame of

$$\mathcal{H}_{eff} = -\hbar\omega_1 I'_x \, . \qquad (1.33)$$

We shall now determine the influence of $\mathcal{H}_{eff}$, on the time evolution of a general proton wavefunction $\Psi_{rot.}$ for a single proton. Let us begin by considering the system at time $t=0^-$, just before the application of the oscillating r.f. field. From Eq. (1.29) we found that the effect on the wavefunction of entering the rotating frame was to introduce a phase shift proportional to time. In comparison to Eq. (1.15), we may incorporate this phase factor into the phase angle ϕ to yield a general wavefunction again defined as

$$|\Psi_{rot.}(0^-)>_{z'} = |c_1|\, e^{i\phi/2}\, |+>_{z'} + |c_2|\, e^{-i\phi/2}\, |->_{z'} \quad . \tag{1.34}$$

where we have reintroduced the subscripts on the kets to represent the direction of measurement which here is along the z' axis of the rotating frame. Now the oscillating field is applied on resonance at time t=0, leading to the effective Hamiltonian of Eq. (1.33), which polarizes the system along the $\pm x'$ direction. By expanding $|\pm>_{z'}$ in terms of the $|\pm>_{x'}$ basis using a rotating frame version of Eq. (1.12), we attain the following

$$|\Psi_{rot.}(0)>_{x'} = (1/\sqrt{2})\, \{\, (c_1+ c_2)|+>_{x'} \; + \; (c_1- c_2)\, |->_{x'}\, \} \tag{1.35}$$

where, for the present, we will not deal explicitly with the phase factors ($c_1 = |c_1|e^{i\phi/2}$, $c_2 = |c_2|\, e^{-i\phi/2}$). Under the influence of the effective rotating frame Hamiltonian $\mathcal{H}_{eff}$ for a time t^-, $|\Psi_{rot.}>_{x'}$ will evolve into

$$|\Psi_{rot.}(t^-)>_{x'} = \exp(-i\mathcal{H}_{eff}t^-)\, |\Psi_{rot.}(0)>_{x'} \quad . \tag{1.36}$$

Because the eigenvalues of the operator I'_x in $\mathcal{H}_{eff}$ are multiples of the energy eigenvalues of $|\Psi_{rot.}>_{x'}$, the operator can simply be replaced by its eigenvalue to yield,

$$\begin{aligned} |\Psi_{rot.}(t^-)>_{x'} = (1/\sqrt{2})\, \{\, & (c_1+c_2)\exp(i\omega_1 t^-/2)\, |+>_{x'} \\ & + (c_1- c_2)\, \exp(-i\omega_1 t^-/2)\, |->_{x'}\} \end{aligned} \tag{1.37}$$

Now at a time t, the oscillating field is turned off, which again polarizes the spins along the z' axis. Upon returning to the basis expansion along the z'-axis we obtain,

$$|\Psi_{rot.}(t)>_{z'} = \{c_1 \cos(\omega_1 t/2) + ic_2 \sin(\omega_1 t/2)\}\ |+>_{z'} + \{c_2 \cos(\omega_1 t/2) + ic_1 \sin(\omega_1 t/2)\}\ |->_{z'} \quad . \qquad (1.38)$$

From Eq. (1.38), we see that the application of such a transverse magnetic field leads to a mixing of the $|+>_{z'}$ and $|->_{z'}$ states. For example, if $\omega_1 t=\pi$, the coefficients have essentially been exchanged (except for a phase factor) by the r.f. pulse, leading to a reversal of the original probability distribution. In addition, simple algebra shows that if $\omega_1 t=\pi/2$ *and the phase factor* $\phi=0$ (recall $c_1 = |c_1|\, e^{i\phi/2}$, $c_2 = |c_2|\, e^{-i\phi/2}$), the probabilities of the particle being in either the $|->_{z'}$ or the $|+>_{z'}$ state in Eq. (1.38) will be equal. There is much more information to glean from this equation, however this may best be done by looking at a physical observable such as the mean value of the magnetic moment $\boldsymbol{\mu}$ in the rotating frame.

Using the general wavefunction $\Psi_{rot.}$ of Eq. (1.38), we now write down the mean values for the Cartesian components of the magnetic moment in the rotating frame.

$$\begin{aligned}
&<\Psi_{rot.}(t)\,|\,\mu'_z\,|\Psi_{rot.}(t)> = \gamma\hbar\,\{(1/2)(|c_1|^2 - |c_2|^2)\cos(\omega_1 t) + |c_1|\,|c_2|\sin(\phi)\sin(\omega_1 t)\}\\
&<\Psi_{rot.}(t)\,|\,\mu'_y\,|\Psi_{rot.}(t)> = \gamma\hbar\,\{-|c_1|\,|c_2|\sin(\phi)\cos(\omega_1 t) + (1/2)(|c_1|^2 - |c_2|^2)\sin(\omega_1 t)\}\\
&<\Psi_{rot.}(t)\,|\,\mu'_x\,|\Psi_{rot.}(t)> = \gamma\hbar\,|c_1|\,|c_2|\cos(\phi) \qquad (1.39)
\end{aligned}$$

where ϕ is the initial phase difference between the rotating frame $|+>_{z'}$ and $|->_{z'}$ states, which is the same as the initial phase difference between the laboratory frame states $|+>_z$ and $|->_z$, as defined in Eq. (1.15). An immediate result from Eq. (1.39) is that the polarized field along the x'-axis does not affect the mean value of μ'_x in any way. Returning to the discussion relating to the previous equation, Eq. (1.38), the condition of $\phi=0$ that leads to population equalization, requires that the mean value of μ'_y be zero at t=0, the start of the r.f. pulse.

There are at least two other important points that arise from Eq. (1.39). First, only two terms in Eq. (1.39) are independent of the phase angle ϕ. If we again consider the magnetization resulting from a large number of incoherent spins, i.e. spins with random phase differences ϕ^i, the magnetization summations that involve a ϕ^i dependence will average to zero. Second, the two terms without a ϕ dependence have the same magnitude, $\gamma\hbar(1/2)(|c_1|^2 - |c_2|^2)$, which is the initial mean value of μ'_z

at t=0, and by setting $\omega_1 t=\pi/2$, this mean value may be fully tipped into the +y'-direction. By performing such a $\pi/2$ pulse simultaneously on a large number of spins, the resulting transverse y' magnetization will be coherent, since the initial phase differences ϕ^i will all be zero. We have thus discovered a way to create phase coherence in the transverse plane. In terms of an initial magnetization vector $\mathbf{M}' = \hat{\mathbf{z}}' M_0$, the results of Eq. (1.39) suggest that $\mathbf{M}'$ will evolve under the Hamiltonian of Eq. (1.33) as follows

$$\hat{\mathbf{z}}' M_0 \xrightarrow{-\omega_1 I_x t} \hat{\mathbf{z}}' M_0 \cos(\omega_1 t) + \hat{\mathbf{y}}' M_0 \sin(\omega_1 t) \qquad (1.40)$$

where above the arrow, we have written the appropriate Hamiltonian that causes the evolution for a time t.

1.4 Magnetic Shielding and the Chemical Shift

At this point, we have only considered isolated proton spins. However, within a molecule, each proton will interact with its surrounding electrons and neighboring protons. If such interactions did not occur, all protons would resonate at the same Larmor frequency, so there would be no easy method to distinguish between them. In this section we shall briefly discuss the magnetic shielding effects on a nucleus due to its electrons and the electrons of neighboring nuclei.

The applied static magnetic field $\mathbf{B_0}$ is the field experienced by a bare proton without any surrounding electrons. Within an atom, the field experienced by the proton is not equal $\mathbf{B_0}$ because of the field arising from the motion of the electrons induced by the $\mathbf{B_0}$ field. In general, this motion of the electrons will produce a field that opposes the applied field. In addition to this atomic shielding mechanism, which is diamagnetic, there is also a paramagnetic shielding effect arising from the interaction of the orbital magnetic moments of the electrons in the molecule (47). The combined atomic and molecular shielding effects lead to a small, but extremely important, change in the magnetic field experienced by the proton that is dependent upon the chemical environment of the proton. We shall define a magnetic shielding constant ζ such that B(nucleus) = $(1-\zeta)\, B_0$. For protons, ζ is only $\sim 10^{-5}$.

Exact calculations of the magnetic shielding constant are possible for simple molecules such as molecular hydrogen (47). In general, however, ζ is determined empirically because it depends not only on the applied magnetic field and type of electronic bonds, but also on the electronegativity of other elements within the molecule, and on interactions of the molecule with other molecules.

The variations of ζ between protons in different chemical environments gives rise to a difference in their resonance frequencies. This difference, or chemical shift, is usually reported in parts per million (ppm), which are independent of the magnetic field strength. Consider two proton frequencies, ω_I and ω_S defined such that

$$\omega_S = \gamma(1-\zeta_S)B_O \qquad \text{and} \qquad \omega_I = \gamma(1-\zeta_I)B_O \tag{1.41}$$

where $\zeta_{S,I}$ are the magnetic shielding constants. If ω_S is the reference frequency, $\omega_{ref.}$, to which all other chemical shifts are referred, we shall define the chemical shift, δ_I, in units of ppm, by

$$\delta_I = 10^6(\omega_I-\omega_{ref})/\omega_{ref} = 10^6(\zeta_{ref}-\zeta_I)/(1-\zeta_{ref}) \sim 10^6(\zeta_{ref}-\zeta_I) \quad . \tag{1.42}$$

The strongly shielded protons in the tetramethylsilane molecule, $Si(CH_3)_4$, are usually chosen as the reference. With this convention, the typical range of proton chemical shifts is from 0 to 10 ppm.

1.5 Indirect Scalar or J-Coupling Interaction

In 1950 the concept of a spin-echo was introduced by Hahn (48). In this paper, it was reported that certain molecules exhibited unexpected cosinusoidal modulations, with periods of tens of milliseconds, in their spin-echo response. Shortly thereafter, Hahn and Maxwell (49) correctly described these modulations by introducing a scalar interaction of the form $\mathbf{I_1}\cdot\mathbf{I_2}$ between two neighboring nuclear spins. However they were unable to propose a physical mechanism giving rise to the interaction, because the direct nuclear dipole-dipole interaction averages to zero in a liquid. The following year, this effect was properly explained by Ramsey and Purcell (50) who suggested that the underlying mechanism was an indirect magnetic

interaction between the two nuclei facilitated by the exchange coupling of the electron spins associated with each nucleus.

To be more specific, let us begin by considering the intra-atomic interaction between a spin one-half nucleus and an electron spin. Such magnetic interactions between a nucleus and an electron are often termed hyperfine interactions. The general form of the interaction Hamiltonian may be described by Eq. (1.17), by replacing the magnetic field **B** with $\mathbf{B}_{elec.}$, which represents the component of magnetic field experienced by the nucleus that arises from the presence of the electron. The existence of $\mathbf{B}_{elec.}$ may arise from three possible hyperfine interactions: dipolar, orbital or contact. Because a net electron spin is unusual in covalent molecular systems, the dipolar interaction need not be considered. Moreover, in a liquid, any dipolar contribution would average to zero, since the orientation of the molecule changes rapidly and randomly in a liquid. The orbital interaction may give rise to a finite $\mathbf{B}_{elec.}$ due to the interaction of the net orbital angular momentum of the electron with the applied external field. This interaction leads to paramagnetic shielding of the nucleus and contributes to the chemical shifts of the resonances as described in the previous section. Nevertheless, because of the spatial dependence of this interaction, it is of insufficient intensity to account for the observed J-coupling effects between two nuclear spins (49). It is the *contact* hyperfine interaction that gives rise to the scalar, or J-, coupling effect. As implied by the word contact, this interaction occurs only when the electron wave function is nonzero at the nucleus.

Information about the spin state of one nucleus is transmitted to other nuclei in the molecule via contact interactions between the nuclei and the electrons in the covalent bonds, which polarize the electron spin densities near the nuclei. To understand this mechanism, we will consider the effect that a nuclear spin has on the spin of a second nucleus which is linked to the first by an electronic covalent bond. The contact interaction between a nuclear spin and the nearby electrons leads to a polarization of the electron density near the nucleus in which the antiparallel alignment of electron and nucleus is favoured. Since the Pauli Exclusion Principle requires that the two electron spins in the covalent bond have antiparallel spins, there will be a higher probability for the electron having a spin state parallel to the first nucleus in other regions of the electron distribution. Other nuclear spins will,

therefore, "see" the spin state of the original nucleus since it has been transmitted to them via polarization of the electron spin states. Therefore, the combined effects of the contact hyperfine interaction and of the electron spin exchange interaction give rise to an indirect coupling between two nuclear spins. Defining this coupling constant as J in Hz (49), the interaction Hamiltonian between two covalently bonded nuclear spins (**I** and **S**) in a static magnetic field becomes

$$\mathcal{H} = -\hbar \left[\omega_I I_Z + \omega_S S_Z - 2\pi J \, \mathbf{I} \cdot \mathbf{S} \right] \quad , \tag{1.43}$$

where ω_I and ω_S are the Zeeman energy frequencies of the I and S spins.

We shall now consider a single proton pair that interact as described by the Hamiltonian in Eq. (1.43). By comparison with the single spin case, one might suspect that the J-coupling interaction operators that are products of transverse operators ($I_X S_X$ and $I_Y S_Y$) might be capable of inducing transitions between states. In fact, this turns out to be true, so, for simplicity, we will begin by considering the weak coupling case where these terms are dropped. The more general case of strong coupling will be considered later in Section 1.5.2.

1.5.1 Weak Coupling

The weak coupling Hamiltonian for two protons in a static magnetic field is

$$\mathcal{H}_{weak} = -\hbar \left[\omega_I I_Z + \omega_S S_Z - 2\pi J \, I_Z S_Z \right] \quad , \tag{1.44}$$

and gives a reliable description of a two-spin system when the two weakly coupled protons are chemically nonequivalent. There are four distinguishable orientations of the system, which are the energy eigenfunctions of Eq. (1.44), and may be defined as $|+_I -_S\rangle$, $|+_I +_S\rangle$, $|-_I +_S\rangle$, and $|-_I -_S\rangle$. A general wavefunction to describe the state of this system at time t=0 would be

$$|\Psi(0)\rangle = c_1|+_I +_S\rangle + c_2|+_I -_S\rangle + c_3|-_I +_S\rangle + c_4|-_I -_S\rangle \quad , \tag{1.45}$$

where $c_{1\text{-}4}$ are again complex coefficients. Using the rules developed for the single spin case, we may now determine the energy eigenvalues of $\mathcal{H}_{weak}$, as listed below

and illustrated in Fig. 1.1.

$$\mathcal{H}_{weak}|+_I+_S\rangle = (\hbar/2)\,(-\omega_I - \omega_S + \pi J)|+_I+_S\rangle = E_{++}|+_I+_S\rangle$$
$$\mathcal{H}_{weak}|+_I-_S\rangle = (\hbar/2)\,(-\omega_I + \omega_S - \pi J)|+_I-_S\rangle = E_{+-}|+_I-_S\rangle$$
$$\mathcal{H}_{weak}|-_I+_S\rangle = (\hbar/2)\,(+\omega_I - \omega_S - \pi J)|-_I+_S\rangle = E_{-+}|-_I+_S\rangle$$
$$\mathcal{H}_{weak}|-_I-_S\rangle = (\hbar/2)\,(+\omega_I + \omega_S + \pi J)|-_I-_S\rangle = E_{--}|-_I-_S\rangle\,. \qquad (1.47)$$

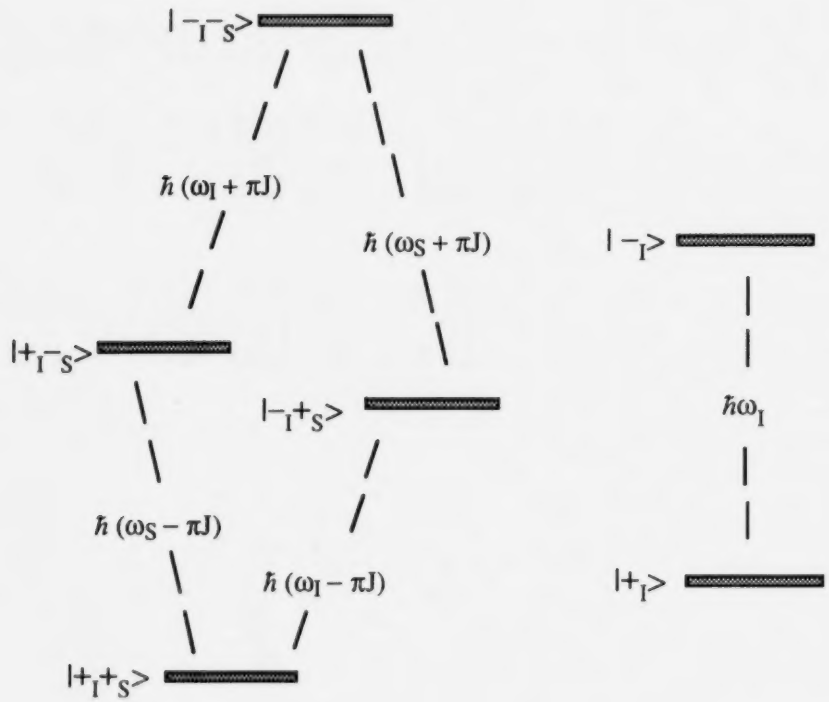

Figure 1.1 The energy levels of a weakly coupled system of proton spins. At left, a two spin system, and at right a single spin system. Some of the energy differences between states are listed.

From the Schrodinger equation, the evolution of $|\Psi>$ under $\mathcal{H}_{weak}$ for a time t will yield

$$|\Psi(t)> = c_1 \exp(-iE_{++}\,t/\hbar)\,|+_I+_S\rangle + c_2 \exp(-iE_{+-}\,t/\hbar)|+_I-_S\rangle$$
$$+ c_3 \exp(-iE_{-+}\,t/\hbar)|-_I+_S\rangle + c_4 \exp(-iE_{--}\,t/\hbar)|-_I-_S\rangle. \qquad (1.47)$$

Just as we did in Section 1.3, we are now prepared to calculate the mean magnetic moment of either spin. For convenience, we shall only calculate the mean values μ^I for spin I. The result for the mean value of μ_z^I follows intuitively from the single spin case, and is just the sum of probabilities of the I spin being up or down.

$$< \Psi(t) \mid \mu_z^I \mid \Psi(t) > = \gamma \hbar (1/2)(|c_1|^2 + |c_2|^2 - |c_3|^2 - |c_4|^2) \tag{1.48}$$

The transverse μ components do not follow quite so easily. We begin with μ_x^I,

$$<\Psi(t)| \mu_x^I |\Psi(t) > = \gamma \hbar (1/2)\{ c_1^* c_3 \exp[-i(\omega_I - \pi J)t] + c_2^* c_4 \exp[-i(\omega_I + \pi J)t] + c_3^* c_1 \exp[i(\omega_I - \pi J)t] + c_4^* c_2 \exp[i(\omega_I + \pi J)t]\} \tag{1.49}$$

Further simplification of this equation may be made by introducing the phase differences between the complex coefficients. We shall define the following phase angles

$$\arg\{c_1^* c_3\} = \phi_{13} \text{ and } \arg\{c_2^* c_4\} = \phi_{24} \ . \tag{1.50}$$

Then Eq. (1.49) reduces to

$$<\Psi(t)| \mu_x^I |\Psi(t) > = \gamma \hbar \{ |c_1| |c_3| \cos [(\omega_I - \pi J)t - \phi_{13}] + |c_2| |c_4| \cos [(\omega_I + \pi J)t - \phi_{24}]\} \tag{1.51}$$

From this equation, we see that if we wanted to measure a finite magnetization M_x^I due to a large number of spins, we would require a phase coherence across the sample between the $\phi^i{}_{13}$ or the $\phi^i{}_{24}$, or between both. In other words, there must be a similar inter-relationship between the states $|+_I +_S>$ and $|-_I +_S>$, and/or between the states $|+_I -_S>$ and $|-_I -_S>$ for each spin system in order to get a nonzero M_x^I. We shall call such a coherence between two states that differ by one in magnetic quantum number a *single* quantum coherence.

Further simplifications can be made if we assume that we have managed to perturb the system from equilibrium such that all the phase differences are zero, and that there is equal probability of the system being in each of its four states. One then obtains the following for the transverse components of μ.

$$< \Psi(t) \mid \mu_x^I \mid \Psi(t) > = (\gamma \hbar/4) [\cos(\omega_I + \pi J)t + \cos(\omega_I - \pi J)t]$$
$$< \Psi(t) \mid \mu_y^I \mid \Psi(t) > = -(\gamma \hbar/4) [\sin(\omega_I + \pi J)t + \sin(\omega_I + \pi J)t] \qquad (1.52)$$

Of course, when J=0 the results are the same as the single spin case in Section 1.3.1. However, when J is nonzero, we see that the mean values of the transverse components of $\boldsymbol{\mu}^I$ not only precess at ω_I, but also modulate at an angular frequency of πJ. It is interesting to note that if t=1/2J, the mean values of both transverse magnetic moment components vanish. This loss can be easily explained by a simple vector model by breaking the cos(πJt) term into two counter-rotating components, which clearly will oppose each other at t=1/2J, as illustrated in Fig. 1.2.

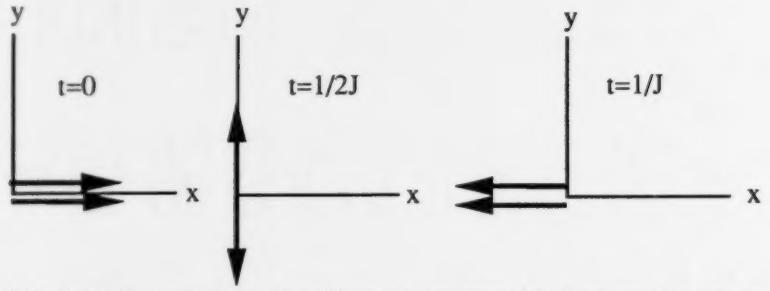

Figure 1.2 An illustration of the effect of varying the time on the mean transverse magnetic moment as defined in Eq. (1.52). In the figure, it is assumed that ω_I=0, thus the two counter-rotating components of $<\mu_x^I>$ rotate at an angular frequency of $\pm\pi J$, which leads to their cancellation when t=1/2J.

Clearly the products of eigenvalue coefficients in the wavefunction $|\psi>$ play a crucial role in determining the mean values of $\boldsymbol{\mu}$. For example, we have seen that the transverse components of $<\mu^I>$ depend upon products such as $c_2^* c_4$ and $c_1^* c_3$, which are single quantum coherences. Nevertheless, neither the I nor S magnetic moment components depend on products such as $c_1^* c_4$ or $c_2^* c_3$ which link either the $|+_I +_S>$ and $|-_I -_S>$ states, or the $|+_I -_S>$ and $|-_I +_S>$ states respectively. Note that the term $c_1^* c_4$ links two states that differ by two in magnetic quantum number (double quantum coherence), while the $c_2^* c_3$ term links states that differ by zero in magnetic quantum number (zero quantum coherence). In the case of a large number of similar spin systems, where the superscript ^{i} refers to the index of each spin system, a constant phase difference throughout the sample between each of the c_2^i and c_3^i terms, or between each of the c_1^i and c_4^i terms would lead to zero or double

quantum coherence respectively. In general, we shall refer to such terms as **multiple quantum coherences** (**MQC**s).

The existence of MQCs has no direct effect on the magnetization because the phase coherences that give rise to an MQC are not relevant to the calculation of mean values of the magnetic moment. However, MQCs can have a very large indirect effect on the observable magnetization - a fact that is central to this thesis. The creation and evolution of MQC will be addressed later. However, for the present, let us attempt to generate an operator whose mean value depends on the interrelationship of two states separated in energy by zero or two quanta.

We now consider the expectation values of the products I_+S_- and I_+S_+ of single spin operators. The effect of such operators on particular eigenstates of the Hamiltonian follows from the single spin case of Eq. (1.10),

$$I_+S_+|-_I-_S> = |+_I+_S> \qquad \text{and} \qquad I_+S_-|-_I+_S> = |+_I-_S>. \tag{1.53}$$

These operators lead to a null result when applied to any other eigenstate. We may now calculate the mean value of these MQC operators using the wavefunction of Eq. (1.47).

$$\begin{aligned} <\Psi(t)|\, I_+S_+\, |\Psi(t)> &= c_1^* c_4 \exp[i(E_{++} - E_{--})t/\hbar] \\ <\Psi(t)|\, I_+S_-\, |\Psi(t)> &= c_2^* c_3 \exp[i(E_{+-} - E_{-+})t/\hbar] \end{aligned} \tag{1.54}$$

Upon substitution for the energy values, and the phase factors we obtain

$$\begin{aligned} <\Psi(t)|\, I_+S_+\, |\Psi(t)> &= |c_1|\,|c_4| \exp[i(\omega_I+\omega_S)t + \phi_{14}\,] \\ <\Psi(t)|\, I_+S_-\, |\Psi(t)> &= |c_2|\,|c_3| \exp[i(\omega_I-\omega_S)t + \phi_{23}\,] \end{aligned} \tag{1.55}$$

From Eq. (1.55), we see that the double quantum coherence (DQC) term evolves at a frequency that is the sum of the two Larmor frequencies, while the zero quantum coherence (ZQC) term evolves at a frequency that is the difference between these two frequencies. The evolution rate of both terms is independent of the J-coupling for this two spin system. During evolution under the Hamiltonian of Eq. (1.42), for weak coupling in a static magnetic field, the DQC and ZQC terms never evolve into observable magnetization. Even though these MQCs are not observable,

they may exist and will evolve according to Eq. (1.55). It should now become obvious that a three-axis vector model of magnetization is insufficient to describe a weakly-coupled two-spin system. Nevertheless, by introducing additional orthogonal axes to represent coherences such as DQC, a vector model may again become feasible.

1.5.2 Strongly Coupled Two Spin System

We will now consider the full Hamiltonian of Eq. (1.43), without dropping any terms as was done for the weak coupling case. Using the raising and lowering operators, the Hamiltonian of Eq. (1.43) may be written as

$$\begin{aligned}\mathcal{H}_{strong} &= -\hbar\,[\omega_I I_z + \omega_S S_z - 2\pi J\, I_z S_z - \pi J\,(I_+ S_- + I_- S_+)] \\ &= \mathcal{H}_{weak} + \hbar\pi J\,(I_+ S_- + I_- S_+)\end{aligned} \tag{1.56}$$

Our first goal is to determine the energy eigenstates for this Hamiltonian. From Eq. (1.53), we found that operators of the form $I_- S_+$ or $I_+ S_-$ can affect eigenstates of the form $|+_I -_S\rangle$ or $|-_I +_S\rangle$, where the effect was to interchange the two states $|-_I +_S\rangle$ and $|+_I -_S\rangle$. However, such operators will annihilate the $|+_I +_S\rangle$ or the $|-_I -_S\rangle$ states. Without hesitation, therefore, we expect that the weak energy eigenfunctions $|+_I +_S\rangle$ and $|-_I -_S\rangle$ will also be energy eigenfunctions of $\mathcal{H}_{strong}$. In addition, because of the interchange arising from the zero quantum operators in $\mathcal{H}_{strong}$, we expect the remaining two energy eigenstates to be linear combinations of $|+_I -_S\rangle$ and $|-_I +_S\rangle$. Of course, the energy eigenfunctions Φ, must be orthonormal so the following choice becomes reasonable

$$\begin{aligned}\Phi_1 &= |+_I +_S\rangle \\ \Phi_2 &= -\sin\theta\,|+_I -_S\rangle + \cos\theta\,|-_I +_S\rangle \\ \Phi_3 &= \cos\theta\,|+_I -_S\rangle + \sin\theta\,|-_I +_S\rangle \\ \Phi_4 &= |-_I -_S\rangle\end{aligned} \tag{1.57}$$

Now by solving the Schrodinger equation $\mathcal{H}_{strong}\Phi_n = E_n\Phi_n$, we may

determine both the energy eigenvalues E_n and θ. E_1 and E_4 follow directly from the weak coupling case, however E_2 and E_3 do not. For example, in the case of Φ_3 we find

$$\mathcal{H}_{strong}\Phi_3 = (\hbar/2)\,[(-\omega_I + \omega_S - \pi J)\cos\theta + 2\pi J\sin\theta\,]\,|+_I -_S\rangle$$
$$+(\hbar/2)\,[(\omega_I - \omega_S - \pi J)\sin\theta + 2\pi J\cos\theta\,]\,|-_I +_S\rangle \qquad (1.58)$$

and clearly,

$$E_3\Phi_3 = E_3(\cos\theta\,|+_I -_S\rangle + \sin\theta\,|-_I +_S\rangle) \qquad (1.59)$$

equating component parts for $|+_I -_S\rangle$ and $|-_I +_S\rangle$ in Eqs. (1.58) and (1.59) leads to two equations

$$E_3\cos\theta = (\hbar/2)\,[(-\omega_I + \omega_S - \pi J)\cos\theta + 2\pi J\sin\theta]$$
$$E_3\sin\theta = (\hbar/2)\,[(\omega_I - \omega_S - \pi J)\sin\theta + 2\pi J\cos\theta] \qquad (1.60)$$

which we may rewrite as

$$E_3\sin 2\theta = (\hbar/2)\,[(-\omega_I + \omega_S - \pi J)\sin 2\theta + 2\pi J\sin^2\theta]$$
$$E_3\sin 2\theta = (\hbar/2)\,[(\omega_I - \omega_S - \pi J)\sin 2\theta + 2\pi J\cos^2\theta] \qquad (1.61)$$

solving for θ yields,

$$\tan 2\theta = (2\pi J)/(\omega_S - \omega_I) = J/(\nu_S - \nu_I), \qquad (1.62)$$

where $\nu_{I,S}$ are the resonance frequencies in Hz. From Eq. (1.61) we may now easily solve for E_3, and following a similar process E_2 can be determined. We now list the four resulting energies for this strongly coupled system, which were originally predicted by Hahn and Maxwell (49).

$$E_1 = E_{++} = (\hbar/2)\,(-\omega_I - \omega_S + \pi J)$$
$$E_2 = (\hbar/2)\,\{-[(\omega_I - \omega_S)^2 + (2\pi J)^2]^{1/2} - \pi J\}$$
$$E_3 = (\hbar/2)\,\{[(\omega_I - \omega_S)^2 + (2\pi J)^2]^{1/2} - \pi J\}$$
$$E_4 = E_{--} = (\hbar/2)\,(+\omega_I + \omega_S + \pi J) \qquad (1.63)$$

In general, because of its added complexity, we would like to avoid using the full strong coupling Hamiltonian whenever possible. By comparing the strong coupling energies and eigenstates with those of the weak coupling approximation in Eqs. (1.45) and (1.46), we see that the strong coupling results reduce correctly to the weak coupling approximation when $(\nu_S - \nu_I) >> J$. For most applications however, the weak coupling approximation will suffice provided $(\nu_S - \nu_I)/J > 5$ (51). This limiting ratio would imply less than 10% mixing of the $|+_I -_S>$ and $|-_I +_S>$ states.

Consider now the effect on a spin wavefunction Ψ of evolution under $\mathcal{H}_{strong}$ from t=0 to a time t,

$$|\Psi_{strong}(t)> = c_1 \exp(-iE_1 t/\hbar)\,|\Phi_1> + c_2 \exp(-iE_2 t/\hbar)\,|\Phi_2> + c_3 \exp(-iE_3 t/\hbar)\,|\Phi_3> + c_4 \exp(-iE_4 t/\hbar)\,|\Phi_4> \quad . \tag{1.64}$$

The mean values of the magnetic moment vector $\boldsymbol{\mu}^I$ can now be determined. Beginning with μ_Z^I, we obtain

$$<\Psi(t)\,|\,\mu_Z^I\,|\Psi(t)> = \gamma\hbar(1/2)\{\,|c_1|^2 - |c_4|^2 - |c_2|^2\cos2\theta + |c_3|^2\cos2\theta - c_2^* c_3 \exp[i(E_3-E_2)t/\hbar)]\sin2\theta - c_3^* c_2 \exp[i(E_2-E_3)t/\hbar)]\sin2\theta\,\} \quad . \tag{1.65}$$

This equation tells us that some of the terms that contribute to the mean value of μ_Z^I oscillate at the zero quantum angular frequency of $[(\omega_I - \omega_S)^2 + (\pi J)^2]^{1/2}$. In the weak coupling approximation $\sin2\theta=0$ and this effect is not observed. However, in the strong coupling case, the sum of $<\mu_Z^I>$ and $<\mu_Z^S>$ does not oscillate and yields the same result as in the weak coupling case of

$$<\Psi(t)\,|\,\mu_Z^I + \mu_Z^S\,|\Psi(t)> = \gamma\hbar(1/2)[\,|c_1|^2 - |c_4|^2] \quad . \tag{1.66}$$

As a final example of the wavefunction approach to spin evolution, we shall find the mean value of $\mu_+^I + \mu_+^S$, which ultimately will be related to the net transverse magnetization.

$$< \Psi(t) \mid \mu_+^I + \mu_+^S \mid \Psi(t) > = \gamma \hbar \{ c_4^* c_3 (\cos\theta + \sin\theta) \exp[i(E_4 - E_3)t/\hbar)] \\ c_4^* c_2 (\cos\theta - \sin\theta) \exp[i(E_4 - E_2)t/\hbar)] \\ c_2^* c_1 (\cos\theta - \sin\theta) \exp[i(E_2 - E_1)t/\hbar)] \\ c_3^* c_1 (\cos\theta + \sin\theta) \exp[i(E_3 - E_1)t/\hbar)] \} \qquad (1.67)$$

Before commenting on Eq. (1.67), we shall define the c coefficients for a special case. Suppose that the spin system has just been altered from equilibrium by a $\pi/2$ radiofrequency pulse similar to that of Section 1.3.2. Then if we ignore J-coupling and precession effects during the pulse, a possible wavefunction at the end of the pulse may be represented by

$$|\Psi_{strong}> = (1/2) (\; |+_I +_S> + |+_I -_S> + |-_I +_S> + |-_I -_S> \;) \qquad (1.68)$$

where the probability of each spin being polarized along the z-axis is equal. Immediately after the pulse, we may rewrite Eq. (1.68) in terms of the basis of Eq. (1.57) leading to

$$|\Psi_{strong}> = (1/2) \; [\; |\Phi_1> + (\cos\theta - \sin\theta)|\Phi_2> + (\cos\theta + \sin\theta)|\Phi_3> + |\Phi_4>] \qquad (1.69)$$

Replacing the $c_{1\text{-}4}$ coefficients of Eq. (1.67), with the coefficients of Eq. (1.69) yields

$$< \Psi(t) \mid \mu_+^I + \mu_+^S \mid \Psi(t) > = (\gamma \hbar/4) \{ (1 + \sin 2\theta) \exp[i(E_4 - E_3)t/\hbar)] \\ (1 - \sin 2\theta) \exp[i(E_4 - E_2)t/\hbar)] \\ (1 - \sin 2\theta) \exp[i(E_2 - E_1)t/\hbar)] \\ (1 + \sin 2\theta) \exp[i(E_3 - E_1)t/\hbar)] \} \qquad (1.70)$$

From Eq. (1.70), we find that the transverse magnetic moment will consist of components which precess at each of four frequencies with characteristic intensities $(1 \pm \sin 2\theta)$. By Fourier transforming this signal, we may obtain the frequency spectrum illustrated in Fig 1.3.

Of equal interest is the case of zero chemical shift difference between the two spins, or from Eq. (1.62), when $\theta = \pi/4$. In such a case we have two magnetically

equivalent spins. Since they are bonded together, J-coupling is still operative, but will it be observable? By examining the spectrum, the answer is that such coupling between magnetically equivalent spins is not observable because the intensities of the two outer lines shrink to zero and the two inner lines coalesce as J approaches zero. The same answer may be derived by looking at the wavefunctions of Eq. (1.57): when $\theta=\pi/4$, $|\Phi_2>$ is purely antisymmetric while the other three states are symmetric. From symmetry considerations, we would expect no transitions between the antisymmetric and symmetric states.

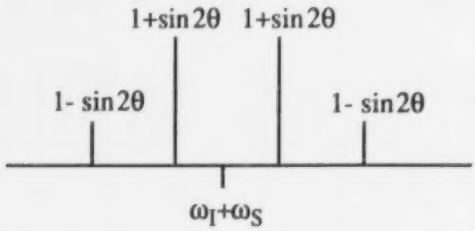

Figure 1.3 A spectrum illustrating the relative intensities of the four frequencies corresponding to the rotating components of the mean transverse magnetic moment of an AB spin system. The angle θ is defined in the text. The four frequencies, $\omega_{1\text{-}4}$, are $\omega_{1\text{-}4}= (1/2)\{\omega_I + \omega_S \pm 2\pi J \pm [(\omega_I-\omega_S)^2 + (2\pi J)^2]^{1/2}\}$. In the weak coupling limit, θ goes to zero and we obtain the normal pair of doublets at frequencies of $\omega_I \pm \pi J$ and $\omega_S \pm \pi J$.

We shall reconsider the effects of J-coupling in Section 1.7, following the introduction of the density operator notation. We shall find that this notation will greatly simplify the calculations of evolution under either weak or strong J-coupling.

1.5.3 Classification of Spin Systems

In order to classify a particular spin system, we will use the Pople notation (52), where each spin is represented by a letter, with closely spaced letters, such as A and B, indicating nuclei with similar chemical shifts so that they are strongly coupled, and distantly spaced letters, such as A and X, indicating nuclei with very different chemical shifts for which the weak coupling approximation is appropriate. The same letter is repeated to indicate equivalent spins, i.e. A_2 for two equivalent spins. In the previous section, it was found that magnetically equivalent nuclei do

not exhibit observable J-coupling effects. Such couplings may therefore be left out of the Hamiltonian that describes the spin system of a given molecule.

Two nuclei are said to be chemically equivalent if they have the same chemical shift. In order for such nuclei to be magnetically equivalent, they must experience identical spin-spin couplings to all other nuclei in the molecule. Molecular asymmetry can often lead to two apparently chemically equivalent protons being nonequivalent. For example, the two protons in a CH_2 group which is directly bonded to a neighboring *chiral* carbon atom, will not be chemically equivalent. This can be visualized most easily by viewing the molecule along the carbon-carbon bond. Three rotational conformations are shown in Fig. 1.4, where the protons of interest are labelled H_A and H_B. The average chemical shift that is detected for H_A is related to the probability of H_A being in each of the three different chemical environments shown in Fig. 1.4 (a), (b) and (c). If the probabilities of the molecule being in each of these three conformations are not equal, the resonant frequencies of H_A and H_B will be different. For example, if conformer (b) is the most likely, then H_A is most likely to be found between P and T, while H_B is most likely to be found between R and T, thus H_A and H_B will have different resonant frequencies.

Even when each conformer of Fig. 1.4 has equal likelihood, the resonant frequencies of H_A and H_B may still be different. For example, H_A in (a) is not equivalent to H_B in (b), because, despite the fact that they have the same neighbors (R and T), Q is in a different chemical environment. Hence, the chemical environments are not necessarily the same for H_A in (a) and for H_B in (b).

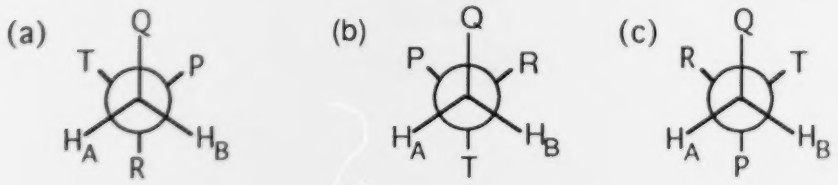

Figure 1.4 Three possible orientations of a molecular fragment linking two carbon atoms, one with two protons H_A and H_B attached to it, via a free-rotating carbon-carbon bond. The molecule is viewed along the carbon-carbon bond which forms the centre of each drawing. P, Q, R and T are other atoms or fragments that are bonded to the carbons.

We are now in a position to introduce the spin systems of the metabolites to be studied in this thesis. The four molecules to be considered are illustrated in Fig. 1.5, and the appropriate spin system classification is listed below each one. In addition, the chemical shifts and J-couplings for each of these metabolites are listed in Table 1.1.

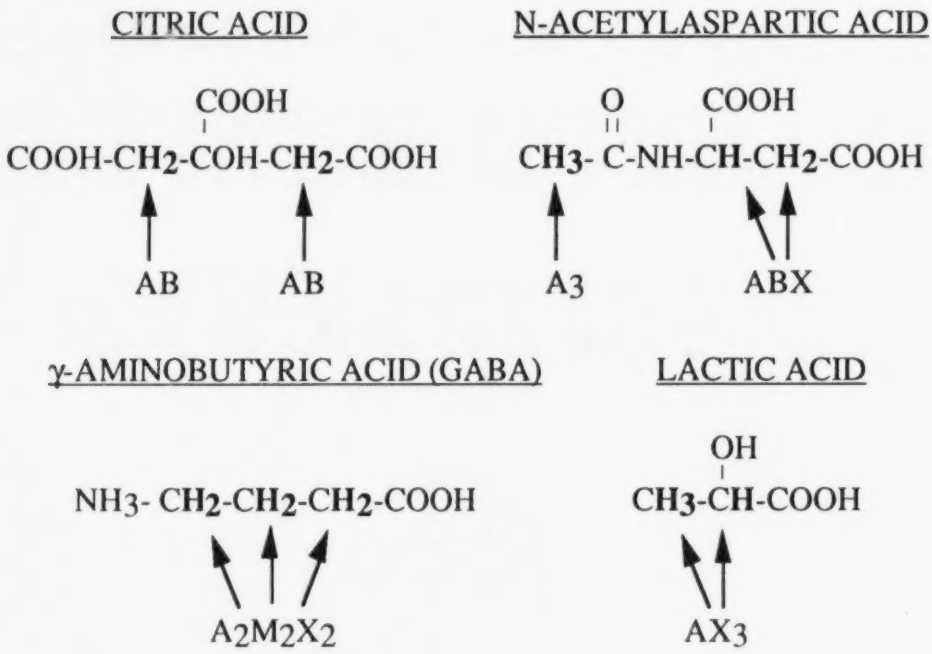

Figure 1.5 The spin systems of the four metabolites to be considered in this thesis. Below each molecule, its spin system is listed in Pople notation (52). Citric acid has two identical AB systems. Couplings between protons separated by more than three bonds need not be considered because they are too small. In an aqueous solution, the NH and OH protons will be in rapid exchange and thus will not be visible. In addition, all four metabolites are weak acids and thus, for MRS purposes, we shall henceforth consider them to be in their dissociated ionic forms (eg. lactate instead of lactic acid).

Table 1.1

Chemical Shifts and J-Couplings of the Targetted Metabolites

Metabolite			Chemical Shift (ppm)	Multiplicity*	J-Couplings (Hz)
Lactate		CH	4.11	quartet	7.3
		CH_3	1.33	doublet	7.3
GABA	X_2	CH_2	2.31	triplet	7.3
	M_2	CH_2	1.91	quintet	7.3
	A_2	CH_2	3.01	triplet	7.3
Citrate	A	CH	2.55	strongly	15.4
	B	CH	2.69	coupled doublets	15.4
NAA		CH_3	2.02	singlet	------
	X	CH	4.40	doublet of doublets	3.7 (J_{AX})
					10.1 (J_{BX})
	B	CH	2.51	strongly coupled	15.7 (J_{AB})
				multiplet	10.1 (J_{BX})
	A	CH	2.70	strongly coupled	15.7 (J_{AB})
				multiplet	3.7 (J_{AX})

*The multiplicity refers to the number of lines one would observe in the frequency spectrum where each line represents a frequency of rotation of the transverse magnetization.

1.6 Density Operator Formalism

As we have seen, the calculations of the mean values of μ for two J-coupled spins are quite lengthy and clumsy. The daunting task that we are now faced with is to calculate mean values over an entire ensemble of spin systems. Up to this point, we have determined mean values by making use of a known wavefunction, for example, suppose the wavefunction Ψ is defined in terms of an orthonormal basis $|u_n\rangle$ such that

$$|\Psi\rangle = \Sigma_p c_p |u_p\rangle \qquad \text{or} \qquad \langle\Psi| = \Sigma_n c_n^* \langle u_n| \tag{1.71}$$

then the mean value of an operator **O** is,

$$\langle O\rangle = \langle\Psi|\mathbf{O}|\Psi\rangle = \Sigma_{n,p} c_n^* \langle u_n|O|u_p\rangle c_p = \Sigma_{n,p} c_n^* c_p O_{np} \ , \tag{1.72}$$

which depends upon the multiplication of the products of the coefficients $c_n^* c_p$ with the corresponding elements of the operator **O** defined as $O_{np}=\langle u_n|O|u_p\rangle$. To use the method of Eq. (1.72) for an ensemble of spins, we would require knowledge of the wavefunction of each spin in the ensemble. In general, this information is unavailable, because we can only determine information about ensemble averages, and thus the wavefunction approach of Eq. (1.72) breaks down. Nevertheless, by introducing the spin density operator, the incomplete information that we possess will be shown to be sufficient for the calculation of mean values of operators acting on the ensemble. Even in cases where the wavefunction can be described, we shall see that mean value calculations can be performed in a much simpler manner by using the density operator approach.

1.6.1 General Equations

We shall initially introduce the density operator for the case of an idealized pure state where all the spin systems in the ensemble can be described by the same wavefunction. In Section 1.6.1.2, we then consider the more general case of a statistical mixture of states where the ensemble cannot be described by a single

wavefunction.

1.6.1.1 Equations for an Idealized Pure State

Assuming that the wavefunction Ψ of Eq. (1.71) describes the ensemble, we can define the mean values by Eq. (1.72). The fact that the coefficients $c_n^* c_p$ of Eq. (1.72) can be represented by $\langle u_p|\Psi\rangle\langle\Psi|u_n\rangle$, suggests the introduction of the spin density operator ρ defined as

$$\rho = |\Psi\rangle\langle\Psi| = \Sigma_{n,p}\, c_n^* c_p\, |u_p\rangle\langle u_n| \quad . \tag{1.73}$$

Unlike the wavefunction that is represented by an expansion of basis vectors $|u_p\rangle$, the density operator is represented by an expansion of basis *operators* $|u_p\rangle\langle u_n|$. From Eq. (1.72), our mean value may now be written as

$$\langle \mathbf{O}\rangle = \Sigma_{n,p}\langle u_n|\mathbf{O}|u_p\rangle\langle u_p|\sigma|u_n\rangle = \Sigma_n \langle u_n|\mathbf{O}\sigma|u_n\rangle \,, \tag{1.74}$$

where the last equality follows from the closure property of the basis, $\Sigma_p |u_p\rangle\langle u_p| = \mathbf{1}$, where $\mathbf{1}$ is the unity operator. This closure property is easily proven below,

$$|\Psi\rangle = \Sigma_p c_p |u_p\rangle = \Sigma_p (\langle u_p|\Psi\rangle)\, |u_p\rangle = \Sigma_p\, |u_p\rangle\langle u_p|\Psi\rangle. \tag{1.75}$$

If we define the trace of an operator as the sum of its diagonal elements, the mean value of $\mathbf{O}$ in Eq. (1.74) becomes simply

$$\langle \mathbf{O}\rangle = \mathrm{Trace}\{\rho\, \mathbf{O}\} \,. \tag{1.76}$$

We now wish to consider the evolution of ρ under a time independent Hamiltonian $\mathcal{H}$. From the wavefunction representation, we know that

$$|\,\Psi(t)\rangle = \exp(-i\,\mathcal{H}t/\hbar)\,|\Psi(0)\rangle \quad \text{and} \quad \langle\Psi(t)| = \langle\Psi(0)\,|\exp(i\,\mathcal{H}t/\hbar) \,, \tag{1.77}$$

so it immediately follows that

$$\rho(t) = \exp(-i\,\mathcal{H}t/\hbar)\rho(0)\exp(i\,\mathcal{H}t/\hbar) \quad . \tag{1.78}$$

For the more general case of a time dependent Hamiltonian, we obtain from the Schrödinger equation

$$i\hbar\, d/dt|\Psi(t)\rangle = \mathcal{H}(t)\,|\Psi(t)\rangle \quad \text{and} \quad -i\hbar\, d/dt\langle\Psi(t)| = \langle\Psi(t)|\mathcal{H}(t) \tag{1.79}$$

and,

$$\dot{\rho}(t) = (i/\hbar)[\rho, \mathcal{H}]\,. \tag{1.80}$$

1.6.1.2 Equations for a Statistical Mixture of States

In general, the state of a system is not perfectly determined, but is a statistical mixture of states. If we assume that there are q such states, each defined by Ψ_q, we shall define ρ as

$$\rho = \Sigma_q\, p_q|\Psi_q\rangle\langle\Psi_q| \tag{1.81}$$

where p_q represents the statistical, fractional population of the state Ψ_q and $\Sigma_q\, p_q=1$. Since each Ψ_q may be expanded in terms of the same basis set $\{|u_n\rangle\}$, the q dependence is only in the coefficients:

$$\rho = \Sigma_{n,p}\,(\Sigma_q p_q c^*_{nq} c_{pq})\,|u_p\rangle\langle u_n| \quad . \tag{1.82}$$

The bracketed term represents the ensemble average of $c^*_n c_p$, which we shall represent by $\overline{c^*_n c_p}$. Hence,

$$\rho = \Sigma_{n,p}\,\overline{c^*_n c_p}\;|u_p\rangle\langle u_n| \quad . \tag{1.83}$$

By comparing Eq. (1.83) to Eq. (1.73), it is clear that the spin density operator ρ for an ensemble of spins will also obey Eqs. (1.76) and (1.78) for the respective calculations of the mean values of an operator O, and of the evolution of ρ under a time-independent Hamiltonian $\mathcal{H}$.

The spin density operator may also be represented by a matrix of its coefficients, (ρ), which for a two vector basis, $\{|u_1\rangle, |u_2\rangle\}$, gives rise to

$$(\rho)=\begin{pmatrix} \overline{c_1^* c_1} & \overline{c_2^* c_1} \\ \overline{c_1^* c_2} & \overline{c_2^* c_2} \end{pmatrix} \quad . \qquad (1.84)$$

In the matrix representation, the diagonal elements are real and represent the fractional populations of spins that are in each state. Clearly then, Trace{ρ}=1. The off-diagonal elements are complex conjugates of each other and will only be nonzero when there is a phase coherence between spins in the $|u_1>$ and $|u_2>$ states.

1.6.2 Bases for an Ensemble of Single Spin Systems

Consider now an ensemble of q single proton spin systems in a static magnetic field along the z-axis. Each spin may be represented by a wavefunction Ψ_q such that $|\Psi_q> = c_{1q}|+> + c_{2q}|->$. Using Eq. (1.83), the density operator of the ensemble will be

$$\rho = \overline{c_1^* c_1}\ |+><+| + \overline{c_1^* c_2}\ |-><+| + \overline{c_2^* c_1}\ |+><-| + \overline{c_2^* c_2}\ |-><-| \qquad (1.85)$$

while the density matrix (ρ) is the same as that of Eq. (1.84). In Eq. (1.85), ρ has been expanded in terms of four orthogonal base operators. In order to gain more insight, and reduce the complexity of calculations, we would like to expand ρ in the more convenient basis set of Cartesian spin operators (53, 54). Using the matrix representation, we can write (ρ) as

$$(\rho)=\begin{pmatrix} \overline{c_1^* c_1} & \overline{c_2^* c_1} \\ \overline{c_1^* c_2} & \overline{c_2^* c_2} \end{pmatrix} = 1/2 \left\{ d_1 \begin{pmatrix} 1 & 0 \\ 0 & 1 \end{pmatrix} + d_2 \begin{pmatrix} 1 & 0 \\ 0 & -1 \end{pmatrix} + d_3 \begin{pmatrix} 0 & 1 \\ 1 & 0 \end{pmatrix} + d_4 \begin{pmatrix} 0 & -i \\ i & 0 \end{pmatrix} \right\} \qquad (1.86)$$

where $d_{1\text{-}4}$ are real constants. By comparing the component matrices of (ρ) to those of the Cartesian spin operators introduced in Section 1.2, we may write (1.86) in matrix or operator form as

$$(\rho)=d_1[\mathbf{1}]+ d_2(I_z)+ d_3(I_x)+ d_4(I_y) \qquad \rho = d_1\mathbf{1}+ d_2 I_z+ d_3 I_x+ d_4 I_y \quad . \qquad (1.87)$$

From Eq. (1.86), we may also solve explicitly for the d coefficients.

$$d_1 = \overline{c_1^* c_1} + \overline{c_2^* c_2} \qquad d_2 = \overline{c_1^* c_1} - \overline{c_2^* c_2}$$
$$d_3 = \overline{c_1^* c_2} + \overline{c_2^* c_1} \qquad d_4 = -i\,(\overline{c_1^* c_2} - \overline{c_2^* c_1}) \tag{1.88}$$

In particular, the coefficient d_2 represents the difference in populations between spins being in the $|+\rangle$ and $|-\rangle$ states. Now suppose we wish to calculate mean values such as $\langle I_x \rangle$, the result would simply be $\langle I_x \rangle = d_3 \mathrm{Trace}\{I_x I_x\} = d_3/2$, because the traces of the other products of I_x with the basis operators of Eq. (1.88) are all zero. Similarly, $\langle I_y \rangle = d_4/2$ and $\langle I_z \rangle = d_2/2$. Hence the mean values of **I** relate directly to coefficients of the density operator.

At thermal equilibrium, we do not expect there to be any phase coherence between the $|+\rangle$ and $|-\rangle$ states, thus $d_3 = d_4 = 0$ in the initial equilibrium density operator ρ_{eq}. Moreover, for calculation purposes, we need not consider the operator **1** in Eq. (1.87) since it has no effect on the mean values of magnetization and remains unchanged under evolution due to Eq. (1.78). The fact that the **1** has no effect on the observable magnetization follows from $\mathrm{Trace}\{\mathbf{1}, I_\alpha\} = 0$, where $\alpha = +, -, x, y,$ or z, and intuitively, from the fact that it is the population *difference* that gives rise to magnetic resonance phenomena. In addition, since we will only be interested in the signal strength relative to its maximum, we need not concern ourselves with the magnitude of the proportionality constant d_2 that is related to the Boltzmann factor. Thus, for a single spin, we shall begin calculations from equilibrium described by a reduced spin density operator $\sigma_{eq} = I_z$ defined in terms of the equilibrium density operator ρ_{eq} as

$$\rho_{eq} = d_1 \mathbf{1} + d_2 I_z = d_1 \mathbf{1} + d_2 \sigma_{eq} . \tag{1.89}$$

The evolution of this operator under various Hamiltonians will be discussed in Section 1.7. At this point, we have seen that the bases for an ensemble of single spin systems can be formed by the Cartesian spin operators, and furthermore that the coefficient of each spin angular momentum operator is directly related to the mean value of that component of **I**. In fact, the three Cartesian basis operators correspond directly to the three Cartesian axes of the classical vector model. In other words, the mean values of a single spin can be equally well described by either the classical or the quantum mechanical MR theory.

1.6.3 Bases for an Ensemble of Two Spin Systems

For a two spin system, the density operator is composed of sixteen basis operators of the form $|\pm_I\pm_S\rangle\langle\pm_I\pm_S|$, and the density matrix has sixteen corresponding entries as listed below,

$$(\rho) = \begin{array}{c} \\ \langle +_I+_S| \\ \langle +_I-_S| \\ \langle -_I+_S| \\ \langle -_I-_S| \end{array} \begin{array}{c} \begin{array}{cccc} |+_I+_S\rangle & |+_I-_S\rangle & |-_I+_S\rangle & |-_I-_S\rangle \end{array} \\ \begin{pmatrix} \overline{c_1^* c_1} & \overline{c_2^* c_1} & \overline{c_3^* c_1} & \overline{c_4^* c_1} \\ \overline{c_1^* c_2} & \overline{c_2^* c_2} & \overline{c_3^* c_2} & \overline{c_4^* c_2} \\ \overline{c_1^* c_3} & \overline{c_2^* c_3} & \overline{c_3^* c_3} & \overline{c_4^* c_3} \\ \overline{c_1^* c_4} & \overline{c_2^* c_4} & \overline{c_3^* c_4} & \overline{c_4^* c_4} \end{pmatrix} \end{array} \tag{1.90}$$

where to the left and above the matrix, the bra and ket that define each row and column are listed. For example, $\langle +_I+_S|\rho\,|-_I+_S\rangle = \overline{c_3^* c_1}$. We may again expand ρ in terms of Cartesian spin operators. The necessary operators may be obtained by forming the direct product between the operators ($\mathbf{1}$, I_x,I_y,I_z) and ($\mathbf{1}$, S_x,S_y,S_z). The resulting products of operators are listed below.

$$\begin{array}{llllll} \mathbf{1} & & & & & \\ I_x & I_y & I_z & S_x & S_y & S_z \\ I_xS_z & I_yS_z & I_zS_x & I_zS_y & & \\ I_xS_x & I_xS_y & I_yS_x & I_yS_y & & \\ I_zS_z & & & & & \end{array} \tag{1.91}$$

These product operators are orthogonal with respect to the formation of a trace. however, they are not normalized. Normalization would require multiplication of $\mathbf{1}$ by 1/2, and multiplication of the two spin operators by 2 ($2I_xS_z$, $2I_xS_y$, etc.). In general, for a system made up of N spins, the normalization condition requires that $\mathrm{Tr}\{\mathbf{O_1},\mathbf{O_2}\} = \delta_{1,2}2^{N-2}$, where $\mathbf{O}_{1,2}$ are product operators and $\delta_{1,2}$ is nonzero only when 1=2.

Each of the operators in Eq. (1.91) may be expanded in terms of the original 16 base operators of the form $|\pm_I\pm_S\rangle\langle\pm_I\pm_S|$, for example, noting the effect of the operator I_x on a wavefunction $|\pm_I\rangle$ (see Section 1.2) we may write,

$$I_xS_x = 1/4\{\ |+_I+_S\rangle\langle-_I-_S| + |-_I+_S\rangle\langle+_I-_S| + |+_I-_S\rangle\langle-_I+_S| + |-_I-_S\rangle\langle+_I+_S|\ \}\ . \qquad (1.92)$$

From Eq. (1.92), it is clear that the operator I_xS_x represents a type of coherence between the states separated by two quanta and also between the states separated by zero quanta. Instead of the Cartesian I_x and I_y operators it is often convenient to introduce the raising and lowering operators as defined in Section 1.2. The basis operators then become

$$\begin{array}{llllll} \mathbf{1} & & & & & \\ I_+ & I_- & I_z & S_+ & S_- & S_z \\ I_+S_z & I_-S_z & I_zS_+ & I_zS_- & & \\ I_+S_+ & I_+S_- & I_-S_+ & I_-S_- & & \\ I_zS_z & & & & & \end{array} \qquad (1.93)$$

With the raising and lowering operators one may distinguish between a zero quantum operator and a double quantum operator as illustrated below.

$$I_+S_+ = |-_I-_S\rangle\langle+_I+_S| \qquad I_+S_- = |-_I+_S\rangle\langle+_I-_S| \qquad (1.94)$$

In the expansion of the density operator the coefficient of I_+S_+ will be $\overline{c_1^*c_4}$ and the coefficient of I_+S_- will be $\overline{c_2^*c_3}$. The single quantum operators in Eq. (1.93) come in two forms, either $S_\pm$ and $I_\pm$, or $I_\pm S_z$ and $S_\pm I_z$. Expanding two such terms we arrive at

$$\begin{aligned} I_+ &= |-_I+_S\rangle\langle+_I+_S| + |-_I-_S\rangle\langle+_I-_S| \\ I_+S_z &= 1/2\{|-_I+_S\rangle\langle+_I+_S| - |-_I-_S\rangle\langle+_I-_S|\ \} \end{aligned} \qquad (1.95)$$

The coefficients for I_+ and I_+S_z in the expansion of the density operator will be $(\ \overline{c_1^*c_3} + \overline{c_2^*c_4}\ )$ and $(1/2)(\ \overline{c_1^*c_3} - \overline{c_2^*c_4}\ )$ respectively. To distinguish between these

two types of single quantum terms, we shall call terms such as I_+S_Z *antiphase* coherences. The remaining term in Eq. (1.91) and (1.93), that we have not yet discussed, is the operator I_ZS_Z which may be written as follows

$$I_ZS_Z = 1/4\{ |+_I+_S\rangle\langle+_I+_S| - |-_I+_S\rangle\langle-_I+_S| - |+_I-_S\rangle\langle+_I-_S| + |-_I-_S\rangle\langle-_I-_S| \} , \quad (1.96)$$

where its coefficient in the expansion of the density operator will thus be $(1/4)(\overline{c_1^* c_1} - \overline{c_2^* c_2} - \overline{c_3^* c_3} + \overline{c_4^* c_4})$ which represents a specific combination of the four populations. We have thus seen that each element in the density matrix is linked to the existence of various types of product operator terms. The connections between the double quantum, DQ, zero quantum, ZQ, population terms, P, and single quantum I and S terms, SQ(I) and SQ(S), to the various elements of the density matrix of Eq. (1.90) are:

$$\begin{array}{c} \\ \langle+_I+_S| \\ \langle+_I-_S| \\ \langle-_I+_S| \\ \langle-_I-_S| \end{array} \begin{array}{c} \begin{array}{cccc} |+_I+_S\rangle & |+_I-_S\rangle & |-_I+_S\rangle & |-_I-_S\rangle \end{array} \\ \begin{pmatrix} P & SQ(S) & SQ(I) & DQ \\ SQ(S) & P & ZQ & SQ(I) \\ SQ(I) & ZQ & P & SQ(S) \\ DQ & SQ(I) & SQ(S) & P \end{pmatrix} \end{array} . \quad (1.97)$$

From our previous work with the wavefunctions, we know that the longitudinal magnetization is proportional to the population differences. The population terms P, arise from a combination of the operators **1**, I_Z, S_Z, and I_ZS_Z. Nevertheless by applying Eq. (1.76), we see that only the density operator coefficients of the I_Z and S_Z operators will affect $\langle I_Z+S_Z\rangle$ since the other traces will be zero. Similarly, the calculation of $\langle I_X+S_X\rangle$ depends purely upon the coefficients of I_X and S_X, while a calculation of $\langle I_++S_+\rangle$ depends purely upon the coefficients of I_- and S_-. In summary then, the existence of a finite magnetization for the **I** spins, depends solely upon the coefficients of I_X, I_Y (or I_+ and I_-) and I_Z, in the density operator expansion. *The ZQ, DQ and antiphase coherences make no contribution to the magnetization.*

1.7 Transformation Equations of the Density Operator

By using a density operator expansion in terms of products of spin operators, we have seen that only the single quantum operators such as I_x and I_y need to be considered at the time of detection, because the terms associated with other products of spin operators do not give rise to transverse magnetization. It is thus sufficient to begin calculations with only the reduced spin density operator σ, rather than the complete density operator ρ. The reduced equilibrium density operator for a two spin system can be described by I_z+S_z. In this section, we shall show how terms in the reduced density operator evolve under the influence of radiofrequency (r.f.) pulses, chemical shift and J-coupling. All evolution effects will be determined by solving Eq. (1.78) with the appropriate time-independent Hamiltonian $\mathcal{H}$. (If $\mathcal{H}$ is time dependent, it shall be reduced to a series of small time-independent parts.) We shall see that the power of the product operator approach lies in its ability to concisely describe such evolutions in terms of simple algebraic transformation equations. This approach was first introduced in 1983 by Sorensen et. al. (53).

From this point onward, we shall always assume, unless otherwise specified,that we are in a rotating frame of reference, unless otherwise specified, that rotates at the proton Larmor frequency, as discussed in Section 1.3.2.

1.7.1 Transformations Under a Radiofrequency Pulse

If a single spin system is exactly on resonance, its Hamiltonian during an r.f. pulse with magnetic field B_1 applied along the x axis of a frame rotating at a frequency of $-\omega_o$ is described by Eq. (1.33) which we rewrite here, dropping the primed notation and recalling that $\omega_1=\gamma B_1$.

$$\mathcal{H} = -\hbar\,\omega_1 I_x \tag{1.98}$$

Beginning with the equilibrium reduced density operator $\sigma_{eq}=\sigma(0)=I_z$, the evolution of σ under this Hamiltonian is described by (1.78), thus we arrive at

$$\sigma(t) = \exp(i\omega_1 I_x t)\, I_z \exp(-i\omega_1 I_x t) \quad . \tag{1.99}$$

This equation may be solved by using the method of Slichter (46) which we now outline. Taking the time derivative of Eq. (1.99) we obtain

$$\begin{aligned}\dot{\sigma}(t)&=i\omega_1\exp(i\omega_1 I_X t)\,[I_X, I_Z]\,\exp(-i\omega_1 I_X t)\\&=\omega_1\exp(i\omega_1 I_X t)\,I_y\,\exp(-i\omega_1 I_X t)\end{aligned}\qquad(1.100)$$

where a dot above the operator indicates time differentiation. The second derivative yields

$$\begin{aligned}\ddot{\sigma}(t)&=i\omega_1\exp(i\omega_1 I_X t)\,[I_X, I_y]\,\exp(-i\omega_1 I_X t)\\&=-\omega_1^2\exp(i\omega_1 I_X t)\,I_Z\,\exp(-i\omega_1 I_X t)\\&=-\omega_1^2\sigma(t)\quad .\end{aligned}\qquad(1.101)$$

This second order differential equation has general solution,

$$\sigma(t) = A\cos(\omega_1 t) + B\sin(\omega_1 t)\qquad(1.102)$$

where A and B are operators that can be evaluated by considering the initial conditions of $\sigma(0)=I_Z$ and $\dot{\sigma}(0)=\omega_1 I_y$, to yield

$$\sigma(t) = I_Z\cos(\omega_1 t) + I_y\sin(\omega_1 t).\qquad(1.103)$$

Using the notation of Section 1.3.2, we may write the net effect of the r.f. pulse as

$$I_Z \xrightarrow{-\omega_1 I_x t} I_Z\cos(\omega_1 t) + I_y\sin(\omega_1 t)\quad .\qquad(1.104)$$

We shall define a counterclockwise rotation, if looking in the direction of the rotation vector, as a negative rotation, thus the effect of Eq. (104) is to cause a counterclockwise rotation about the +x axis. By defining the r.f. pulse angle $\theta=-\omega_1 t$, we may represent a positive or clockwise rotation about the +x axis by

$$I_Z \xrightarrow{\theta I_x} I_Z\cos\theta - I_y\sin\theta\quad .\qquad(1.105)$$

Similarly, it can be shown that

$$I_y \xrightarrow{\theta I_x} I_y \cos\theta + I_z \sin\theta$$
$$I_x \xrightarrow{\theta I_x} I_x . \qquad (1.106)$$

We shall refer to this rotation, under the influence of the Hamiltonian of Eq. (1.98) as a θ_x pulse (ie. 90°_x etc.) where the subscript x refers to the direction of the applied r.f. field in the rotating frame as defined above.

If the r.f. magnetic field is applied with a 90^o phase shift, the effective Hamiltonian in the rotating frame will be proportional to I_y and rotations will then be about the y-axis leading to

$$I_z \xrightarrow{\theta I_y} I_z \cos\theta + I_x \sin\theta$$
$$I_x \xrightarrow{\theta I_y} I_x \cos\theta - I_z \sin\theta$$
$$I_y \xrightarrow{\theta I_y} I_y . \qquad (1.107)$$

The validity of the above equations depends upon the assumption that the r.f. Hamiltonian dominates during the r.f. pulse so that any effects due to either chemical shift precession or J-coupling can be neglected during that time. In cases where the proton spin of interest is on resonance and the r.f. pulse duration is short (~500 μs, or less), the above equations are quite accurate. We shall comment further on the validity of this assumption in Section 1.9.

In general cases of spin systems with more than one spin, for example a two spin I and S system, the effects of an r.f. pulse may be determined by treating each spin separately since the operators in the dominating r.f. pulse Hamiltonian will commute.

1.7.2 Transformations Under Chemical Shift Precession

If a single spin system is placed in a static magnetic field it will precess under the effects of the Zeeman Hamiltonian. In the rotating frame, this Hamiltonian will depend upon the rotating frame chemical shift ω_I^{rot} which is the difference between the carrier (and rotating frame) frequency $\omega_{r.f.}$ and the laboratory frame resonant frequency ω_I^{lab}, such that $\omega_I^{rot}=\omega_{r.f.}-\omega_I^{lab}$, and

$$\mathcal{H} = \hbar \omega_I^{rot} I_z \,. \tag{1.108}$$

As discussed at the start of Section 1.7, from here on we shall always assume that we are in a rotating frame of reference and shall drop the *rot.* superscript. In a manner analagous to that for the r.f. pulse, we then obtain the following transformations,

$$\begin{aligned} I_x &\xrightarrow{\omega_I I_z t} I_x \cos(\omega_I t) + I_y \sin(\omega_I t) \\ I_y &\xrightarrow{\omega_I I_z t} I_y \cos(\omega_I t) - I_x \sin(\omega_I t) \\ I_z &\xrightarrow{\omega_I I_z t} I_z \,. \end{aligned} \tag{1.109}$$

Evolution under chemical shift precession may be described somewhat more concisely by using the raising and lowering operators. In that case, we have

$$\begin{aligned} I_+ &\xrightarrow{\omega_I I_z t} I_+ \exp(-i\omega_I t) \\ I_- &\xrightarrow{\omega_I I_z t} I_- \exp(i\omega_I t) \\ I_z &\xrightarrow{\omega_I I_z t} I_z \,. \end{aligned} \tag{1.110}$$

On the other hand, the raising and lowering operators are somewhat more unwieldy at describing the effects of an r.f. pulse, and that treatment is relegated to Appendix A. In cases of weakly coupled spin systems, the effects of chemical shift precession on each spin may be treated separately because, for example, the operators **I** and **S** commute.

1.7.3 Transformations Under Two-Spin Weak J-Coupling

The Hamiltonian representing the weak J-coupling interaction between two spins is

$$\mathcal{H} = 2\pi J\hbar\, I_Z S_Z \,. \tag{1.111}$$

Because the chemical shift Hamiltonian and the weak J-coupling Hamiltonian commute, we may consider the effects of J-coupling separately from the chemical shift effects. The evolution of the reduced density operator under the Hamiltonian of Eq. (1.111) is

$$\sigma(t) = \exp(-i2\pi J I_Z S_Z t)\sigma(0)\exp(i2\pi J I_Z S_Z t) \quad . \tag{1.112}$$

The solution to Eq. (1.112) may be obtained by using the same method as used in the r.f. pulse case (46). To illustrate this method for the Hamiltonian of Eq. (1.111), we shall begin with $\sigma(0)=I_X$. Taking the time derivative of Eq. (1.112) we obtain

$$\begin{aligned}\dot{\sigma}(t) &= -i2\pi J\exp(-i2\pi J I_Z S_Z t)\,[I_Z S_Z, I_X]\exp(i2\pi J\, I_Z S_Z t) \\ &= 2\pi J\exp(-i2\pi J I_Z S_Z t)\, I_Y S_Z \exp(i2\pi J\, I_Z S_Z t)\end{aligned} \tag{1.113}$$

The second derivative yields

$$\begin{aligned}\ddot{\sigma}(t) &= -i(2\pi J)^2\exp(-i2\pi J I_Z S_Z t)\,[I_Z S_Z, I_Y S_Z]\exp(i2\pi J\, I_Z S_Z t) \\ &= -(2\pi J)^2\exp(-i2\pi J I_Z S_Z t)\,[I_Z, I_Y]\,(S_Z)^2\exp(i2\pi J\, I_Z S_Z t) \\ &= -(2\pi J)^2\,\sigma(t)\end{aligned} \tag{1.114}$$

Considering the initial conditions of $\sigma(0)=I_X$ and $\dot{\sigma}(0)=2\pi J I_Y S_Z$, the solution of Eq. (1.114) becomes

$$\sigma(t) = I_X\cos(\pi J t) + 2I_Y S_Z\sin(\pi J t) \quad . \tag{1.115}$$

One may then write the transformation equation as

$$I_X \xrightarrow{2\pi J I_Z S_Z t} I_X\cos(\pi J t) + 2\, I_Y S_Z \sin(\pi J t) \quad . \tag{1.116}$$

Similarly, it can be shown that

$$I_y \xrightarrow{2\pi J I_z S_z t} I_y \cos(\pi J t) - 2 I_x S_z \sin(\pi J t)$$
$$I_z \xrightarrow{2\pi J I_z S_z t} I_z . \qquad (1.117)$$

For the case of products of spin operators, the effects of the Hamiltonian on each spin can be handled separately. For example, consider the case of evolution from an initial state described by $\sigma(0) = 2I_xS_z$:

$$\begin{aligned}\sigma(t) &= \exp(-i2\pi J I_z S_z t)\, 2I_xS_z \exp(i2\pi J I_z S_z t) \\ &= 2\exp(-i2\pi J I_z S_z t)\, I_x \exp(i2\pi J I_z S_z t)\, S_z \end{aligned} \qquad (1.118)$$

This result is simply the multiplication of Eq. (1.116) by $2S_z$. The behaviour of two spin product operators under spin-spin coupling is summarized below:

$$2I_xS_z \xrightarrow{2\pi J I_z S_z t} 2I_xS_z \cos(\pi J t) + I_y \sin(\pi J t)$$
$$2I_yS_z \xrightarrow{2\pi J I_z S_z t} 2I_yS_z \cos(\pi J t) - I_x \sin(\pi J t)$$
$$2I_xS_x \xrightarrow{2\pi J I_z S_z t} 2I_xS_x$$
$$2I_xS_y \xrightarrow{2\pi J I_z S_z t} 2I_xS_y$$
$$2I_yS_y \xrightarrow{2\pi J I_z S_z t} 2I_yS_y \qquad (1.119)$$

These transformations may also be described in terms of products involving raising and lowering operators as detailed in Appendix A. For example, noting that $I_+ = I_x + iI_y$, we may derive the following result from Eqs. (1.116) and (1.117),

$$I_+ \xrightarrow{2\pi J I_z S_z t} I_+ \cos(\pi J t) - i2I_+S_z \sin(\pi J t) \quad . \qquad (1.120)$$

1.7.4 Transformations Under Two-Spin Strong J-Coupling

When considering the case of strong coupling, it is no longer possible to consider the effects of chemical shift and J-coupling separately because these two parts of the Hamiltonian do not commute. Nevertheless, as outlined in Ref. 55, it is

still possible to write the Hamiltonian as two commuting parts, $\mathcal{H}_0$ and $\mathcal{H}_1$.

$$\mathcal{H}_0=\bar{\omega}\,(A_Z+B_Z)+2\pi J A_Z B_Z$$
$$\mathcal{H}_1=\delta\omega(A_Z-B_Z)+2\pi J(A_X B_X+A_y B_y) \quad , \tag{1.121}$$

where A and B are the spin angular momentum operators for nuclei A and B respectively, where $\delta\omega=(\omega_A-\omega_B)/2$, $\bar{\omega}=(\omega_A+\omega_B)/2$ with ω_A and ω_B representing the respective chemical shift frequencies of the spins A and B. In deriving the transformation equations for this system, Kay and McClung (55) made use of the spherical angular momentum operators (56, 57), which may be defined in terms of the raising and lowering operators as

$$I_+=(-1/\sqrt{2})\,I_+ \quad \text{and} \quad I_-=(1/\sqrt{2})\,I_- \tag{1.122}$$

where the spherical angular momentum operators have been italicized. Following their convention, we shall make use of the spherical product operator notation with $A_\pm$ and $B_\pm$ representing the respective spherical angular momentum operators.

The transformation equations may again be derived by the procedure outlined by Slichter (46). As an example of this procedure (55), consider the evolution of an initial reduced density operator defined by $\sigma(0)=A_+$ under $\mathcal{H}_1$. The first derivative yields

$$\begin{aligned}\dot{\sigma}(t)&=i\exp(-i\mathcal{H}_1 t)\,[\mathcal{H}_1, A_+]\exp(i\mathcal{H}_1 t)\\ &=i\exp(-i\mathcal{H}_1 t)\{-\delta\omega A_+ + \pi J 2A_Z B_+\}\exp(i\mathcal{H}_1 t)\end{aligned} \tag{1.123}$$

The second derivative leads to

$$\begin{aligned}\ddot{\sigma}(t)&=-\delta\omega\exp(-i\mathcal{H}_1 t)\,[\mathcal{H}_1, A_+]\exp(i\mathcal{H}_1 t)+\pi J\exp(-i\mathcal{H}_1 t)\,[\mathcal{H}_1, 2A_Z B_+]\exp(i\mathcal{H}_1 t)\\ &=-\delta\omega\exp(-i\mathcal{H}_1 t)\{-\delta\omega A_+ + \pi J\,2A_Z B_+\}\exp(i\mathcal{H}_1 t)\\ &\quad+\pi J\exp(-i\mathcal{H}_1 t)\{\pi J A_+ + \delta\omega\,2A_Z B_+\}\exp(i\mathcal{H}_1 t)\\ &=-\{(\delta\omega)^2+(\pi J)^2\}\,\sigma(0)\end{aligned} \tag{1.124}$$

Defining $\Lambda=\{(\delta\omega)^2+(\pi J)^2\}^{1/2}$, and considering the initial conditions $\sigma(0)=A_+$, and

$\dot{\sigma}(0)=-i\delta\omega A_+ + i\pi J 2A_Z B_+$, the general solution may be written as

$$\sigma(t)= A_+\cos(\Lambda t) - (i/\Lambda)(\delta\omega A_+ + \pi J 2A_Z B_+) \sin(\Lambda t) \qquad (1.125)$$

The appropriate transformation equation is thus

$$A_+ \xrightarrow{\mathcal{H}_1 t} A_+\{\cos(\Lambda t) - i(\delta\omega/\Lambda) \sin(\Lambda t)\} + i2A_Z B_+(\pi J/\Lambda) \sin(\Lambda t) \qquad (1.126)$$

The remaining transformation equations from Ref. 55 are detailed in Appendix B. Some of the effects of strong coupling are discussed in greater detail in Chapters 4 and 5.

In Section 1.7, we have derived transformation equations for one and two spin systems. How do we deal with the case of larger spin systems such as the four spin system of lactate or the six spin system of GABA? In the weak coupling approximation, the equations derived for the two spin system may be used since the various parts of the chemical shift and J-coupling Hamiltonians will all commute allowing us to consider each individual coupling or chemical shift separately. *This cannot be done in the case of strong coupling*, because as we have seen in the two spin case, the various parts of the Hamiltonian do not commute. Thus we must derive a new set of transformation equations if we wish to consider larger strongly coupled systems. Kay and McClung have derived the appropriate equations for a three spin ABX system (55). Larger spin systems have yet to be considered, and judging by the complexity of the three spin case, it is questionable whether such derivations would be valuable, because the value of the product operator approach lies in its ability to *concisely* describe evolutions.

1.8 Multiple Quantum Coherences

In general, spectroscopists wish to either maximize or minimize the intensity of MQCs. The minimization of MQCs will lead to a much simpler and more easily predicted spin response to the pulse sequence of interest, while the maximization of MQCs will often further complicate the response. Nevertheless, the presence of

MQCs can introduce an additional method of discrimination between spin systems, and hence, its maximization is often desirable. Following a discussion of the creation and detection of MQC in Section 1.8.1 and 1.8.2 respectively, we shall introduce static magnetic field gradient pulses in Section 1.8.3, which can serve as a discrimination mechanism for the performance of multiple quantum filtering as discussed in Section 1.8.4. For simplicity, the discussion will focus on a two-spin weakly J-coupled system.

1.8.1 Creation of Multiple Quantum Coherences

In the presence of antiphase coherences such as I_xS_z, it can easily be seen that MQC may be created by performing a $90^o{}_x$ pulse on the spin system, resulting in the system being converted into MQC of the form I_xS_y. We begin then, by considering the creation of antiphase coherence.

By considering Eq. (1.118) for J-coupling evolution, we see that the antiphase coherence I_xS_z may be created from I_y following an evolution period of length $\tau=1/2J$. The spin system will also be affected by chemical shift evolution during this τ period. However, the effects of chemical shift evolution may be removed by placing a 180^o pulse at the middle of the evolution period. We now illustrate the creation of antiphase coherence and the refocussing capacity of a 180^o pulse by considering the response of the I spin of a two spin system to the pulse sequence $\{90^o{}_x - \tau/2 - 180^o{}_y - \tau/2\}$, where evolution under both J-coupling and chemical shift occur during the $\tau/2$ periods. Considering only the I spin, the reduced density operator, σ_I, following the first pulse may be represented by

$$\sigma_I(0^+)=I_y. \tag{1.127}$$

Because the chemical shift precession and weak J-coupling Hamiltonians commute, we may deal first with the evolution due to chemical shift precession for a time $\tau/2$ which leads to an intermediate density operator $\sigma_I{}^{int}$

$$\sigma_I{}^{int}(\tau/2)=I_y\cos(\omega_I\tau/2) - I_x\sin(\omega_I\tau/2). \tag{1.128}$$

Consideration of the effects of J-coupling for the same time period then results in

$$\sigma_I(\tau/2)=I_y\cos(\omega_I\tau/2)\cos(\pi J\tau/2) - I_x\sin(\omega\tau/2t)\cos(\pi J\tau/2)$$
$$-2I_xS_z\cos(\omega_I\tau/2)\sin(\pi J\tau/2) +2I_yS_z\sin(\omega_I\tau/2)\sin(\pi J\tau/2). \quad (1.129)$$

The $180^o{}_y$ pulse inverts the x and z spin operators, then further chemical shift evolution during the second $\tau/2$ period yields

$$\sigma_I^{int}(\tau)=I_y\cos^2(\omega_I\tau/2)\cos(\pi J\tau/2) + I_y\sin^2(\omega\tau/2t)\cos(\pi J\tau/2)$$
$$-2I_xS_z\cos^2(\omega_I\tau/2)\sin(\pi J\tau/2) - 2I_xS_z\sin^2(\omega_I\tau/2)\sin(\pi J\tau/2).$$
$$=I_y\cos(\pi J\tau/2) - 2I_xS_z\sin(\pi J\tau/2). \quad (1.130)$$

Finally, J evolution over this same $\tau/2$ period yields

$$\sigma_I(\tau)=I_y\cos^2(\pi J\tau/2) - 4I_xS_z\sin(\pi J\tau/2)\cos(\pi J\tau/2) - I_y\sin^2(\pi J\tau/2)$$
$$=I_y\cos(\pi J\tau) - 2I_xS_z\sin(\pi J\tau) \ . \quad (1.131)$$

Note that the chemical shift effects have been completely refocussed at time τ.

By choosing $\tau=1/2J$, we may create pure antiphase coherence, which may be transformed into MQC by the application of a $90^o{}_x$ pulse. Thus the following pulse sequence will lead to maximal creation of MQC of the form $2I_xS_y$ (and also $2S_xI_y$) $\{90^o{}_x$ - 1/4J - $180^o{}_y$ - 1/4J - $90^o{}_x\}$(58). While this sequence leads to maximal creation of MQC, some MQC may be created following any pulse sequence consisting of two 90^o pulses separated by a delay.

1.8.2 Detection of Multiple Quantum Coherences

Now that the MQC has been created, we wish to detect it. In a pulsed MRS experiment, the detected signal arises from a rotating transverse magnetization that gives rise to a changing magnetic field which in turn induces an electromotive force in the detection coil. In general, this signal is detected in quadrature so the detected signal is related to the measurement of $< I_+>$ or $< S_+>$. Therefore, from Eq. (1.76), the detectable terms in the density operator must produce a nonzero trace when multiplied by I_+ or S_+, which implies that the observable terms in the density

operator are related to the coefficients of the spin operators I_- and S_- in the density operator, because Trace$\{I_+I_-\}$ and Trace$\{S_+S_-\}$ are the only nonzero traces. In particular, neither antiphase nor multiple quantum coherences are directly detectable, because the trace of these terms with I_+ is zero.

It is worth emphasizing that, unlike typical absorption spectroscopic experiments, the detected signal in a pulsed MRS experiment is proportional to the transverse magnetization. For example, a conventional absorption spectroscopy experiment might entail shining a polychromatic light source through a gas, then from analysis of the missing light frequency components, the transition frequencies that led to absorption by the gas could be determined. Such an experiment measures transition frequencies, for instance, if a multiple quantum absorption transition occurred in the gas with sufficient intensity, it could be detected since that frequency component would be reduced in the detected light signal. Unlike this experiment, a pulsed MRS experiment detects only tranverse magnetization which produces magnetic dipole radiation that is detected by the receiving coil.

In a simple MRS experiment, we indirectly detect the equilibrium z-magnetization by converting it into transverse magnetization. In a similar manner, we can detect MQC, indirectly, by converting it into transverse magnetization. In essence, we shall simply reverse the process that led to the creation of MQC from transverse magnetization. For example, continuing from the last section, the density operator σ_I following the sub-sequence $\{90^o_x$ - 1/4J - 180^o_y - 1/4J - $90^o_x\}$ is,

$$\sigma_I(1/2J)=2I_xS_y \tag{1.132}$$

A further 90^o_x pulse, will convert this MQC into the antiphase coherence $-2I_xS_z$. Under the influence of the sub-sequence $\{\ \tau_1/2$ - 180^o_y - $\tau_1/2\ \}$, the density operator becomes

$$\sigma_I(1/2J+\tau_1)=-2I_xS_z\cos(\pi J\tau_1) - I_y\sin(\pi J\tau_1) \tag{1.133}$$

By choosing $\tau_1=1/2J$, we obtain pure transverse magnetization. Recalling that the detectable magnetization is proportional to the coefficients of the I_- term in the density operator, and that $I_y=(1/2i)(I_+-I_-)$, the only term of interest in Eq. (1.133) is

$$\sigma_I(1/J) = (1/2i)\, I_- \quad . \qquad (1.134)$$

Initially we converted transverse magnetization to MQC through application of the subsequence $\{90^o_x - 1/4J - 180^o_y - 1/4J - 90^o_x\}$, then, by applying a further subsequence $\{90^o_x - 1/4J - 180^o_y - 1/4J\}$, the MQC was converted back to transverse magnetization that can be detected. At this point, this circular process seems somewhat redundant, however, by subjecting the MQC to a static magnetic field gradient pulse, it will be shown below that it is possible to filter out other transverse magnetization signals that do not arise from the MQC of interest.

1.8.3 Gradient Dephasing of Coherences

Static magnetic field gradient pulses may be used for coherence selection, where the purpose of the gradient pulses is to dephase unwanted coherences that may lead to detectable transverse magnetization (59-61). During the gradient pulse, the z-component of the magnetic field experienced by nuclei in the sample will depend on their spatial location. The variation in the z-component of magnetic field may be chosen to be along any axis and is typically linear. The gradient pulse may be applied along any axis,. During the application of a static magnetic field gradient $\mathbf{G}$, the transverse magnetization of spins at a location $\mathbf{r}$ will precess in the laboratory frame at frequency

$$\omega = -\gamma\,[B_O + \mathbf{G}\cdot\mathbf{r}] \quad . \qquad (1.135)$$

The effect of the gradient is somewhat similar to the chemical shift, however, the chemical shift is *spin* dependent while the effect of the gradient is *spatially* dependent. If the gradient is applied along the r-axis for a time t_g, then immediately after the pulse, the spins at a location $\mathbf{r}$ have accumulated an additional phase angle θ_g of

$$\theta_g = -\gamma\, G r\, t_g. \qquad (1.136)$$

Thus, the effect of the gradient pulse is to create a spatially dependent phase distribution across the sample (See Fig. 1.6). If the gradient pulse is of sufficient length and strength, the transverse magnetization may be completely dephased. For example, suppose that a sample of protons is 2 cm in length and that a gradient pulse of 1 ms duration is applied along this length. The expression for the maximum phase

angle θ_{max} (in degrees) accumulated by peripheral spins in the sample at the end of the gradient pulse would be

$$\theta_{gmax} = -1532\ G \quad , \tag{1.137}$$

where G is measured in Gauss/cm (=10mT/m). In this thesis, gradient strengths on the order of 5 Gauss/cm are typical, and with such a pulse, gradient-sensitive coherences can be effectively dephased.

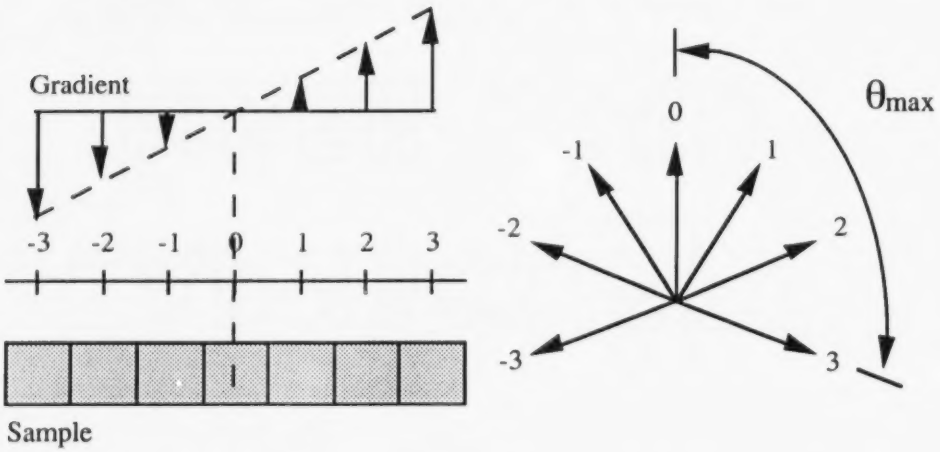

Figure 1.6 The dephasing effect of a gradient pulse on transverse magnetization (coherence order -1). On the left is an illustration of the static magnetic field gradient that varies along the axis of the sample (shaded). On the right, the effect of this gradient on transverse magnetization within each region of the sample is illustrated. the maximum phase angle, θ_{max}, accumulated by peripheral components of transverse magnetization is shown.

The effect of a gradient pulse applied along the r-axis on spins at a location **r** on the spin operator for nucleus I are

$$\begin{aligned} I_+ &\xrightarrow{\theta_g t} I_+ \exp(-i\theta_g t) \\ I_- &\xrightarrow{\theta_g t} I_- \exp(i\theta_g t) \\ I_z &\xrightarrow{\theta_g t} I_z \, , \end{aligned} \tag{1.138}$$

where we have used the definition of θ_g in Eq. (1.136), and made use of the raising and lowering spin operators.

Now, in the case of coupled spin systems, the effects of a gradient pulse on each operator may be treated separately because the **I** and **S** spin operators commute. It is useful to define the coherence order, p, as the difference in the magnetic quantum numbers between the two states linked by the spin operator. For example, for a single spin system, $I_+=|+><-|$ so $p=(1/2)-(-1/2)=+1$, or for two spins, $I_+S_+=|++><--|$ so $p=1-(-1)=+2$, and $I_+S_-=|+-><-+|$ so $p=0-0=0$. The effect of a gradient pulse on a coherence of order p at a location **r** may thus be described by

$$\theta_g=-p\gamma G r\, t_g \quad . \tag{1.139}$$

In practice, the gradient pulse is never perfectly rectangular, so Eq. (1.139) is rewritten as

$$\theta_g=-p\gamma \int G r dt \quad , \tag{1.140}$$

where the integration is performed over the gradient pulse time t_g. From Eq. (1.140), we see that the application of a gradient pulse may allow for discrimination between coherences based on their coherence order. In order to make use of this property, the coherence of interest must be converted back to transverse magnetization and rephased. We deal with this in the next section. However, we wish to first illustrate how the gradient rephasing process can often lead to significant signal losses due to incomplete rephasing of coherences.

Consider a single spin subjected to the subsequence of Fig. 1.7 consisting of a 90^o_x pulse sandwiched between two identical gradient pulses G that are applied along the r-axis. Beginning with a reduced density operator, σ_1, defined by

$$\sigma_1(0)=(1/2)(I_+ + I_-) \quad , \tag{1.141}$$

and applying the gradient pulse, which leads to a dephasing angle ζ, ($\zeta=-\gamma G r t_g$) of the spins at a location **r**, we obtain

$$\sigma_1(0)=(1/2)(I_+ e^{-i\zeta} + I_- e^{i\zeta}) \quad . \tag{1.142}$$

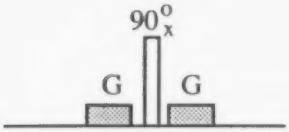

Figure 1.7 A 90° radiofrequency pulse, preceded and followed by a static magnetic field gradient pulse G.

From Appendix A, we note that a 90°_{x} has the following effect on a raising or lowering operator

$$I_{\pm} \xrightarrow{90^{\circ}I_x} (1/2)(I_{+}+I_{-}) \pm iI_z \ . \tag{1.143}$$

Considering only the transverse coherences produced by the 90°_{x} pulse, at time $t=0^{+}$, the density operator becomes

$$\sigma_1(0^{+})=(1/4)\{(I_{+}+I_{-})e^{-i\zeta} + (I_{+}+I_{-})e^{i\zeta}\} \ , \tag{1.144}$$

which upon application of the second gradient pulse results in

$$\sigma_1(0^{++})=(1/4)\{I_{+}e^{-i2\zeta}+I_{-}e^{i2\zeta} + I_{+}+I_{-}\} \ , \tag{1.145}$$

where one half of the signal remains dephased. If the 90° r.f. pulse was replaced by a 180° r.f. pulse, the coherences would simply be inverted and all the signal would be rephased. However, when the dephasing and rephasing gradient pulses are separated by a 90° r.f. pulse, or a cascade of r.f. pulses, complete rephasing of the dephased coherences cannot be assumed.

1.8.4 Multiple Quantum Filtering

We shall now reconsider the pulse sequence discussed in Section 1.8.2, with the added insertion of two gradient pulses as illustrated in Fig 1.8. Just prior to the first gradient pulse, the I spin density operator of the two spin system is in the state described by Eq. (1.132). From symmetry, the reduced density operator σ is

$$\sigma(1/2J)=2I_xS_y+2I_yS_x=-i(I_{+}S_{+} - I_{-}S_{-}) \ . \tag{1.146}$$

where we have used the raising and lowering operator notation which indicates that the terms of Eq. (1.146) are double quantum coherences.

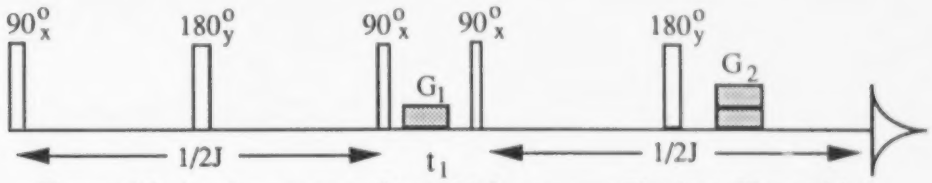

Figure 1.8 A pulse sequence for multiple quantum filtering. The multiple quantum coherences are created by the second 90^{o}_{x} r.f. pulse, and evolve in the t_1 period, before being converted back to single quantum coherences by the final 90^{o}_{x} r.f. pulse. The shaded pulses G_1 and G_2 are static magnetic field gradient pulses. If $G_2 = \pm 2\, G_1$, the sequence selects double quantum coherence, and if $G_2 = 0$ it will select zero quantum coherence. For the example in the text, there is no zero quantum coherence.

The application of the rectangular gradient pulse G_1 dephases a coherence of order p at a location **r** by $-p\theta$, where θ is described by Eq. (1.136). Immediately following G_1, and ignoring chemical shift and J-coupling evolution during the pulse, we obtain

$$\sigma(1/2J+t_1) = -i\,(I_+S_+e^{-i2\theta} - I_-S_-\,e^{i2\theta}) \quad . \tag{1.147}$$

Immediately after the next 90^{o}_{x} r.f. pulse, the DQ coherences in Eq. (1.147) will be converted into the following antiphase coherences,

$$\begin{aligned}\sigma(1/2J+t_1+) = (1/2)\{ & [(I_+ + I_-)S_Z + (S_+ + S_-)I_Z]e^{-i2\theta} \\ & + [(I_+ + I_-)S_Z + (S_+ + S_-)I_Z]e^{i2\theta}\} \quad .\end{aligned} \tag{1.148}$$

Considering only the terms that may evolve into detectable transverse magnetization of the spin I, the application of the gradient pulse G_2 leads to further dephasing by an angle ϕ where $\phi = -\gamma G_2 r t_g$ thus,

$$\sigma(1/2J+t_1+t_g) = (1/2)\{ Le^{i\phi}S_Z\, e^{-i2\theta} + Le^{i\phi}S_Z\, e^{i2\theta}\} . \tag{1.149}$$

Evolution over the final $\{1/2J - 180^{o}_{y} - 1/2J\}$ period leads to the following terms

$$\sigma(1/J+t_1)=(1/4)\, I_- e^{i\phi}(e^{-i2\theta}+ e^{i2\theta}) . \qquad (1.150)$$

With no gradient present, we obtain the same result as in Eq. (1.134). If $\phi = \pm 2\theta$, we obtain one half of the previous result. The loss of one half of the signal is due to the fact that only one of the two DQ coherence terms in Eq. (1.147) is rephased. However, in this case, it is possible to retain all of the signal by making the final 90^o_x r.f. pulse frequency selective such that only the S spins are excited (**20**). For more complicated spin systems, retention of all of the signal is rarely possible, because not all of the coherence pathways can be rephased simultaneously.

In this section, we indirectly detected DQ coherence by choosing $G_2=\pm 2G_1$ in the sequence of Fig. 1.7. This ratio of gradient pulse strengths ensured that the refocussed transverse magnetization was in the DQ state during the t_1 period. For example, single quantum coherences ($p=\pm 1$) in the t_1 period would only be dephased by an angle $\pm\theta$, and gradient-insensitive coherences ($p=0$) such as zero quantum coherence or longitudinal magnetization will receive no dephasing at all during the t_1 period. If any of these $p=0$ or ± 1 coherences are converted into detectable transverse magnetization by the final 90^o_x r.f. pulse, they would not be fully rephased since the final gradient pulse is chosen such that $\phi=\pm 2\theta$.

This destruction of unwanted coherences is not dependent on chemical shift. Thus two completely overlapping resonances may be separated if they exhibit different J-coupling patterns as will be demonstrated in Chapter 3 where multiple quantum filtering is used to edit GABA. For spin systems like GABA, the J evolution is more complicated than the two spin system treated here, and the potential losses due to incomplete coherence rephasing are also greater; these two factors require that the editing pulse sequence be carefully crafted in order to maximize the rephased signal, while still ensuring adequate dephasing of the unwanted coherences.

1.9 Introduction to *In Vivo* Proton Magnetic Resonance Spectroscopy

In this section, we detail the main difficulties that are encountered when performing proton MRS in an *in vivo* environment, which include dominating water and lipid resonances, low metabolite concentrations, limited spectral resolution and the need for localization. Perhaps the simplest problem to solve is that of the dominating water resonance. The water protons resonate in a reasonably empty region of the spectrum, so they may be easily suppressed by a 90° frequency selective r.f. pulse followed by a dephasing gradient pulse. The other problems of low metabolite concentration, spectral overlap (including lipids), and localization are not dealt with so easily, and are discussed separately in the next three sections.

1.9.1 Metabolite Concentrations

The limit of detectability in an *in vivo* proton MRS experiment depends on many biological and instrumental factors, but a rough practical limit of detection is on the order of 1 mM for a volume of ~2 mL. Unfortunately, many of the most interesting metabolites, such as dopamine and serotonin, are present at much lower concentrations. Nevertheless, there are a number of important metabolites that are above the threshold of detectability. For example, in the human brain, where proton MRS shows the most promise, the metabolites listed in Table 1.2 are of sufficient concentration to be potentially visible when performing *in vivo* proton MRS.

The specific metabolites that we are concerned with in this thesis are NAA, lactate and GABA in the brain, and citrate in the prostate gland which has a normal concentration of 50 mM (62). All of these metabolites are of sufficient concentration to be visible. However, normal concentrations of both lactate and GABA are on the verge of detectability, thus for these metabolites, the utmost care should be taken in selecting a pulse sequence that will maximize their intensities.

Table 1.2

Concentrations of MR Visible Metabolites in Human Brain*

Metabolite	Grey Matter Concentration (mM)	White Matter Concentration (mM)
N-acetyl compounds (NA)	12.7±0.4	13.6±0.3
N-acetyl Aspartate (NAA)	11.7±2.2	8.8±1.0
Creatine and Phosphocreatine (Cr/PCr)	11.1±0.4	9.8±0.2
Glutamate (Glu)	12.5±3.0	8.1±1.5
Myo-Inositol (Ins)	9.9±0.7	10.3±0.7
Glutamine (Gln)	5.5±1.9	3.1±1.3
Taurine	4.7±1.1	3.5±2.0
Choline	2.0±0.1	2.4±0.1
Lactate	0.8±0.7	1.0±0.7
N-Acetylaspartyl-Glutamate (NAAG)	0.0±2.2	2.4±2.2
GABA	1.6±0.9	1.3±1.3
Aspartate(Asp)	2.4±0.7	0.6±0.8

* All concentrations were determined by *in vivo* proton MRS results from References 7-9. Notice that many metabolites have a high level of uncertainty, this uncertainty arises from the inaccuracies of complete spectral modelling of overlapping metabolites.

1.9.2 Spectral Overlap

In most *in vivo* proton MRS studies, the majority of resonances of interest appear in the 1.0 to 4.0 ppm range, which at the typical magnetic field strength of 1.5 T, represents a frequency range of only 190 Hz. Within this small spectral window, the many metabolites of interest often exhibit a high degree of spectral overlap. As

an example of the severity of metabolic spectral overlap, a 100 MHz (2.35 T) proton spectrum from a perchloric acid extract of rat brain (63) is shown in Fig 1.9. A stick spectrum illustrating the major components of this rat brain spectrum is also shown in this figure. By comparing these spectra, it is clear that *approximate* intensities of resonances such as NAA, PCr/Cr, choline and myo-inositol could be obtained directly from Fig. 1.9. However, accurate determination of the intensities of resonances such as GABA would not be possible due to spectral overlap.

Under *in vitro* high resolution MR conditions, such spectral overlap would be of minor consequence since any overlapping peaks could easily be separated by a wide battery of two-dimensional MR experiments. However, *in vivo* MR examination times should realistically be kept to durations of less than one hour which, when coupled with the low metabolite concentrations, severely limits the applicability of multidimensional methods. For example, a scanning time on the order of 10 min is usually required for a one-dimensional proton MRS acquisition, while a 16 step two-dimensional experiment would take 3.7 hours. In addition, even if the patient attempts to remain motionless for 3.7 hours, the patient's body is still a dynamic system undergoing respiration, cardiac motion, peristalsis, motion of blood and cerebrospinal fluid, all of which may degrade methods that depend on long-term stability. Thus differentiation between overlapping peaks must generally be accomplished in one dimension.

The human brain is composed mainly of water, protein and fat, all of which are undesirable in the proton spectrum. However, in brain, the short relaxation times of most of the large fat and protein molecules leads to only broad baseline contributions to the spectrum. Nevertheless, some macromolecular proteins may still cause significant spectral overlap at very short echo times (64). Outside of the brain, lipid resonances due mainly to free fatty acids, can cause a high degree of spectral overlap. For example, observation of the lactate resonance in human muscle usually requires some form of spectral editing (20, 65). However, direct observation of lactate is possible within the brain (1,7).

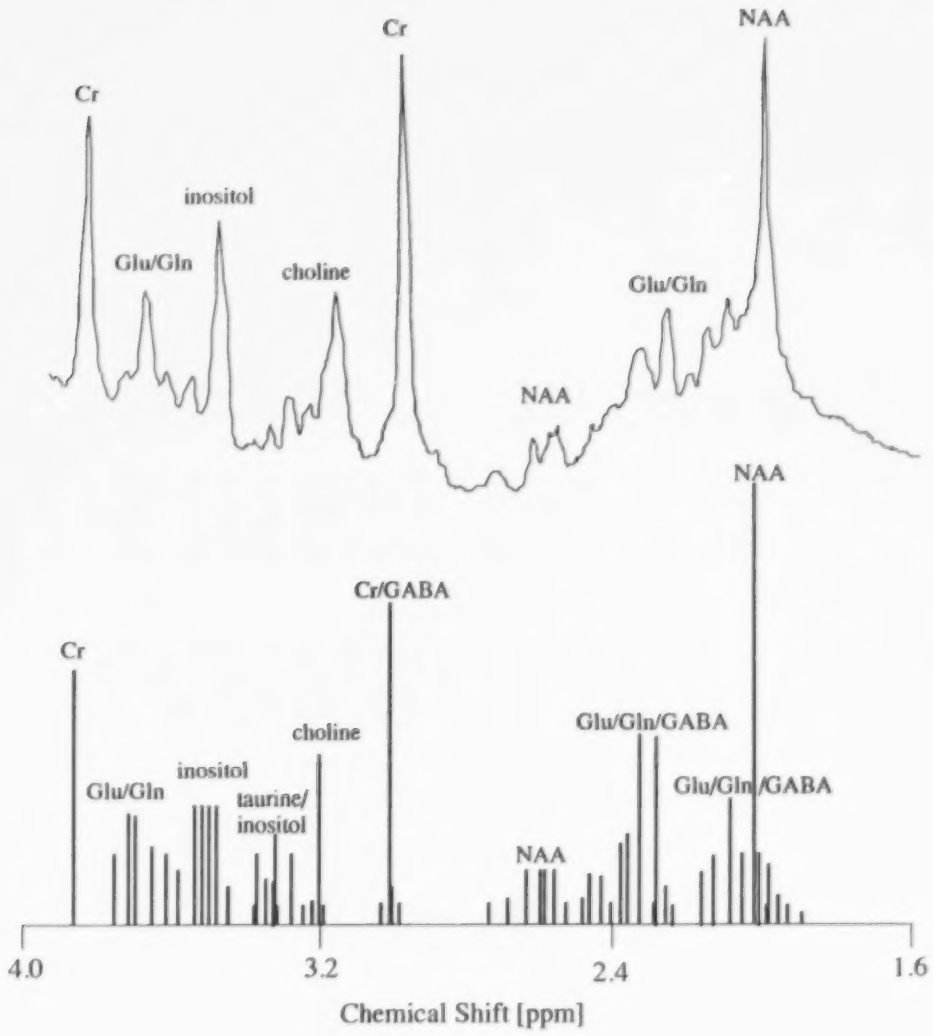

Figure 1.9 Top: 100 MHz proton spectrum from a perchloric acid extract of rat brain. Bottom: A stick spectrum of the main constituents in the rat brain spectrum. The abbreviations are the same as those used in Table 1.2.

In conclusion, most resonances in *in vivo* proton spectra do exhibit some degree of spectral overlap. In many cases this spectral overlap is minimal and direct calculations of peak intensities may be made. Often, however, the peak of interest is completely overlapped and some form of spectral editing, or complete spectral modelling (7) becomes necessary.

1.9.3 Localization

In order to maximize the diagnostic value of a proton spectrum, some form of localization is required. The most commonly used methods of single voxel localization in proton MRS are the Point RESolved Spectroscopy (PRESS) sequence (36-38) and the STimulated Echo Acquisition Mode (STEAM) sequence (35). Both methods rely on static magnetic field (B_O) gradients to achieve localization. Other common localization methods include Image Selected *In vivo* Spectroscopy (ISIS), where B_O gradients and 180^o r.f. pulses select a volume by subtraction of multiple scans (66); and surface coils where an inhomogeneous r.f. field selects the region of interest (67). However, surface coils are only useful near the surface of the patient, and the subtraction of scans in the ISIS sequence make it vulnerable to patient motion and ineffective for localized shimming. In this section, we shall only discuss the more prevalent STEAM and PRESS sequences.

In both the PRESS and the STEAM sequences, the volume is selected by three slice selective r.f. pulses. The slice selectivity is achieved by simultaneous application of a shaped r.f. pulse and a B_O gradient pulse. The gradient pulse creates a spatial Larmor frequency dependence across the sample, and since the shaped r.f. pulse is designed to excite only a specific frequency region, spatial selectivity is achieved along the direction of the gradient. For example, a typical sinc r.f. pulse of 1ms duration will excite a frequency bandwidth of ~7000 Hz (68). The Larmor frequency difference, Δf, between two points separated by r=1 cm along the direction of a gradient pulse G will be $\Delta f = \gamma G r$, which equals 7000 Hz when G=16.6 mT/m. Since modern MR scanners are equipped with gradients strengths on the order of 20 mT/m, and since proton MRS is typically performed on voxels larger than 1 mL, the r.f. pulse lengths can potentially be on the order of 1 ms *provided that the maximum allowable r.f. peak power is not exceeded.* In fact, the constraint on *in vivo* r.f. power absorption is often the limiting factor when attempting to minimize the duration of a frequency selective pulse. For example, typical parameters for the slice-selective 90^o r.f. pulses in the STEAM sequence applied to proton spectroscopy of brain are [1.6 ms, ~10 mT/m, 0.9 cm] (8,69) or [2.6 ms, 4mT/m, 1.6 cm] (6, 70) where we have listed the pulse duration, the gradient strength and the selected slice width respectively.

The r.f. pulse transformation equations introduced in Section 1.7.1, assumed that both the Larmor frequency precession and the J-coupling evolution can be ignored during the r.f. pulse. In the case of a slice selective pulse, the Larmor precession can no longer be ignored because the gradient leads to a wide frequency distribution. Nevertheless, by computer modelling of the effects of simultaneous r.f. excitation and Larmor precession, r.f. pulses have been designed for uncoupled spins that can produce experimental frequency profiles resembling a "top hat" for both 90^o and 180^o r.f. excitation (71-75). (These pulses often vary not only the r.f. amplitude and phase, but also the gradient amplitude and phase.). Thus, by using an optimal slice selective pulse, the spins within the slice receive excitation that can be approximated by the equations of Section 1.7.1.

For J-coupled spins, it would seem reasonable to ignore the effects of proton-proton J-coupling during an r.f. pulse of duration ~3 ms, since one would expect that little J modulation would occur in this short time, for example, if J=7 Hz and t=3 ms, then $\cos(\pi Jt)=0.999$. This hypothesis has been shown to be valid theoretically (76, 77), even when the r.f. pulse is applied to purely antiphase coherence (77). However, optimal slice-selective r.f. pulses must again be used.

One of the goals of this thesis is to obtain concise analytical expressions for the response of various spin systems to the PRESS and the STEAM sequences. The most attractive method for obtaining such expressions is the product operator approach. However, this approach cannot easily describe the case of *simultaneous* time-dependent r.f. excitation, J-coupling modulation, and Larmor frequency precession. Nevertheless, the results of other numerical methods discussed above, have shown that for properly chosen slice-selective r.f. pulses, the net result can be described quite accurately by the simple r.f. transformations of Section 1.7.1. *Thus, for the purposes of this thesis, we shall use approximations of the PRESS and the STEAM sequences that make use of nonselective r.f. pulses rather than spatially selective pulses.* The PRESS and the STEAM sequences, along with the approximation sequences to be used in this thesis, are illustrated in Figs. 1.10 and 1.11.

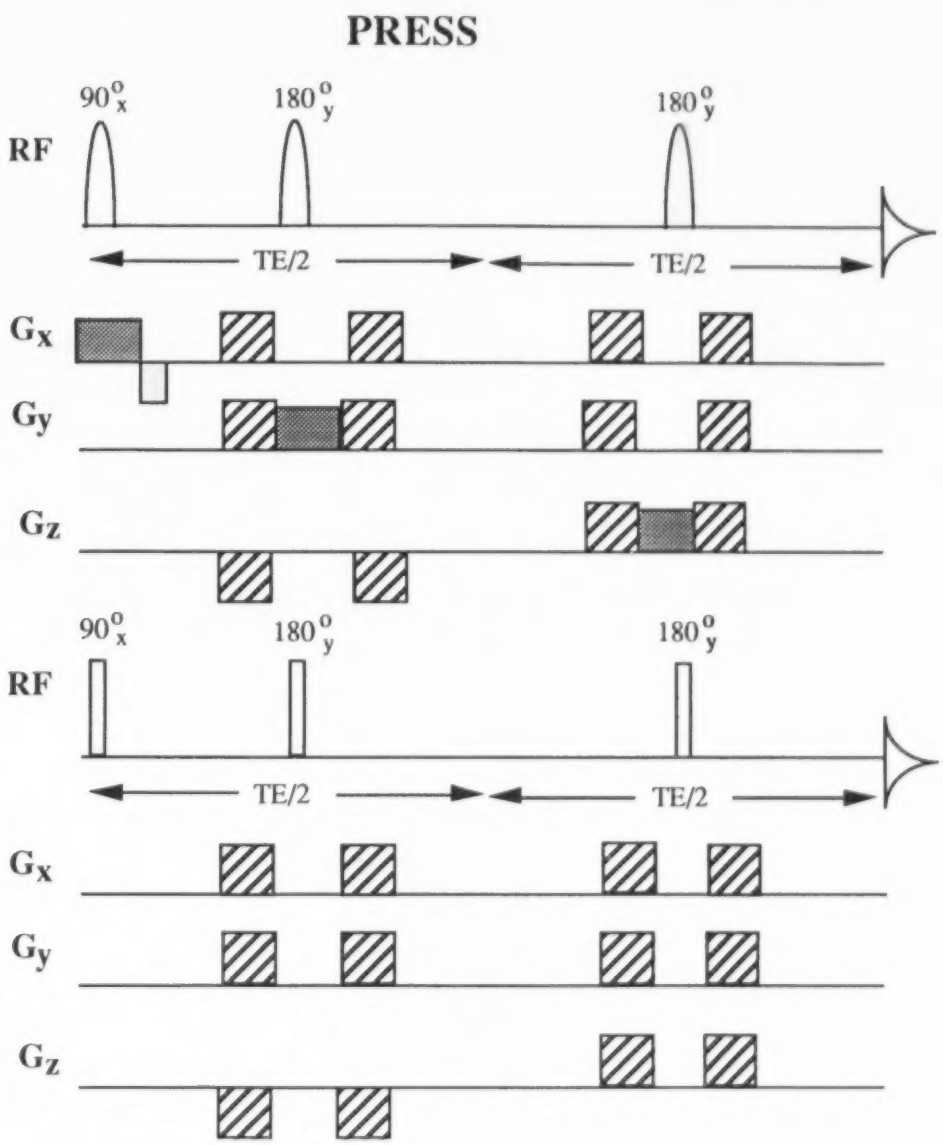

Figure 1.10 An illustration of the PRESS localization sequence which forms a double spin echo. The striped gradients are for coherence selection and ensure the dephasing of spins that are not inverted by the 180° pulses. The darkly shaded gradients are for slice selection. The lightly dotted gradient pulse is a compensation pulse to refocus losses due to gradient dephasing during the first r.f. pulse. The lower sequence is the approximation used in this thesis. It does not use slice selection, but maintains the same coherence pathways as the complete sequence.

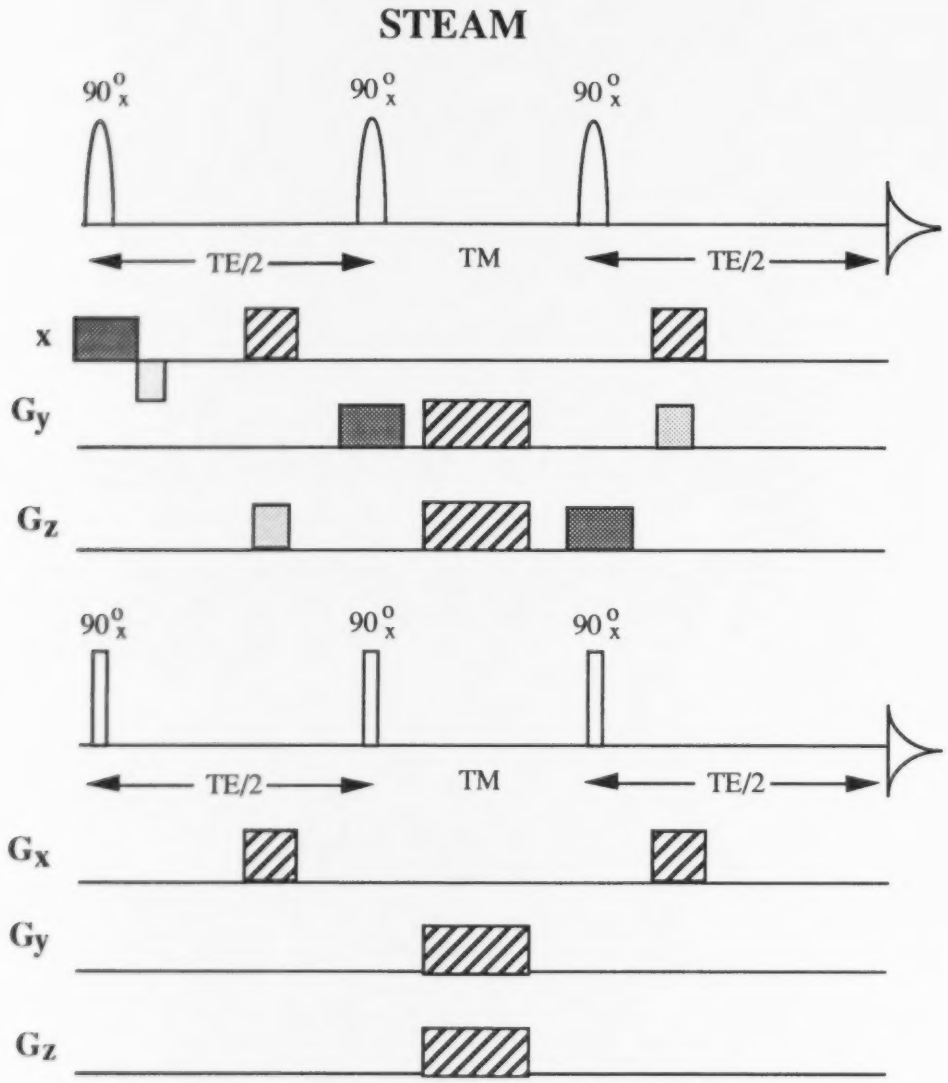

Figure 1.11 The STEAM sequence consisting of three 90° r.f. pulses that create a stimulated echo. Because of gradient dephasing during the pulse sequence, one half of the maximum available signal is lost. The striped gradient pulses perform coherence selection. The dotted gradient pulses are compensation gradients that refocus gradient dephasing during the r.f. pulses. The shaded gradients are slice selective gradients. The lower sequence is the approximation used in this thesis.

1.10 Clinical Relevance of the Targetted Metabolites

The four targetted metabolites are N-Acetylaspartate, GABA, and lactate in the brain, and citrate in the prostate gland. These four metabolites were chosen firstly because of their potential clinical importance, and, secondly, because they are J-coupled spin systems with poorly understood responses to MRS sequences. Each of these four metabolites may potentially have an important impact on the value of clinical MRS examinations.

1.10.1 Lactate

In the absence of oxygen, the breakdown of glucose or glycogen to produce energy, shifts to an anaerobic pathway that leads to the production of lactate. An increase in the level of lactate, therefore, serves as an indicator of increased anaerobic respiration which may be due to an impaired oxygen supply. For example, increases in lactate have been observed in tumours (3,32), and in areas affected by cerebral infarcts (1,78). In stroke, it has been suggested that there is a link between the level of lactate and the functional outcome (79). In addition, the measurement of lactate in tumours may correlate with the effectiveness of tumour therapy (80).

1.10.2 GABA

GABA is the most prevalent inhibitory neurotransmitter in the brain. GABA is known to play a role in depression, anxiety and epilepsy (81-85). The exact nature of its role in these disorders remains unclear. However, it has been postulated that GABA may modulate the activity of norepinephrine, serotonin, and dopamine (83). The application of drugs that inhibit the synaptic reuptake of GABA have lead to numerous effects on human subjects. For example, normal volunteers have exhibited manic and schizophrenic behavior for many days following a small dose of GABA uptake inhibitor (83). Presently, GABA uptake inhibitors are used clinically to combat depression, epilepsy and anxiety (81, 82). By using *in vivo* proton MRS to observe GABA, the effect of various drug therapies on the GABA concentration can be monitored. Moreover, the relationship between GABA concentration and the onset of various neural disorders can be probed.

1.10.3 Citrate

Citrate is secreted by the prostate and binds to zinc in semen. It has been suggested that citrate may serve as an energy source for spermatozoa (86). Citrate has been implicated as a potential indicator of prostatic cancer since its concentration is significantly reduced in adenocarcinoma relative to that in benign hyperplasia and normal prostatic tissue (62, 87-90). Recent studies have shown that these differences can be observed with *in vivo* proton MRS (91, 92). The incidence of prostatic cancer in American males over 80 years old is 53%, and in 1988 alone, ~26 000 American males died from prostatic cancer (93). In order to reduce this high mortality, a screening method is required to detect this disease while it is still localized to the prostate, i.e. before it metastasizes. *In vivo* proton MRS of citrate may fulfill this role.

1.10.4 N-Acetylaspartate

The exact function of NAA in brain remains unclear. However, NAA has been implicated as a marker of intact neurons in the adult brain (94-104). It has thus been suggested that a measurement of NAA directly reflects the degree of neuronal loss. Abnormalities in the level of NAA in brain have been measured by proton MRS in patients with neurogenitive disorders, stroke and tumours (100-105). It has been postulated that the measurement of NAA may be used to find evidence of degenerative neuronal disorders before such evidence can be detected by MRI (105).

1.11 References and Selected Bibliography

1. H. Bruhn, J. Frahm, M.L. Gyngell, K.D. Merboldt, W. Hanicke, and R. Sauter, *Magn. Reson. Med.* **9**, 126 (1989).
2. R. Kreis, T. Ernst, and B.D. Ross, *Magn. Reson. Med.* **30**, 424 (1993).
3. F.D. Jungling, A.K. Wakhloo, and J. Hennig, *Magn. Reson. Med.* **30**, 155 (1993).
4. J.W. Hugg, K.D. Laxer, G.B. Matson, A.A. Maudsley, and M.W. Weiner, *Ann. Neurol.* **34**, 788 (1993).
5. M.S. Knaap, J. Grond, P.R. Luyten, J.A. den Hollander, J.J.P. Nauta, and J. Valk, *Ann. Neurol.* **31**, 202 (1992).
6. T.M. Michaelis, K.D. Merboldt, H. Bruhn, W. Hanicke, M.L. Gyngell, H. Bruhn, and J. Frahm, *NMR in Biomed.* **4**, 90 (1991).
7. S.W. Provencher, *Magn. Reson. Med.* **30**, 672 (1993).
8. R. Kreis, T. Ernst, and B.D. Ross, *J. Magn. Reson.* **B102**, 9 (1993).
9. T.M. Michaelis, K.D. Merboldt, H. Bruhn,W. Hanicke, and J. Frahm, *Radiology* **187**, 219 (1993).
10. M. Von Kleinlin, J.P. Albrand, B. Authier, P. Blondet, S. Lotito, and M. Decorps, *J. Magn. Reson.* **75**, 371 (1987).
11. G.C. McKinnon and P. Boesiger, *Magn. Reson. Med.* **8**, 355 (1988).
12. A. Knuttel and R. Kimmich, *J. Magn. Reson.* **83**, 335 (1989).
13. I.M. Brereton, G.J. Galloway, S.E. Rose, and D.M. Doddrell, *J. Magn. Reson.* **83**, 190 (1989).
14. A. Knuttel and R. Kimmich, *Magn. Reson.Med.* **10**, 404 (1989).
15. A. Knuttel and R. Kimmich, *Magn. Reson.Med.* **10**, 411 (1989).
16. W. Nosel, L.A. Trimble, J.F. Shen, P.S. Allen, *Magn. Reson.Med.* **11**, 398 (1989).
17. R.E. Hurd and D.M. Freeman, *Proc. Natl. Acad. Sci. USA* **86**, 4402 (1989).
18. I.M. Brereton, S.E. Rose, G.J. Galloway, L.N. Moxon, and D.M. Doddrell, *Magn. Reson. Med.* **16**, 460 (1990).
19. S. Crozier, I.M. Brereton, S.E. Rose, J. Field, G.F. Shannon, and D.M. Doddrell, *Magn. Reson. Med.* **16**, 496 (1990).
20. L.A. Trimble, J.F. Shen, A.H. Wilman, and P.S. Allen, *J. Magn. Reson.* **86**, 191 (1990).
21. A. Knuttel and R. Kimmich, *J. Magn. Reson.* **86**, 253 (1990).
22. W. Zhang and C. Ho, *J. Magn. Reson.* **86**, 253 (1990).
23. J.F. Shen and P.S. Allen, *J. Magn. Reson.* **90**, 606 (1990).
24. J.F. Shen and P.S. Allen, *J. Magn. Reson.* **92**, 398 (1991).
25. J.F. Shen and P.S. Allen, *J. Magn. Reson.* **92**, 550 (1991).
26. W.I. Jung and O. Lutz, *J. Magn. Reson.* **94**, 587 (1991).
27. W. Zhang, D.S. Williams, and C. Ho, *J. Magn. Reson.* **95**, 581 (1991).
28. W.I. Jung and O. Lutz, *J. Magn. Reson.* **96**, 237 (1992).
29. A.H. Wilman and P.S. Allen, *J. Magn. Reson.* **B101**, 102 (1993).
30. A.H. Wilman and P.S. Allen, *J. Magn. Reson.* **B101**, 168 (1993).
31. R. Reddy, V.H. Subramanian, B. J. Clark, and J.S. Leigh, *J. Magn. Reson.* **B102**, 20 (1993).
32. A.A. den Graaf, P.R. Luyten, J.A. den Hollander, W. Heindel, and W.M. Bovee, *Magn. Reson. Med.* **30**, 231 (1993).
33. R.V. Mulkern and J.L. Bowers, *Magn. Reson. Med.* **30**, 518 (1993).
34. W. Zhang and C. Ho, *J. Magn. Reson.* **B103**, 120 (1994).

35. J. Frahm, KD. Merboldt, and W. Hanicke, *J. Magn. Reson*, **72**, 502 (1987).
36. R.E. Gordon and R.J.Ordridge, Abstracts of the Society of Magnetic Resonance in Medicine, Third Annual Meeting, New York,, 272, 1984.
37. R.J. Ordridge, M.R. Bendall, R.E. Gordon, and A. Conelly, *in* "Magnetic Resonance in Biology and Medicine,"(G. Govil, C.L. Khetrapal, and A. Saran, Ed.s), pp. 387-397, McGraw-Hill, New Dehli,1985.
38. P.A. Bottomley, *Ann. N.Y. Acad. Sci.*, **508,** 333 (1987).
39. O. Stern, *Z. Phys.*, **7**, 249 (1921).
40. W. Gerlach and O. Stern, *Ann. Phys. Leipzig* **74**, 673 (1224).
41. I. Estermann and O. Stern, *Z. Phys.*, **85**, 17 (1933).
42. J.J. Sakurai, *Modern Quantum Mechanics*, Addison-Wesley, New York 1985.
43. H.A. Bethe, *Intermediate Quantum Mechanics*, 3rd Ed., Benjamin Cummings, Menlo Park, Calif. 1986.
44. F. Reif, "Fundamentals of Statistical and Thermal, Physics," McGraw-Hill, New York 1965.
45. C.E. Hayes, W.A. Edelstein, J.F. Schenk, O.M.Mueller, and M. Eash, *J. Magn. Reson.*, **63**,, 622 1985.
46. C.P. Slichter, "Principles of Magnetic Resonance,"3rd. ed., Springer-Verlag, New York 1989.
47. N.F. Ramsey, *Phys. Rev.* **78,** 699 (1950).
48. E.L. Hahn, *Phys. Rev.* **80,** 580 (1950).
49. E.L. Hahn and D.E. Maxwell, *Phys. Rev.* **84,** 580 (1951).
50. N.F. Ramsey and E.M. Purcell, Interactions Between Nuclear Spins, *Phys. Rev.* **85,** 143 (1952).
51. E.D. Becker, "High Resolution NMR," 2nd ed., Academic Press, New York 1980.
52. J.A. Pople, W.G. Schneider, and H.J. Bernstein, "High Resolution Nuclear Magnetic Resonance," McGraw-Hill, New York,1959.
53. O. W. Sorensen, G.W. Eich, M.H. Levitt, G. Bodenhausen, and R.R. Ernst, *Prog. in NMR Spect.*, **16**, 163 (1983).
54. R.R. Ernst, G. Bodenhausen, and A. Wokaun, "Principles of Nuclear Magnetic Resonance in One and Two Dimensions," Clarendon Press, Oxford 1987.
55. L.E. Kay and R.E.D. McClung, *J. Magn. Reson.* **77**, 258 (1988).
56. M.E. Rose, "Elementary Theory of Angular Momentum," Wiley, New York 1957.
57. T.T. Nakashima and R.E.D. McClung, *J. Magn. Reson.* **70**, 187 (1986).
58. W.P. Aue, E. Bartholdi, and R.R. Ernst, *J. Chem. Phys.* **69**, 567 (1980).
59. R.L. Vold, J.S. Waugh, M.P. Klein, and D.E. Phelps, *J. Chem. Phys.* **48**, 3831 (1968).
60. A.A. Maudsley, A. Wokaun, and R.R. Ernst, *Chem. Phys. Lett.* **55**, 9 (1978).
61. A. Bax, P.G. De Gong, A.F. Mehlkoph, and J. Smidt, *Chem. Phys. Lett.* **69**, 567 (1980).
62. F. Schick, H. Bongers, S. Kurz, W.I. Jung, M. Pfeffer and O. Lutz, *Magn. Reson Med.* **29**, 38 (1993).
63. G.B. Baker, J.T. Wong, J.M. Yeung, and R.T. Coutts, *J. Affective Disorders* **21**, 207 (1991).
64. K.L. Behar and T. Ogino, *Magn. Reson. Med.* **30**, 38 (1993).
65. H. Bruhn, J. Frahm, M.L. Gyngell, KD. Merboldt, W. Hanicke, and R. Sauter, *Magn. Reson. Med.*, **17**, 82 (1991).
66. R.J. Ordidge, A. Conelly, and J.A. Lohman, *J. Magn. Reson.* **66**, 283 (1986).

67. J.J.H. Ackerman, T.H. Grove, G.G. Wong, D.G. Gadian, and G.K. Radda, *Nature (London)* **283**, 167 (1980).
68. M. Garwood, *in* "Advanced Magnetic Resonance Spectroscopy, pp.147-157, Society of Magnetic Resonance in Medicine,Berkeley 1993.
69. T. Ernst, R. Kreis, and B.D. Ross, *J. Magn. Reson.*, **B102**, 1 (1993).
70. J. Frahm, T. Michaelis, K.D. Merboldt, H. Bruhn, M.L. Gyngell, and W. Hanicke, *J. Magn. Reson.* **90**, 464 (1990).
71. M.S. Silver, R.I. Joseph, and D.I. Hoult, *J. Magn. Reson.* **59**,, 347 (1984)
72. S. Conelly, D. Nishimura, and A Macovski, *J. Magn. Reson.* **78**,, 440 (1988).
73. J. Pauly, D. Nishimura, and A. Macovski, *J. Magn. Reson.* **81**,, 347 (1989).
74. S. Conelly, D.G. Nishumura, and A. Macovski, *J. Magn. Reson.* **83**, 549 (1989).
75. J.M. Pauly, B.S. Hu, S.J. Wang, and D.G. Nishimura, *Magn. Reson. Med.* **21**, 12 (1993).
76. J. Slotboom, A.H. Mehlkopf, and W.M. Bovee, *J. Magn. Reson.* **A108**, 38 (1994).
77. R. Thompson, personal communication.
78. J.W. Berkelbach, V.D. Sprenkel, P.R. Luyten, P.C. van Rijen, C.A. Tulleken, and J.A. den Hollander, *Stroke* **19**, 1556 (1988).
79. G.D. Graham, P. Kalvach, A.M. Blamire, L.M. Brass, P.B. Fatad, Z. Rattner, O.A. Petoff, and J.W. Prichard, *Proc. Society of Magn. Reson. in Med. Twelfth Meeting*,, 1483 (1993).
80. Y. Luo, M. Terpstra, H. Merkle, and M. Garwood, *Proc. Society of Magn. Reson. in Med. Twelfth Meeting*,, 19 (1993).
81. F. Fonnum, *in* " Psychopharmacology: The Third Generation of Progress," (H.Y. Meltzer, ED.), pp. 173-182, Raven Press, New York, 1987.
82. K.G. Lloyd and P.L. Moreselli, *in* " Psychopharmacology: The Third Generation of Progress," (H.Y. Meltzer, ED.), pp. 183-195, Raven Press New York, 1987.
83. A.J. Sedman, G.P. Gilmet, A.J. Sayed and E.L. Posvar, *Drug Development Research*, **21**, 235 (1990).
84. R.R. Matsumoto, *Brain Research Reviews* **14**, 203 (1989).
85. N. Davidson, "Neurotransmitter Amino Acids," Academic Press, London 1976.
86. A. Krongrad and M.J. Droller, *in* "Prostatic Disorders," (D.F. Paulson, ED.), pp 107-124, Lea and Febifer, London, 1989.
87. M.E. Yacoe, G. Sommer, and D. Peehl, *Magn. Reson Med.* **19**, 429 (1991).
88. J. Kurhanewicz, R. Dahiya, J.M. Macdonald, L.H. Chang, T.L. James, and P. Narayan, *Magn. Reson Med.* **29**, 149 (1993).
89. M.L. Schliebler, K.K. Miyamoto, M. White, S.J. Maygarden, and J.L. Mohler, *Magn. Reson Med.* **29**, 285 (1993).
90. T.G. Pretlow, B.E. Harris, E.L. Bradley, *Cancer Research* **45**, 442 (1985).
91. J. Kurhanewicz, D.B. Vigneron, S.J. Nelson, H. Hricak, S. Moyher, P. Carrol, T.L. James, and P. Narayan, Abstracts of the Society of Magnetic Resonance in Medicine, 12th Annual Meeting, New York, p. 212, 1993.
92. A. Heerschap, G. de Jager, A. de Koster, J. Barentz, J. de la Rosette, F. Debruyne, and J. Ruijs, Abstracts of the Society of Magnetic Resonance in Medicine, 12th Annual Meeting, New York, p. 213, 1993.
93. R.W. deCere White, *in* "Prostatic Disorders," (D.F. Paulson, ED.), pp 261-272, Lea and Febifer, London, 1989.
94. J.V. Nadler, and J.R. Cooper, *J. Neurochem.* **19**, 313 (1972).
95. K.J. Koller, R. Zaczek, and J.T. Koyle *J. Neurochem.* **43**, 1136 (1984).

96. D.L. Birken, and W.H. Oldendorf, *Neurosci. Biobehav. Rev.* **13**, 23 (1989).
97. S.S. Gill, R.K. Small, D.G.T. Thomas, and P. Patel, *NMR Biomed* **2**, 196 (1989).
98. J.R. Moffett, A.M.A. Namboodiri, C.B. Cangro, and J.H. Neale, *NeuroReport* **2**, 131 (1991).
99. J. Urenjak, S.R. Williams, D.G. Gadian and M. Noble, *J. Neurochem.* **59**, 55 (1992).
100. O.A.C. Petroff, G.D. Graham, A.M. Blamire, M. Al-Rayess, D.L. Rothman, P.B. Fayad, L.M. Brass, R.G. Shulman, and J.W. Prichard, *Neurology* **42**, 1349 (1992).
101. C.C. Ford, R.H. Griffey, N.A. Matwiyoff, and G.A. Rosenberg, *Neurology* **42**, 1408 (1992).
102. J.H. Duijn, G.B. Matson, A.A. Maudsley, J.W. Hugg, and M.W. Weiner, *Radiology* **183**, 711 (1992).
103. C.M. Segebarth, D.F. Balerieux, P.R. Luyten, and J.A. den Hollander *Magn. Reson. Med.* **13**, 62 (1990).
104. J.W. Hugg, K.D. Laxer, G.B. Matson, A.A. Maudsley, and M.W. Weiner, *Ann. Neurol.* **34**, 788 (1993).
105. M.S. van der Knapp, J. van der Ground, P.R. Luyten, J.A. den Hollander, J.J.P. Nauta, and J. Valk, *Ann. Neurol.* **31**, 202 (1992).

Chapter 2

In vivo NMR Detection Strategies for γ-Aminobutyric Acid Utilizing Proton Spectroscopy and Coherence Pathway Filtering with Gradients[1]

2.1 Introduction

The inhibitory neurotransmitter γ-aminobutyric acid (GABA) may play a significant role in several neurological disorders such as depression, spasticity, epilepsy, tardive dyskinesia, schizophrenia and mania (1-3). The ability to monitor *in vivo*, changes in its concentration would be of substantial value in research into the etiology of these disorders and in the clinical monitoring of various drug therapies. However, the non-invasive detection of GABA by means of localized, but unedited, *in vivo* proton spectroscopy is hindered by the overlapping resonances of creatine (Cr), glutamate (Glu), glutamine (Gln), and N-acetylaspartate (NAA) (4-7). These complications stem from the broad lines and the limited chemical shift dispersion usually encountered in in-vivo spectroscopy. The assignment of small overlapping bumps in an *in vivo* spectrum solely on the basis of a chemical shift value is difficult at best, but in a crowded *in vivo* spectrum it is susceptible to significant error at worst. Two-dimensional (2D) techniques are not considered entirely appropriate *in vivo* due to examination time limitations and susceptibility to patient motion. Single shot, one-dimensional spectroscopic editing techniques that eliminate the interfering resonances while still retaining a significant portion of the signal from the metabolite of interest are a promising alternative. The purpose of this paper is to evaluate a series of single shot editing techniques that enable GABA to be differentiated from its overlapping neighboring resonances.

The evaluation made below assumes the weak coupling approximation for the $A_2M_2X_2$ spin system of GABA. Such an approximation is sufficiently close at field strengths around 2T to form the basis of a definitive evaluation of several editing strategies. In the weak coupling approximation, the proton spectrum of GABA consists of two triplets at 3.01 ppm (A_2) and 2.30 ppm (X_2) respectively, and

---

[1] A version of this chapter was published. A.H. Wilman and P.S. Allen, *J. Magn. Reson.* **B101**, 165 (1993).

a quintet at 1.91 ppm (M_2). *In vivo* at 100 MHz, the GABA M_2 quintet at 1.91 ppm is hidden by the wings of the normally stronger NAA peak at 2.02 ppm, as well as the Glu multiplet centred at 2.08 ppm. The GABA X_2 triplet at 2.30 ppm interferes with the Glu multiplet at 2.34 ppm which is the X_2 part of an $AMPX_2$ system. Distinguishing between either set of these multiplets is difficult because the Glu spin system is somewhat similar to that of GABA and its normal concentration is higher than that of GABA. The GABA A_2 triplet at 3.01 ppm lies beneath the creatine singlet at 3.03 ppm. This is probably the best single scan editing alternative at field strengths normally used for *in vivo* studies since editing may be performed by discriminating solely against the uncoupled methyl resonance of Cr.

To our knowledge, the only successful method of GABA editing using proton spectroscopy *in vivo* is the homonuclear, double-resonance, difference spectroscopy experiment performed on rat brain at 8.5 T (4,8). In addition to the problems of stability and dynamic range, which affect all subtraction techniques, GABA difference spectroscopy requires that subtraction take place between an in-phase and an antiphase multiplet. This leads to partial cancellation and an inevitable loss of signal that is at least a factor of two for the triplets. Despite these drawbacks, the difference method has been effective at 8.5 T. However at much lower field strengths, small subtraction errors become more significant due to the complete spectral overlap of the GABA peaks and a much lower signal to noise ratio.

Instead of a subtraction methodology, we have evaluated methods that achieve full editing in a single scan. In the following sections we focus on the A_2 triplet of GABA and show that a triple quantum coherence (TQC) filter, utilizing a spin selective read pulse, produces up to 25% of the full spin echo signal, provides suppression of the overlapping Cr peak by a factor of greater than 1600 and avoids the stability and dynamic range problems encountered with subtraction methods. This editing efficiency should provide a GABA/Cr signal ratio at ~3 ppm of 14 for normal brain concentrations of GABA and Cr (9,10).

2.2 Analysis

The objective of the analysis is to determine the preferred method of spectral editing for observing the 3.0 ppm GABA triplet *in vivo*. For example, which, if any, order of multiple quantum coherence (MQC) would it be most profitable to filter, or alternatively, would it be preferable to create correlated z-order. The multiple quantum filters are evaluated in two groups, namely, the even (zero and double) and the odd (single and triple) ordered filters. The pulse sequences that give rise to these filters are illustrated in Fig. 2.1 and are considered sequentially in the analysis. The evaluation criteria are first, the preservation of the magnitude of the output GABA signal for each editing strategy, and secondly the efficiency with which each pulse sequence will suppress unwanted neighboring signals. Each of these issues is dealt with analytically in this section, before experimental confirmation is provided in the next section.

In the following analysis the product operator notation is used (11,12) where A_{ju}, M_{ju}, X_{ju} are the spin operators for the A, M and X spins respectively, where $j=\alpha, \beta$ denotes a particular spin of each pair and where, u=x,y,z denotes the rotating frame component. The effects of both longitudinal and transverse relaxation have been neglected. Naturally, when these relaxation effects are taken into account, the optimum evolution time will be somewhat shorter than that used here.

Irrespective of the order of the filter, each of the pulse sequences illustrated in Fig. 2.1 begins with a $\{90^{o}_{x} - \tau/2 - 180^{o}_{y} - \tau/2\}$ sub-sequence where $\tau = 1/2J$ and J is the scalar coupling constant ($J_{MX} = J_{AM} = J$). At the end of this sub-sequence the density operator σ, ignoring constant terms, can be written

$$\sigma(\tau-) = 4A_yM_{\alpha z}M_{\beta z} + 4X_yM_{\alpha z}M_{\beta z} - 16M_yA_{\alpha z}A_{\beta z}X_{\alpha z}X_{\beta z} \qquad (2.1)$$

where $(\tau-)$ denotes the instant immediately prior to a pulse at time τ and the operators $S_u = S_{\alpha u} + S_{\beta u}$ with S = A, M or X.

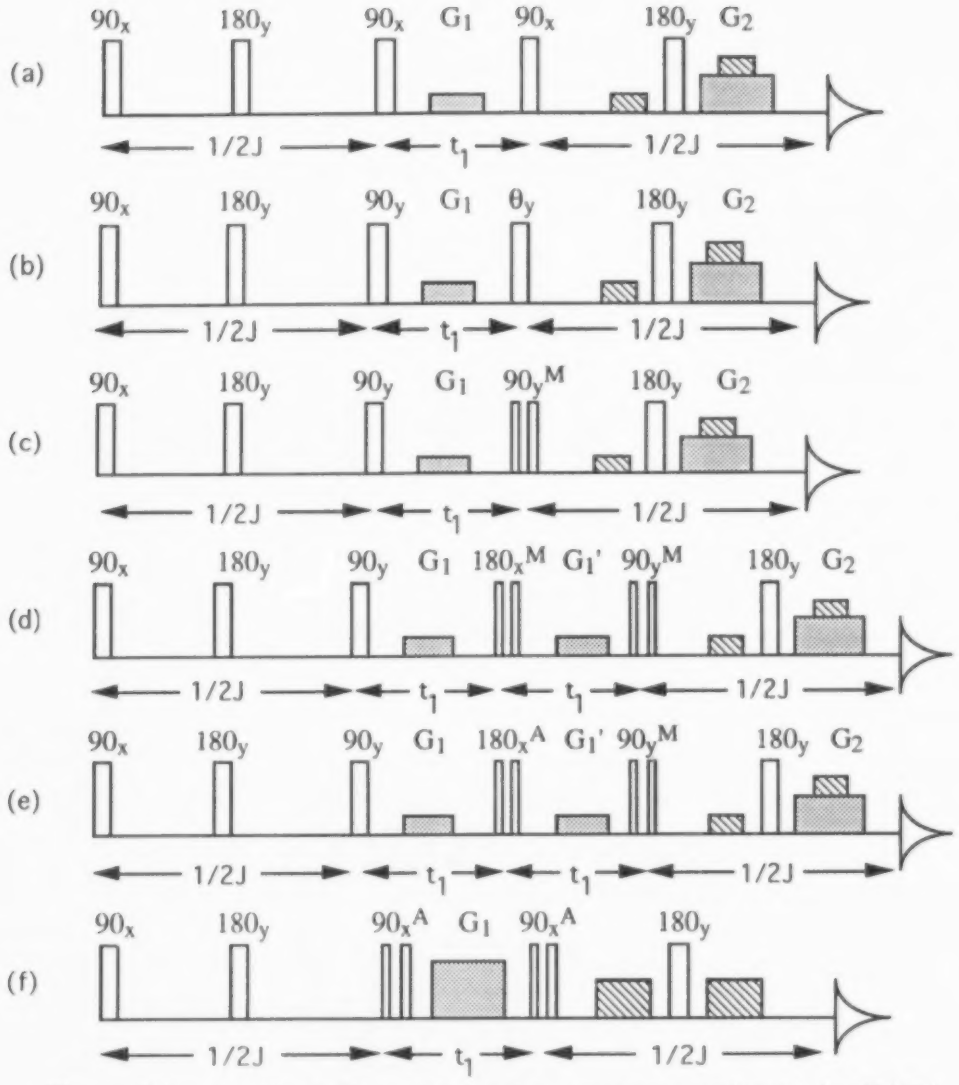

Figure 2.1 An illustration of the pulse sequences evaluated for GABA editing. The coherence filtering gradient pulses are shaded. The hatched pulses are "crusher" gradients used only on the final 180° pulse to eliminate imperfections in that pulse. The sequences are (a) a conventional multiple quantum filter used for either ZQC or DQC filtering of GABA (for DQC filtering $G_2=2G_1$ while for ZQC filtering $G_2=0$); (b) TQC filter with variable read pulse angle, $G_2=3G_1$; (c) TQC filter with spin selective read pulse, $G_2=3G_1$; (d) combination triple and single quantum filter, $G_2=2G_1=2G_1'$; (e) combination triple and single quantum filter, $G_2=4G_1=4G_1'$; and (f) longitudinal z-order filter. All pulses are hard pulses except for the spectrally selective pulses in sequences (c) to (f), illustrated by two closely spaced boxes, which are simple jump-return 1-1 pulses. The timing parameters were $t_1=9$ ms and 1/2J=68.5 ms (J=7.3Hz).

2.2.1 Even Ordered Filters

To transform the antiphase coherence of Eq. (2.1) into even orders of MQC a nonselective 90^{o}_{x} pulse is applied at t= τ, (13) (see Fig. 2.1a) after which the density operator becomes,

$$\sigma(\tau+) = 4A_zM_{\alpha y}M_{\beta y} + 4X_zM_{\alpha y}M_{\beta y} - 16M_zA_{\alpha y}A_{\beta y}X_{\alpha y}X_{\beta y} \quad . \qquad (2.2)$$

Confining our attention to the A_2 triplet, which is described by the first term in Eq. (2.2), we may define a component density operator, σ_A, for this triplet that includes both zero and double quantum coherences (ZQC and DQC respectively). Application of the first filter gradient at this point in time dephases each order of MQC by -pϕ, where p is the order of coherence and $\phi = \gamma \int \mathbf{G}\cdot\mathbf{r}\, dt$, is the phase angle accumulated by spins at a location **r**, under the influence of a gradient **G** (14). For simplicity, further evolution of the spins during the short t_1 gradient period is neglected in this section. The effects of evolution under a weak scalar coupling and chemical shift during this period are accounted for later in the Results section. Following the filter gradient G_1 we may write,

$$\sigma_A(\tau+t_1-) = A_z(M_{\alpha-}M_{\beta+} + M_{\alpha+}M_{\beta-} - M_{\alpha+}M_{\beta+}e^{-i2\phi} - M_{\alpha-}M_{\beta-}ei^{2\phi}) \qquad (2.3)$$

where the raising and lowering operators are denoted by M_{j+} and M_{j-} .

The final 90^{o}_{x} read pulse will transform Eq. (2.3) into successive orders of MQC of which only the single quantum coherence (SQC) antiphase terms will evolve into observable magnetization. Retaining only these antiphase terms gives

$$\sigma_A(\tau+t_1+) = -(1/2i)\,(A_+-A_-)\,M_{\alpha z}M_{\beta z}\,(2 + e^{i2\phi} + e^{-i2\phi}). \qquad (2.4)$$

During the final 1/2J period there will be no further change in coherence level and antiphase magnetization evolves back into in-phase magnetization. For brevity, in the following analysis, we shall take this evolution for granted and draw our final conclusions from the antiphase terms. In the experimental pulse sequences (Fig. 2.1), the final filter gradient follows the final 180^{o}_{y} refocussing pulse, however if we choose to ignore this pulse, then the polarity of the final filter gradient must be

reversed relative to that shown in Fig. 2.1.

It is clear from Eq. (2.4) that by using no final filter gradient only those terms arising from the ZQC of Eq. (2.3) will contribute to the signal to yield one half of the total triplet amplitude available from a simple spin echo sequence. Alternatively, by applying a final filter gradient that is twice the area of the first, one or other of the DQC terms will be refocussed depending on the relative polarities of the two gradients, to yield one quarter of the maximum spin echo triplet signal. The proportion of the spin echo amplitude that is available from each of the pulse sequences of Fig. 2.1 is listed in Table 2.1. Although recruitment of ZQC provides greater signal intensity, its insensitivity to field gradients is also shared by longitudinal magnetization, which degrades its ability to suppress unwanted signals and may necessitate reversion to subtraction techniques (15).

Table 2.1

The Percentage A_2 Triplet Signal Intensity* From GABA And The Creatine Suppression Factors For Various Editing Sequences

Pulse Sequence		Theoretical intensity $t_1 = 0$	Theoretical intensity+ $t_1 = 9$ms	Experimental intensity# $t_1 = 9$ms	Creatine suppression factor
(a)	DQC	25	14	14	250
(a)	ZQC	50	50	50	1
(b)	TQC with $\theta=90^o$	12.5	11	10	1600
(c)	TQC with selective M spin read pulse	25	21	18	1600
(d)	TQC plus SQC with $G_2=2G_1$	100	65	59	2
(e)	TQC plus SQC with $G_2=4G_1$	25	16	12	1000
(f)	correlated z order	100	100	99	2

* The intensities are expressed as a percentage of that obtainable in a spin echo experiment.

\+ The values in this column take account of the evolution under weak scalar coupling during t_1.

\# ±5%

2.2.2 Odd Ordered Filters

To convert the antiphase coherences expressed in Eq. (2.1) into SQC, TQC and quintuple quantum coherence, a nonselective 90^{o}_{y} pulse is applied at time $t = \tau$ (13). The density operator for a weakly coupled $A_2M_2X_2$ system immediately after this pulse can be written

$$\sigma(\tau+) = 4A_yM_{\alpha x}M_{\beta x} + 4X_yM_{\alpha x}M_{\beta x} - 16M_yA_{\alpha x}A_{\beta x}X_{\alpha x}X_{\beta x} \qquad (2.5)$$

Again confining our attention to the A_2 triplet which is described by the first term in Eq. (2.5), we may write the component density operator $\sigma_A(\tau+)$ for this triplet, that includes only SQC and TQC, as

$$\sigma_A(\tau+) = (1/2i)\,(A_+-A_-)(M_{\alpha+}M_{\beta+} + M_{\alpha+}M_{\beta-} + M_{\alpha-}M_{\beta+} + M_{\alpha-}M_{\beta-})\,. \qquad (2.6)$$

If we drop the SQC terms, since they will not be rephased by later filter gradients that are set to discriminate against the SQC of all other molecular species, Eq. (2.6) will evolve during the application of the first filter gradient into,

$$\sigma_A(\tau+t_1-) = (1/2i)\,(A_+M_{\alpha+}M_{\beta+}e^{-i3\phi} - A_-M_{\alpha-}M_{\beta-}e^{i3\phi}) \quad . \qquad (2.7)$$

At this point several alternative strategies are open to us, and the relative merits of each one, first with regard to signal amplitude maximization, and second with regard to the optimization of signal discrimination, both need to be determined. For example, if, as in Fig. 2.1b, a non-selective read pulse θ_y is applied at $t = \tau+t_1$, the density operator is transformed into one which contains the following terms that may evolve into in-phase triplet magnetization,

$$\sigma_A(\tau+t_1+) = (1/4i\,)M_{\alpha z}M_{\beta z}\sin^2\theta\,[\,(A_+e^{-i3\phi} - A_-\,e^{\,i3\phi})(1+\cos\theta) + (A_+e^{\,i3\phi} - A_-e^{-i3\phi})(1-\cos\theta)]\quad . \qquad (2.8)$$

Optimization of the read pulse tip angle dependence (Fig. 2.1b) enables one to obtain an 18.5% increase in signal over the 1/8 of the total triplet signal that would result if θ_y were 90^{o}_{y} (see Fig. 2.2). This optimization occurs when $\theta_y = 70.5^{o}$ or 109.5^{o} depending on which TQC pathway is refocussed by appropriate choice of

filter gradient polarities (16).

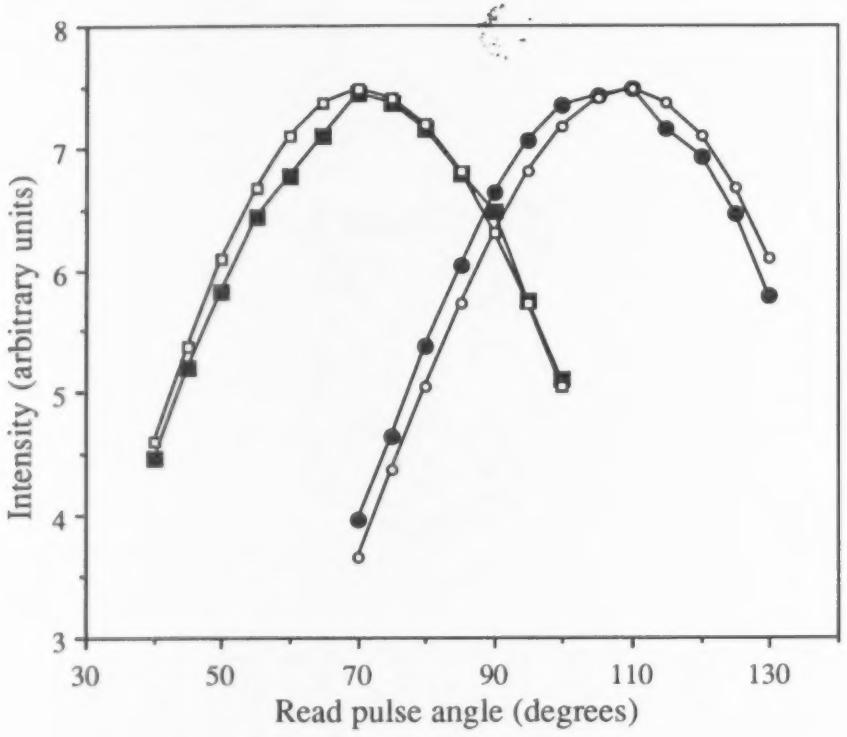

Figure 2.2 The relationship between the intensity of the GABA triplet peak at 3.0 ppm and the tip angle of the read pulse in sequence (b). The theoretical curves representing Eq. (2.8) are denoted by the full line. In the absence of the final 180° pulse, the ■ and ● curves correspond respectively to the experimental data for gradient filters of opposite polarity, $G_1 = -3G_2$, and same polarity, $G_1 = 3G_2$.

Notwithstanding this low triplet intensity, the triple quantum filter should give excellent suppression of resonances from uncoupled spins since it very effectively dephases both SQC and longitudinal magnetization pathways. To recoup more GABA signal and also retain this suppression efficiency, one may also choose to make the read pulse spectrally selective, so that the tip angle dependence of the antiphase coherence following that pulse stems from the manipulation of one chemically shifted species only. This leads to a dependence on a single

trigonometric function of θ, e.g. $\sin^2\theta$ in Eq. (2.8), rather than a compromising combination of sines and cosines that has a maximum value of less than unity. In this way, the sequence in Fig 2.1c yields one quarter of the spin-echo triplet by utilizing a selective 90^o read pulse that acts only on the M_2 spins. The use of a spectrally selective read pulse has previously been applied to the case of DQC filtering of lactate (17,18).

A further exploitation of selective excitation, that also leads to increases in detectable GABA signal, is to use a selective refocussing pulse to interchange coherence levels in the middle of the t_1 interval as illustrated in Figs. 2.1d and 2.1e. This has the effect of combining the SQC and TQC in the A_2 triplet signal in a way that is entirely analogous to that used to combine the zero and double quantum coherences of the lactate doublet (18). Following the composite of a selective refocussing pulse sandwiched between two equal amplitude gradients, the TQC and SQC terms of Eq. (2.6) are respectively converted to SQC and to TQC plus SQC. The accumulated phase of the resulting terms depends not only on which chemically shifted species is refocussed, but also on the relative polarity of the two equal amplitude filter gradients. For example, when the selective refocussing pulse irradiates the M_2 spins as in Fig. 2.1d, and when the gradients G_1 and G_1' are unipolar, the A_2 triplet terms of Eq. (2.6) are transformed, immediately prior to the read pulse, to

$$\begin{aligned}\sigma_A(\tau+2t_1-) = -(i/2)(&A_+M_{\alpha-}M_{\beta-}e^{-i2\phi} - A_-M_{\alpha+}M_{\beta+}e^{\,i2\phi} + A_+M_{\alpha-}M_{\beta+}e^{-i2\phi} \\ &+ A_+M_{\alpha+}M_{\beta-}e^{-i2\phi} + A_+M_{\alpha+}M_{\beta+}e^{\,-i2\phi} - A_-M_{\alpha+}M_{\beta-}e^{\,i2\phi} \\ &- A_-M_{\alpha-}M_{\beta+}e^{\,i2\phi} - A_-M_{\alpha-}M_{\beta-}e^{\,i2\phi})\end{aligned} \qquad (2.9)$$

where both the TQC and SQC terms accumulate a phase differential of 2ϕ. A selective $90^o{}_y$ read pulse at $t=\tau+2t_1$ that also irradiates only the M_2 spins then produces the following observable triplet terms,

$$\begin{aligned}\sigma_A(\tau+2t_1+) = -(i/2)\, M_{\alpha z}M_{\beta z}\,(&A_+e^{-i2\phi} - A_-\,e^{\,i2\phi} + A_+e^{\,-i2\phi} + A_+e^{-i2\phi} \\ &+ A_+e^{-i2\phi} - A_-\,e^{\,i2\phi} - A_-e^{\,i2\phi} - A_-e^{\,i2\phi}) \\ = -2i\, M_{\alpha z}M_{\beta z}\,(&A_+e^{-i2\phi} - A_-\,e^{\,i2\phi})\end{aligned} \qquad (2.10)$$

that can be totally refocussed to give the full spin echo signal by applying a final filter gradient G_2 of twice the intensity of the G_1 gradient and of opposite sign. Although this sequence maximizes the triplet intensity, one might anticipate poor suppression of uncoupled spin resonances. This is because the coherences are combined in such a way as to make the relationship between the three filter gradients for the combined refocussing of TQC and SQC, also appropriate for terms that remain in the single quantum state throughout.

A different outcome of the coherence transfer strategy is obtained by choosing the selective 180^o pulse to act on the A spins as in Fig 2.1e. In this case, one is able to refocus, with $G_2=\pm 4G_1$, only one quarter of the spin-echo triplet signal, however, one would anticipate good suppression of unwanted resonances.

2.2.3 Correlated Z Order

Finally, the technique of editing by means of correlated z-order needs to be considered. In the modified version of ECZOTIC (19) shown in Fig. 2.1f, a spectrally selective $90^o{}_x$ pulse acting on the A_2 spins at $t = \tau = 1/2J$ will create such a z-ordered state, which can be represented for the A_2 triplet by the density operator term,

$$\sigma_A(\tau+) = 4A_zM_{\alpha z}M_{\beta z} \qquad (2.11)$$

The second selective $90^o{}_x$ pulse on the A_2 spins, following complete dephasing of all the transverse terms by G_1 will result in the total transformation of this z-order to antiphase coherence, and hence the recovery of all of the spin echo triplet intensity in the refocussed signal.

Although this maximizes the triplet signal, the sole reliance on field gradient insensitivity for editing purposes leads correlated z-order filtering to have the same difficulty in suppressing unwanted z magnetization as ZQC filters. In the case of the GABA triplet, the overlapping singlet peak has no distant coupling partner and it is not possible to convert the GABA A spins to longitudinal spin order without also converting some of the overlapping peak to gradient-insensitive longitudinal

magnetization. Where the correlated z-order method gives better discrimination, as has been demonstrated (19,20), is in cases where chemically selective pulses allow for discrimination between species.

2.3 Methods and Results

An experimental test of the foregoing analysis was carried out at 100 MHz using 0.5 ml samples of either aqueous solutions of brain metabolites or brain extracts. A 100 mM solution of GABA in D_20 was used to verify the sequence dependence of the triplet amplitude, whereas the discrimination characteristics of the sequences were determined experimentally from a solution bearing approximately the same concentration ratio of creatine to GABA as normal brain. To minimize the eddy current effects of the switched gradients, a homemade 10 cm diameter gradient coil set was employed inside the 40 cm bore magnet. Gradient pulse lengths were set at 2 ms with a 7 ms settling time. The maximum gradient strength (60 mT/m) was used in each case for the strongest gradient in the filter. Frequency selectivity was achieved from the 10 mm diameter, 5 turn solenoidal coil by the most simple means using jump-return (1-1) pulses.

The experimentally measured intensities of the GABA A_2 triplet relative to that for a spin echo acquisition are listed in Table 2.1, along with the theoretical predictions at $t_1 = 0$ and at $t_1 = 9$ ms accounting for the evolution under weak J coupling. We attribute the small overestimate of the theoretical predictions to be due to a neglect of the effects of strong coupling. The bimodal enhancement of the TQC filter output as a function of the read pulse tip angle described by Eq. (2.8) is demonstrated by the data shown in Fig. 2.2.

The ability of each sequence to discriminate the GABA A_2 triplet at 3.01 ppm from the overlapping 3.03 ppm creatine singlet resonance is illustrated in Fig. 2.3 and also quantified in Table 2.1. These tests were carried out without the benefits of phase cycling in order to determine whether or not each editing scheme was truly a single scan editing method. Fig. 2.3A shows the performance of those sequences that demonstrate little or no discrimination, namely, the ZQC filter version of sequence (a), the combination SQC and TQC filter of sequence (d), with $G_1=2G_2$, and the z-order filter of sequence (f). The performance of those sequences that

provide substantial discrimination is shown in Fig. 2.3B. A separate test was carried out on creatine alone to find the exact levels of creatine suppression listed in Table 2.1. Finally, the efficiency of the filtering for GABA was demonstrated (Fig. 2.4) in a perchloric acid extract from rat brain using the TQC filter sequence (c).

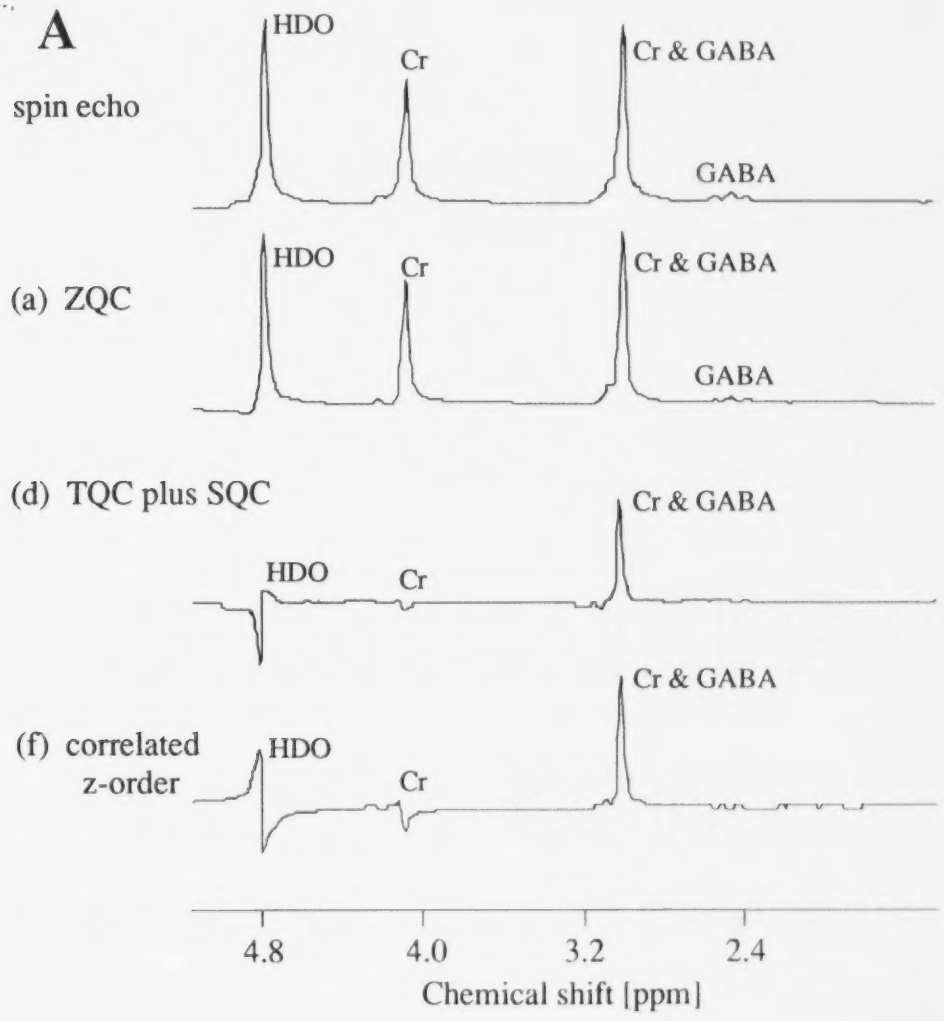

Figure 2.3A The 100 MHz proton spectrum obtained from a sample of 400 mM creatine and 70 mM GABA in D_2O using the editing pulse sequences listed at the left. These spectra correspond to unsuccessful editing of the 3.0 ppm triplet. All spectra were acquired with one scan. The creatine suppression ratios are listed in Table 2.1.

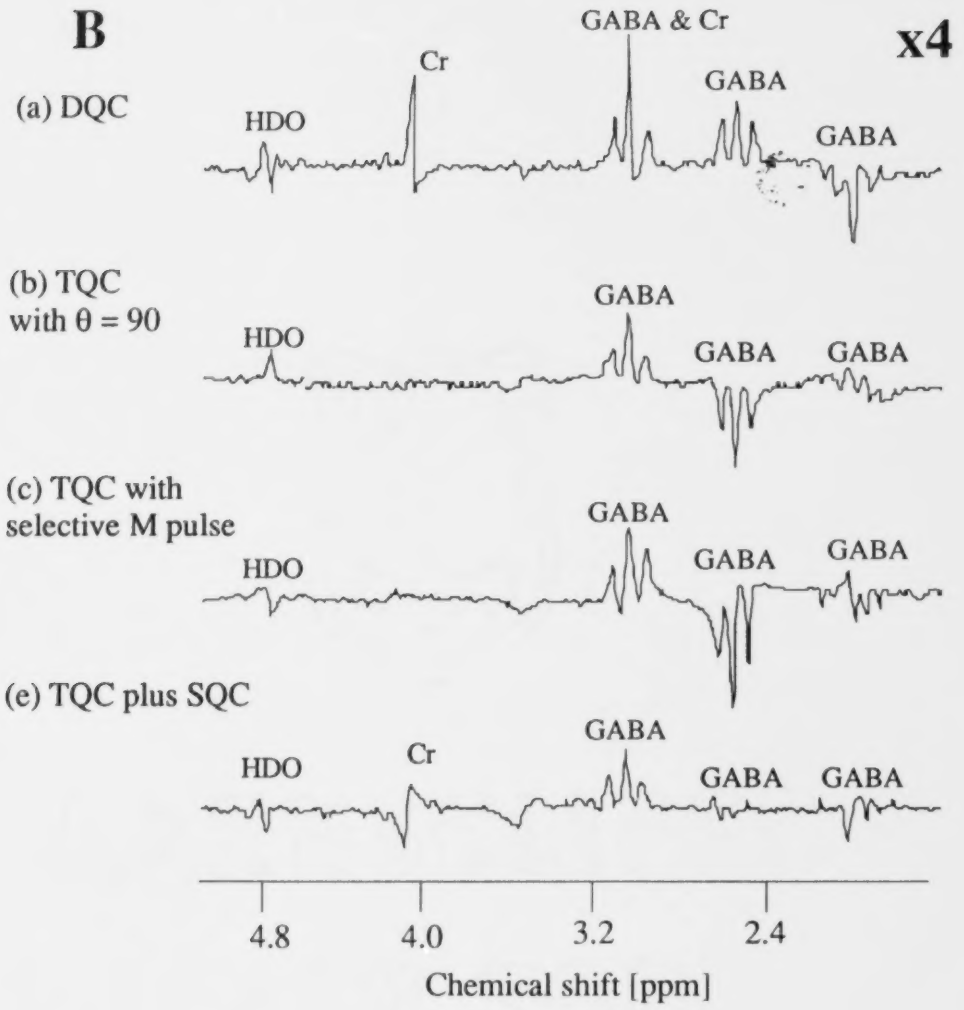

Figure 2.3B The 100 MHz proton spectrum obtained from a sample of 400 mM creatine and 70 mM GABA in D_2O using the editing pulse sequences listed at the left. These spectra correspond to successful editing of the 3.0 ppm triplet. All spectra were acquired with 32 signal averaging scans but no phase cycling. The creatine suppression ratios are listed in Table 2.1.

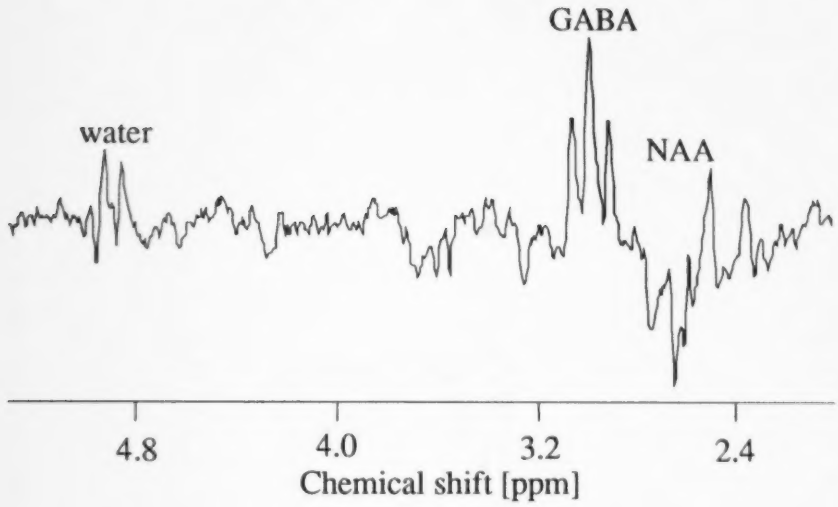

Figure 2.4 A 100 MHz proton spectrum of the perchloric acid extract from rat brain obtained in 512 scans with TQC filter with selective read pulse, sequence (c). The modifications were: a 1331 water presaturation pulse preceding the editing sequence, conversion of the first hard 90^{o}_{x} to a jump-return pulse nulled on water, and the use of full phase cycling. The water suppression is on the order of 20,000. The GABA signal intensity was enhanced approximately three-fold by injecting the rat with phenelzine approximately 3 hours prior to decapitation (23).

2.4 Discussion and Conclusions

Both theoretical analysis and experimental measurement at 100 MHz are in agreement in showing that at the lower field strengths (~1.5T) of clinical NMR units, pure TQC filtering provides the most effective single shot means of editing for GABA. The partial loss of the GABA A_2 triplet signal in comparison to its spin echo value is offset by the ≥1600 fold suppression of the overlapping Cr singlet. Because of this excellent suppression, not only of Cr but of all singlets, one is also able to maximize the receiver gain and avoid dynamic range problems, which enables one to partially compensate for the reduction in GABA signal. Both theory and experiment are also particularly clear in showing that for techniques which rely solely on filtering by gradient insensitivity, such as ZQC or longitudinal spin order filtering, adequate single-scan editing is not achieved, in spite of the larger GABA signal. This is because of the poor discrimination of such methods against the

overlapping Cr methyl singlet. The best compromise between suppression of Cr and the preservation of GABA was found to be the TQC filter with selective read excitation of the 1.9ppm GABA quintet. To bring about localization *in vivo*, the TQC editing sequence can be preceded by ISIS volume selection (21), as described by Thomas et al. for double quantum filters (22).

2.5 References

1. F. Fonnum, *in* "Psychopharmacology: The Third Generation of Progress," (H.Y. Meltzer, ED.), pp. 173-182, Raven Press, New York, 1987.
2. K.G. Lloyd and P.L. Moreselli, *in*" Psychopharmacology: The Third Generation of Progress," (H.Y. Meltzer, ED.), pp. 183-195, Raven Press, New York, 1987.
3. A.J. Sedman, G.P. Gilmet, A.J. Sayed and E.L. Posvar, *Drug Development Research*, **21**, 235 (1990).
4. D.L. Rothman, K.L. Behar, H.P. Hetherington, and R.G. Shulman, *Proc. Natl. Acad. Sci. USA* **81**, 6630 (1984).
5. P.A. Bottomley, W.A. Edelstein, T.H. Foster, and W.A. Adams, *Proc. Natl. Acad. Sci. USA* **82**, 2148 (1985).
6. P.R. Luyten and J.A. den Hollander, *Radiology* , **161**,795 (1986)
7. C.C. Hanstock, D.L. Rothman, J.W. Prichard, T. Jue, and R.G. Shulman, *Proc. Natl. Acad. Sci. USA*, **85**, 1821 (1988).
8. N.E. Preece, S.R. Williams, G. Jackson, J.S. Duncan, J. Houseman and D.G. Gadian, "Proceedings, 10th Meeting of the Society of Magnetic Resonance, San Francisco, 1991," p1000.
9. P.A. Narayana, L.K. Fotedar, E.F. Jackson, T.P. Bohan, I.J. Butler and J.S. Wolinsky, *J. Magn. Reson.* **83**, 44 (1989).
10. T.L. Perry, S. Hansen and S.S. Gandham, *J. Neurochem.* **36**, 406 (1981).
11. O.W. Sorensen, G.W. Eich, M.H. Levitt, G. Bodenhausen, and R.R. Ernst, *Prog. in NMR Spectroscopy* **16**, 163 (1983).
12. K.J. Packer and K.M. Wright, *Mol. Phys.*, **50,** 797 (1983).
13. W.P. Aue, E. Bartholdi, and R.R. Ernst, *J. Chem. Phys.* **64**, 2229 (1976).
14. A. Bax, P.G. De Jong, A.F. Mehlkopf, and J. Smidt, *Chem. Phys. Lett.* **69**, 567 (1980).
15. C.H. Sotak and D.M. Freeman, *J. Magn. Reson.* **77**, 382 (1988).
16. J.S. Shen and P.S. Allen,*J. Magn. Reson.* **90**, 606 (1990).
17. R.E. Hurd and D.M. Freeman, *Proc. Natl. Acad. Sci. USA* , **86**, 4402 (1989).
18. L.T. Trimble, J.S. Shen, A.H. Wilman, and P.S. Allen, *J. Magn. Reson.* **86**, 191 (1990).
19. I.M. Brereton, G.J. Galloway, S.E. Rose, and D.M. Doddrell, *J. Magn. Reson.* **83**, 190 (1989).
20. I.M. Brereton, G.J. Galloway, S.E. Rose, and D.M. Doddrell, *Magn. Reson. Med.* **16**, 460 (1990).
21. R.G. Ordridge, A. Conelly, and A.B. Lohman, *J. Magn. Reson.* **66**, 283 (1986).
22. M.A. Thomas, H.P. Heatherington, D.J. Meyerhoff, and D.B. Tweig, *J. Magn. Reson.* **93**, 485 (1991).
23. G.B. Baker, J.T.F. Wong, and R.T. Coutts, *J Affective Disorders*, **21**, 207 (1991).

Chapter 3

Shortened Double-Quantum Filtering, with Inphase or Two-Spin Antiphase Detection, for γ-Aminobutyric Acid Editing in Proton Spectroscopy of Brain[1]

3.1 Introduction

The inhibitory neurotransmitter γ-aminobutyric acid (GABA) is suspected of playing an important role in such prevalent neural disorders as depression, epilepsy and schizophrenia (1-4). The ability to monitor *in vivo*, changes in the concentration of GABA would not only allow further investigation of the role of GABA in these disorders but would also facilitate studies to test the efficacy of pharmaceutical intervention. However, the detection of the GABA spectrum in brain by *in vivo* proton MRS is hindered by a series of overlapping resonances (5-10). In particular, the 3.0 ppm GABA triplet, which is the most likely editing candidate of the three GABA resonances, lies beneath the methyl creatine (Cr) singlet.

Multiple quantum filters (MQF's) are an excellent candidate for the editing of this 3.0 ppm triplet, since MQF's can very effectively suppress singlet resonances. In a previous evaluation of the editing efficiency of several MQF's, a triple quantum filter (TQF) performed best, increasing the GABA/Cr signal ratio from 0.03 to 14, i.e. by ~450 (11). Nevertheless, like most refocussed MQF's, the duration of the TQF was ~1/J=137 ms, where J is the coupling constant. Since this long length may lead to significant transverse relaxation losses, as well as the inherent filter losses, a shorter MQF would be much preferable. Here, we report significant reductions (1/2 or 1/4 of the usual 1/J) in the duration of a double quantum filtering (DQF) sequence applied to the 3.0 ppm triplet of the $A_2M_2X_2$ system of GABA. Moreover, not only do the sequences reported here dramatically reduce the length of the filter, but they also increase the inherent signal yield of the filter, by more than 50% when compared to either the best performing TQF sequence, or to typical DQF methods with $\tau=1/2J$ (11). Previous work on reducing the duration of a DQF sequence applied to a doublet has also appeared (12).

---

[1] A version of this chapter has been submitted for publication. A.H. Wilman and P.S. Allen, *J. Magn. Reson.* (1994).

At present, the only successful *in vivo* demonstration of GABA editing for proton MRS of human brain is spin-echo difference spectroscopy (13-15). This method requires a pulse sequence duration of 1/2J, yields a maximum of 50% of the available triplet magnetization by subtraction but is quite vulnerable to motion artifacts. In comparing the shortened DQF GABA editing techniques introduced here to difference spectroscopy, the shortened DQF methods were found to be as effective in terms of signal yield and editing capability, but with the added advantage of single-scan editing that eliminates subtraction and its inherent problem of stability. In addition, the DQF method may be performed with a sequence that is one-half the sequence duration in difference spectroscopy and thus suffers considerably smaller relaxation loss. Furthermore, since the filtering is performed by spectrally-insensitive gradient dephasing, rather than by subtraction, manually interactive adjustments to optimize the cancellation of the overlapping Cr singlet are quite unnecessary. However, such adjustments are required with difference spectroscopy because of the fundamental differences between the two sequences that are used to produce the difference spectrum (15).

3.2 Theory

The objective of the analysis was to determine the yield of the shortened DQF sequences illustrated in Fig. 3.1 when applied to the GABA 3.0 ppm triplet. In this analysis the product-operator notation has been used (16,17), where A_{ju}, M_{ju}, X_{ju}, are the spin operators for the A, M and X spins, respectively, of the GABA $A_2M_2X_2$ system, where j=1,2 denotes a particular spin of each pair and where u= x, y, z denotes the Cartesian rotating frame component. The effects of both longitudinal and transverse relaxation have been neglected, as have the J coupling effects during the t_1 period, because it is assumed that the t_1 interval is short (less than 10 ms). Furthermore, the X spins of the $A_2M_2X_2$ system of GABA need not be considered, because they are not directly coupled to the A spins, and thus will not contribute to observable A magnetization under the weak coupling assumption for any of the proposed sequences shown in Fig. 3.1.

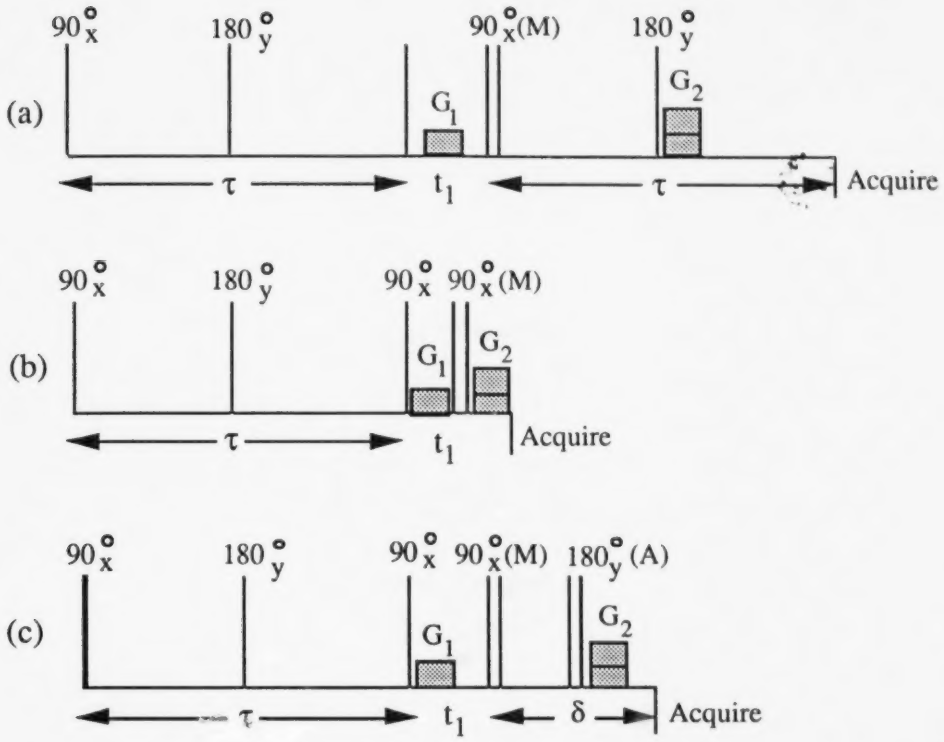

Figure 3.1 An illustration of the DQC pulse sequences that were used for editing the GABA triplet at 3.0 ppm. The sequences are (a) a typical DQC filter; (b) a DQC filter with antiphase multiplet detection; and (c) a DQC filter with antiphase multiplet detection as well as a short period, δ ~16 ms, to accommodate hardware limitations and facilitate a 180° selective pulse on the A spins to refocus both J and chemical shift dispersion. The coherence pathway filtering gradient pulses G_1 and G_2 were of 1 ms duration and were chosen such that $G_2=2G_1$. The t_1 time was 6 ms. All three sequences use a selective 1-1 read pulse that acts on the M spins but not on the A spins.

We will begin the analysis by considering a DQF sequence similar to that shown in Fig. 1a, but with a nonselective $90°_x$ read pulse (18). Once the response to this nonselective pulse sequence has been obtained, the GABA editing sequences illustrated in Fig. 3.1 will be discussed. In all of the sequences to be considered, the density operator, σ, for the A and M spins becomes after the first $90°_x$ pulse

$$\sigma(0^+) = -A_y - M_y . \qquad (3.1)$$

Considering first those terms that begin with the A triplet, before considering the terms that are transferred from the M spins to the A spins, and confining our attention only to the A spins, we have following the $\{\tau/2-180°_y-\tau/2\}$ subsequence and immediately prior to the second $90°_x$ pulse, the density operator

$$\sigma_A(\tau^-) = -A_y \cos^2(\pi J\tau) + 2A_x (M_{1z} + M_{2z})\cos(\pi J\tau) \sin(\pi J\tau) + 4A_y M_{1z} M_{2z} \sin^2(\pi J\tau) \quad . \tag{3.2}$$

Immediately following the second $90°_x$ pulse, these terms are converted to

$$\sigma_A(\tau^+) = -A_z \cos^2(\pi J\tau) - 2A_x (M_{1y} + M_{2y})\cos(\pi J\tau) \sin(\pi J\tau) + 4A_z M_{1y} M_{2y} \sin^2(\pi J\tau) \tag{3.3}$$

Only terms that include double quantum coherence (DQC) need to be considered, since the other terms will not survive the editing process that is accomplished by means of the gradients . Application of the first filter gradient will dephase each order of coherence by $-p\phi$, where p is the order of the coherence and $\phi = \gamma \int \mathbf{G} \bullet \mathbf{r}\, dt$, is the phase angle accumulated by spins at a location $\mathbf{r}$, under the influence of a gradient $\mathbf{G}$ (19). Keeping only the double quantum terms, and including the effects of the gradient G_1, the density operator immediately prior to the read pulse becomes

$$\sigma_A(\tau+t_1^-) = -(1/2i)\,[A_+M_+e^{-i(2\phi+\delta\omega t_1)} + A_-M_-e^{i(2\phi+\delta\omega t_1)}] \cos(\pi J\tau) \sin(\pi J\tau) - A_z\,[M_{1+}M_{2+}e^{-i2\phi} + M_{1-}M_{2-}e^{i2\phi}] \sin^2(\pi J\tau) \tag{3.4}$$

where the chemical shift offset is $\delta\omega = \omega_A - \omega_M$, and where we have assumed that the M spins are on resonance. Furthermore we have neglected evolution under J during this t_1 interval, since it is assumed to be small.

If the $90°_x$ read pulse were non-selective, it would convert the above DQC terms to the following antiphase magnetization terms

$$\sigma_A(\tau+t_1^+) = -(1/2)\,[A_xM_z\,e^{-i(2\phi+\delta\omega t_1)} + A_xM_z\,e^{i(2\phi+\delta\omega t_1)}] \cos(\pi J\tau) \sin(\pi J\tau) - A_y\,[M_{1z}M_{2z}e^{-i2\phi} + M_{1z}M_{2z}e^{i2\phi}] \sin^2(\pi J\tau)\,. \tag{3.5}$$

The application of a final gradient of twice the strength of the initial one, would cause one half of each term to be rephased (20). Following the final τ period, which includes this final gradient pulse, and considering only the real part (when $\sin(\delta\omega t_1)\neq 0$ there is also an imaginary part), Eq. (3.5) would evolve into

$$\sigma_A(2\tau+t_1) = -(1/2)\, A_y \cos(\delta\omega t_1)\cos^2(\pi J\tau)\sin^2(\pi J\tau) + (1/4)\, A_y \sin^4(\pi J\tau)\,. \qquad (3.6)$$

Turning to the terms that begin as M magnetization at the start of the pulse sequence, the M spins are influenced during the first $\{\tau/2-180°_y-\tau/2\}$ subsequence by eight J coupling interactions ($A_{1z}M_{2z}$, $X_{1z}M_{1z}$, etc.). Restricting consideration to terms that evolve under the A with M couplings, one arrives at the intermediate density operator σ_M^{int}.

$$\sigma_M^{int}(\tau^-) = -M_y\cos^2(\pi J\tau) + 2M_xA_z\cos(\pi J\tau)\sin(\pi J\tau) + 4M_yA_{1z}A_{2z}\sin^2(\pi J\tau) \qquad (3.7)$$

The influence of the M with X couplings will add an additional $\cos^2(\pi J\tau)$ modulation to each of the terms in Eq. (3.8), as well as creating additional terms that cannot be converted into A magnetization in the final evolution period. By the end of the first τ period the only term that may ultimately lead to observable A magnetization during acquisition is

$$\sigma_M(\tau^-) = 2M_xA_z\cos^3(\pi J\tau)\sin(\pi J\tau)\,. \qquad (3.8)$$

Following the second $90°_x$ pulse, Eq. (3.8) transforms into the DQC terms,

$$\sigma_M(\tau^+) = -(1/2i)\,[M_+A_+ - M_-A_-]\cos^3(\pi J\tau)\sin(\pi J\tau)\,. \qquad (3.9)$$

Application of the first gradient together with chemical shift evolution during t_1 and followed by the nonselective $90°_x$ read pulse leads, in a similar manner to the A spin case, to the following antiphase A terms,

$$\sigma_M(\tau+t_1^+) = -(1/2)\,[A_xM_z\,e^{-i(2\phi+\delta\omega t_1)} + A_xM_z\,e^{i(2\phi+\delta\omega t_1)}]\cos^3(\pi J\tau)\sin(\pi J\tau)\,. \qquad (3.10)$$

Application of the final gradient G_2, and evolution during the final τ period leads to

$$\sigma_M(2\tau+ t_1) = - (1/2)\, A_y \cos(\delta\omega t_1)\cos^4(\pi J\tau)\, \sin^2(\pi J\tau) \quad , \qquad (3.11)$$

where we have again dropped the imaginary part of the expression. The net in-phase magnetization, S, at the time of acquisition, including both the terms of Eq. (3.6) and the transfer terms of Eq. (3.11), is then

$$S(2\tau+t_1) = - (1/2) \cos(\delta\omega t_1)\cos^2(\pi J\tau)\, \sin^2(\pi J\tau)\ [1 + \cos^2(\pi J\tau)\ ] + (1/4)\, \sin^4(\pi J\tau) \quad , \qquad (3.12)$$

where a value of S=1 corresponds to a complete recovery of all of the triplet magnetization. The maximum value of S from Eq. (3.12) is 0.25 and it occurs when $\tau \sim 1/(4J)$ and $\cos(\delta\omega t_1)=-1$. This equals the yield of the typical DQF of length 1/J, however it is obtained with one half of the sequence duration (11) thus with substantially less transverse relaxation loss.

The yield of a DQF sequence may also be increased, as has been demonstrated previously for the lactate doublet (20,21), by changing the read pulse to a selective pulse. Making the read pulse selective in the DQF sequence of Fig. 3.1a, i.e. acting only on the M spins, the second term in Eq. (3.4) will not be recovered because the read pulse does not act on the A spins. However, the other term in Eq. (3.4) as well as the terms of Eq.(3.9), will be increased by a factor of 2 in a manner similar to that described elsewhere for lactate DQF (20) or for GABA TQF (11). The net real inphase magnetization with the selective read pulse sequence of Fig 3.1a is then

$$S(2\tau+t_1) = -\cos(\delta\omega t_1)\cos^2(\pi J\tau)\, \sin^2(\pi J\tau)\ [1 + \cos^2(\pi J\tau)] \qquad (3.13)$$

Since the t_1 chemical shift factor is now global, the spectrum may still be phased to yield the maximum even if $\cos(\delta\omega t_1)\neq\pm 1$. In the case of GABA, this maximum occurs at τ=32 ms and yields 38.5% of the 3.0 ppm triplet signal, where approximately one third of this yield is due to magnetization transferred to the triplet from the 1.9 ppm GABA M_2 quintet. It is thus important that the first two 90° pulses excite both the 3.0 ppm and the 1.9 ppm GABA multiplets, so that this transfer of

magnetization can take place. Lastly, it is interesting to note, see Ref. 11, that when a selective read pulse is applied to the typical DQF of length 1/J, there is not an increase, but a loss in the GABA 3.0 ppm triplet signal because in the typical filter, the DQ coherences are formed from a combination of operator terms similar to $A_zM_{1x}M_{2x}$, and in this case both the M and A spins must receive excitation from the read pulse in order to produce antiphase A magnetization.

3.2 .1 Detection Of Antiphase Multiplets

In general, the detection of antiphase (or oppositely going) multiplets has been eschewed by the *in vivo* community, because of concern over the destructive interference between adjacent but opposing peaks. This concern is undoubtedly justified in the case of doublets like the methyl signal from lactate, or in the case of triplets arising from the three-spin antiphase operator terms of GABA (see Fig. 3.2a), where, in both cases, the opposing peaks are only separated by J which is ~7 Hz. However, as is shown below for GABA, opposing multiplet peaks may be generated from two-spin antiphase coherence that are separated not by J, but by 2J, thus leading to minimal destructive interference.

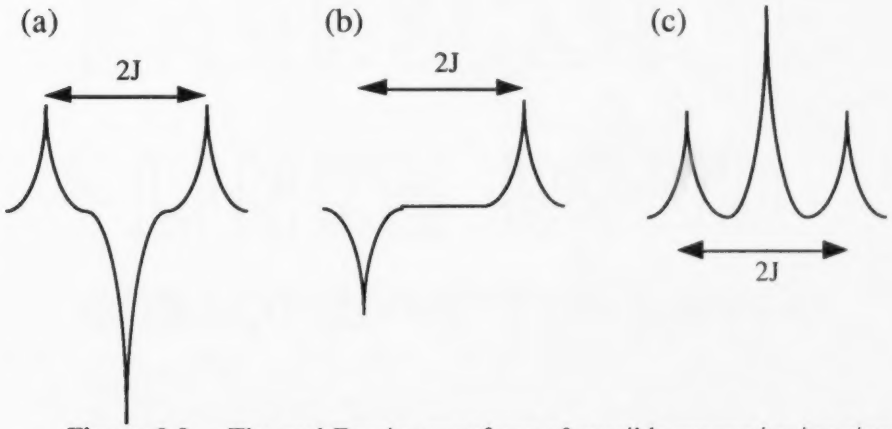

Figure 3.2 The real Fourier transform of possible magnetization signals arising from the A_2 triplet of GABA. At the start of acquisition, the density operator terms were assumed to be the following: (a) three spin antiphase coherence (e.g., $A_yM_{1z}M_{2z}$); (b) two spin antiphase coherence (e.g., A_xM_{1z}); and (c) in-phase magnetization (e.g., A_y). During the acquisition period, these terms evolve to produce the observable signals as illustrated. In all cases the separation between the two outer peaks is 2J or 14.6 Hz for GABA.

For example, if the final τ interval prior to acquisition is eliminated (see Fig. 3.1b), and acquisition begins immediately following the second gradient, the real terms at the start of acquisition that may evolve into observable triplet magnetization are from two spin antiphase terms, i.e.,

$$\sigma(\tau+t_1^+) = - A_x M_z \cos(\delta\omega t_1)\cos(\pi J\tau)\sin(\pi J\tau)[1 + \cos^2(\pi J\tau)]. \quad (3.14)$$

During the acquisition time t_{aq} evolution of Eq. (3.14) will give rise to the following signal that will appear as two opposing peaks upon Fourier transformation, (at $t_{aq}=0$, S=0)

$$S(\tau+ t_1+ t_{aq}) = -(1/2)\cos(\delta\omega t_1)\cos(\pi J\tau)\sin(\pi J\tau)[1+\cos^2(\pi J\tau)] \sin(2\pi J t_{aq})\cos(\omega_A t_{aq}). \quad (3.15)$$

This signal arising from two-spin antiphase terms produces opposing GABA peaks that are separated not by J, but by 2J or 14.6 Hz (see Fig. 3.2b) thus leading to minimal destructive interference between the two peaks when the linewidths are less than 10 Hz full-width-half-maximum (FWHM). For example, if the shim on the brain volume of interest is 5 Hz FWHM, the destructive interference of the opposing peaks separated by 2J, leads only to a 3% reduction in the maximum intensity of each opposing peak, while a shim of 10 Hz would lead only to a 10% reduction.

Because of the antiphase nature of the doublet, the component peak height, H, given by Eq. (3.16), becomes a more appropriate measure of the multiplet intensity than its total area,

$$H(\tau+ t_1) = (1/2)\cos(\delta\omega t_1)\cos(\pi J\tau)\sin(\pi J\tau)[1 + \cos^2(\pi J\tau)] \quad (3.16)$$

where H is normalized such that a value of unity corresponds to the maximum possible height of the central peak of an in-phase GABA triplet (see Fig. 3.2c). The maximum value of Eq. (3.16), namely 0.394 occurs at a τ value of 28 ms, much shorter than 1/2J. In Fig. 3.3, the τ dependence of the in-phase triplet intensity, Eq. (3.13), for the DQF sequence of Fig 3.1a is compared with that of the antiphase doublet intensity, Eq. (3.16), for the truncated DQF sequence of Fig. 3.1b.

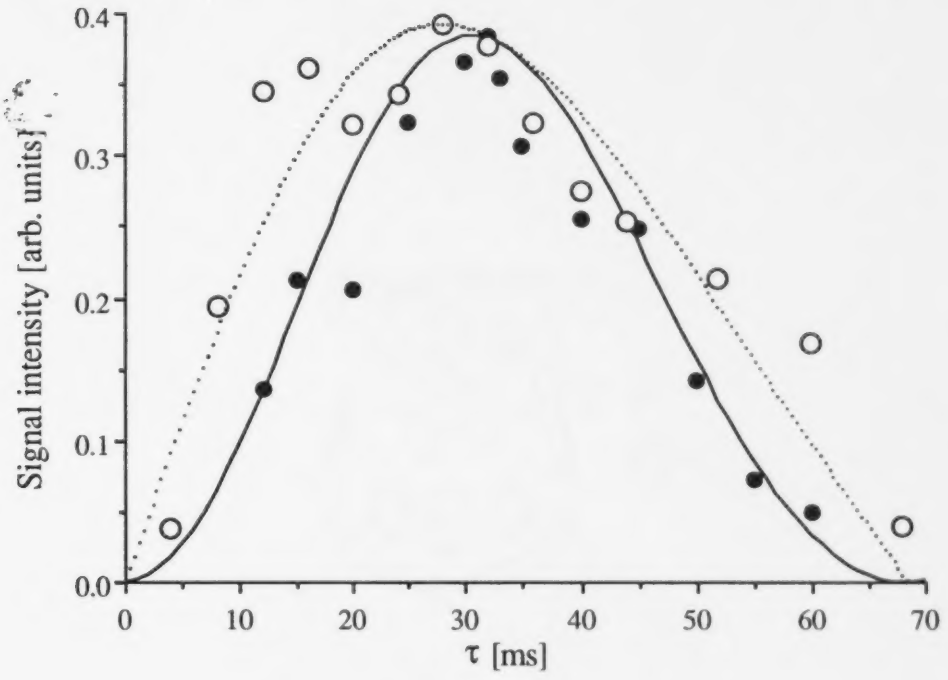

Figure 3.3 The relationship between the intensity of the GABA signal at 3.0 ppm and the evolution time τ of the corresponding DQC filter. The circles represent the experimental data and the curves are plots of the theoretical equations. The DQC filter of Fig. 3.1a is represented by solid dots and a solid curve, while the DQC filter of Fig. 3.1c is represented by open circles and a dashed curve. For the antiphase multiplet case, the maximum height of one peak in the antiphase pair was used as the intensity measure. For the inphase case, the area under the complete GABA multiplet was the intensity measure. In both cases a value of unity corresponds to the maximum available GABA multiplet signal, height (antiphase case) or area (in phase case), i.e. that available following a 90^{o} acquire experiment.

The sequence of Fig. 3.1b is demanding of the system hardware. For example, available gradient strength may require the G_2 pulse to be longer than a few milliseconds, or either eddy currents or gradient driver settling time may require a significant delay following G_2. Under such circumstances the sequence of Fig. 3.1c will retain some of the benefits of that in Fig. 3.1b. Incorporation of an additional period δ ($\delta<\tau$) during which a frequency selective inversion pulse is applied, (acting

on the 3.0 ppm A spins but nulling the 1.9 ppm M spins) will accommodate hardware deficiencies, and refocus the J coupling and the chemical shift dispersion of the A spins. The resulting 3.0 ppm signal for this sequence will be the same as that of Fig. 3.1b except for additional transverse relaxation losses during the δ period. Thus, excluding relaxation losses, the theoretical response to the sequence of Fig. 3.1c is the same as that of the sequence of Fig. 3.1b and may be described by Eq. (3.16).

3.3 Methods

In order to verify the τ dependence of the DQF sequences, an experimental test was carried out at 100 MHz using a solution of GABA in D_2O. Once the optimal values for the DQF sequences had been determined, a comparison with difference spectroscopy was also performed. In the first stage of this comparison, in order to determine the 3.0 ppm GABA signal yield, each sequence was applied to a solution of GABA in D_2O. In the second stage, where the purpose was to determine the GABA editing efficiency with true brain metabolite concentrations, each method was used to edit GABA from a rat brain extract.

The difference spectrum was obtained by subtracting the signals from two successive spin echo scans. Alternate scans used an additional M selective 180° pulse. (See Refs. 12-14.) Selectivity was accomplished by means of a four component DANTE (Delays Altering with Nutations for Tailored Excitation) pulse (22). Only the raw editing sequences were tested, and no additional water suppression pulses were added to improve the appearance of either sequence.

The perchloric acid extract (23) of rat brain was obtained from rats injected three hours prior to death (23) with the antidepressant phenelzine (30 mg/kg), a drug that is known to increase the GABA level (23). In order to minimize dynamic range effects when performing difference spectroscopy and thereby allow a direct comparison with the DQF sequences, the water content of the brain extract was reduced to 10% by evaporation and then reconstituted by D_2O replacement.

All solutions were ~0.5 mL and were placed in a 10 mm diameter, solenoidal

radiofrequency coil. The gradient pulses were produced from a homemade 10 cm diameter gradient-coil set placed inside the 40 cm bore, 2.35 T magnet. The gradient pulses were 1 ms in duration followed by a 5 ms settling time, with a maximum strength of 30 mT/m. This total delay of 6 ms necessitated the use of the sequence of Fig. 3.1c, rather than that of Fig. 3.1b, so that losses due to chemical shift dispersion and to J coupling evolution during the G_2 pulse delay could be recovered.

3.4 Results and Discussion

Both the theoretical and experimental τ dependencies are shown in Fig. 3.3 for the response of the 3.0 ppm GABA triplet to each of the two DQFs illustrated in Figs. 1a and 1c, namely, the inphase multiplet detection of Eq. (3.13) or the antiphase multiplet detection of Eq. (3.16). For the case of inphase detection using the sequence of Fig. 3.1a, the τ value for maximum area was 31 ms. For the case of antiphase multiplet detection using the sequence of Fig. 3.1c, the maximum height occurred at τ=28 ms. In Fig. 3.3, the slight differences between the experimental results and the theoretical predictions may be due to the effects of strong coupling.

Although Fig. 3.3 verifies the τ dependence clearly, it cannot be used to compare the efficacy of inphase and antiphase multiplet detection because a different intensity measure is used in each case. The reason for maintaining two different measures is as follows. When using the antiphase multiplet sequence of Fig. 3.1b or 3.1c, the shape of the 3.0 ppm GABA signal is independent of τ, in that there are two equal and opposing peaks separated by 2J as in Fig. 3.2b. This constant shape is due to the fact that only two-spin antiphase terms are present at the start of acquisition. However, in the case of the inphase DQF sequence of Fig. 3.1a, the shape varies significantly with changing τ, as is illustrated in Fig. 3.4, and there is a clear opportunity for averaging due to *in vivo* line broadening. The changing shape is due to the evolutionary variation of the relative contributions of inphase, two-spin antiphase, and three-spin antiphase terms in the density operator which may all be present at the start of acquisition.

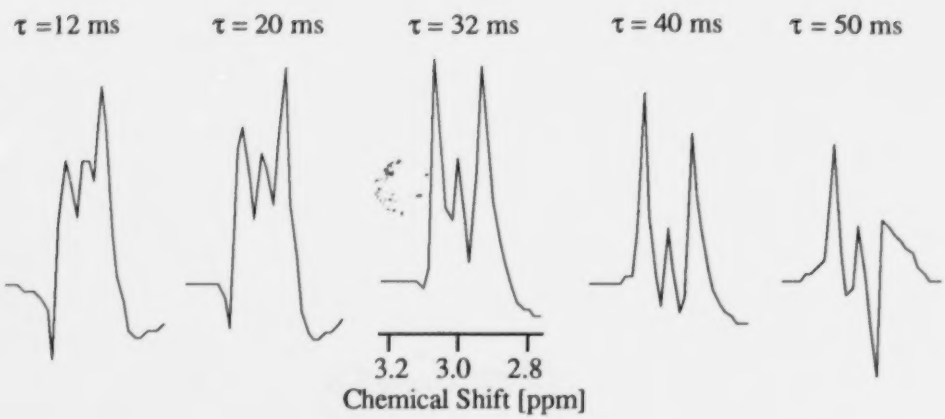

Figure 3.4 Selected spectra of the GABA 3.0 ppm multiplet obtained at 2.35 T using the DQC filter of Fig. 3.1a. The τ timings are listed in the figure. The changing shape of the triplet arises from the evolving combinations of inphase and antiphase magnetization that appear at the start of acquisition and evolve during the acquisition period as detailed in Eq. (3.17).

A theoretical description of this changing shape follows from consideration of the evolution of the two-spin antiphase coherence $2A_xM_z$ over the final τ period in the sequence of Fig. 3.1a. Ignoring the gradient G_2, at the end of this τ period, and just prior to acquisition, this term has evolved into

$$2A_xM_z \xrightarrow{\tau} [A_y+4A_yM_{1z}M_{2z}]\cos(\pi J\tau)\sin(\pi J\tau) + 2A_xM_z[\cos^2(\pi J\tau)-\sin^2(\pi J\tau)]\,. \qquad (3.17)$$

From Eq. (3.17), it is clear that when τ≤12 ms (~1/11J), the two-spin antiphase term dominates (see Fig. 3.2b), while when τ=32 ms (~1/4J), the intensity is dominated by the interaction of the inphase and three-spin antiphase terms, which, following acquisition and Fourier transformation, may be visualized as an adding of the spectrum in Fig. 3.2a to that of Fig. 3.2c.

A comparison of optimal yields is illustrated in Fig. 3.5, where the 3.0 ppm multiplet of GABA obtained in response to each of the DQF sequences with τ=28 ms, and to a 68 ms (1/2J) spin-echo difference sequence, is shown. The percentage of the GABA signal height obtained by each method was compared to that obtained

from a 90°-acquire experiment, yielding 50% for the spin-echo difference method (Fig. 3.5a), and 36% for both DQF sequences (Figs. 3.5b and 3.5c). The theoretical predictions were 50%, 38.5% and 39.5% respectively.

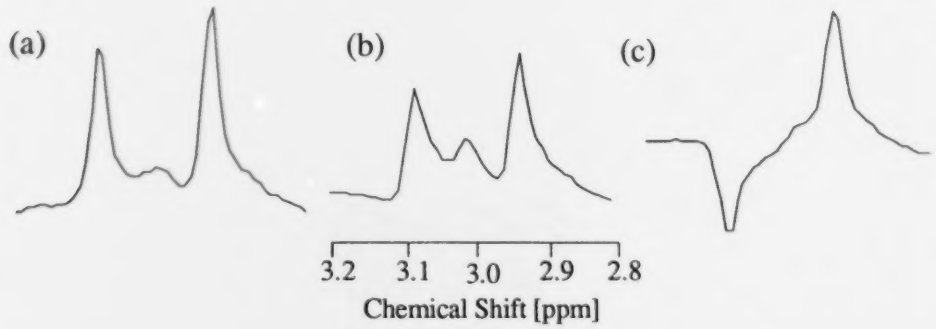

Figure 3.5 A comparison of the GABA 3.0 ppm multiplet obtained from a GABA phantom at 2.35 T, using difference spectroscopy and the DQC filters of Fig. 3.1. The methods used were (a) a 68 ms spin-echo difference technique; (b) a DQC filter obtained with the sequence of Fig. 3.1a with τ=28 ms, and (c) a DQC filter obtained with the sequence of Fig. 3.1c with τ=28 ms and δ=16 ms. All sequences were acquired using 4 scans. The percentage of the maximum available GABA 3.0 ppm signal yield was 50%, 36% and 36% for sequences (a),(b) and (c) respectively.

The relative editing ability of the DQFs and spin-echo difference methods in relation to the observation of the 3.0 ppm GABA multiplet from a perchloric acid extract of rat brain is illustrated in Fig. 3.6. The poor water suppression shown in Fig. 3.6a is of little consequence, since it does not obscure the GABA signal and since its improvement by prior water presaturation can be readily implemented. Of far greater importance is the ability of each method to eliminate the overlapping Cr resonance. From Fig. 3.6, it appears that all three sequences adequately suppressed the 3.0 ppm Cr resonance by at least a factor of 50; however, the exact suppression level is somewhat uncertain because of the direct overlap of the Cr and GABA resonances.

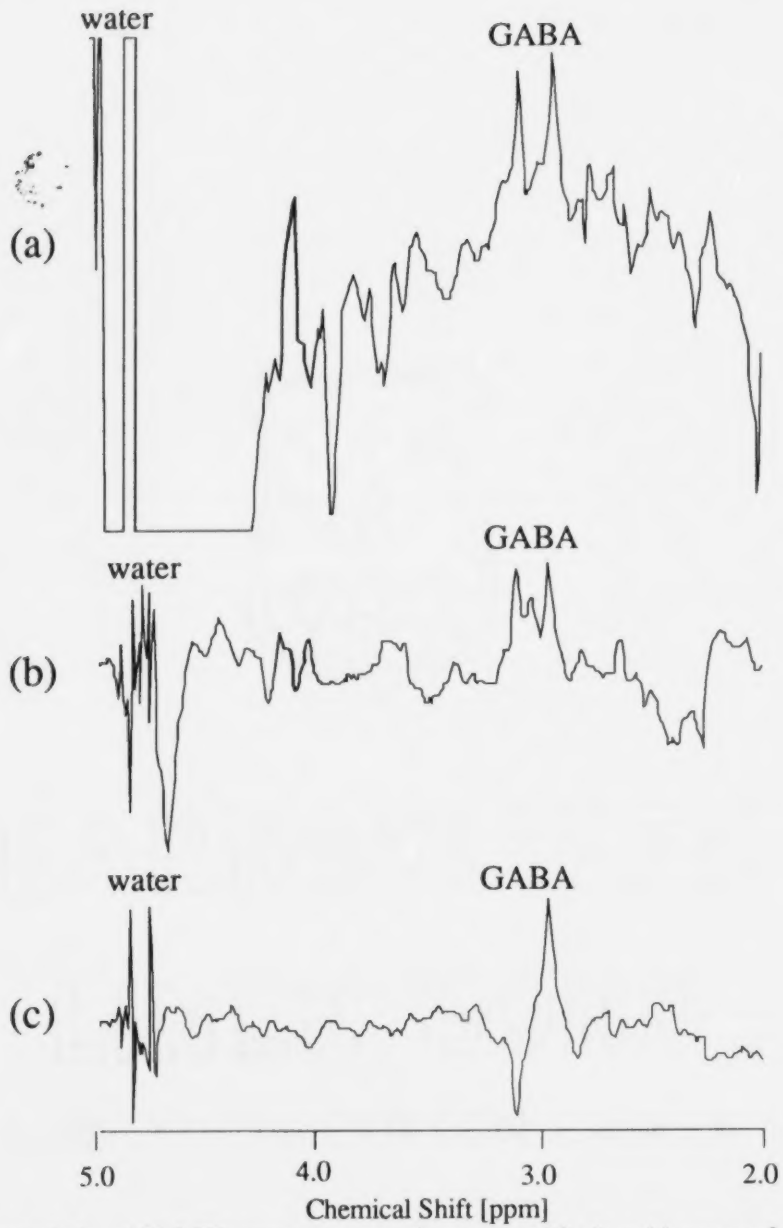

Figure 3.6 100 MHz proton spectra from a perchloric acid extract from the brain of a phenelzine treated rat (27), taken up in a 10% water and 90% D_2O solution. The methods used were (a) a 68 ms spin-echo difference experiment; (b) the DQC filter of Fig. 3.1a with τ=32 ms; and (c) the DQC filter of Fig. 3.1c with τ=28 ms and δ=16 ms. Prior to Fourier transformation, exponential line broadening of 2 Hz was applied. All spectra were acquired with 64 scans, and no additional water suppression pulses were used. The water suppression was ~13, 1600 and 2500 for (a), (b) and (c) respectively.

The exact suppression levels were determined by repeating the same experimental test with the resonant frequency shifted such that the water resonance was at the same frequency offset, and hence experienced the same radiofrequency excitation, as the 3.0 ppm Cr resonance in the original test. The results of this additional test predicted that the overlapping Cr singlet was suppressed by ~70, 1100 and 1700 for the case of Fig. 3.6a, b and c respectively. The lower Cr suppression performance for the spin-echo difference method is due to the inevitable differences in Cr response between the two scans that are subtracted. For example, in the more demanding *in vivo* case of Ref. 15, the spectrum from the spin-echo scan with the DANTE pulse needed artificial enhancement by 7% before subtraction, in order to minimize the Cr contribution. Without such an enhancement, following subtraction, 3.5% of the Cr signal would have remained leading to a suppression factor of 28.6.

Finally, it has been reported recently (15) that the edited 3.0 ppm resonance in *in vivo* proton spectra of human brain may include, in addition to GABA, a component due to macromolecular protons. From *in vivo* rat brain pulse-acquire experiments (24), it has been reported that the 3.0 ppm contribution from macromolecular protons is roughly 40% of the intensity of the GABA peak in normal rat brain and that the macromolecular proton resonance exhibits J coupling to a resonance at 1.7 ppm. Such a coupling is similar to the J coupling of GABA protons giving rise to its 3.0 ppm and 1.9 ppm multiplets. Thus when performing the DQF methods *in vivo*, one can also expect some interference from underlying macromolecular protons. As research into these macromolecules and their associated T_2 times continues, it may become possible to quantify more exactly the contribution that the macromolecules make to the 3.0 ppm resonance. Until that time, absolute *in vivo* quantification of GABA will be somewhat uncertain.

3.5 Conclusions

From a previous analysis (11) we concluded that a TQF sequence provided the most efficient editing of GABA from the Cr methyl singlet. This TQF has a duration of ~1/J (136 ms), a Cr suppression factor of 1600, and yields ~25% of the GABA intensity. The principal weakness of the TQF is the transverse relaxation loss accrued during the sequence length of ~1/J. By exploiting the τ dependence of different terms in the density operator, we have demonstrated in this work that DQFs can be constructed of duration ~1/2J (68 ms), or less, that can suppress Cr to the order of 1700 and at the same time yield up to 39% of the GABA signal. When losses due to transverse relaxation are included, the superiority of the new DQF methods becomes clear. For example, assuming a liberal T_2 of 200 ms *in vivo*, the GABA signal intensity using the new DQF methods is at least 200% greater than that from the previously reported TQF method.

Moreover, the results of this study indicate that the DQF sequences introduced here can compete with difference spectroscopy for editing the GABA 3.0 ppm triplet. The strength of the MQF methods is that they suppress the overlapping Cr (as well as other neighboring resonances) much more effectively than difference editing does. In addition, because they accomplish this editing without subtraction they do not share difference editing's vulnerability to motion artefacts. The weakness of MQF methods is loss of signal intensity due to inherent filter losses and to transverse relaxation losses. With the DQF's proposed here we have enhanced the basic signal to better than three quarters of the difference editing technique as well as shortening the sequence length of difference editing sequences reported in the literature. In terms of the enhancement of the GABA/Cr ratio, difference spectroscopy enhanced this ratio ~35 times, the inphase multiplet DQF method increased it by ~400, whereas the antiphase multiplet DQF method enhanced this ratio by ~600 times.

3.6 References

1. Lloyd, K.G., Zivkovic, B., Scatton, B., Morselli, P.L., and Bartholini, G., *Prog. Neuro-Psychopharmacol. Biol. Psychiatry* **13**, 341 (1989).
2. F. Fonnum, *in* " Psychopharmacology: The Third Generation of Progress," (H.Y. Meltzer, ED.), pp. 173-182, Raven Press, New York, 1987.
3. K.G. Lloyd and P.L. Moreselli, *in* " Psychopharmacology: The Third Generation of Progress," (H.Y. Meltzer, ED.), pp. 183-195, Raven Press, New York, 1987.
4. A.J. Sedman, G.P. Gilmet, A.J. Sayed and E.L. Posvar, *Drug Development Research*, **21**, 235 (1990).
5. P.A. Bottomley, W.A. Edelstein, T.H. Foster, and W.A. Adams, *Proc. Natl. Acad. Sci. USA* **82**, 2148 (1985).
6. P.R. Luyten and J.A. den Hollander, *Radiology* , **161**,795 (1986)
7. C.C. Hanstock, D.L. Rothman, J.W. Prichard, T. Jue, and R.G. Shulman, *Proc. Natl. Acad. Sci. USA*, **85**, 1821 (1988).
8 J. Frahm, H. Bruhn, M.L. Gyngell, K.D. Merboldt, W. Hanicke, and R. Sauter, *Magn. Reson. Med.* **11**, 47 (1989).
9 D.L. Rothman, C.C. Hanstock, O.A.C. Petroff, E.J. Novotny, J.W. Prichard, and R.G. Shulman, *Magn. Reson. Med.* **25**, 94 (1992).
10 B.D. Ross, *NMR in Biomed.*, **4** 59 (1991).
11. A.H. Wilman, and P.S. Allen, *J. Magn. Reson.* **B 101**, 165 (1993).
12. J.S. Shen and P.S. Allen, *J. Magn. Reson.* **92**, 398 (1991).
13. D.L. Rothman, K.L. Behar, H.P. Hetherington, and R.G. Shulman, *Proc. Natl. Acad. Sci. USA* **81**, 6630 (1984).
14. N.E. Preece, S.R. Williams, G. Jackson, J.S. Duncan, J. Houseman and D.G. Gadian, "Proceedings, 10th Meeting of the Society of Magnetic Resonance, San Francisco, 1991," p1000.
15. D.L. Rothman, O.G. Petroff, K.L. Behar, and R.H. Mattson, *Proc. Natl. Acad. Sci. USA* **90**, 5662 (1993).
16. O.W. Sorensen, G.W. Eich, M.H. Levitt, G. Bodenhausen, and R.R. Ernst, *Prog. in NMR Spectroscopy* **16**, 163 (1983).
17. K.J. Packer and K.M. Wright, *Mol. Phys.*, **50,** 797 (1983).
18. W.P. Aue, E. Bartholdi, and R.R. Ernst, *J. Chem. Phys.* **64**, 2229 (1976).
19. A. Bax, P.G. De Jong, A.F. Mehlkopf, and J. Smidt, *Chem. Phys. Lett.* **69**, 567 (1980).
20. L.T. Trimble, J.S. Shen, A.H. Wilman, and P.S. Allen, *J. Magn. Reson.* **86**, 191 (1990).
21. R.E. Hurd and D.M. Freeman, *Proc. Natl. Acad. Sci. USA* , **86**, 4402 (1989).
22. G.A. Morris, and R. Freeman, *J. Magn. Reson.* **29**, 433 (1978).
23. G.B. Baker, J.T.F. Wong, J.M. Yeung, and R.T. Coutts, *J Affective Disorders*, **21**, 207 (1991).
24. K.L. Behar, and T. Ogino, *Magn. Reson. Med.* **30**, 38 (1993).

CHAPTER 4

An Analytical and Experimental Evaluation of STEAM Versus PRESS for the Observation of the Lactate Doublet[1]

PRESS (1,2,3) and STEAM (4) are two of the most common methods of localization used in performing ^1H MRS in-vivo. The response of uncoupled spins to either of these sequences is simple and easily predicted. However coupled spin systems, such as the AX_3 spin system of lactate do not, in general, behave in the same simple manner. For example, the evolution of the various spin-spin coherences during the intervals between the 90º pulses of the STEAM sequence makes the response of coupled spins to this sequence very dependent on those intervals, as well as on the coupling scheme of the spins. The different response of coupled spins to the PRESS and the STEAM sequences becomes particularly important, when, as has happened in the study of multiple sclerosis (MS) lesions, lactate has not been observed by several laboratories using STEAM (5,6,7) but has been reported by a laboratory using PRESS (8). In such circumstances it is essential to establish whether the differential observation of lactate follows from the NMR methodology or whether it only reflects differences in the pathology of the MS lesions studied by the different groups.

The response of an AX_3 spin system to PRESS is well documented (9,10). Its response to STEAM, however, has not to our knowledge been subjected to a rigorous analytical and experimental evaluation, although several authors have demonstrated empirically the two periodicities of the lactate doublet signal on the mixing time, TM, of the STEAM sequence (11-13). Analytical evaluations of the response to STEAM have been published for an AX system (13,14) and for the triplet of an AX_2 system (15). In the present communication we report the analytical derivation of four periodicities in the response of an AX_3 doublet to the STEAM sequence, confirm the three major periodicities experimentally and compare this response with that of the same doublet to PRESS. The analytical derivation will first enable previous STEAM

---

[1] A version of this chapter has been published. A.H. Wilman and P.S. Allen, *J. Magn. Reson.* **B101** 102 (1993).

data to be analysed retrospectively to determine the extent to which the lactate doublet has been suppressed by an inappropriate choice of interpulse intervals, and secondly to provide a quantitative yardstick for choosing STEAM pulse intervals in future experiments.

During the application of STEAM or PRESS in-vivo, spatially selective, soft pulses are employed. For the purpose of this analysis we have approximated this excitation by means of radiofrequency (r.f.) and gradient pulses that are rectangular and consecutive, but which nevertheless maintain the same coherence pathways as the sequences used in-vivo. In the case of STEAM, we have adopted the same approximation sequence (illustrated in Fig.4.1) as Hagberg et al (15). This sequence comprises alternate r.f. and gradient pulses, where we have chosen the G_2 gradient in the TM period to be sufficiently large that only terms which were gradient insensitive during TM could be refocussed in the second TE/2 period. Also, the presence of the two G_1 gradients ensured that refocussed spins were in the single quantum state during both TE/2 periods.

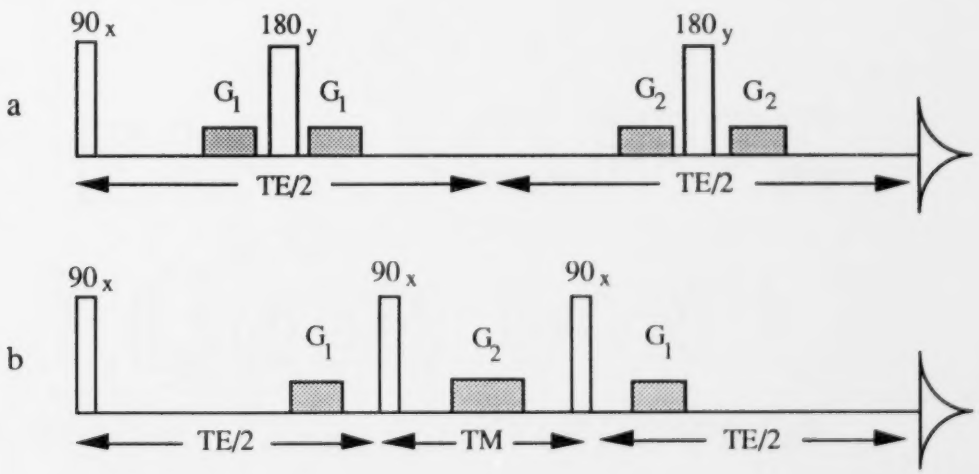

Figure 4.1 The pulse sequences used for experimental and theoretical analysis, where (a) is an approximation of the PRESS sequence and (b) is an approximation of the STEAM sequence. G_1 and G_2 are orthogonal field gradients.

Using the spherical product operator approach (16,17) the response to the STEAM sequence of Fig. 4.1 can be obtained from the initial density operator $\sigma(0)=$

$X_z + A_z$, where X represents the doublet terms, A is the quartet term and $X_u = \sum_i X_{iu}$ with u=x,y or z and i=1,2 and 3. The ultimate doublet signal will result firstly from terms that reflect the evolution of the initial doublet term in the density operator and secondly from magnetization transferred between quartet and doublet. Confining our attention initially to the doublet terms, the doublet density operator, σ_X, after the first 90^o_x pulse, becomes

$$\sigma_X(0+) = -(i/\sqrt{2})(X_+ + X_-) \tag{4.1}$$

During the evolution in time TE/2, a gradient G_1 of duration t_1 is applied, whose effect at a location r is to dephase a coherence of order p by an amount $-p\gamma(\mathbf{G_1}\cdot\mathbf{r})t_1$ where γ is the gyromagnetic ratio (18). Following this gradient, and immediately prior to the second 90^o_x pulse, the doublet terms will have evolved into

$$\begin{aligned}\sigma_X(TE/2-) = &-(i/\sqrt{2})(X_+e^{-i\theta} + X_-e^{i\theta})\cos(\pi JTE/2) \\ &-(\sqrt{2})(X_+e^{-i\theta} - X_-e^{i\theta})A_z\sin(\pi JTE/2),\end{aligned} \tag{4.2}$$

where $\theta = \{\delta\omega TE/2 + \gamma(\mathbf{G_1}\cdot\mathbf{r})t_1\}$ represents the dephasing due to the doublet chemical shift ω_X relative to the transmitter frequency, and to the gradient G_1. In anticipation of the refocussing effects of the gradient in the second TE/2 period, we shall in the TM period confine our attention to those terms in σ_X which are insensitive to G_2. Accordingly $\sigma_X(TE/2+)$, immediately after the second 90^o_x pulse, reduces to

$$\begin{aligned}\sigma_X(TE/2+) = &-(1/2)(X_ze^{-i\theta} + X_ze^{i\theta})\cos(\pi JTE/2) \\ &-(i/2)(A_+X_{-z}e^{i\theta} + A_+X_-e^{-i\theta} - A_-X_+e^{i\theta} - A_-X_+e^{-i\theta})\sin(\pi JTE/2).\end{aligned} \tag{4.3}$$

During the TM period the terms in Eq. (4.3) will evolve into

$$\begin{aligned}\sigma_X(TE/2+TM-) = &-(1/2)X_z(e^{-i\theta} + e^{i\theta})\cos(\pi JTE/2) \\ &-(i/2)[A_+X_-(e^{i(\theta+\delta\omega TM)} + e^{-i(\theta-\delta\omega TM)}) \\ &-A_-X_+(e^{i(\theta-\delta\omega TM)} - e^{-i(\theta+\delta\omega TM)})]\sin(\pi JTE/2)\cos^2(\pi JTM),\end{aligned} \tag{4.4}$$

where $\delta\omega = \omega_X - \omega_A$, the chemical shift difference between the doublet and quartet and where the antiphase two spin coherence terms, which give rise to no observable

magnetization in the detection period, have been omitted. The final 90°_{x} pulse yields,

$$\sigma_X(TE/2+TM+) = (i/2\sqrt{2})\,(X_+ + X_-)\,(e^{-i\theta}+e^{i\theta})\cos(\pi JTE/2) + (1/2\sqrt{2})\,(X_+ - X_-)\,A_z(e^{-i\theta}+e^{i\theta})\sin(\pi JTE/2)\cos^2(\pi JTM)\cos(\delta\omega TM), \quad (4.5)$$

where only inphase and antiphase doublet terms have been retained. Evolution under scalar coupling, chemical shift and the final gradient G_1 during the final TE/2 gives rise to the following observable terms,

$$\sigma_X(TE+TM) = (i/4\sqrt{2})[(X_+ + X_-)[\,2\cos^2(\pi JTE/2) - \sin^2(\pi JTE/2)\cos^2(\pi JTM)\cos(\delta\omega TM)]]. \quad (4.6)$$

Turning secondly to the magnetization transferred between the quartet and the doublet, the equilibrium operator for the quartet, A_z, becomes, following the first 90°_{x} pulse and evolution under J coupling, chemical shift and the gradient G_1, during the first TE/2 period,

$$\sigma_A(TE/2-) = (\sqrt{2})(A_-e^{i\phi} - A_+e^{-i\phi})\,X_z\cos^2(\pi JTE/2)\sin(\pi JTE/2), \quad (4.7)$$

where all terms that cannot transfer transverse magnetization to the doublet by means of this pulse sequence have been neglected and where $\phi = (\omega_A TE/2 + \gamma(\mathbf{G_1}\cdot\mathbf{r})t_1)$. Following the second 90°_{x} pulse, the terms from Eq. (4.7), which are insensitive to gradients during TM evolve as shown in Eq. (4.8),

$$\sigma_A(TE/2+TM-) = -(i/2)[A_-X_+e^{i(\phi-\delta\omega TM)} - A_+X_-e^{i(\phi+\delta\omega TM)} - A_+X_-e^{-i(\phi-\delta\omega TM)} + A_-X_+e^{-i(\phi+\delta\omega TM)}]\cos^2(\pi JTE/2)\sin(\pi JTE/2)\cos^2(\pi JTM). \quad (4.8)$$

The remaining terms are omitted because they will not be refocussed in the acquisition period.

Applying the final 90°_{x} pulse and accounting for the evolution during the final TE/2 period yields the following observable doublet terms,

$$\sigma_A(TE+TM) = (i/4\sqrt{2})(X_+e^{-i\delta\omega TE/2} + X_-e^{i\delta\omega TE/2}) \sin^2(\pi JTE/2)\cos^2(\pi JTE/2)\cos^2(\pi JTM)\cos(\delta\omega TM). \quad (4.9)$$

Combining Eq. (4.9) and Eq. (4.6) provides the terms from which the real part of the net doublet magnetization at the end of the STEAM sequence can be calculated. Assuming quadrature detection with a 90º receiver phase shift (aligned along the y axis of the rotating frame), the net doublet signal S(t) is

$$S(t) = (1/2)\{\cos^2(\pi JTE/2) - (1/2)\sin^2(\pi JTE/2)[1 - \cos^2(\pi JTE/2)\cos(\delta\omega TE/2)]\cos^2(\pi JTM)\cos(\delta\omega TM)\} \quad (4.10)$$

The first term, deriving from σ_X, represents magnetization that was longitudinal during the TM period. The second term reflects the zero quantum coherence (ZQC) state during TM. It includes contributions from both the doublet and the quartet.

The response of an AX_3 doublet to PRESS is exactly the same as that of a simple AX system, ie., the J modulation is $\cos(\pi JTE)$. This dependence leads to a maximum at TE=n/J where n is an integer (9,10).

The three major periodicities of Eq. (4.10) were verified experimentally at 100 MHz using a phantom of lithium lactate in D_2O. They are plotted in Figs. 4.2 to 4.4. In all the graphs the solid lines represent the theoretical curves and the points are experimental data. The theoretical curves include a factor to accommodate transverse relaxation, the characteristic time of which was measured to be (600 ± 40 ms). Longitudinal relaxation losses were minimal and have been neglected.

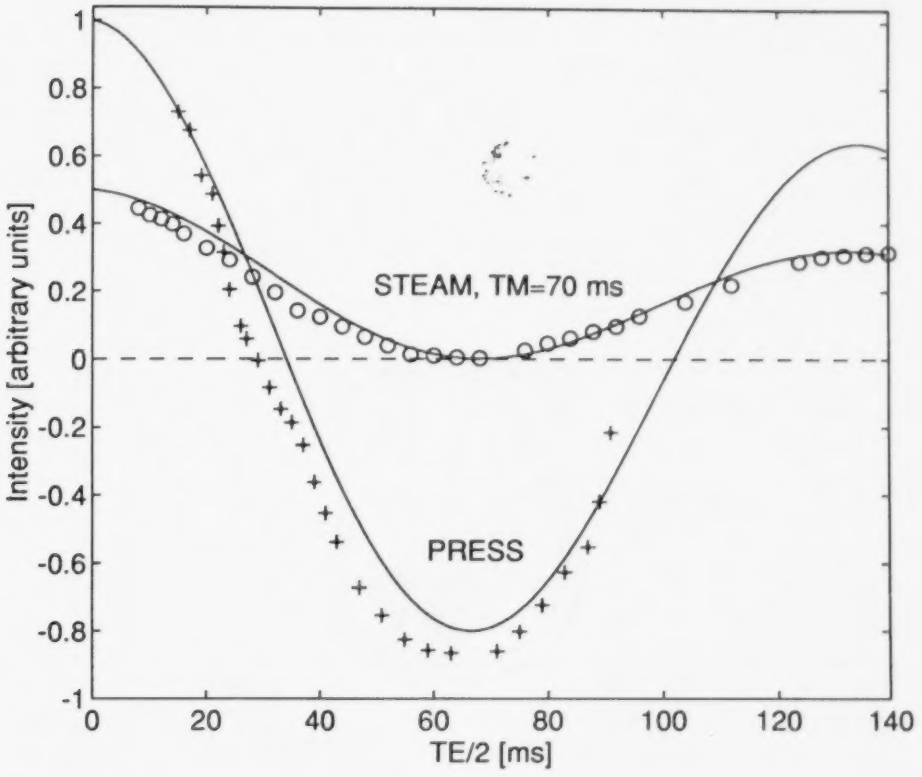

Figure 4.2 A comparative illustration of the TE dependence of the lactate doublet intensity, as observed using PRESS (●), and STEAM with TM=70ms~1/2J (□). The solid lines are the theoretical curves and the points are the experimental data. J=7.3Hz was assumed and a transverse relaxation decay (T_2=600ms) was also incorporated into the theoretical curves.

Fig. 4.2 provides a comparison of the echo time dependence of PRESS and STEAM (TM=70 ms), when the value of TM of the STEAM sequence is chosen to ensure that the ZQC term in Eq. (4.10) is nulled through its (πJTM) dependence. Clearly PRESS gives rise to the greater signal at most echo times, however its advantage over STEAM can easily be less than the often quoted factor of two, for example, when 15<TE/2<30 at TM=70 ms. When the ZQC is not nulled, Eq. (4.10) shows that three additional periodicities arise, namely, a higher freqency term in TE/2 plus two in TM. Focussing first on the major (πJTE/2) periodicity, the TE dependent minima at TE=(2n+1)/J (n is an integer) become TM dependent, but the corresponding TE dependent maxima are unchanged.

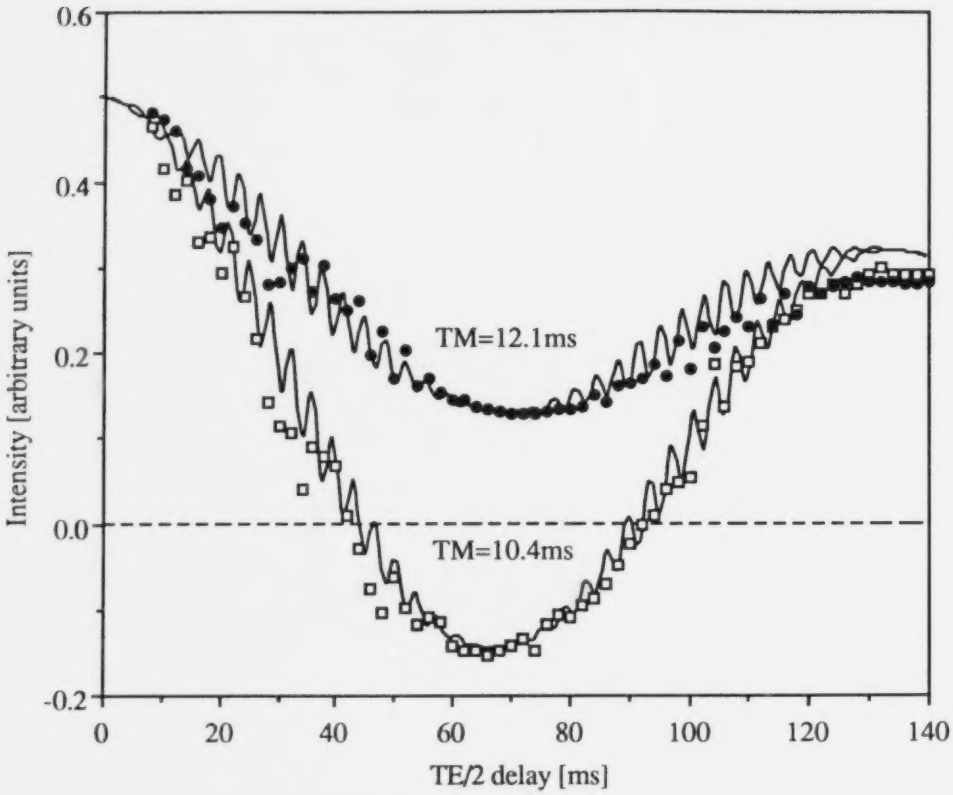

Figure 4.3 An illustration of the secondary TM dependence of the TE dependent lactate doublet intensity using TM=10.4ms (□), and 12.1ms (●). The solid lines are the theoretical curves and the points are the experimental data. J=7.3Hz was assumed and a transverse relaxation decay (T_2=600ms) was also incorporated into the theoretical curves.

This secondary TM dependence of the first TE minimum is illustrated in Fig.4.3, where the difference between the TM=10.4 ms and the TM=12.1 ms curves reflect a sign change in the cos(δωTM) term in the ZQC component of Eq. (4.10). The value of cos(δωTM) for the two curves in Fig.4.3 is respectively 0.7 and -0.7. The minor higher frequency oscillation in the ZQC component due to the cos(δωTE/2) modulation arises from magnetization transferred from the quartet. The amplitude of this higher frequency oscillation is similar to the scatter in our data points and although the correct periodicity of the data points does seem to be present in places, we do not feel able to claim that this periodicity was verified experimentally.

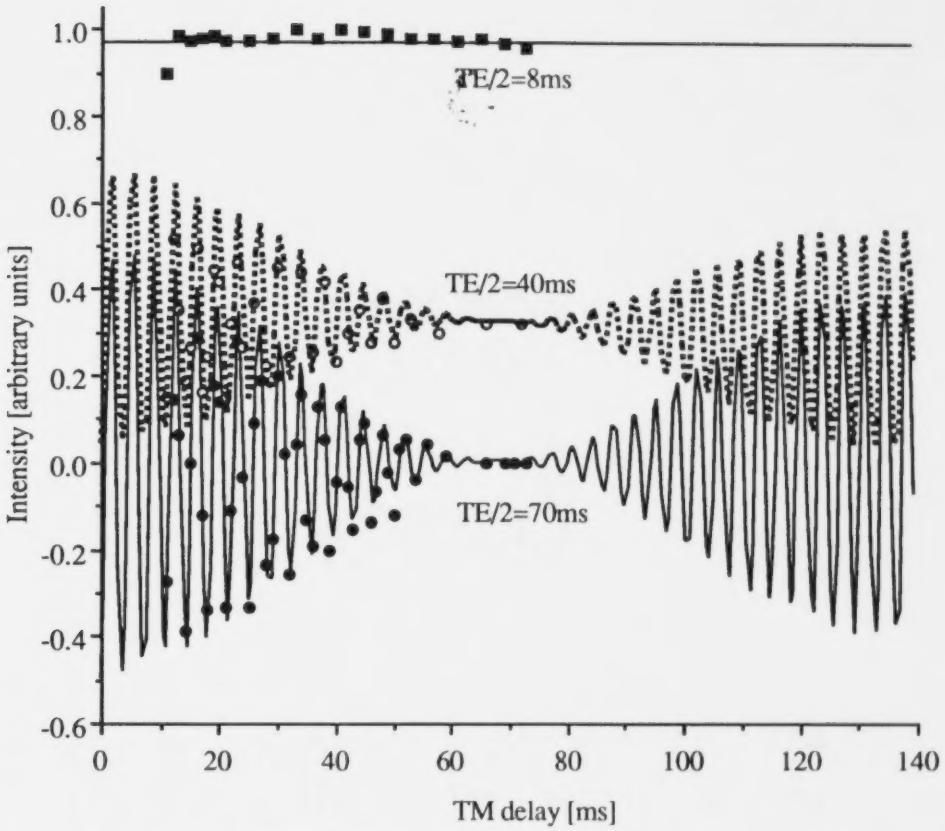

Figure 4.4 An illustration of the TM periodicities of the lactate doublet intensity when observed by STEAM at the half echo times TE/2=8ms (■), 40ms (○), and 70ms(●). The lines represent the theoretical curves and the points are experimental data. J=7.3Hz was assumed.

The two TM periodicities which also arise from the ZQC term of Eq. (4.10) are clearly illustrated for three TE values in Fig. 4.4. Individual reports of the existence of each of these TM periodicities have been made previously by Sotak and coworkers (11,12) from experimental observations at TE=1/J. Equation (4.10) and Fig. 4.4, however, emphasize in addition to the TM dependence of the ZQC component, the significant effects that TE has on that TM dependence, a point not previously made. This stresses the need to carefully control both TE and TM in order to optimize the STEAM signal. For example, the ($\delta\omega$TM) period, which is field dependent, is particularly rapid and easy to adjust wrongly. Nonetheless, from

the TM and TE values quoted in References 5,6 and 7, it appears that for each reference some data was in fact acquired with an appropriate choice of pulse intervals, thereby increasing.the confidence that abnormal lactate levels were not missed through an inappropriate choice of these times, and supporting the conclusion of reference (8) that only very new lesions show elevated lactate.

In summary, provided one fully accounts for the evolution of the multiple quantum coherences in the TM period, in-vivo localization and editing sequences based on STEAM can be effective alternatives to PRESS. For example, if in the case of lactate observation the STEAM sequence includes a frequency selective metabolite inversion pulse in the TM interval (19), that inverts the 1.33 ppm methyl doublet, but subjects the 4.11 ppm methine quartet to no excitation, then one must take account of the fact that all the ZQC filtered terms in Eq. (4.10) would be converted to double quantum coherence in the TM period and be subsequently dephased. In such a case, only those terms that passed through TM in the longitudinal state would be observable, namely the first term in Eq. (4.10). In other examples, the greater complexity of the STEAM response can be used to advantage where peak verification is required (12). On occasions where the complexity is undesirable, e.g. in applications involving longitudinal relaxation, it may be eliminated by setting TE/2 = n/J (for weakly coupled systems of single J) or by choosing TM = (2n + 1)/2J (for the doublet of an AX_3 system for example, but not for an AX system).

4.1 References

1. R.E. Gordon and R.J.Ordridge, Abstracts of the Society of Magnetic Resonance in Medicine, Third Annual Meeting, New York, p272, 1984.
2. R.J. Ordridge, M.R. Bendall, R.E. Gordon, and A. Conelly, *in* "Magnetic Resonance in Biology and Medicine,"(G. Govil, C.L. Khetrapal, and A. Saran, Ed.s) p. 387-397, McGraw-Hill, New Dehli,1985.
3. P.A. Bottomley, *Ann. N.Y. Acad. Sci.*, **508,** 333 (1987).
4. J. Frahm, KD. Merboldt, and W. Hanicke, *J. Magn. Reson*, **72**, 502 (1987).
5. R.A.Koopmans, G. Zhu, D.K.B. Li, P.S. Allen, M. Javidan, and D.W. Paty, Abstracts of the Society of Magnetic Resonance in Medicine, Ninth Annual Meeting, New York, p1205, 1990.
6. P.V. Hecke, G.Marchal, K.Johannik, P.Demaerel, G.Wilms, H.Carton, and A.L.Baert, *Mag. Res. Med.*, **18**, 199 (1991).
7. H.B.W.Larson, P. Christiansen, M.Jensen, J. Frederiksen, A,Heltberg, J.Olesen, and O.Henriksen, *Mag. Res. Med.*, **22**, 23 (1991).
8. D.L. Arnold, P.M. Matthews, G. Francis, and J.Antel, *Mag. Res. Med.*, **14**, 154 (1990).
9. W.I.Jung, M.Bunse, H.Bongers, F. Schick, and O.Lutz, Abstracts of the Society of Magnetic Resonance in Medicine, Tenth Annual Meeting, San Francisco, p1066, 1991.
10. W.I. Jung and O.Lutz, *J. Magn. Reson*, **96**, 237 (1992).
11. C.H. Sotak and D.M. Freeman, *J. Magn. Reson*,**77**, 382 (1988).
12. C.H. Sotak and J.R. Alger, *Mag. Res. Med.*, **17**, 533 (1991).
13. Th. Ernst and J. Hennig, *Mag. Res. Med.*, **21**, 82 (1991).
14. R.Kimmich, E.Rommel, and, A.Knuttel, *J. Magn. Reson*, **81**, 333 (1989).
15. G. Hagberg, N. Beckmann, and J. Seelig, SMRM Abstracts (1991) p1107.
16. O.W Sorensen, G.W.Eich, M.H. Levitt , G. Bodenhausen and R.R. Ernst *Prog. NMR Spectrosc.*, **16**, 163 (1983).
17. T.T. Nakashima and R.E.D. McClung, *J. Magn. Reson*, **70**, 187 (1986).
18. A.Bax, P.G.DeJong, A.F.Mehlkopf, and J.Smidt, *Chem. Phys. Lett.* **69**,567 (1980).
19. G. Zhu, D. Gheorghiu, and P.S. Allen, *NMR in Biomedicine*, **5**, 209 (1992).

Chapter 5

The Response of the Strongly Coupled AB System of Citrate to Typical Proton MRS Localization Sequences[1]

5.1 Introduction

The level of citrate, a secretory product of the normal prostate, may serve as a method of differentiating adenocarcinoma from benign prostatic hyperplasia (BPH) and from normal prostatic tissue, since the citrate concentration is generally regarded as being significantly decreased in adenocarcinoma (1-8) relative to that in BPH and the normal peripheral zones. Using proton MRS, recent *in vivo* observations of citrate in human prostate confirm this finding of a decreased citrate level in adenocarcinoma (9, 10).

The most commonly used localisation sequences in proton MRS, which were also the sequences used in the recent *in vivo* studies of human prostate (6,9,10), are PRESS (11,12) and STEAM (13,14). The response of uncoupled spins to either of these sequences is simple and easily predicted. However, the response of strongly coupled spin systems, such as the AB system of citrate is much more complex. Empirical results on the response of the citrate multiplet have elucidated the echo-time, TE, modulations obtained from the PRESS sequence at 1.5 T (6), and the mixing-time, TM, modulations obtained from the STEAM sequence with a fixed TE (15). Using the density matrix approach (16), Mulkern et al. (17-19) have recently evaluated the echo-time dependence of the spectrum of the citrate AB system as obtained from the radiofrequency pulses of the PRESS sequence. In addition, they have derived the spectrum obtained from a sequence of three 90^{o} pulses (17,18). However, this sequence does not include the essential gradient pulses of the STEAM sequence, which determine not only the localisation, but also the coherence pathway selection of that sequence. Inclusion of the gradient pulses for the PRESS sequence is not so critical.

---

[1] A version of this chapter has been accepted for publication. A.H. Wilman and P.S. Allen, *J. Magn. Reson.* (1994).

In the present paper, and in contrast to Mulkern, we use the product operator approach (20) as applied to strongly coupled systems (21), to develop an analytical framework enabling the determination of all the echo-time modulations that affect the actual observability of citrate in response to both the PRESS and the STEAM sequences. The response to either sequence exhibits a strong field dependence in the range commonly used for *in vivo* proton MRS. Furthermore, because the field dependence of the AB spectrum, when observed under *in vivo* conditions, undermines the signal-to-noise benefits normally accruing to an increasing Zeeman energy, higher field strengths are not automatically favoured. To estimate the benefit of increasing the field strength, while at the same time eliminating the influence of changes in the noise characteristics as the Larmor frequency changes, the signal intensity from the two central, but *in vivo* broadened, lines of the AB spectrum have been compared with that from an equivalently broadened line from uncoupled spins.

5.2 Analysis

At 2.35 T, the field strength used for experimental verification, the AB system of citrate is very strongly coupled with a chemical-shift-difference to scalar-coupling-constant ratio, δ/J, of approximately unity, thus making the typical weak-coupling spherical product operator analysis invalid. Instead, one may still use the spherical product operator notation but in combination with the transformational equations developed in Ref. 21 for an AB system under the influence of Zeeman and strong scalar coupling. In Ref. 21, Kay and McClung split the AB Hamiltonian into two commuting parts, $\mathcal{H}_0$ and $\mathcal{H}_1$, and then separately derived the evolution of the spherical AB product operators under each part. The two parts of the Hamiltonian are as follows,

$$\mathcal{H}_0 = \overline{\omega}\,(A_Z + B_Z) + 2\,\pi\,J A_Z\,B_Z \tag{5.1}$$

$$\mathcal{H}_1 = \delta\omega\,(A_Z - B_Z) - 2\,\pi\,J\,(A_+\,B_- + A_-\,B_+) \tag{5.2}$$

where A_m and B_m are the m components of the spherical spin angular momentum

operators (22, 23) with m = +, -, z for spins A and B, where $\delta\omega$ is the chemical shift difference between the A and B spins, and where $\overline{\omega}$ is the average chemical shift. If Λ is the strong coupling frequency, then,

$$\delta\omega=(\omega_A-\omega_B)/2 \quad ; \quad \overline{\omega}=(\omega_A+\omega_B)/2 \quad ; \quad \Lambda=[\delta\omega^2+(\pi J)^2]^{1/2}. \tag{5.3}$$

For example, each part of the Hamiltonian affects the time evolution of the in-phase A magnetisation as follows,

$$A_+ \xrightarrow{\mathcal{H}_1 t} A_+a_1(t) + 2B_+A_z\,a_2(t) \quad , \quad A_+ \xrightarrow{\mathcal{H}_0 t} A_+b_1(t) + 2A_+B_zb_2(t) \tag{5.4}$$

where the time dependent coefficients a and b are as defined in Ref. 21, namely,

$$a_1(t) = \cos(\Lambda t) - i(\delta\omega/\Lambda)\sin(\Lambda t) \qquad a_2(t) = i(\pi J/\Lambda)\sin(\Lambda t)$$
$$b_1(t) = \cos(\pi Jt)\exp(-i\,\overline{\omega}\,t) \qquad b_2(t) = -i\sin(\pi Jt)\exp(-i\,\overline{\omega}\,t). \tag{5.5}$$

Although strongly coupled systems are like weakly coupled ones in that coherence orders only change during rf pulses, and do not change during evolution (22, 24, 25), they are however, unlike weakly coupled systems, in that evolution under $\mathcal{H}_1$ allows for interchange between in-phase A magnetisation and antiphase B magnetisation through the a_2 coefficient. It is because of this a_2 coefficient that the chemical shift is not fully refocussed in a spin-echo sequence. Furthermore, because of this lack of refocussing, the response to PRESS differs significantly from that to the spin-echo sequence. Note that in the weak coupling limit, $\delta\omega >> \pi J$, the a_2 coefficient goes to zero and a_1 becomes simply $\exp(-i\delta\omega\, t)$.

Using the methods introduced by Kay and McClung (21), the response of citrate to both the STEAM and PRESS sequences has been obtained. For the purpose of this analysis, the STEAM and the PRESS sequences were approximated as illustrated in Fig. 5.1, using consecutive rather than concurrent radiofrequency (rf) and gradient pulses. Nevertheless, these sequences still maintain the same coherence pathways as the sequences used *in vivo* (26, 27). Perfect quadrature detection was also assumed so that the observable signals are associated with only the A- and B- density operator terms (22).

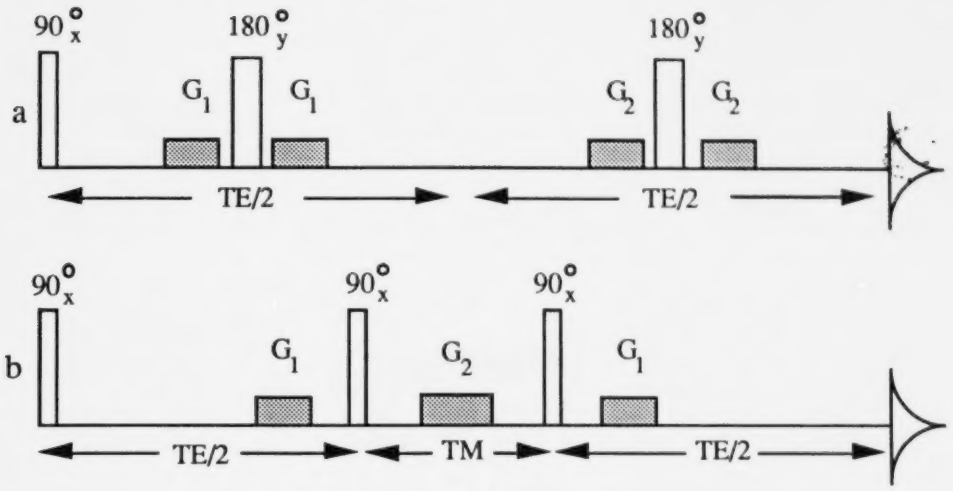

Figure 5.1. The pulse sequences used for both theoretical and experimental analysis of the PRESS and STEAM localisation sequences. G_1 and G_2 are field gradient pulses. Panel (a) is an approximation of the PRESS sequence and panel (b) is an approximation of the STEAM sequence.

For comparison with the results derived later, the response to a simple spin-echo sequence, which was originally derived by Abragam using the density matrix approach (28), and which also follows directly from Eq. (23) of Ref. 21, is listed below, where the total real signal, S, available following a spin-echo sequence of total length t_E is,

$$S(t_E) = [(\delta\omega/\Lambda)^2 + (\pi J/\Lambda)^2\cos(\Lambda t_E)]\cos(\pi J t_E) + (\pi J/\Lambda)\sin(\pi J t_E)\sin(\Lambda t_E)\,. \qquad (5.6)$$

The signal S represents the total transverse magnetisation that is present at the start of the acquisition period which is directly proportional to the total area under the Fourier transform. In the weak coupling limit, Eq. (5.6) reduces to simply $\cos(\pi J t_E)$, as does the response to PRESS in that same limit.

5.2.1 PRESS

If A and B represent the spins of the citrate AB system, the initial spherical density operator of that system is $\sigma(0) = A_z + B_z$. Following the first $90^o{}_x$ radiofrequency (rf) pulse of a PRESS sequence (Fig. 5.1a), the density operator becomes

$$\sigma(0+) = (-i/\sqrt{2})\,(A_+ + A_- + B_+ + B_-), \tag{5.7}$$

where we note that in the spherical angular momentum operator notation (22, 23), the Cartesian spin angular momentum operators A_x and A_y are defined by $A_y = (i/\sqrt{2})\,(A_+ + A_-)$ and $A_x = (-i/\sqrt{2})\,(A_+ - A_-)$. The $A_+ + B_+$ terms produced by this first pulse can be neglected since these terms return to +1 coherence states prior to acquisition, hence making them unobservable to perfect quadrature detection (22). In contrast to the forthcoming analysis of the STEAM sequence, the gradient pulses need not be considered either, because the $180^o{}_y$ pulses allow for total rephasing of the magnetization.

Immediately prior to the first $180^o{}_y$ pulse, the terms of interest arising from Eq. (5.7) have evolved into

$$\sigma(\tau_1-) = (-i/\sqrt{2})\,\{A_-\,\alpha(\tau_1) + B_-\,\beta(\tau_1) + 2A_-B_z\,\gamma(\tau_1) + 2B_-A_z\,\varepsilon(\tau_1)\} \tag{5.8}$$

where
$$\begin{aligned}
\alpha(\tau_1) &= a_1(-\tau_1)b_1(-\tau_1) + a_2(-\tau_1)b_2(-\tau_1),\\
\beta(\tau_1) &= a_1(+\tau_1)b_1(-\tau_1) + a_2(-\tau_1)b_2(-\tau_1),\\
\gamma(\tau_1) &= a_1(-\tau_1)b_2(-\tau_1) + a_2(-\tau_1)b_1(-\tau_1),\\
\varepsilon(\tau_1) &= a_1(+\tau_1)b_2(-\tau_1) + a_2(-\tau_1)b_1(-\tau_1),
\end{aligned} \tag{5.9}$$

and where $\tau_1 = TE/4$ for the PRESS sequence. The first $180^o{}_y$ pulse transforms these terms as follows,

$$\sigma(\tau_1+) = (-i/\sqrt{2})\,\{A_+\alpha(\tau_1) + B_+\beta(\tau_1) - 2A_+B_z\,\gamma(\tau_1) - 2B_+A_z\,\varepsilon(\tau_1)\}\ . \tag{5.10}$$

During the $\tau_2 = TE/2$ time interval, between the two $180^o{}_y$ pulses, the terms of Eq. (5.10) will evolve under $\mathcal{H}_0$ and $\mathcal{H}_1$ to be transformed by the final $180^o{}_y$ pulse

to give the following density operator.

$$\begin{aligned}\sigma(\tau_1+\tau_2+) = (-i/\sqrt{2})\{&A_-[\alpha(\tau_1)a_1(\tau_2)b_1(\tau_2) + \beta(\tau_1)a_2(\tau_2)b_2(\tau_2) - \gamma(\tau_1)a_1(\tau_2)b_2(\tau_2) \\ &- \varepsilon(\tau_1)a_2(\tau_2)b_1(\tau_2)] \\ &+ B_-[\alpha(\tau_1)a_2(\tau_2)b_2(\tau_2) + \beta(\tau_1)a_1(-\tau_2)b_1(-\tau_2) - \gamma(\tau_1)a_2(\tau_2)b_1(\tau_2) \\ &- \varepsilon(\tau_1)a_1(-\tau_2)b_2(\tau_2)] \\ &- 2A_-B_Z[\alpha(\tau_1)a_1(\tau_2)b_2(\tau_2) + \beta(\tau_1)a_2(\tau_2)b_1(\tau_2) - \gamma(\tau_1)a_1(\tau_2)b_1(\tau_2) \\ &- \varepsilon(\tau_1)a_2(\tau_2)b_2(\tau_2)] \\ &- 2B_-A_Z[\alpha(\tau_1)a_2(\tau_2)b_1(\tau_2) + \beta(\tau_1)a_1(-\tau_2)b_2(\tau_2) - \gamma(\tau_1)a_2(\tau_2)b_2(\tau_2) \\ &- \varepsilon(\tau_1)a_1(-\tau_2)b_1(\tau_2)]\}. \end{aligned} \tag{5.11}$$

Note that evolution during this τ_2 period, has led to a complete mixing of states; for example, the in-phase A magnetisation with coefficient $\alpha(\tau_1)$ in Eq. (5.10), now contributes not only to the in-phase and antiphase A magnetisation of Eq. (5.11), but also to the in-phase and antiphase B magnetisation.

Evolution during the final τ_3 = TE/4 period preceding acquisition, where the signal acquired is proportional to the sum of the A_- and B_- terms, gives rise to the terms given in Eq. (5.12). For PRESS, the acquisition has been performed along the -y axis (not the +y axis as in the spin-echo, and the STEAM case to be considered later) in order to yield a signal that is initially positive, namely,

$$\begin{aligned} S(TE) = &[\alpha(\tau_1)\alpha(\tau_3) + \gamma(\tau_1)\gamma(\tau_3)]\, a_1(\tau_2)b_1(\tau_2) \\ &+ [\beta(\tau_1)\beta(\tau_3+\varepsilon(\tau_1)\varepsilon(\tau_3)]\, a_1(-\tau_2)b_1(\tau_2) \\ &+ [\alpha(\tau_1)\beta(\tau_3) + \gamma(\tau_1)\varepsilon(\tau_3) + \alpha(\tau_3)\beta(\tau_1) + \gamma(\tau_3)\varepsilon(\tau_1)]\, a_2(\tau_2)b_2(\tau_2) \\ &- [\alpha(\tau_1)\varepsilon(\tau_3) + \beta(\tau_1)\gamma(\tau_3) + \alpha(\tau_3)\varepsilon(\tau_1) + \beta(\tau_3)\gamma(\tau_1)]\, a_2(\tau_2)b_1(\tau_2) \\ &- [\alpha(\tau_1)\gamma(\tau_3) + \alpha(\tau_3)\gamma(\tau_1)]\, a_1(\tau_2)b_2(\tau_2) \\ &- [\beta(\tau_1)\varepsilon(\tau_3) + \beta(\tau_3)\varepsilon(\tau_1)]\, a_1(-\tau_2)b_2(\tau_2) \end{aligned} \tag{5.12}$$

which on substitution for the various coefficients gives,

$$\begin{aligned} S(TE) = &[(\delta\omega/\Lambda)^2 + (\pi J/\Lambda)^2\cos(\Lambda TE)]\cos(\pi JTE) \\ &+ 2(\pi J/\Lambda)[(\delta\omega/\Lambda)^2 + (\pi J/\Lambda)^2\cos(\Lambda TE/2)]\sin(\pi JTE)\sin(\Lambda TE/2)\,. \end{aligned} \tag{5.13}$$

5.2.2 STEAM

The response to the STEAM sequence (Fig. 5.1b) was derived in a similar manner. Following the first 90^{o}_{x} pulse only the +1 coherence states need be considered, since the -1 states will not be rephased into observable magnetisation at the time of acquisition because of the two G_1 gradient pulses (27). For example, -1 coherence levels that receive the first G_1 gradient pulse, must be in the +1 state at the time of the second, identical G_1 pulse in order to be rephased; however, the quadrature detection process will only detect terms proportional to the -1 levels so these terms are irrelevant. Immediately prior to the second 90^{o}_{x} pulse the expression for the density operator is somewhat similar to Eq. (5.8) except that the +1 coherences are retained at the time $\tau = TE/2$.

$$\sigma(\tau) = (-i/\sqrt{2}) \{ A_+ \alpha(-\tau) + B_+ \beta(-\tau) + 2A_+B_Z \gamma(-\tau) + 2B_+A_Z \varepsilon(-\tau) \} \qquad (5.14)$$

Following the second 90^{o}_{x} pulse only those terms that are converted by that pulse to zero quantum coherence (ZQC) or to longitudinal magnetization need to be retained, since any gradient-sensitive terms (nonzero orders of coherence) will be dephased by the TM gradient pulse G_2. The terms of interest immediately after this second pulse are shown in Eq. (5.15).

$$\sigma(\tau+) = (-1/2)\{ A_Z \alpha(-\tau) + B_Z \beta(-\tau) + 2A_+B_- (1/2)[\gamma(-\tau)-\varepsilon(-\tau)] + 2A_-B_+ (1/2)[\varepsilon(-\tau)-\gamma(-\tau)] \} \qquad (5.15)$$

The four operators A_Z, B_Z, $2A_+B_-$, and $2A_-B_+$, all commute with the Hamiltonian H_O, thus during the TM period the evolution of this truncated density operator is completely described by the evolution under $\mathcal{H}_1$. The effect of $\mathcal{H}_1$ on the coherence-level-zero operators of Eq. (5.15) is to allow interchange amongst all four states. By the end of the TM period, such interchange leads to the following expression

$$\begin{aligned}\sigma(\tau+TM)=(-i/\sqrt{2})\{ & A_Z [\alpha(-\tau)r_1(TM) + \beta(-\tau)r_2(TM) + (1/2)(\gamma(-\tau) - \varepsilon(-\tau))r_3(TM) \\ & + (1/2)(\varepsilon(-\tau)-\gamma(-\tau))r_3(-TM)] \\ & + B_Z [\alpha(-\tau) r_2(TM) + \beta(-\tau)r_1(TM) - (1/2)(\gamma(-\tau) - \varepsilon(-\tau))r_3(TM) \\ & - (1/2)(\varepsilon(-\tau)- \gamma(-\tau))r_3(-TM)]\end{aligned}$$

$$+ 2A_+B_- [\ \alpha(-\tau)r_3(TM) - \beta(-\tau)r_3(TM) + (1/2)(\gamma(-\tau)-\varepsilon(-\tau))r_4(TM) + (1/2)(\varepsilon(-\tau)-\gamma(-\tau))r_2(TM)]$$
$$+ 2A_-B_+ [\ \alpha(-\tau)r_3(-TM) - \beta(-\tau)r_3(-TM) + (1/2)(\gamma(-\tau)-\varepsilon(-\tau))r_2(TM) + (1/2)(\varepsilon(-\tau)-\gamma(-\tau))r_4(-TM)]\}\quad , \qquad (5.16)$$

where r_1 to r_4 are (21)

$$r_1(TM) = (1/2)\{1+ [(\delta\omega)^2 + (\pi J)^2\cos(2\Lambda TM)]/\Lambda^2\}$$
$$r_2(TM) = (1/2)(\pi J/\Lambda)^2\{1 - \cos(2\Lambda TM)\}$$
$$r_3(TM) = (1/2)(\pi J/\Lambda)\ \{(\delta\omega/\Lambda)[\cos(2\Lambda TM) - 1] - i\sin(2\Lambda TM)\}$$
$$r_4(TM)=(1/2)\{\cos(2\Lambda TM) + (1/\Lambda)^2[(\pi J)^2 +(\delta\omega)^2\cos(2\Lambda TM)] - i2(\delta\omega/\Lambda)\sin(2\Lambda TM)\} \qquad (5.17)$$

In Eq. (5.16), the longitudinal terms with an r_1 coefficient represent magnetisation that remained in that same longitudinal state during the TM period; similarly the ZQC terms associated with r_4 also remained in the same ZQC state. However, the terms with an r_2 coefficient arose from a transfer between the A_Z and B_Z states during TM, and finally, the r_3 coefficient is associated with the transfer between the longitudinal and ZQC states. It is worth noting that in the weak coupling approximation, $r_1 \rightarrow 1$, and $r_4 \rightarrow \exp(-2\delta\omega TM)$, but both r_2 and r_3 tend to zero.

Following the final 90^o_x pulse of the STEAM sequence, one need only consider the -1 coherence levels which evolve for a further τ=TE/2 period before acquisition. At the end of this second TE/2 period, the total observable signal $S(2\tau+TM)$, acquired along the +y axis, is

$$S(2\tau+TM) = \alpha(\tau)\ [\alpha(-\tau)r_1(TM) + \beta(-\tau)r_2(TM) + (1/2)(\gamma(-\tau)-\varepsilon(-\tau))r_3(TM) + (1/2)(\varepsilon(-\tau)-\gamma(-\tau))r_3(-TM)]$$
$$+ \beta(\tau)\ [\alpha(-\tau)r_2(TM) + \beta(-\tau)r_1(TM) - (1/2)(\gamma(-\tau)-\varepsilon(-\tau))r_3(TM) - (1/2)(\varepsilon(-\tau)-\gamma(-\tau))r_3(-TM)]$$
$$+ (1/2)(\varepsilon(\tau)-\gamma(\tau))[\alpha(-\tau)r_3(TM) - \beta(-\tau)r_3(TM) +(1/2)(\gamma(-\tau)-\varepsilon(-\tau))r_4(TM) + (1/2)(\varepsilon(-\tau)-\gamma(-\tau))r_2(TM)]$$
$$+ (1/2)(\gamma(\tau)-\varepsilon(\tau))[\alpha(-\tau)r_3(-TM) - \beta(-\tau)r_3(-TM) + (1/2)(\gamma(-\tau)-\varepsilon(-\tau))r_2(TM) + (1/2)(\varepsilon(-\tau)-\gamma(-\tau))r_4(-TM)]\quad , \qquad (5.18)$$

which on substitution for the various coefficients yields

$$S(TE+TM) = (1/2)\ \{\ [\cos(\Lambda TE/2)\cos(\pi JTE/2) + (\pi J/\Lambda)\sin(\Lambda TE/2)\sin(\pi JTE/2)]^2$$
$$+ (\delta\omega/\Lambda)^2 \sin^2(\Lambda TE/2)\cos^2(\pi JTE/2)\ [(\delta\omega/\Lambda)^2 + (\pi J/\Lambda)^2\cos(2\Lambda TM)]$$
$$- (\delta\omega/\Lambda)^2 \sin^2(\Lambda TE/2)\sin^2(\pi JTE/2)\cos(2\Lambda TM)$$
$$- (\pi J/\Lambda)(\delta\omega/\Lambda)^2 \sin^2(\Lambda TE/2)\sin(\pi JTE)\sin(2\Lambda TM)\ \}. \qquad (5.19)$$

In the weak coupling limit Eq. (5.19) reduces to

$$S_{weak}(TE+TM) = (1/2)\ \{\cos^2(\pi JTE/2)$$
$$- (1/2)\sin^2(\pi JTE/2)[1 - \cos(\delta\omega TE)]\cos(2\delta\omega TM)\ \}. \qquad (5.20)$$

5.2.3 Signal to Noise Comparison with Uncoupled Spins

In this section, the magnetic field strength dependence of the signal-to-noise ratio, S/N, of the spectrum from citrate is compared to that of uncoupled spins. While this analysis is independent of the pulse sequence used, it is assumed that the citrate multiplet is detected in-phase. In general, the in-phase spectrum of an AB system can be represented by four lines as is illustrated in Fig. 5.2. The inner lines are separated by $[(\Lambda/\pi)-J]$ Hz and each has a relative intensity of $(1/4)[1+ (\pi J/\Lambda)]$ (28,29). These expressions reflect a field dependence whereby the separation between the inner lines increases with increasing field, while the relative intensity contained within them decreases, a fact that has been well documented in a qualitative manner (6). It is possible, however, to make a more valuable quantitative statement about the field dependent observability of the citrate AB multiplet by comparing its amplitude with that of the singlet from an equal number of uncoupled spins.

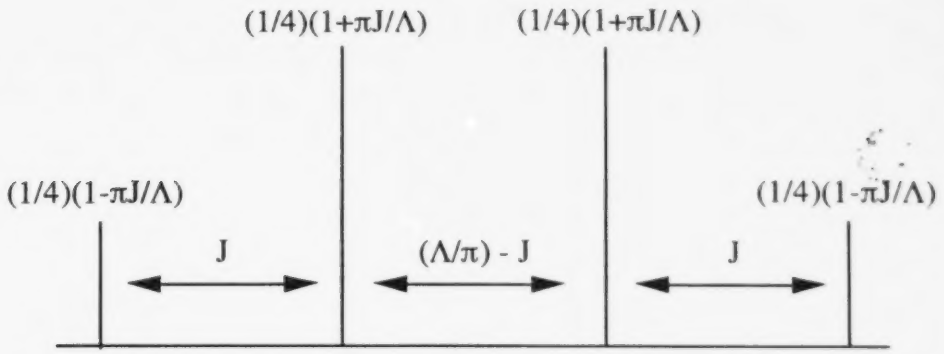

Figure 5.2 A schematic in-phase AB spectrum (1), indicating the relative intensities and separations of the multiplet lines. The separations are denoted in units of Hz.

At the field strengths employed in *in vivo* work, the two central lines of the citrate multiplet overlap and dominate the intensity. By assuming that these two central lines are Lorentzian, the field dependence of the ratio, R(f), of the maximum amplitude of the combined central peaks, relative to that for the amplitude of an uncoupled singlet with the same number of spins and same T_2^* can be calculated from Eq. (5.21).

$$R(f)= (1/4)[1+ (\pi J/\Lambda)]\ MAX\{\ [1+ (2\pi(f - f_1)T_2^*)^2\ ]^{-1} + [1+ (2\pi(f - f_2)T_2^*)^2\ ]^{-1}\}\ , \qquad (5.21)$$

where $f_{1,2} = \pm (1/2)[(\Lambda/\pi) - J]$ Hz and MAX refers to the maximum value over the whole multiplet.

5.3 Experimental Methods

An experimental test of the response of the citrate multiplet to the spin-echo, PRESS and STEAM sequences was carried out at 2.35 T on a 100 mM phantom solution of trilithium citrate in D_2O. The sample was placed in a 5 mm NMR tube and surrounded by a 1 cm diameter, 4 turn solenoidal coil. The 90° pulse length was 16 μs. The experimental STEAM and PRESS sequences used were exactly as

outlined in Fig. 5.1. To minimize the eddy-current effects of the switched gradients, a homemade 10 cm diameter gradient-coil set was employed inside the 40 cm bore magnet. The gradient pulses were 2 ms in duration with a 5 ms settling time. and a maximum strength of 40 mT/m.

As a prelude to these tests, experimental determinations were made of J (15.4 Hz), and of $\delta\omega$ (13.2π rad/s). In addition, the characteristic transverse relaxation time T_2 (400 $\pm$ 40 ms) was determined from a comparison of the experimental and theoretical spin-echo responses of the citrate multiplet. Longitudinal relaxation losses during the pulse sequences were minimal and have been neglected. Experimental measurement of the citrate multiplet intensity was accomplished by measuring the total area under the multiplet. This area corresponds to the total inphase magnetisation available at the start of the acquisition period and corresponds directly with the results of the theoretical calculations.

5.4 Results

Figure 5.3 provides a comparison of the analytical equations for the response to the spin-echo and PRESS sequences, namely Eqs. (5.6) and (5.13) respectively, and the experimental response at 2.35 T (100 MHz). The theoretical weak coupling response to each of the sequences, ie. cos(πJTE), is also shown.

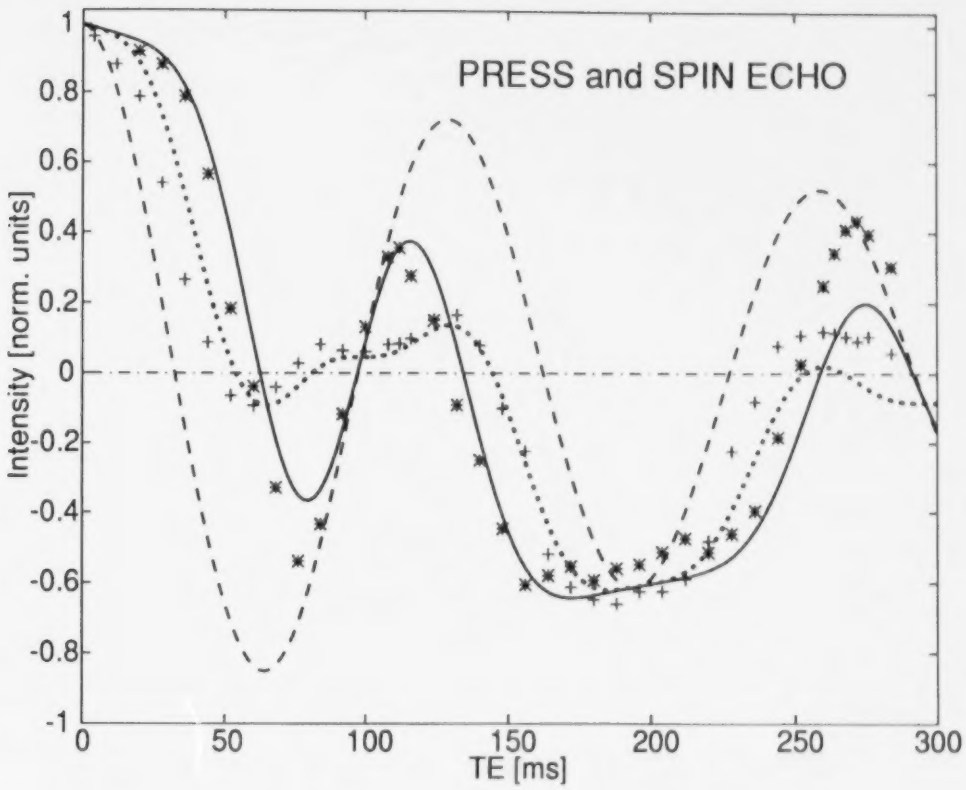

Figure 5.3 The TE dependence of the citrate AB multiplet intensity acquired in response to the spin-echo and the PRESS sequences performed at 100 MHz. The lines are the theoretical curves and the points are the experimental data, where the solid line, Eq. (5.13), and (*) represent PRESS results, and the dotted line of Eq. (5.6) and (+) correspond to a spin-echo experiment. The dashed curve illustrates the weak coupling approximation which is the same for both the spin-echo and the PRESS responses. The theoretical curves include a relaxation time T_2 of 400 ms.

Selected spectra illustrating the response to PRESS at 100 MHz are shown in Fig. 5.4. For the purpose of this illustration, the TE timings were chosen to emphasize the slow changes up to TE=36 ms, the first null at TE=60 ms, and the first complete inversion at TE=76 ms. A more detailed set of spectra illustrating the response of citrate to the PRESS sequence at 1.5 T is provided by Ref. 6.

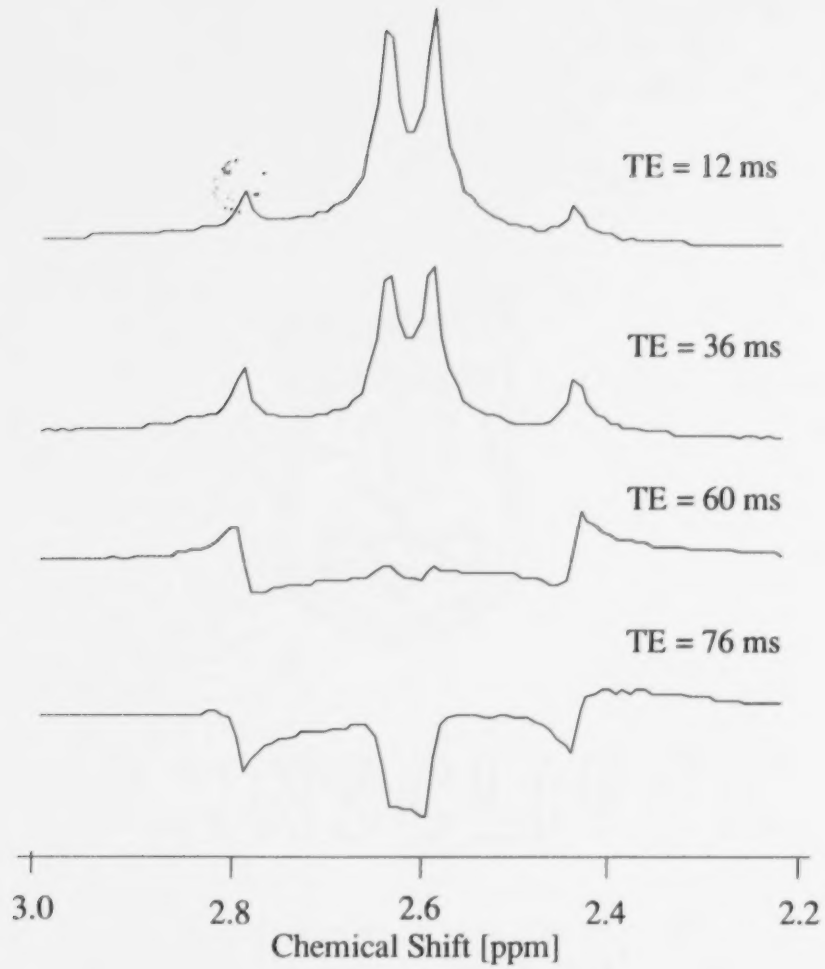

Figure 5.4 An illustration of the TE dependence of 100 MHz proton spectra obtained from a phantom of trilithium citrate using the PRESS sequence.

The response of the citrate AB system to the STEAM sequence is shown in Fig. 5.5, where the experimental and theoretical TE modulations at 2.35 T are given for a TM of 8ms. Fig. 5.6 provides selected spectra obtained in this test corresponding to the first experimental minimum at TE/2=22 ms, the local maximum at TE/2=40 ms, and the first null at TE/2=74 ms. In addition to the TE time dependence, the AB response to the STEAM sequence also exhibits significant TM dependent modulations which are illustrated in Fig. 5.7.

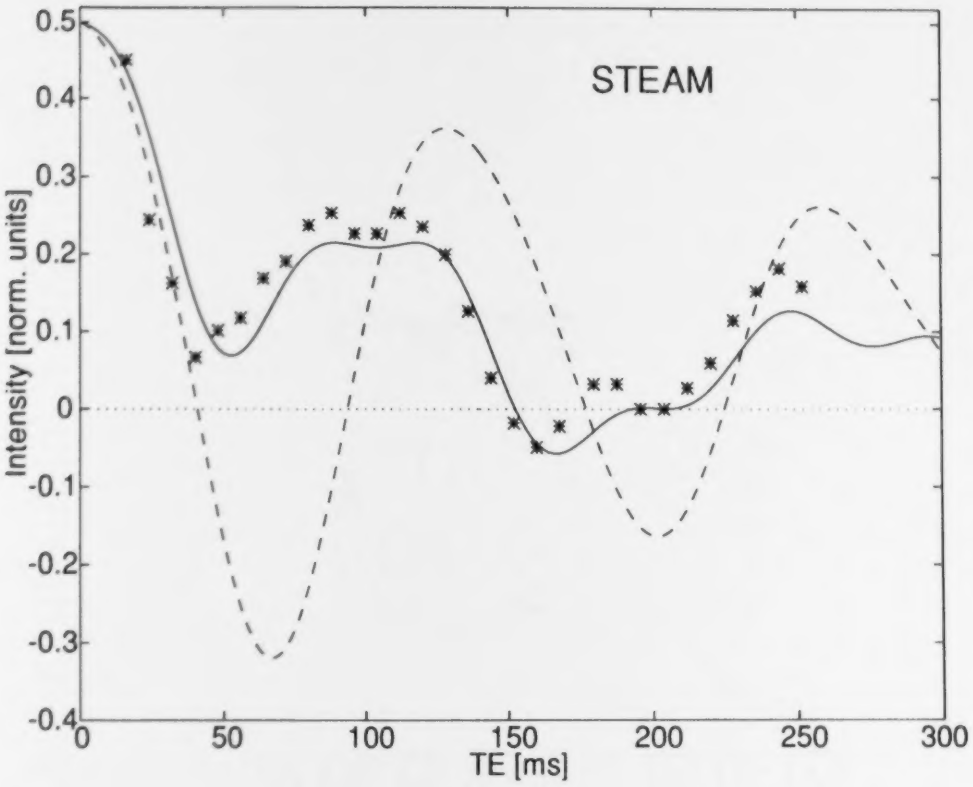

Figure 5.5 The TE dependence of the citrate AB signal intensity at 100 MHz obtained in response to a STEAM sequence with a TM = 8 ms. The solid line is the theoretical curve of Eq. (5.19) and (∗) are the experimental data. The dashed curve illustrates the weak coupling approximation of Eq. (7.20). A relaxation time T_2 of 400 ms was incorporated into the theoretical curves.

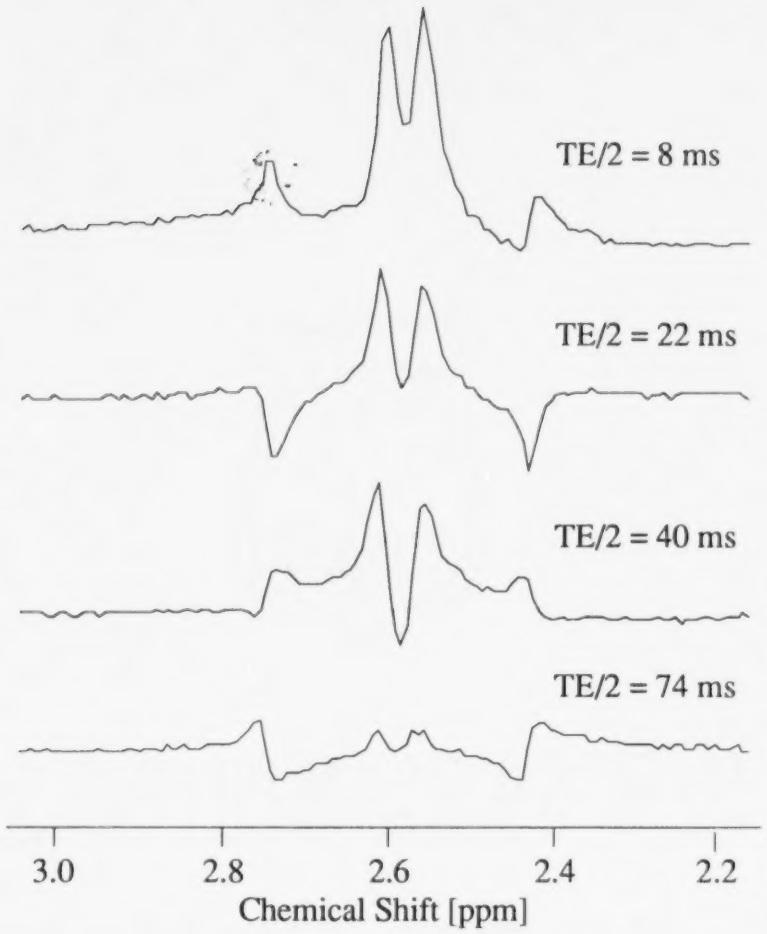

Figure 5.6 An illustration of the TE dependence of 100 MHz proton spectra obtained from a phantom of trilithium citrate using the STEAM sequence with a TM=8 ms.

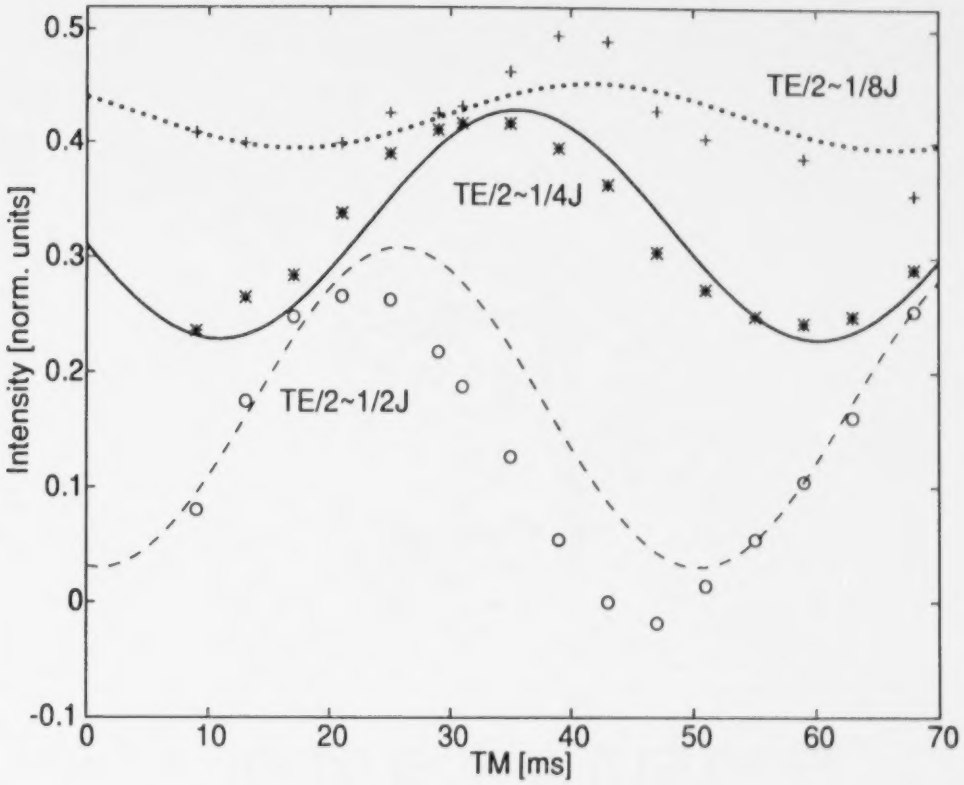

Figure 5.7 An illustration of the TM periodicities of the citrate AB multiplet intensity when observed by STEAM at the half echo times TE/2 = 8 ms ~1/8J (+), 15.7 ms ~1/4J (*), and 31.4 ms ~1/2J (o). The curves represent the theoretical expressions derived from Eq. (5.19), and the points are the experimental data.

The details of the citrate response to the *in vivo* localisation sequences also depends to a large degree on the magnetic field strength. First of all, the effect that varying the magnetic field strength has on the echo-time modulations of the citrate response to the PRESS or the STEAM sequence is illustrated in Figs. 5.8 and 5.9 respectively. In these curves, only the change in echo-time modulation with field strength is illustrated. Of course, changes in magnetic field strength also influence the signal-to-noise ratio. The effect of magnetic field strength on the achievable S/N is shown in Fig. 5.10, where the field dependence of the maximum height of the combined central peaks of the citrate AB multiplet is shown relative to that obtainable for uncoupled spins as calculated using Eq. (5.21).

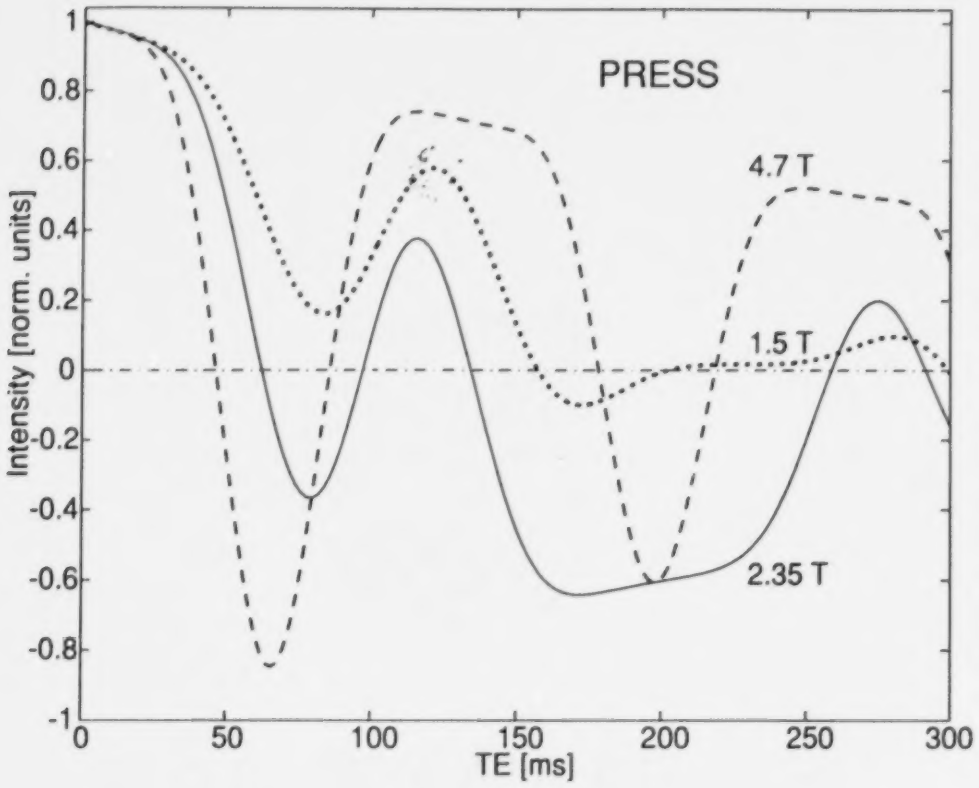

Figure 5.8 The normalised theoretical relationship between the citrate AB signal intensity and TE for the PRESS sequence at three different magnetic field strengths (1.5 T - dotted line, 2.35 T - solid line, and 4.7 T - dashed line). A relaxation time T_2 of 400 ms was assumed at each field strength.

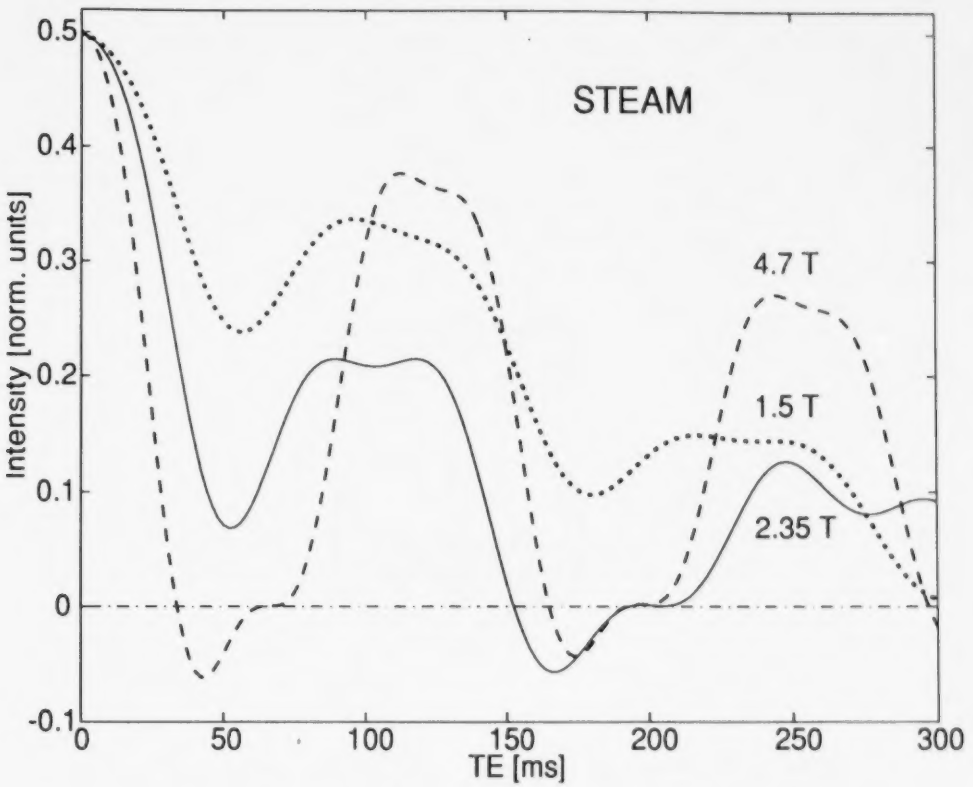

Figure 5.9 The normalised theoretical relationship between the citrate AB signal intensity and TE for the STEAM sequence at three different magnetic field strengths (1.5 T - dotted line, 2.35 T - solid line, and 4.7 T - dashed line) and with TM=8 ms. A relaxation time T_2 of 400 ms was assumed at each field strength.

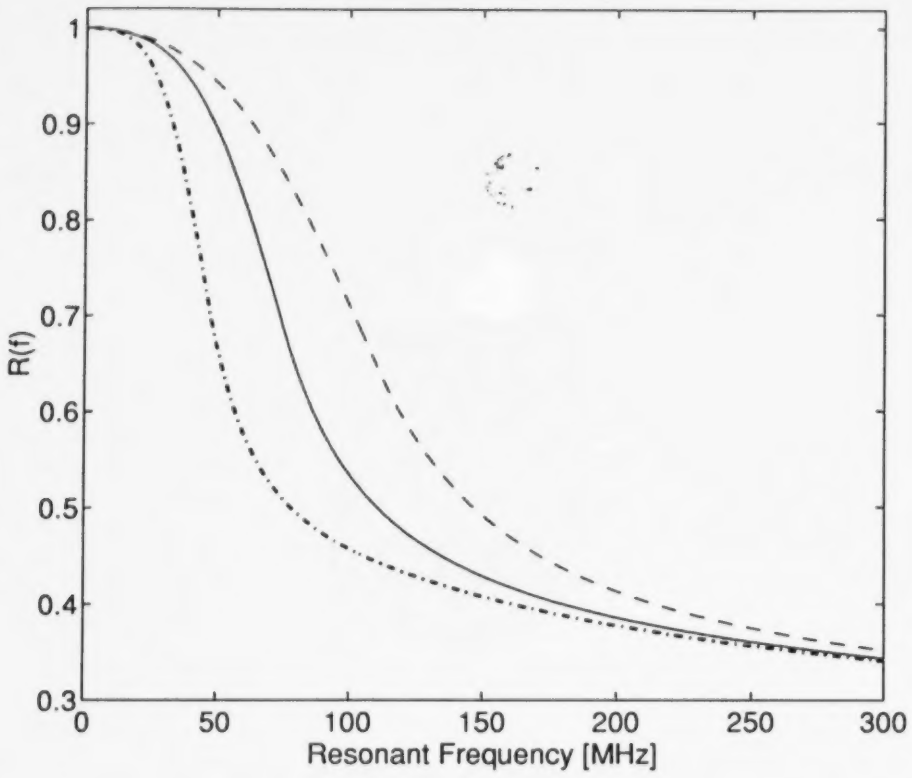

Figure 5.10 The ratio R(f) of the maximum height of the in-phase citrate AB multiplet spectrum to the maximum height of a singlet from the same number of uncoupled spins is plotted against the magnetic field strength B_o for various half height linewidths namely, 2 Hz (dotted line), 5 Hz (solid line) and 10 Hz (dashed line). The curves were generated from Eq. (5.21).

5.5 Discussion And Conclusions

Although the actual response of the citrate AB system to *in vivo* localisation sequences is known to differ substantially from that predicted by the weak coupling approximation (6, 15, 17-19), not all of the important variations affecting the observability of the signal at different echo times and field strengths have been previously quantified. The well defined cosinusoid variation with echo time predicted by the weak coupling approximation gives way to a non-periodic variation whose maxima and null values are quite field dependent. For example in the case of the PRESS sequence at 2.35 T, a negative maximum at TE = 1/J or ~ 65 ms, predicted by weak coupling turns into a signal null as demonstrated by both the theoretical and experimental curves of Fig. 5.3. In the case of STEAM, the predicted null at TE/2 ~ 48 ms is in fact a maximum at 2.35 T, and there is no inversion at shorter TE/2. In addition, the TM dependence of the response to the STEAM sequence is in fact modulated at a frequency of 2Λ, rather than the lesser frequency of $2\delta\omega$ as predicted by the weak coupling approximation of Eq. (5.20). The different modulation frequency has been observed experimentally (15).

When performing PRESS or STEAM at any field strength, careful choice of TE, and TM, is essential to ensure that one obtains the optimum citrate intensity. The appropriate timing parameters for either of these localisation sequences for any strongly coupled AB system at any field strength, are now given a quantitative basis by Eqs. (5.13) and (5.19). By making use of the formulas developed here, it will be possible to optimize the citrate intensity subject to any individual constraint.

From an experimental point of view, the presence of significant strong coupling effects is neither purely advantageous nor disadvantageous. For example, for both the PRESS and the STEAM sequences, the reduction in TE modulation as the strong coupling effects increase (illustrated in Figs. 5.8 and 5.9) may be exploited at shorter TE to yield a notable increase in signal intensity relative to that for a similar weakly coupled spin system. However, the S/N benefits achieved by increasing field strength are significantly less for citrate than the corresponding gain experienced by uncoupled spins (see Fig. 5.10). For instance, if we assume for simplicity that there is a linear increase in S/N with field, then only a 1.4 fold improvement would be observed in citrate intensity on changing the field strength

from 1.5 T to 4.0 T as compared to a 2.7 fold improvement for uncoupled spins, assuming in addition that the full width at half height of a single peak is 5 Hz. The improvement limitations in signal intensity for strongly coupled AB systems are compounded by the fact that the echo-time-dependent modulations of signal intensity are much more marked at higher field strengths for this AB system, reducing even further the advantages of higher field strengths for the observation of citrate.

5.7 References

1. K.R. Halliday, C.Fenoglio-Preiser, and L.O. Sillerud, *Magn. Reson Med.* **7**, 384 (1988).
2. L.O. Sillerud, K.R. Halliday, R.H. Griffey, C. Fenoglio, and S. Sheppard, *Magn. Reson. Med.* **8**, 224 (1988).
3. M.E. Yacoe, G. Sommer, and D. Peehl, *Magn. Reson Med.* **19**, 429 (1991).
4. J. Kurhanewicz, R. Dahiya, J.M. Macdonald, L.H. Chang, T.L. James, and P. Narayan, *Magn. Reson Med.* **29**, 149 (1993).
5. M.L. Schliebler, K.K. Miyamoto, M. White, S.J. Maygarden, and J.L. Mohler, *Magn. Reson Med.* **29**, 285 (1993).
6. F. Schick, H. Bongers, S. Kurz, W.I. Jung, M. Pfeffer and O. Lutz, *Magn. Reson Med.* **29**, 38 (1993).
7. A.H. Fowler, A.A. Pappas, J.C. Holder, A.E. Finkbeiner, G.V. Dalrymple, M.S. Mullins, J.R. Sprigg, and R.A. Komoroski, *Magn. Reson Med.* **25**, 140 (1992).
8. T.G. Pretlow, B.E. Harris, E.L. Bradley, *Cancer Research* **45**, 442 (1985).
9. J. Kurhanewicz, D.B. Vigneron, S.J. Nelson, H. Hricak, S. Moyher, P. Carrol, T.L. James, and P. Narayan, Abstracts of the Society of Magnetic Resonance in Medicine, 12th Annual Meeting, New York, p. 212, 1993.
10. A. Heerschap, G. de Jager, A. de Koster, J. Barentz, J. de la Rosette, F. Debruyne, and J. Ruijs, Abstracts of the Society of Magnetic Resonance in Medicine, 12th Annual Meeting, New York, p. 213, 1993.
11. R.E. Gordon and R.J. Ordidge, Abstracts of the Society of Magnetic Resonance in Medicine, 3rd Annual Meeting, New York, p. 272, 1984.
12. R. J. Ordidge, M.R. Bendall, R.E. Gordon, and A. Connelly, *in* "Magnetic Resonance in Biology and Medicine" (G. Govil, C.L. Khetrapal, and A. Saran, Eds.), pp. 387-397, McGraw-Hill, New Dehli, 1985.
13. P.A. Bottomley, *Ann. N.Y. Acad. Sci.* **508**, 333 (1987).
14. J. Frahm, K.D. Merboldt, and W. Hanicke, *J. Magn. Reson.* **72**, 502 (1987).
15. J. Kurhanewicz, Y. Xu, D.B. Vigneron, S.J. Nelson, W. Chew, J.M. Macdonald, L.-H. Chang, T.L. James, and P. Narayan, Abstracts of the Society of Magnetic Resonance in Medicine, 11th Annual Meeting, Berlin, p. 3810, 1992.
16. C.P. Slichter, "Principles of Magnetic Resonance," 3rd ed., Springer-Verlag, New York, 1990.
17. R.V. Mulkern, J.L. Bowers, and D. Williamson, Abstracts of the Society of Magnetic Resonance in Medicine, 12th Annual Meeting, New York, p. 919,

1993.
18. R.V. Mulkern, and J.L. Bowers, *Concepts in Magn. Reson.* (in press).
19. R.V. Mulkern, and J. L. Bowers, *Magn. Reson. Med.* **30**, 518 (1993).
20. O.W. Sorensen, G.W. Eich, M.H. Levitt, G. Bodenhausen, and R.R. Ernst, *Prog. NMR Spectrosc.*, **16**, 163 (1983).
21. L.E. Kay, and R.E.D. McClung, *J. Magn. Res.* **77**, 258 (1988).
22. T.T. Nakashima and R.E.D. McClung, *J. Magn. Res.* **70**, 187 (1986).
23. M.E. Rose, "Elementary Theory of Angular Momentum," Wiley, New York, 1957.
24. A. D. Bain, *J. Magn. Res.* **56**, 418 (1984).
25. G. Bodenhausen, H. Kogler, and R.R. Ernst, *J. Magn. Res.* **58**, 370 (1984).
26. G. Hagberg, N. Beckmann, and J. Seelig, Abstracts of the Society of Magnetic Resonance in Medicine, 10th Annual Meeting, San Francisco, p. 1107, 1991.
27. A.H. Wilman and P.S. Allen, *J. Magn. Res.*, Series B **101**, 102 (1993).
28. A. Abragam, "Principles of Nuclear Magnetism," Oxford University Press, Oxford U.K., 1961.
29. E.D. Becker, "High Resolution NMR," 2nd ed., Academic Press, New York, 1980.

Chapter 6

Double Quantum Filtering of Citrate for *In vivo* Observation[1]

Because adenocarcinoma of the prostate has become one of the most common malignancies in North American men, its differential diagnosis from benign prostate hyperplasia and the normal peripheral zone of the prostate has taken on a significantly important role. The level of citrate, a secretory product of the normal prostate, as determined non-invasively by NMR spectroscopy, may prove to afford such a differential diagnosis, since it is generally regarded as decreased in adenocarcinoma (1-6) and possibly increased in prostatic hyperplasia (2,7). *In vivo* observations of citrate in normal human prostate with a signal-to-noise ratio of <20, (its concentration is ~60 mM) have already been performed by proton MRS (6,8). While there is some spectral overlap of the ~2.6 ppm citrate multiplet with the glutamine (Gln) multiplet centred at 2.46 ppm and the creatine plus phosphocreatine singlet (Cr) at 3.03 ppm, its high concentration in normal prostate allows for unedited observation with little interference from its neighbors. However, in cases of adenocarcinoma of the prostate when the citrate concentration can be at least ten-fold lower than normal (4), accurate detection of citrate becomes more vulnerable to interference from the neighboring resonances. In such cases, some form of citrate spectral editing could be advantageous.

Double quantum filtering (DQF) has already demonstrated its usefulness as an editing method for the weakly coupled spins of lactate in *in vivo* proton MRS (9,10). The immediate advantage of DQF is that all uncoupled resonances are drastically reduced in each scan, independently of chemical shift location, through the use of static magnetic field gradients. At first sight, a secondary advantage in the case of citrate is that the scalar coupling constant, J, between the methylene protons is much greater (15.4 Hz) than that normally encountered in the multiple spin systems of metabolites. This large J appears to provide a means to discriminate

---

[1] A version of this chapter has been accepted for publication. A.H. Wilman and P.S. Allen, *J. Magn. Reson.*, (1994).

against other coupled resonances such as the overlapping Gln peak, which couples to its neighboring spins with coupling constants of only 7.9 Hz and 3.6 Hz (11). Moreover, since the DQF sequence-evolution-time, τ, is chosen to be 1/2J in typical weak coupling applications (12), one might anticipate that effective DQF could be accomplished with a total sequence duration of as little as 65 ms in the citrate case, thus minimizing transverse relaxation losses.

The purpose of this study was to investigate the feasibility of detecting the strongly coupled AB system of citrate by means of a DQF sequence. In particular, this study evaluates how τ and the magnetic field strength affect the spectral response of the citrate multiplet, so that τ may be optimized at each field strength and so that the degree to which the large J facilitates sequence shortening can be determined.

The evolution-time dependence of an AB system response to an unrefocussed DQF sequence has previously been derived by density matrix calculations (13) and by product operator notation (14,15). Unlike previous work on DQF of an AB system, the filtering reported here, and illustrated in Fig. 6.1, is achieved by a pair of static magnetic field gradient pulses, where $G_2=\pm 2G_1$.

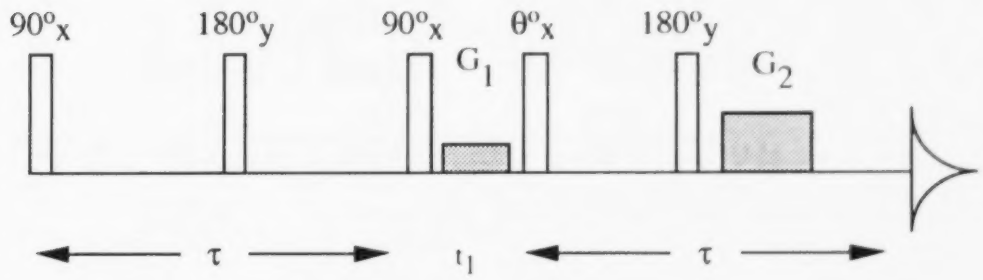

Figure 6.1 The pulse sequence used for double quantum filtering. G_1 and G_2 are static field gradient pulses with $G_2=2G_1$. The read pulse angle θ is variable yielding a maximum citrate signal intensity when $\theta=60°$. The t_1 time was 10 ms.

The response to this refocussed DQF sequence, when the read pulse angle θ is 90^o, has been derived using Eq. (28) of Ref. 14 and symmetry considerations to give the normalized τ dependence $f(\tau)$ shown in Eq. (6.1),

$$f(\tau)=(1/2)\{[(\delta\omega/\Lambda)^2 + (\pi J/\Lambda)^2\cos(\Lambda\tau)]\sin(\pi J\tau) - (\pi J/\Lambda)\sin(\Lambda\tau)\cos(\pi J\tau)\}^2 \quad (6.1)$$

where $\delta\omega=(\omega_A-\omega_B)/2$ is the chemical shift difference between the A and B spins, and $\Lambda=[\delta\omega^2 +(\pi J)^2]^{1/2}$ is the strong coupling frequency and where the normalization of $f(\tau)$ has been performed such that the total available citrate signal at each field strength following a single 90^o pulse is unity.

The response function $f(\tau)$ modulates the DQF signal in a manner that is illustrated in Fig. 6.2 for three values of $\delta\omega$ corresponding to field strengths of 1.5 T, 2.35 T and 4.0 T. Two points are clear from Fig. 6.2. First, the irregularities in the τ dependence of $f(\tau)$ emphasise the care needed in choosing a value for τ. Secondly, the proportion of the total available signal which is accessible at τ values short enough to limit transverse relaxation losses (ie. $\tau < T_2$ *in vivo*) varies markedly with field strength. This variation with field strength is sufficient, at some τ values, to exceed both the field dependence of the magnetization and the field dependence of the citrate intensity fraction appearing in the inner peaks of the AB multiplet (6,16). The predictions of Eq. (6.1)were verified experimentally at 2.35 T on a trilithium citrate solution (Fig. 6.2) and typical spectra are shown in Fig. (6.3). At 2.35 T, J was found to be 15.4 Hz, $\delta\omega=13.2\pi$ rad/s and the characteristic T_2 in solution was 400±40 ms. Both analysis and experiment, at 2.35 T, indicate that the maximum citrate intensity occurs when $\tau\sim1.3/J$ or 86 ms.

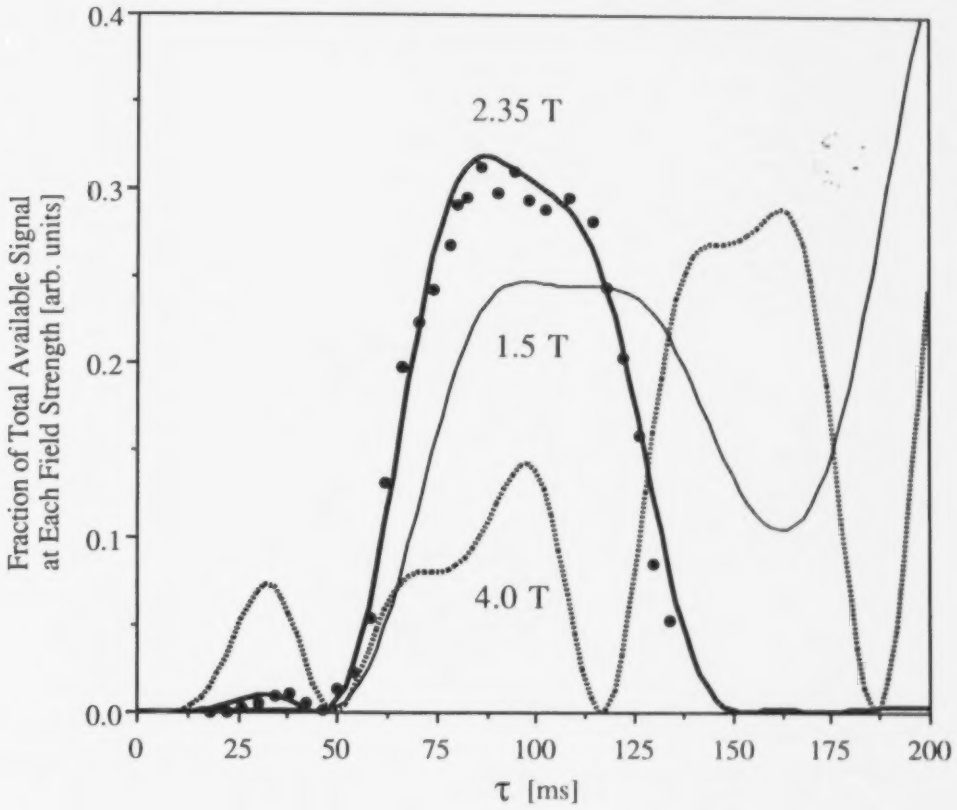

Figure 6.2 The τ time dependence of the fractional citrate signal intensity acquired from the DQF sequence of Fig.6.1 with $\theta=90^0$. The theoretical curves, illustrating the modulation due to $f(\tau)$ of Eq. (6.1), at 2.35 T (thick), 1.5 T (thin) and 4.0 T (dashed), represent the fraction of the total citrate signal available at each field strength. The theoretical curve for 2.35 T also includes the transverse relaxation decay using the measured solution T_2 at 2.35 T of 400 ms. The solid dots represent experimental data acquired at 2.35 T on a trilithium citrate phantom.

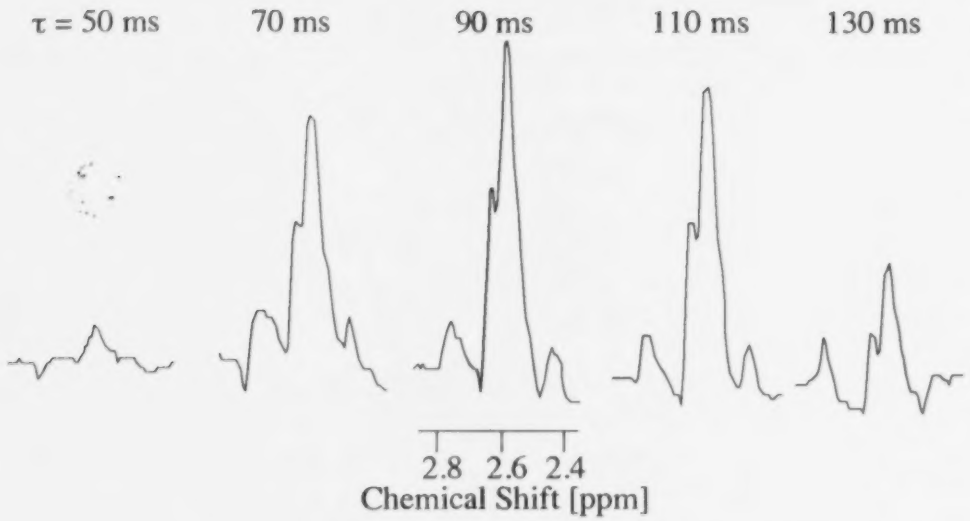

Figure 6.3 Proton spectra of citrate obtained on a trilithium citrate phantom at 2.35 T using the sequence of Fig. 6.1 with $\theta=90^o$ and $G_2=+2G_1$. The τ values are listed above each spectrum. The spectra all received the same phase correction. In some cases, the spectra do not seem perfectly phased because there is a portion of antiphase magnetization that also contributes to the signal.

The read pulse angle θ and the relative gradient polarity may also affect the citrate signal intensity. For example, with θ equal to 90^o and $G_2=\pm 2G_1$, only one half of the double quantum coherence will be converted into observable magnetization (17). However this yield may be increased by up to 30%, in a manner similar to that for an AX system, by changing θ to 60^o when $G_2=+2G_1$, or to 120^o when $G_2=-2G_1$ (18). Including transverse relaxation losses during the τ periods as well as the read pulse tip angle dependence and assuming both gradients have the same polarity, the normalized citrate intensity $S(\tau,\theta)$ is given by

$$S(\tau,\theta)=f(\tau)\sin\theta\,\cos^2(\theta/2)\exp(-2\tau/T_2)\,. \qquad (6.2)$$

Table 6.1 lists the quantitative results of a verification of this dependence of the citrate signal intensity on the read pulse angle and the relative gradient pulse polarity for the DQF sequence, where the optimal τ value of 1.3/J was used in the experiment.

Table 6.1

The Relative Citrate Signal Intensity Obtained in Solution At 2.35 T With the DQF Sequence of Fig. 6.1 for Various Read Pulse Angles and Gradient Polarities*

Pulse Sequence	Theoretical intensity $T_2=\infty$	Theoretical intensity T_2=400 ms	Experimental# intensity
(a) 90^o-acquire	1.00	1.00	1.00
(b) DQF with $\theta=90^o$ $G_2=+2G_1$	0.50	0.32	0.34
(c) DQF with $\theta=60^o$ $G_2=+2G_1$	0.65	0.42	0.44
(d) DQF with $\theta=90^o$ $G_2=-2G_1$	0.50	0.32	0.31
(e) DQF with $\theta=120^o$ $G_2=-2G_1$	0.65	0.42	0.39

* All DQF sequences used the optimal τ value for 2.35 T of 86 ms.
# The experimental data have an error of ±5% and were obtained from a trilithium citrate phantom.

In summary, we have established that the response of the AB system of citrate to a DQF sequence is critically dependent on the evolution time τ in a manner that is strongly field dependent. It follows from the dependencies of this response that at typical *in vivo* field strengths it would be inappropriate to base the choice of τ on criteria that are valid in the weak coupling approximation, i.e. that $\tau=1/2J\sim32.5$ ms. Moreover at 1.5 T and 4.0 T, the sequence lengths for maximum signal are much greater than the T_2 that one might expect for citrate protons in the prostate, and hence, *in vivo* DQF is unlikely to be considered useful at these field strengths because of the substantial loss of signal intensity. Even at 2.35 T, where the optimal τ is 86 ms, significant T_2 attenuation will decrease the signal maximum. For example, assuming a liberal *in vivo* T_2 of 200 ms, the 65% maximum of the DQF sequence at τ=86 ms would be reduced to 28% of the total citrate signal. In conclusion therefore, the promise of short DQF sequences for citrate detection, suggested at first sight by the large coupling constant, is in fact negated by the effects of the strong coupling regime active at *in vivo* field strengths.

6.1 References

1. K.R. Halliday, C.Fenoglio-Preiser, and L.O. Sillerud, *Magn. Reson Med.* **7**, 384 (1988).
2. L.O. Sillerud, K.R. Halliday, R.H. Griffey, C. Fenoglio, and S. Sheppard, *Magn. Reson Med.* **8**, 224 (1988).
3. M.E. Yacoe, G. Sommer, and D. Peehl, *Magn. Reson Med.* **19**, 429 (1991).
4. J. Kurhanewicz, R. Dahiya, J.M. Macdonald, L.H. Chang, T.L. James, and P. Narayan, *Magn. Reson Med.* **29**, 149 (1993).
5. M.L. Schliebler, K.K. Miyamoto, M. White, S.J. Maygarden, and J.L. Mohler, *Magn. Reson Med.* **29**, 285 (1993).
6. F. Schick, H. Bongers, S. Kurz, W.I. Jung, M. Pfeffer and O. Lutz, *Magn. Reson Med.* **29**, 38 (1993).
7. T.G. Pretlow, B.E. Harris, E.L. Bradley, *Cancer Research* **45**, 442 (1985)
8. J.A. Sanders, D.M. Thomasson, and L.O. Sillerud, *in* "Society of Magnetic Resonance in Medicine, Eleventh Annual Meeting,1992" p. 3305.
9. C.H. Sotak,D.M. Freeman, and R.E. Hurd, *J. Magn. Res.*, **78**, 355 (1988).
10. R.E. Hurd, and D.M. Freeman, *Proc. Natl. Acad. Sci. USA* **86,** 4402 (1989).
11. K.L. Behar, and T. Ogino, *Magn. Reson Med.* **17**, 285 (1991).
12. R.R. Ernst, G. Bodenhausen, and A. Wokaun,"Principles of Nuclear Magnetic Resonance in One and Two Dimensions," Carendon Press, Oxford,1987.
13. A. Bax, and R. Freeman, *J. Magn. Res.*, **41**, 507 (1980).
14. L.E. Kay, and R.E.D. McClung, *J. Magn. Res.*, **77**, 258 (1988).
15. T. Nakai, and C.A. McDowell, *Molecular Phys.* (in press).
16. E.D. Becker, " High Resolution NMR," Academic Press, Orlando, 1980.
17. L.A. Trimble, J.F. Shen, A.H. Wilman, and P.S. Allen, *J. Magn. Res.*, **86,** 191 (1990).
18. J.F. Shen, and P.S. Allen, *J. Magn. Res.*, **90,** 606 (1990).

Chapter 7

Observing N-acetylaspartate Via Both Its N-acetyl and Its Strongly Coupled Aspartate Groups In *In Vivo* Proton Magnetic Resonance Spectroscopy[1]

7.1 Introduction

The brain metabolite N-acetyl aspartate (NAA) is suspected of being a specific indicator of neuronal dysfunction in the mature mammalian brain (1-6). Using *in vivo* proton magnetic resonance spectroscopy (MRS), changes in the level of NAA can be monitored noninvasively to provide information that is potentially a measure of neuronal viability. For example, using proton MRS, decreased NAA levels in adult humans have been linked to neuronal loss in chronic infarcts (7-9), intracranial tumors (10), epileptogenic foci (11), chronic multiple sclerosis plaques (12), and other cerebral disorders (13). Changes in the NAA level have also been recorded for various metabolic disorders in infants (13,14). However, in the developing brain, NAA may not be solely confined to neurons, since it is also known to exist in some types of glial precursor cells (6). Nevertheless, in the adult human brain, a large body of evidence does support a high correlation between the level of NAA and neuronal viability.

In *in vivo* proton MRS, NAA is usually quantified by means of its 2.02 ppm methyl singlet. Underlying this singlet are multiplet resonances of glutamate, centred at 2.06 ppm, and to a lesser extent glutamine, centred at 2.14 ppm. In addition, resonances from other metabolite molecules with acetyl groups may also appear in this 2.0 ppm region. For example, in white matter, the acetyl group of N-acetylaspartylglutamate (NAAG) appears at 2.05 ppm (15). At typical *in vivo* field strengths (1.5 T), separation of the 2.02 ppm peak into NAA and NAAG components is unikely to be successful because of the high degree of overlap. Moreover, in cases of severe neuronal loss where the NAA level is low, spectral overlap from glutamate will further degrade the reliability of NAA quantification based solely on its 2.02 ppm singlet.

---

[1] A version of this chapter has been submitted for publication. A.H. Wilman and P.S. Allen, *J. Magn. Reson.* (1994).

Potentially, a more reliable method of quantification is to take advantage of all of the resonances of NAA (16-18), which include not only the 2.02 ppm methyl singlet, but also the ABX system with the AB aspartate multiplet centred at 2.60 ppm, and the X aspartate multiplet at 4.40 ppm. Although observation of the 4.40 ppm resonance is, of course, unrealistic *in vivo* due to the overlapping water resonance, the 2.60 ppm multiplet can be clearly observed, though it has not usually been considered in the NAA quantification process in practice. Nevertheless, Provencher has demonstrated that, despite minor interference at 2.60 ppm from aspartate (2.76 ppm) and glutamine (2.46 ppm), the NAA and NAAG components may be separated if both the 2.02 ppm N-acetyl singlet and the 2.60 ppm aspartyl resonances are employed (16).

The 2.6 ppm aspartate multiplet of NAA can thus provide crucial information for the quantification process. However, in response to either the PRESS (19-21) or the STEAM sequence(22), this multiplet exhibits complex echo-time, TE, modulations, and thus if a poor choice of TE is made, the utility of this multiplet can easily be compromised by low signal-to-noise. The goal of this paper is therefore to evaluate the complex echo time modulations of the intensities of the NAA 2.6 ppm aspartate multiplet in response to typical localization techniques in order to quantify the observable NAA spectrum. It will also be shown that these modulations are extraordinarily field-dependent, and that, somewhat fortuitously, 1.5 T is an excellent choice of field strength to observe the aspartate multiplet at long TE.

7.2 Theory

The 2.60 ppm multiplet of NAA originates from two strongly coupled spins (J=15.5 Hz) that form the AB part of the aspartyl ABX spin system. The shape of this multiplet, at various field strengths, is illustrated in Fig. 7.1.

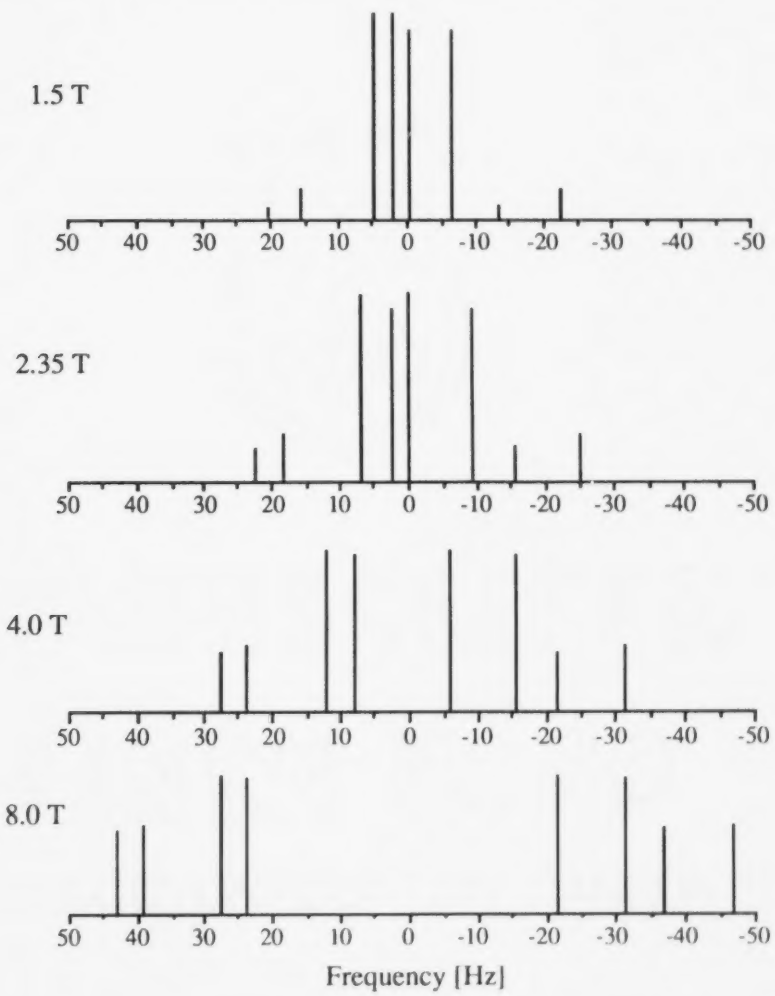

Figure 7.1 Schematic in-phase stick spectra from the AB part of the ABX system of NAA at four different field strengths. For each spectrum, the sum of all the spectral lines was normalized to the same value.

In order to analyze this a strongly coupled multiplet, we have used the product operator description of an ABX system as outlined by Kay and McClung (23),

wherein the Hamiltonian for the evolution of an ABX system under Zeeman and strong scalar coupling is split into two commuting parts, $\mathcal{H}_0$ and $\mathcal{H}_1$:

$$\mathcal{H}_0 = \overline{\omega}\,(A_Z + B_Z) + \omega_X X_Z + 2\pi\, J_{AB} A_Z B_Z + 2\pi\, \overline{J}\,(A_Z + B_Z) X_Z \qquad (7.1)$$

$$\mathcal{H}_1 = \delta\omega\,(A_Z - B_Z) + 2\pi\delta J (A_Z - B_Z) X_Z - 2\pi\, J_{AB}(A_+ B_- + A_- B_+) \qquad (7.2)$$

where A_m, B_m and X_m are the m components of the spherical spin angular momentum operators (24, 25) with m = +, -, z for spins A, B and X. Also in Eqs. [1] and [2], ω_X represents the resonance frequency of the X spin; and $\delta\omega$ and $\overline{\omega}$ represent, respectively, the chemical shift difference and the average chemical shift between the A and B spins such that $\delta\omega=(\omega_A-\omega_B)/2$, and $\overline{\omega}=(\omega_A+\omega_B)/2$. In addition, δJ and $\overline{J}$, represent the difference and average of the coupling constants between the X spin and the A and B spins and are defined as $\delta J=(J_{AX} - J_{BX})/2$ and $\overline{J} = (J_{AX} + J_{BX})/2$.

As an example of the resulting product operator transformation equations, we list in Eqs. (7.3) and (7.4), the result of the evolution of the transverse magnetization operator A_+ under each part of the Hamiltonian, namely, $\mathcal{H}_0$ and $\mathcal{H}_1$

$$A_+ \xrightarrow{\mathcal{H}_0 t} A_+ g_1(t) + 2A_+B_Z g_2(t) + 2A_+X_Z g_3(t) + 4A_+B_Z X_Z g_4(t) \qquad (7.3)$$

$$A_+ \xrightarrow{\mathcal{H}_1 t} A_+ f_1(t) + 2A_+X_Z f_2(t) + 2A_Z B_+ f_3(t) + 4A_Z B_+ X_Z f_4(t) \qquad (7.4)$$

where the time dependent coefficients f and g are as defined in Ref. 23, namely,

$$\begin{aligned}
f_1(t) &= (1/4)\{c_-\exp(i\Lambda_+ t) + c_+\exp(-i\Lambda_+ t) + d_-\exp(i\Lambda_- t) + d_+\exp(-i\Lambda_- t)\} \\
f_2(t) &= (1/4)\{c_-\exp(i\Lambda_+ t) + c_+\exp(-i\Lambda_+ t) - d_-\exp(i\Lambda_- t) - d_+\exp(-i\Lambda_- t)\} \\
f_3(t) &= (i/2)\{(\pi J/\Lambda_+)\sin(\Lambda_+ t) + (\pi J/\Lambda_-)\sin(\Lambda_- t)\} \\
f_4(t) &= (i/2)\{(\pi J/\Lambda_+)\sin(\Lambda_+ t) - (\pi J/\Lambda_-)\sin(\Lambda_- t)\}
\end{aligned} \qquad (7.5a)$$

with,

$$\Lambda_{\pm}=[(\delta\omega\pm\pi\delta J)^2+(\pi J_{AB})^2]^{1/2}\ ,\ c_{\pm} = 1 \pm (\delta\omega+ \pi\delta J)/\Lambda_{+}\ ,\ d_{\pm} = 1 \pm (\delta\omega-\pi\delta J)/\Lambda_{-} \quad (7.5b)$$

and

$$\begin{aligned} g_1(t) &= \cos(\pi \bar{J} t)\cos(\pi J_{AB} t)\exp(-i\,\bar{\omega}\, t) \\ g_2(t) &= -i\cos(\pi \bar{J} t)\sin(\pi J_{AB} t)\exp(-i\,\bar{\omega}\, t) \\ g_3(t) &= -i\sin(\pi \bar{J} t)\cos(\pi J_{AB} t)\exp(-i\,\bar{\omega}\, t) \\ g_4(t) &= -\sin(\pi \bar{J} t)\sin(\pi J_{AB} t)\exp(-i\,\bar{\omega}\, t)\ . \end{aligned} \quad (7.5c)$$

Because changes in coherence order will only occur during radiofrequency pulses (25-27), the coherence order here, like that in weakly coupled systems, is not affected by evolution under $\mathcal{H}_0$ or $\mathcal{H}_1$. However, unlike weakly coupled systems, exchange between in-phase A and antiphase B magnetization can take place during evolution under $\mathcal{H}_1$, through the coefficients f_3 and f_4. In the weak coupling limit of $\delta\omega >> \pi J_{AB}$, f_3 and f_4 are zero, as one would expect. Eqs. (7.3) and (7.4) may also be reduced to those for a strongly coupled AB system by setting $\delta J = \bar{J} = 0$ ($J_{AX}=J_{BX}=0$), which reduces the coefficients g_3 and g_4, as well as f_3 and f_4, to zero.

The PRESS and STEAM sequences used both for the theoretical analysis and the experimental verification, are illustrated in Fig. 7.2. In the following analysis, the effects of longitudinal relaxation have been neglected, but the effects of transverse relaxation have been accounted for in the Results section. Perfect quadrature detection was assumed so that the observable signals are associated with only the -1 coherence levels in the product operator representation (25, 27). Only the detectable A and B magnetization of the ABX system was considered because the initial longitudinal X magnetization at 4.40 ppm will be largely destroyed during the water suppression which normally precedes the *in vivo* localization sequence (28,29). It is thus appropriate to begin the analysis of each sequence with the initial density operator, σ, containing no X term as follows,

$$\sigma(0)= A_Z+B_Z\ . \quad (7.6)$$

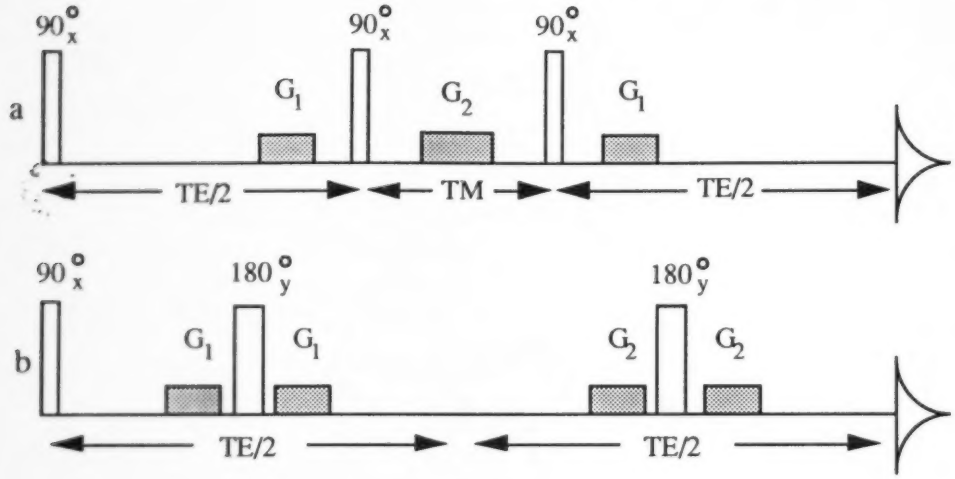

Figure 7.2 The pulse sequences used for both theoretical and *in vitro* experimental analysis of the PRESS and STEAM localization sequences. G_1 and G_2 are field gradient pulses. Panel (a) is an approximation of the STEAM sequence and panel (b) is an approximation of the PRESS sequence. The STEAM sequence was performed with TM=5.4 ms. For water suppression, both sequences were preceded by a selective 1331 binomial pulse on the water resonance followed by a 5 ms duration, 10 G/cm dephasing gradient pulse with a 10 ms settling time.

7.2.1 Spin Echo

The response of the 2.6 ppm NAA multiplet to a simple spin-echo sequence $\{90^o_x\text{- }\tau\text{ -}180^o_y\text{- }\tau\text{- acquire}\}$ was considered first. Immediately after the initial 90^o_x radiofrequency (rf) pulse, the density operator becomes

$$\sigma(0^+)= (-i/\sqrt{2})\,(A_+ + A_- + B_+ + B_-) \quad . \tag{7.7}$$

The -1 coherence states produced by this pulse can be neglected, since they will be converted to unobservable +1 states following the suceeding 180^o_y pulse. Using Table 3 of Ref. (23) it can be shown that at the end of the first τ period, the terms of interest in Eq. (7.7) will have evolved into

$$\begin{aligned}\sigma(\tau)= (-i/\sqrt{2})\,[&A_+c_1(\tau) + B_+c_2(\tau) + 2A_+X_Zc_3(\tau) + 2B_+X_Zc_4(\tau) + 2A_ZB_+c_5(\tau) \\ &+ 2A_+B_Zc_6(\tau) + 4A_ZB_+X_Zc_7(\tau) + 4A_+B_ZX_Zc_8(\tau)] \quad ,\end{aligned} \tag{7.8}$$

where

$$c_1(\tau)=g_1(\tau)f_1(\tau) + g_2(\tau)f_3(\tau) + g_3(\tau)f_2(\tau) + g_4(\tau)f_4(\tau)$$
$$c_2(\tau)=g_1(\tau)f_1(-\tau) + g_2(\tau)f_3(\tau) + g_3(\tau)f_2(-\tau) + g_4(\tau)f_4(\tau)$$
$$c_3(\tau)=g_1(\tau)f_2(\tau) + g_2(\tau)f_4(\tau) + g_3(\tau)f_1(\tau) + g_4(\tau)f_3(\tau)$$
$$c_4(\tau)=g_1(\tau)f_2(-\tau) + g_2(\tau)f_4(\tau) + g_3(\tau)f_1(-\tau) + g_4(\tau)f_3(\tau)$$
$$c_5(\tau)=g_1(\tau)f_3(\tau) + g_2(\tau)f_1(-\tau) + g_3(\tau)f_4(\tau) + g_4(\tau)f_2(-\tau).$$
$$c_6(\tau)=g_1(\tau)f_3(\tau) + g_2(\tau)f_1(\tau) + g_3(\tau)f_4(\tau) + g_4(\tau)f_2(\tau)$$
$$c_7(\tau)=g_1(\tau)f_4(\tau) + g_2(\tau)f_2(-\tau) + g_3(\tau)f_3(\tau) + g_4(\tau)f_1(-\tau)$$
$$c_8(\tau)=g_1(\tau)f_4(\tau) + g_2(\tau)f_2(\tau) + g_3(\tau)f_3(\tau) + g_4(\tau)f_1(\tau)\ . \qquad (7.9)$$

Following the 180^o_y pulse, Eq. (7.8) becomes

$$\sigma(\tau^+)= (-i/\sqrt{2})\ [A_-c_1(\tau) + B_-c_2(\tau) - 2A_-X_Zc_3(\tau) - 2B_-X_Zc_4(\tau) - 2A_ZB_-c_5(\tau)$$
$$- 2A_-B_Zc_6(\tau) + 4A_ZB_-X_Zc_7(\tau) + 4A_-B_ZX_Zc_8(\tau)]\ . \qquad (7.10)$$

Evolution during a further period τ will give rise to observable inphase magnetization and, assuming that the receiver is aligned along the -y axis, the detectable multiplet signal S will be determined by the operator $(i/\sqrt{2})(A_-+B_-)$. Thus during the second τ period, we are concerned with evolution *into* the inphase states A_- and B_-, which is the reverse of the first τ period (Eq. (7.8)) where we were concerned with evolution *from* the inphase states A_+ and B_+. By making use of the symmetry of the strong coupling equations in Table 3 of Ref. (23), we may immediately write down the observable AB multiplet signal, S, at the end of this second τ period

$$S(2\tau) = 0.5\ [c_1(\tau)c_1(-\tau) + c_2(\tau)c_2(-\tau) - c_3(\tau)c_3(-\tau) - c_4(\tau)c_4(-\tau) - c_5(\tau)c_5(-\tau)$$
$$- c_6(\tau)c_6(-\tau) + c_7(\tau)c_7(-\tau) + c_8(\tau)c_8(-\tau)]\ , \qquad (7.11)$$

where S is normalized, such that the maximum available multiplet signal is one. Upon substitution of the various coefficients, Eq. (7.11) yields

$$S(2\tau) = \cos(2\pi\ \bar{J}\tau)\cos(2\pi\ J_{AB}\tau)$$
$$\{\cos(\Lambda_+\tau)\cos(\Lambda_-\tau) + [(\delta\omega^2 - (\pi\delta J)^2 - (\pi J_{AB})^2)/(\Lambda_+\Lambda_-)]\ \sin(\Lambda_+\tau)\sin(\Lambda_-\tau)\}$$
$$+ \cos(2\pi\ \bar{J}\tau)\ \sin(2\pi\ J_{AB}\tau)$$
$$[(\pi J_{AB}/\Lambda_+)\sin(\Lambda_+\tau)\cos(\Lambda_-\tau) + (\pi J_{AB}/\Lambda_-)\sin(\Lambda_-\tau)\cos(\Lambda_+\tau)] \qquad (7.12)$$

When $\Lambda_{\pm} >> \pi J_{AB}$, Eq. (7.12) reduces to the appropriate weak coupling response of

$$S_{weak}(2\tau) = \cos(2\pi J_{AB}\tau)\cos(2\pi \bar{J}\tau)\cos(2\pi\delta J\tau)$$
$$= 0.5 \cos(2\pi J_{AB}\tau)\,[\cos(2\pi J_{AX}\tau)+\cos(2\pi J_{BX}\tau)] \quad , \qquad (7.13)$$

and in addition, by setting $\bar{J}=\delta J=0$, Eq. (7.12) reduces to the correct equation for the spin-echo response of an AB system (23).

7.2.2 STEAM

In the STEAM sequence illustrated in Fig. 7.2a, the effect of gradient dephasing during the first TE/2 period, from the gradient pulse G_1, will be corrected in the second TE/2 period, provided the initial coherence order is inverted prior to the second G_1 gradient pulse. Since only the -1 coherence states are observable,we may account for the net effect of the two G_1 gradient pulses by initially considering only the +1 coherence states. At the end of the first 90^o-TE/2 period, the density operator may thus be described by Eq. (7.8) with τ=TE/2. Following the second 90^o_x pulse and the application of the dephasing TM gradient pulse G_2, only the gradient-insensitive longitudinal and zero quantum coherence terms need be considered. These terms are

$$\sigma(TE/2^+) = -0.5\,[A_Zc_1(\tau) + B_Zc_2(\tau) + (A_+X_- - A_-X_+)c_3(\tau)+(B_+X_- - B_-X_+)c_4(\tau)$$
$$+ (B_+A_- - B_-A_+)c_5(\tau)+ (A_+B_- - A_-B_+)c_6(\tau)$$
$$- 2B_Z(A_+X_- + A_-X_+)c_7(\tau) - 2A_Z(B_+X_- + B_-X_+)c_8(\tau)] \quad . \qquad (7.14)$$

If the TM interval is chosen such that $\cos(2\Lambda_{\pm}TM)=1$, TM modulations in the terms in Eq. (7.14) that do not include X contributions, may be eliminated (23). The effect of the TM evolution on the remaining zero quantum X terms (A_+X_-, $A_ZB_+X_-$, etc.) is unknown, since a product operator description of the zero quantum X terms of an ABX system has yet to be elucidated. (Ref. 23 only derived the transformational equations for the ±1 coherences of the X part of an ABX system.) For the purposes of this analysis, we will assume that the TM interval is short so that minimal J coupling evolution takes place before the final 90^o pulse. Immediately after this final 90^o_x read pulse, the density operator becomes,

$$\sigma(TE/2+TM^{+}) = (0.5i/\sqrt{2})\ \{A_{-}c_1(\tau) + B_{-}c_2(\tau) - A_{-}X_Zc_3(\tau) - B_{-}X_Zc_4(\tau) - A_ZB_{-}\ [c_5(\tau) - c_6(\tau)] - A_{-}B_Z[c_6(\tau) - c_5(\tau)] + 2A_ZB_{-}X_Zc_7(\tau) + 2A_{-}B_ZX_Zc_8(\tau)\}\ . \qquad (7.15)$$

Following further evolution for a time τ=TE/2, we may again use the symmetry of the equations to arrive at the net signal S(TE+TM),

$$S(TE+TM) = 0.25\{c_1(\tau)c_1(-\tau) + c_2(\tau)c_2(-\tau) - 0.5c_3(\tau)c_3(-\tau) - 0.5c_4(\tau)c_4(-\tau) - 0.5\ [c_5(\tau)-c_6(\tau)]c_5(-\tau) - 0.5\ [c_6(\tau)-c_5(\tau)]c_6(-\tau) + 0.5c_7(\tau)c_7(-\tau) + 0.5c_8(\tau)c_8(-\tau)\}\ , \qquad (7.16)$$

where it is assumed that the receiver is aligned along the +y axis, (as opposed to the -y for the spin-echo and PRESS sequences) in order to yield an initially positive result. After a lengthy simplification, Eq. (7.16) may be rewritten as,

$$\begin{aligned} S(TE+TM) = {} & 0.25\cos(2\pi\,\bar{J}\tau)\cos(2\pi\,J_{AB}\tau)\{\cos(\Lambda_+\tau)\cos(\Lambda_-\tau) \\ & + [(1.5\delta\omega^2 - 1.5(\pi\delta J)^2 - (\pi J_{AB})^2)/(\Lambda_+\Lambda_-)]\sin(\Lambda_+\tau)\sin(\Lambda_-\tau)\} \\ & +0.25\cos(2\pi\,\bar{J}\tau)\sin(2\pi\,J_{AB}\tau) \\ & [(\pi\,J_{AB}/\Lambda_+)\sin(\Lambda_+\tau)\cos(\Lambda_-\tau) + (\pi\,J_{AB}/\Lambda_-)\sin(\Lambda_-\tau)\cos(\Lambda_+\tau)] \\ & +0.125\cos(2\pi\bar{J}\tau)\{\cos(\Lambda_+\tau)\cos(\Lambda_-\tau) + [(\pi J_{AB})^2/(\Lambda_+\Lambda_-)] \\ & \sin(\Lambda_+\tau)\sin(\Lambda_-\tau)\} \\ & +0.125 \\ & -0.125\sin^2(\pi J_{AB}\tau)\{[(\delta\omega + \pi\delta J)/\Lambda_+]^2\sin^2(\Lambda_+\tau) \\ & +[(\delta\omega - \pi\delta J)/\Lambda_-]^2\sin^2(\Lambda_-\tau)\}. \end{aligned} \qquad (7.17)$$

When $\Lambda_{\pm} >> \pi J_{AB}$, Eq. (7.17) reduces to the appropriate weak coupling response of

$$\begin{aligned} S_{weak}(TE+TM) = {} & 0.125\{\cos(\pi\,J_{AB}TE)\,[\cos(\pi\,J_{AX}TE) + \cos(\pi\,J_{BX}TE)] \\ & +\cos^2(\pi\,J_{AB}TE/2)\,[\cos^2(\pi\,J_{AX}TE/2) + \cos^2(\pi\,J_{BX}TE/2)] \\ & +2\sin^2(\pi\,J_{AB}TE/2)\cos(\pi\,J_{AX}TE/2)\cos(\pi\,J_{BX}TE/2)\cos(\delta\omega TE)\}. \end{aligned} \qquad (7.18)$$

In addition, by setting $\bar{J}$=δJ=0, Eq. (7.17) reduces to the equation for an AB system that has been derived elsewhere (30) .

7.2.3 PRESS

In the case of the PRESS sequence, illustrated in Fig. 7.2b, only the terms that have coherence order of -1 in the first TE/4 period need to be considered, since the +1 states will not be observable at the time of acquisition. Moreover, for the purposes of this analysis, the gradient pulses G_1 and G_2 need not be considered since these pulses simply ensure the dephasing of any coherence that does not receive complete inversion by each of the 180° pulses. Thus, immediately following the first $180°_y$ pulse at the end of the first τ_1=TE/4 period, the system has evolved into an expression somewhat similar to Eq. (7.10) of the spin-echo case,

$$\sigma(\tau_1)= (-i/\sqrt{2}) [A_+c_1(-\tau_1) + B_+c_2(-\tau_1) - 2A_+X_Zc_3(-\tau_1) - 2B_+X_Zc_4(-\tau_1) - 2A_ZB_+c_5(-\tau_1) - 2A_+B_Zc_6(-\tau_1) + 4A_ZB_+X_Zc_7(-\tau_1) + 4A_+B_ZX_Zc_8(-\tau_1)] \quad (7.19)$$

Now during the next TE/2 period, each of the eight terms in Eq. (7.19) evolves into sixteen different terms, none of which can be neglected. Because of the complexity of this evolution, we will treat the effects of $\mathcal{H}_1$ and $\mathcal{H}_0$ separately. Following evolution under only the influence of $\mathcal{H}_1$ for a further time τ_2=TE/2, one obtains

$$\sigma_1(\tau_1+\tau_2)= (-i/\sqrt{2}) [A_+d_1(\tau) + B_+d_2(\tau) + 2A_+X_Zd_3(\tau) + 2B_+X_Zd_4(\tau) + 2A_ZB_+d_5(\tau) + 2A_+B_Zd_6(\tau) + 4A_ZB_+X_Zd_7(\tau) + 4A_+B_ZX_Zd_8(\tau)] \quad (7.20)$$

where $\tau=\tau_1+\tau_2$=3TE/4, and the coefficients d_n, n=1,8 are given by

$$\begin{aligned}
d_1(\tau)&= f_1(\tau_2)c_1(-\tau_1) - f_2(\tau_2)c_3(-\tau_1) - f_3(\tau_2)c_5(-\tau_1) + f_4(\tau_2)c_7(-\tau_1)\\
d_2(\tau)&= f_1(-\tau_2)c_2(-\tau_1) - f_2(-\tau_2)c_4(-\tau_1) - f_3(\tau_2)c_6(-\tau_1) + f_4(\tau_2)c_8(-\tau_1)\\
d_3(\tau)&=-f_1(\tau_2)c_3(-\tau_1) + f_2(\tau_2)c_1(-\tau_1) + f_3(\tau_2)c_7(-\tau_1) - f_4(\tau_2)c_5(-\tau_1)\\
d_4(\tau)&=-f_1(-\tau_2)c_4(-\tau_1) + f_2(-\tau_2)c_2(-\tau_1) + f_3(\tau_2)c_8(-\tau_1) - f_4(\tau_2)c_6(-\tau_1)\\
d_5(\tau)&=-f_1(-\tau_2)c_5(-\tau_1) + f_2(-\tau_2)c_7(-\tau_1) + f_3(\tau_2)c_1(-\tau_1) - f_4(\tau_2)c_3(-\tau_1)\\
d_6(\tau)&=-f_1(\tau_2)c_6(-\tau_1) + f_2(\tau_2)c_8(-\tau_1) + f_3(\tau_2)c_2(-\tau_1) - f_4(\tau_2)c_4(-\tau_1)\\
d_7(\tau)&= f_1(-\tau_2)c_7(-\tau_1) - f_2(-\tau_2)c_5(-\tau_1) - f_3(\tau_2)c_3(-\tau_1) + f_4(\tau_2)c_1(-\tau_1)\\
d_8(\tau)&= f_1(\tau_2)c_8(-\tau_1) - f_2(\tau_2)c_6(-\tau_1) - f_3(\tau_2)c_4(-\tau_1) + f_4(\tau_2)c_2(-\tau_1)\,. \quad (7.21)
\end{aligned}$$

Further evolution under $\mathcal{H}_0$ for the same τ_2=TE/2 period, followed by the application of the last $180°_y$ pulse, yields

$$\sigma_1(\tau_1+\tau_2)= (-i/\sqrt{2})\,[A_p_1(\tau) + B_p_2(\tau) - 2A_X_Zp_3(\tau) - 2B_X_Zp_4(\tau) - 2A_ZB_p_5(\tau) - 2A_B_Zp_6(\tau) + 4A_ZB_X_Zp_7(\tau) + 4A_B_ZX_Zp_8(\tau)] \quad , \qquad (7.22)$$

where

$$\begin{aligned}
p_1(\tau)&=g_1(\tau_2)d_1(\tau) + g_2(\tau_2)d_6(\tau) + g_3(\tau_2)d_3(\tau) + g_4(\tau_2)d_8(\tau)\\
p_2(\tau)&=g_1(\tau_2)d_2(\tau) + g_2(\tau_2)d_5(\tau) + g_3(\tau_2)d_4(\tau) + g_4(\tau_2)d_7(\tau)\\
p_3(\tau)&=g_1(\tau_2)d_3(\tau) + g_2(\tau_2)d_8(\tau) + g_3(\tau_2)d_1(\tau) + g_4(\tau_2)d_6(\tau)\\
p_4(\tau)&=g_1(\tau_2)d_4(\tau) + g_2(\tau_2)d_7(\tau) + g_3(\tau_2)d_2(\tau) + g_4(\tau_2)d_5(\tau)\\
p_5(\tau)&=g_1(\tau_2)d_5(\tau) + g_2(\tau_2)d_2(\tau) + g_3(\tau_2)d_7(\tau) + g_4(\tau_2)d_4(\tau)\\
p_6(\tau)&=g_1(\tau_2)d_6(\tau) + g_2(\tau_2)d_1(\tau) + g_3(\tau_2)d_8(\tau) + g_4(\tau_2)d_3(\tau)\\
p_7(\tau)&=g_1(\tau_2)d_7(\tau) + g_2(\tau_2)d_4(\tau) + g_3(\tau_2)d_5(\tau) + g_4(\tau_2)d_2(\tau)\\
p_8(\tau)&=g_1(\tau_2)d_8(\tau) + g_2(\tau_2)d_3(\tau) + g_3(\tau_2)d_6(\tau) + g_4(\tau_2)d_1(\tau) \quad . \qquad (7.23)
\end{aligned}$$

The evolution during the final τ_3=TE/4 period, follows from symmetry with the first TE/4 period yielding a net signal S of,

$$S(TE) = 0.5\,[c_1(-\tau_3)p_1(\tau) + c_2(-\tau_3)p_2(\tau) - c_3(-\tau_3)p_3(\tau) - c_4(-\tau_3)p_4(\tau) - c_5(-\tau_3)p_5(\tau) - c_6(-\tau_3)p_6(\tau) + c_7(-\tau_3)p_7(\tau) + c_8(-\tau_3)p_8(\tau)] \quad . \qquad (7.24)$$

This result reduces to the same weak coupling approximation as in the spin-echo case of Eq. (7.13), and its reduction to an AB system also agrees with the PRESS calculation in Ref. 30. We have not reduced Eq. (7.24) to an expression involving only multiples of sine and cosine terms, because the reduction would require at least 131 072 addition and multiplication operations, (assuming that two such operations are required to reduce an f or g coefficient to a sine or cosine expression) which is 64 times more complicated than the reduction of the spin-echo or STEAM results.

7.3 Methods and Results

An experimental test of the response of the ~2.6 ppm NAA multiplet to the spin-echo, PRESS and STEAM sequences was carried out at 2.35 T on a pH balanced phantom (100 mM) solution of NAA in D_2O. As a prelude to these tests, a one pulse acquire spectrum was used to determine the parameters J_{AB} (15.5 Hz), J_{AX} (10.1Hz), J_{BX} (3.7 Hz), and $\delta\omega$ (-19.3π rad/s). Substituting for these parameters, the strong coupling frequencies, $\Lambda_{\pm}$, are Λ_{-}=27.5π rad/s and Λ_{+}=22.6π rad/s. In addition, the transverse relaxation time, T_2, was measured to be 730 $\pm$ 30 ms, by fitting the theoretical and experimental spin-echo responses at 2.35 T. This T_2, has been incorporated into all of the theoretical curves.

The PRESS and STEAM sequences used for the *in vitro* experiments were exactly as shown in Fig. 7.2. The spin-echo sequence used was {90^o_x -TE/2- 180^o_y - TE/2 - acquire}. All sequences were preceded by a water suppresion procedure that was accomplished by applying a frequency selective 90° pulse (binomial 1331) to the water resonance followed by a strong dephasing gradient pulse. The bandwidth of the selective pulse ensured that the 4.40 ppm X resonance of NAA was also suppressed, while the 2.6 ppm AB resonances were unaffected.

Fig. 7.3 provides a comparison of the integrated intensity of the 2.6 ppm multiplet at 2.35 T (100 MHz) to the spin-echo and the PRESS sequences. The analytical equations and the experimental data, namely Eq. (7.12) and (*) for the spin-echo, and Eq. (7.24) and (+) for PRESS, are shown in this figure. In addition, Eq. (7.13), which is the theoretical weak coupling response to both sequences, is also plotted.

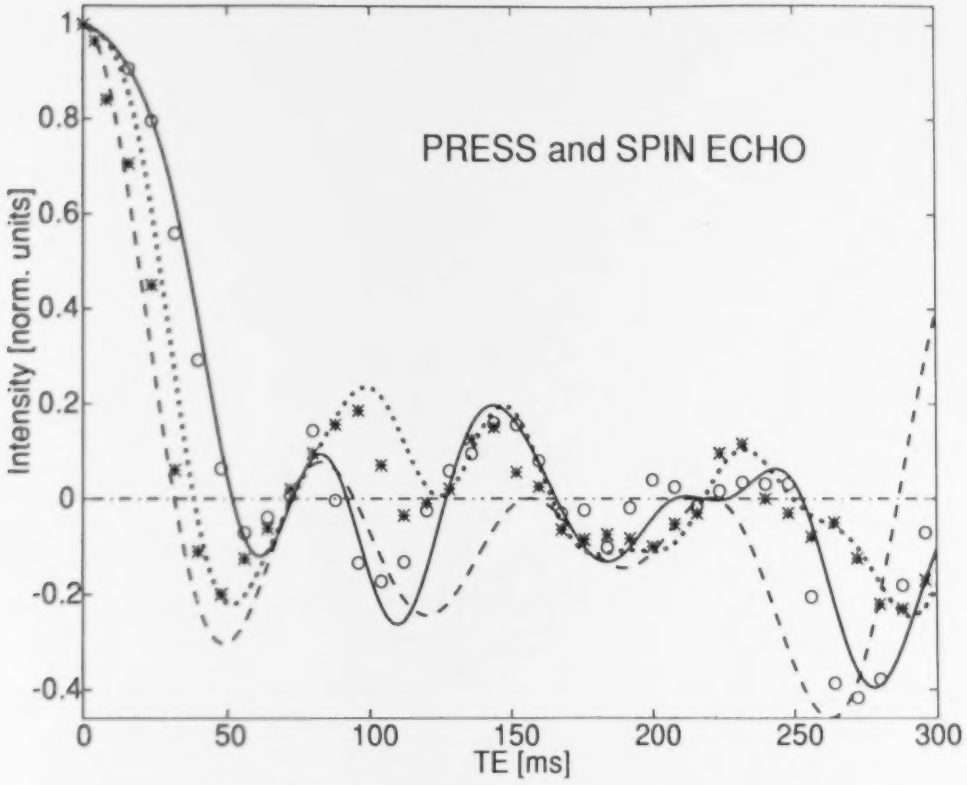

Figure 7.3 An illustration of the TE dependence of the NAA AB multiplet intensity acquired at 100 MHz in response to a spin-echo or the PRESS sequence of Fig. 7.2(b). • • • calculated spin-echo response [Eq. (7.12)], and (*) the spin-echo experimental data; — calculated PRESS response [Eq. (7.24)], and (o) experimental PRESS response; – – the weak coupling approximation [Eq. (7.13)] which is the same for both the spin-echo and the PRESS responses. All theoretical curves include a relaxation time T_2 of 730 ms.

Selected spectra illustrating the response to the PRESS sequence at 100 MHz are shown in Fig. 7.4. For the purpose of this illustration, the TE timings were chosen to emphasize the minimal change in the shape of the multiplet up to TE=24 ms; the first null at TE~48 ms; a partial inversion corresponding to the local minimum at TE=104 ms; and a more complete inversion at TE=272 ms.

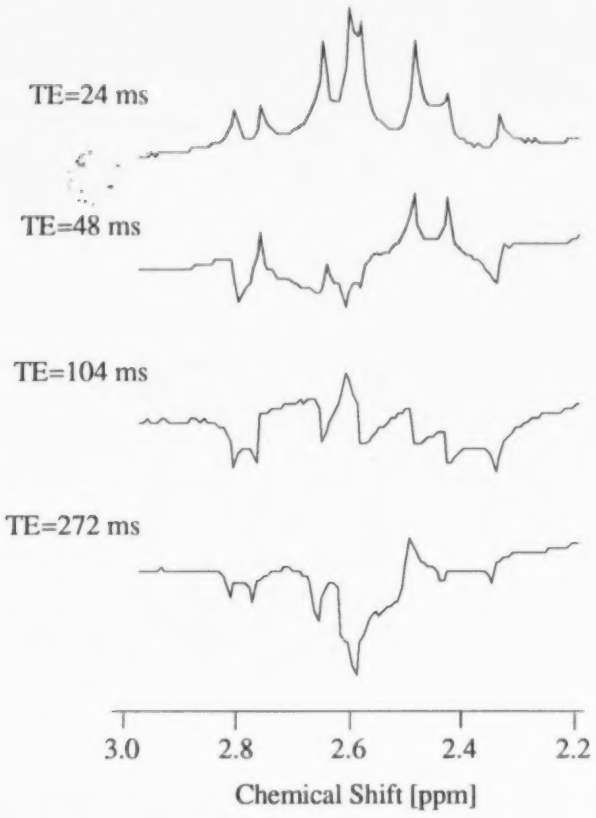

Figure 7.4 An illustration of the TE dependence of 100 MHz proton spectra obtained from a phantom of NAA using the PRESS sequence.

The response of the AB part of the ABX system of NAA to the STEAM sequence is shown in Fig. 7.5, where the experimental (*) and theoretical (Eq. (7.17)) TE modulations at 2.35 T are illustrated for a TM of 5.4 ms. Fig. 7.6 shows particular spectra selected from this test and corresponding to a minimal change at TE/2=10 ms; the first experimental minimum at TE/2=18 ms; the first local maximum at TE/2=38 ms; and the long echo maximum at TE/2=190 ms.

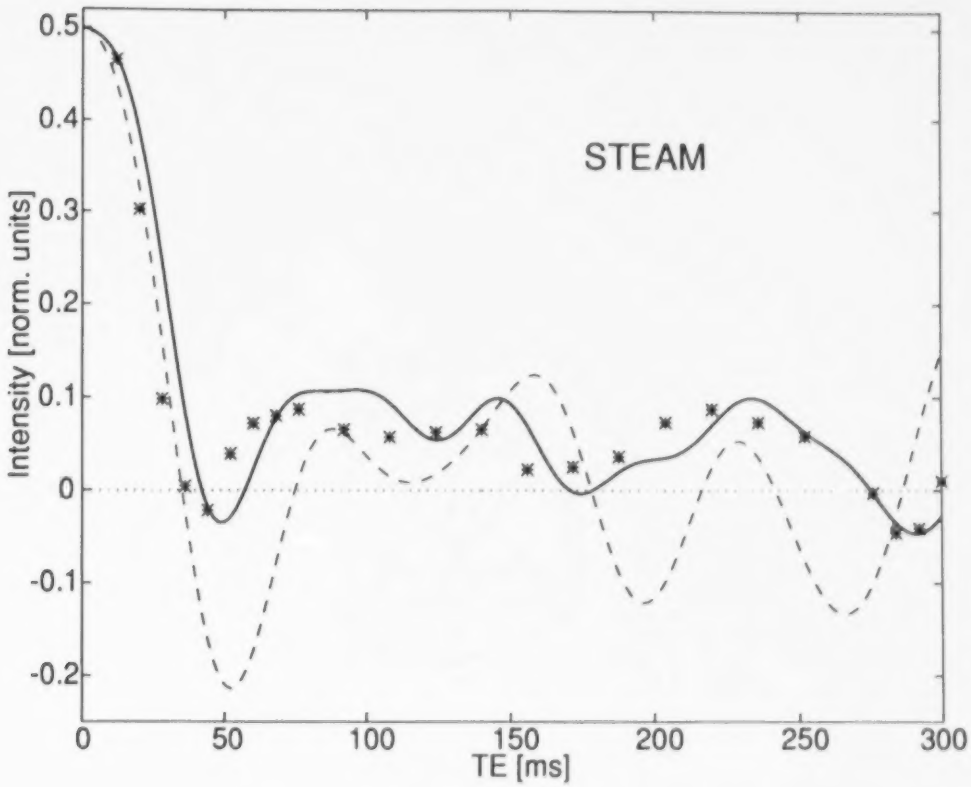

Figure 7.5 The TE dependence of the NAA AB signal intensity at 100 MHz obtained in response to the STEAM sequence illustrated in Fig. 2(a) with TM = 5.4 ms. — calculated response [Eq. (7.17)] and (∗) experimental data; – – weak coupling approximation [Eq. (7.18)]. A relaxation time T_2 of 730 ms was incorporated into the theoretical curves.

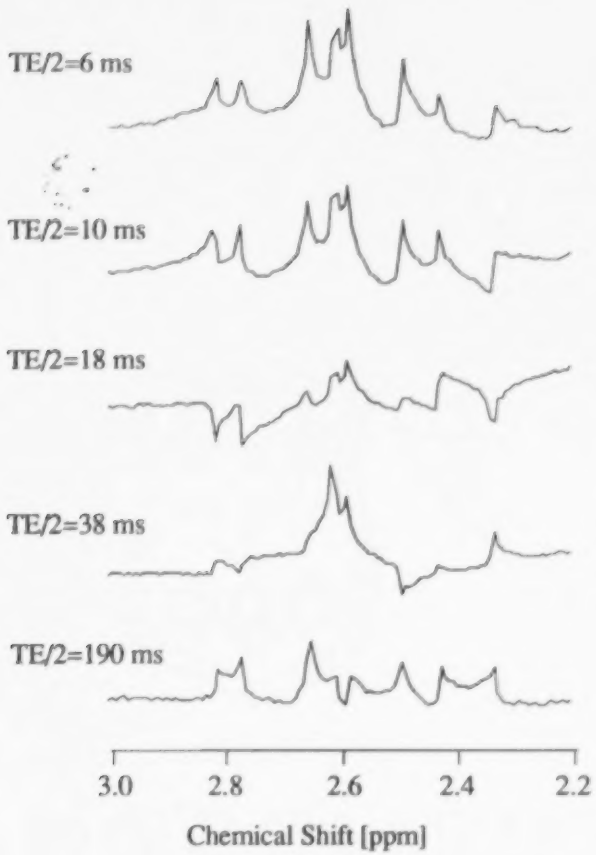

Figure 7.6 An illustration of the TE/2 dependence of 100 MHz proton spectra obtained from a phantom of NAA using the STEAM sequence with a TM=5.4 ms.

Because the degree of strong coupling is field dependent, the response of the 2.6 ppm NAA multiplet to the *in vivo* localization sequences is also dependent on the magnetic field strength. The magnetic field strength dependence of the echo-time modulations of the NAA aspartyl multiplet response to the spin-echo, PRESS and STEAM sequences is illustrated in Figs. 7.7, 7.8 and 7.9 respectively. It must be emphasized that the curves in Figs. 7.7-7.9 represent only the changes in echo-time modulation with field strength, and do not include the two opposing signal-to-noise effects that arise with changing field from the changing spectral shape (as illustrated in Fig. 7.1), and the changing Zeeman energy.

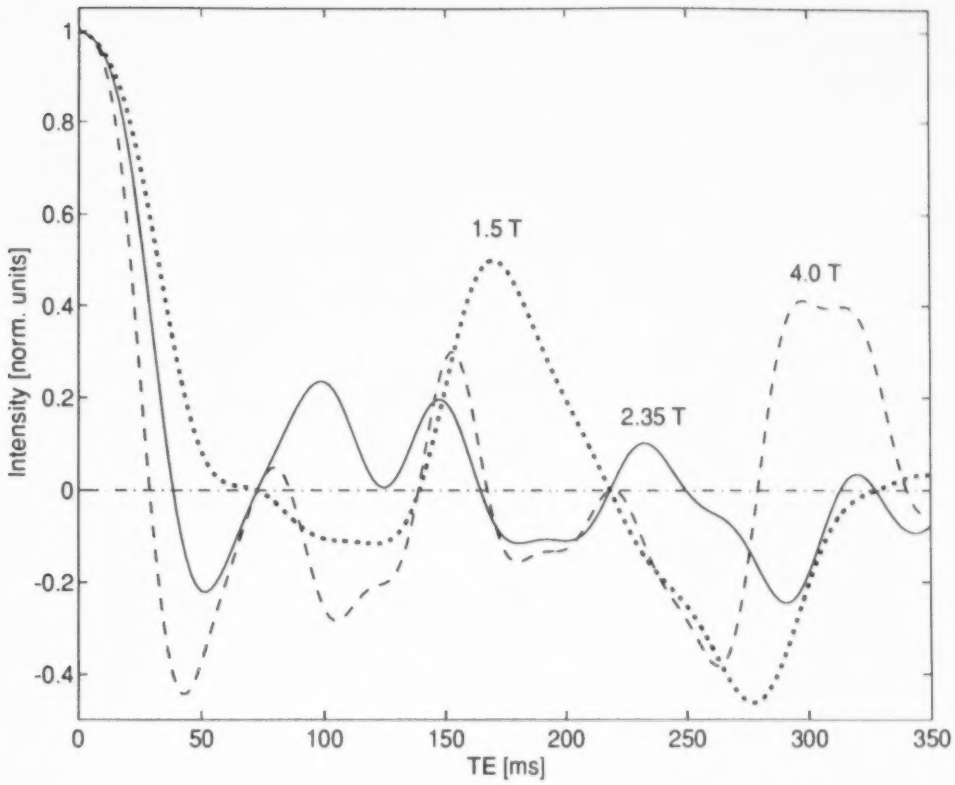

Figure 7.7 The normalised theoretical relationship between the NAA AB signal intensity and TE for the spin-echo sequence at three different magnetic field strengths (1.5 T • • •, 2.35 T —, and 4.0 T – –) . A relaxation time T_2 of 730 ms was assumed at each field strength.

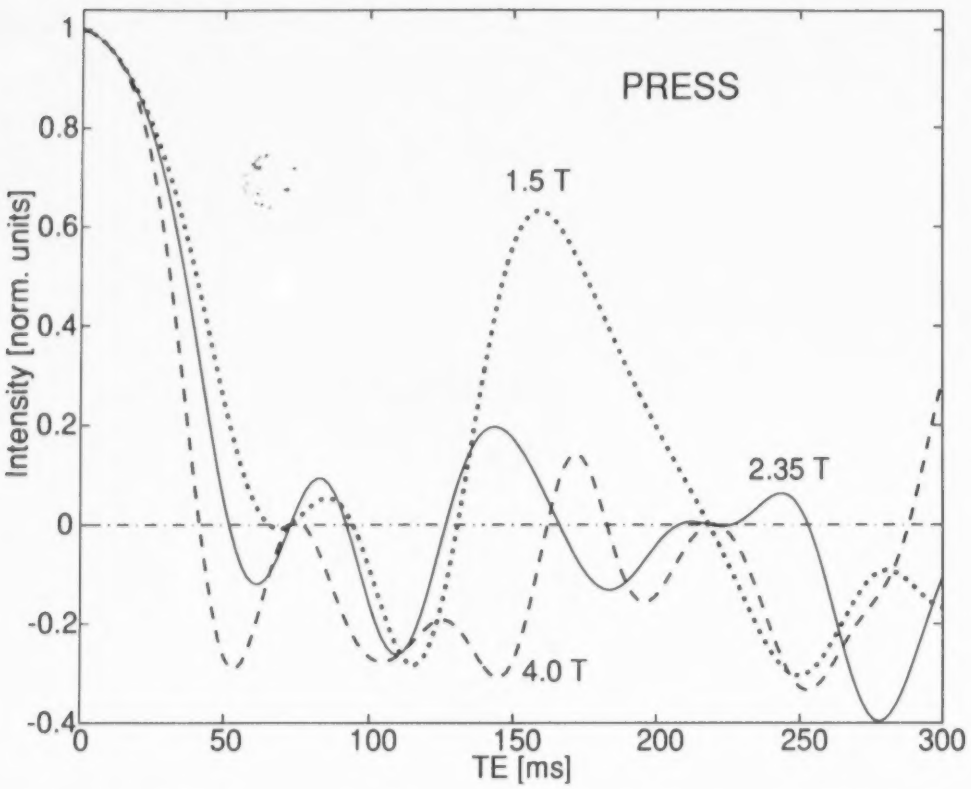

Figure 7.8 The normalised theoretical relationship between the NAA AB signal intensity and TE for the PRESS sequence at three different magnetic field strengths (1.5 T • • •, 2.35 T —, and 4.0 T – –). A relaxation time T_2 of 730 ms was assumed at each field strength.

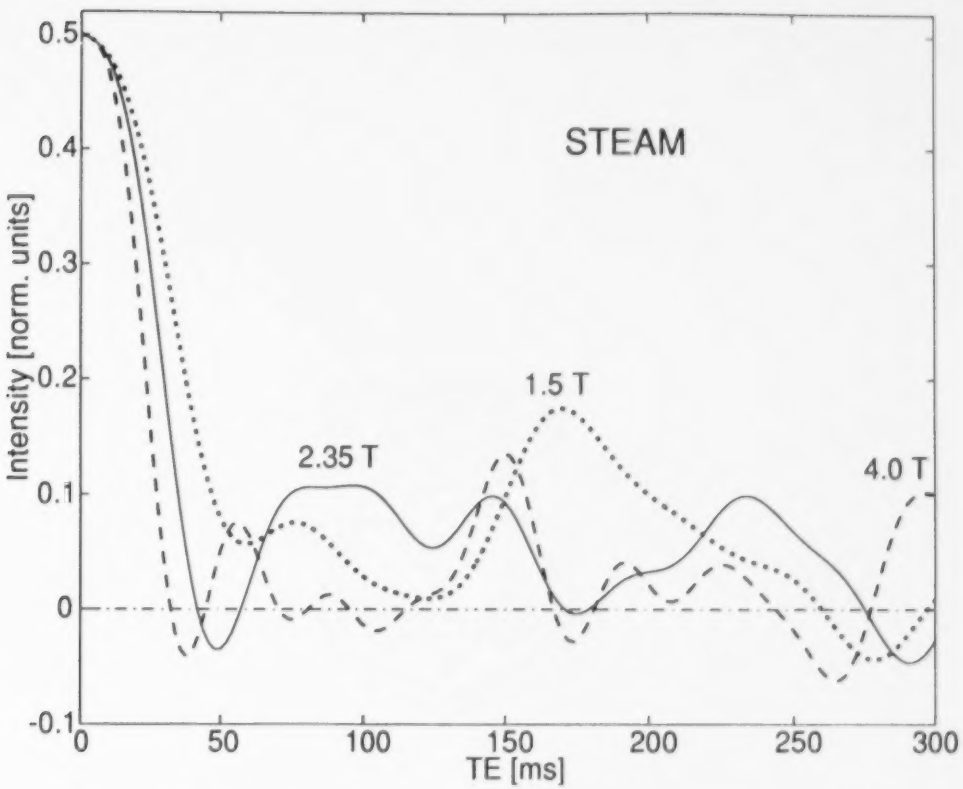

Figure 7.9 The normalised theoretical relationship between the NAA AB signal intensity and TE for the STEAM sequence at three different magnetic field strengths (1.5 T • • •, 2.35 T —, and 4.0 T – –) and with TM=5.4 ms. A relaxation time T_2 of 730 ms was assumed at each field strength.

From the data of Figs. 7.8 and 7.9, the optimal sequence and the optimal long TE timing for a field strength of 1.5 T are PRESS with TE~163 ms. Figure 7.10 illustrates the proton spectrum obtained *in vivo* from a 27 mL region of mainly white matter using these optimal conditions in a typical *in vivo* manisfestation of the PRESS sequence. For comparison purposes, an additional spectrum was obtained at TE=70.5 ms, which corresponds to a null of the AB multiplet response to the PRESS sequence at 1.5 T (see Fig. 7.8).

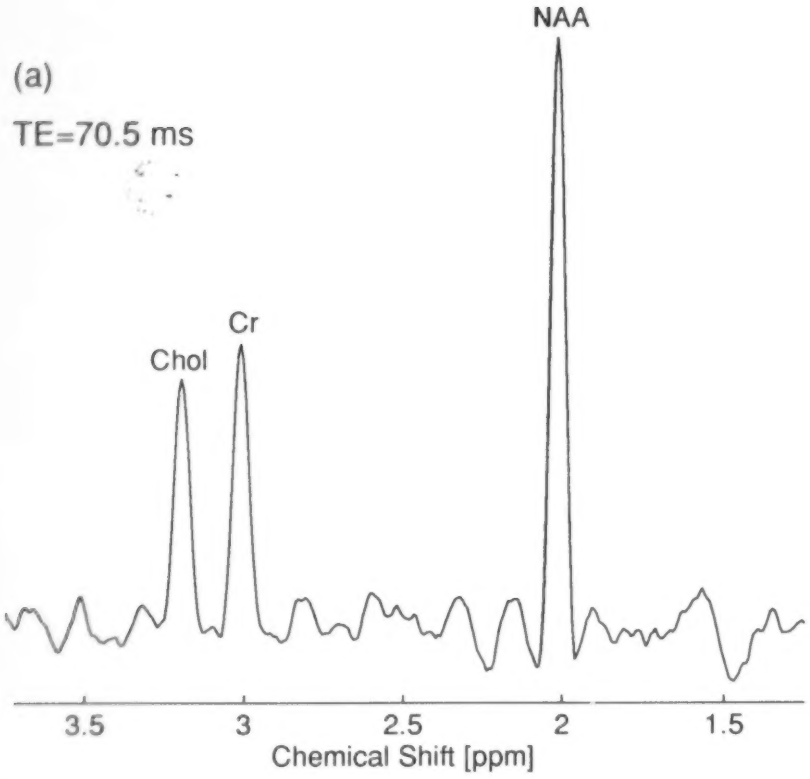

Figure 7.10 An illustration of *in vivo* human brain spectra obtained by using the full PRESS sequence at 1.5 T. The volume selected was 27 mL of predominantly white matter located in the parietal lobe. 128 scans were used, and 1 Hz line broadening was applied prior to Fourier transformation. The echo times were chosen from the thick dashed 1.5 T curve of Fig. 7.8 in order to illustrate extreme choices of TE for the observation of the AB part of the NAA ABX system: (a) a poor choice, TE=70.5 ms.

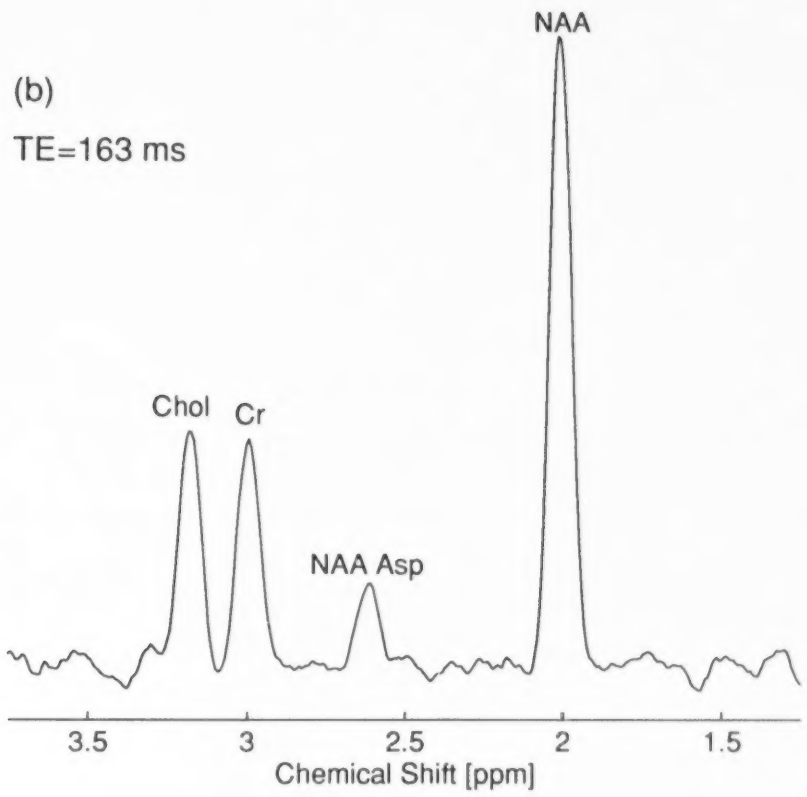

Figure 7.10 (b) a good choice, TE=163 ms.

7.4 Discussion and Conclusions

While one can alleviate concern over significant J modulation losses by performing a short TE (<20 ms) experiment, such experiments are not always possible because they place demands on the capabilities of the gradient system which may be too high. Moreover, the richness of the short echo spectrum introduces a greater potential for spectral overlap and greater difficulty in baseline fitting. For NAA measurement, a longer TE time may be beneficial since broad macromolecular resonances will be attenuated, along with the underlying glutamate and glutamine signals to give a cleaner reference baseline. However, one typical consequence of this longer TE is the loss of the 2.6 ppm NAA aspartyl resonances, which may prove to be particularly important for separating the contributions of NAA and NAAG. Nevertheless, at some field strengths, careful selection of the pulse sequence and TE can allow for clear observation of the NAA aspartate resonance, with good signal-to-noise, at longer TE times. By choosing such an echo time, for example TE=163 ms for PRESS at 1.5 T, both NAA peaks remain available for the fitting process, while other coupled resonances such as glutamine or glutamate are substantially reduced (see Fig. 7.10).

Not all field strengths, however, allow for long TE acquisition with good S/N for this multiplet because the NAA aspartate modulations exhibit a strong magnetic field dependence. The dramatic field strength dependence of the aspartyl resonances is a direct consequence of the strong J coupling in this ABX system. The inadequacy of the weak coupling approximation is illustrated by the fact that it predicts a TE response that is independent of field strength for both the PRESS and STEAM sequences. Even though the product operator calculations for the response of the AB part of a strongly coupled ABX system to the STEAM and PRESS sequences are lengthy and time-consuming, the effort invested has nevertheless been worthwhile since, using the formulas developed here, the NAA 2.6 ppm multiplet intensity can be predicted for any given TE or field strength. In addition, these same formulae may be applied to other ABX systems that may be observed in *in vivo* proton MRS such as aspartic acid or the aspartyl group of NAAG.

7.5 References

1. J.V. Nadler, and J.R. Cooper, *J. Neurochem.* **19**, 313 (1972).
2. K.J. Koller, R. Zaczek, and J.T. Koyle *J. Neurochem.* **43**, 1136 (1984).
3. D.L. Birken, and W.H. Oldendorf, *Neurosci. Biobehav. Rev.* **13**, 23 (1989).
4. S.S. Gill, R.K. Small, D. Thomas, and P. Patel, *NMR Biomed* **2**, 196 (1989).
5. J.R. Moffett, A.M.A. Namboodiri, C.B. Cangro, and J.H. Neale, *NeuroReport* **2**, 131 (1991).
6. J. Urenjak, S.R. Williams, D.G. Gadian and M. Noble, *J. Neurochem.* **59**, 55 (1992).
7. O.A.C. Petroff, G.D. Graham, A.M. Blamire, M. Al-Rayess, D.L. Rothman, P.B. Fayad, L.M. Brass, R.G. Shulman, and J.W. Prichard, *Neurology* **42**, 1349 (1992).
8. C.C. Ford, R.H. Griffey, N.A. Matwiyoff, and G.A. Rosenberg, *Neurology* **42**, 1408 (1992).
9. J.H. Duijn, G.B. Matson, A.A. Maudsley, J.W. Hugg, and M.W. Weiner, *Radiology* **183**, 711 (1992).
10. C.M. Segebarth, D.F. Balerieux, P.R. Luyten, and J.A. den Hollander *Magn. Reson. Med.* **13**, 62 (1990).
11. J.W. Hugg, K.D. Laxer, G.B. Matson, A.A. Maudsley, and M.W. Weiner, *Ann. Neurol.* **34**, 788 (1993).
12. D.L. Arnold, P.M. Matthews, and G.S. Francis, *Ann. Neurol.* **31**, 235 (1992).
13. M.S. van der Knapp, J. van der Ground, P.R. Luyten, J.A. den Hollander, J.J.P. Nauta, and J. Valk, *Ann. Neurol.* **31**, 202 (1992).
14. R. Kreis, T. Ernst, and B.D. Ross, *Magn. Reson. Med.* **30**, 424 (1993).
15. J. Frahm, T. Michaelis, K.D. Merboldt, W. Hanicke, M.L. Gyngell, and H. Bruhn, *NMR in Biomed.* **4**, 201 (1991).
16. S.W. Provencher, *Magn. Reson. Med.* **30**, 672 (1993).
17. R. Kreis, T. Ernst, and B.D. Ross, *J. Magn. Reson.* **B 102**, 9 (1993).
18. T. Michaelis, K.D. Merboldt, W. Hanicke, M.L. Gyngell, H. Bruhn, and J. Frahm, *NMR in Biomed.* **4**, 90 (1991).
19. R.E. Gordon and R.J. Ordridge, Abstracts of the Society of Magnetic Resonance in Medicine, 3rd Annual Meeting, New York, p. 272, 1984.
20. R.J. Ordridge, M.R. Bendall, R.E. Gordon, and A. Conelly, *in* "Magnetic Resonance in Biology and Medicine" (G. Govil, C.L. Khetrapal, and A. Saran, Eds.), pp 387-397, McGraw-Hill, New Dehli, 1985.
21. P.A. Bottomley, *Ann. N.Y. Acad. Sci.* **508**, 333 (1987).
22. J. Frahm, K.D. Merboldt, and W. Hanicke, *J. Magn. Reson.* **72**, 502 (1987).
23. L.E. Kay and R.E.D. McClung, *J. Magn. Reson.* **77**, 258 (1988).
24. M.E. Rose, "Elementary Theory of Angular Momentum," Wiley, N.Y., 1957.
25. T.T. Nakashima and R.E.D. McClung, *J. Magn. Reson.* **70**, 187 (1986).
26. A.D. Bain, *J. Magn. Reson.* **56**, 418 (1984).
27. G. Bodenhausen, H. Kogler, and R.R. Ernst, *J. Magn. Reson.* **58**, 370 (1984).
28. A. Haase, J.Frahm, W. Haenicke, D.Matthei, *Phys. Med. Biol.* **30**,341 (1985).
29. C.T.W. Moonen and P.C.M. Van Zijl, *J. Magn. Reson.* **88**, 28 (1990).
30. A.H. Wilman and P.S. Allen, *J. Magn. Reson.* (in press)1994.

CHAPTER 8

Conclusions

The main purpose of this thesis was twofold. First, it has been to devise editing techniques for proton spectroscopy that take advantage of multiple quantum coherence filtering. In particular, the weakly coupled A_2 triplet of the $A_2M_2X_2$ system of GABA, and the strongly coupled AB system of citrate have been addressed. Secondly, it has been to evaluate analytically and experimentally the complex J-modulations arising in the response of coupled spin systems to the STEAM and the PRESS localization sequences. In particular, the response of the weakly coupled AX_3 system of lactate, as well as that of the strongly coupled AB system of citrate and ABX aspartic system of NAA, have been treated. In all cases, the theoretical results derived via the product operator approach were in close agreement with the experimental data obtained at 2.35 T.

8.1 The Measurement of the Intensity of the Spin Response

The interpretation of experimental *in vivo* spectra has to contend with the line broadening characteristics of the *in vivo* milieu. Under such circumstances adjacent but antiphase multiplet peaks can suffer significant cancellation. This is particularly true in the case of lactate, where the antiphase peaks are separated by only 7 Hz, or citrate, where at 1.5 T the inner peaks are separated by 2 Hz. The normal method of quantification of experimental *in vivo* spectra is measurement of peak area, which is affected by overlap cancellation. The calculations presented here predict the total in phase magnetization present at the start of acquisition which is a direct reflection of the total area under the Fourier transformation of the time domain signal. However, the measurement of peak area does not fully represent the exact spectral shape of a given multiplet. For example, a measurement of zero area may occur when there is no observable signal in the spectrum, but it may also occur when there are significant antiphase peaks which cancel each other out to give zero area. As an illustration, consider the lactate doublet spectra of Fig. 8.1 which were acquired by the STEAM and the PRESS sequences of Fig. 4.1.

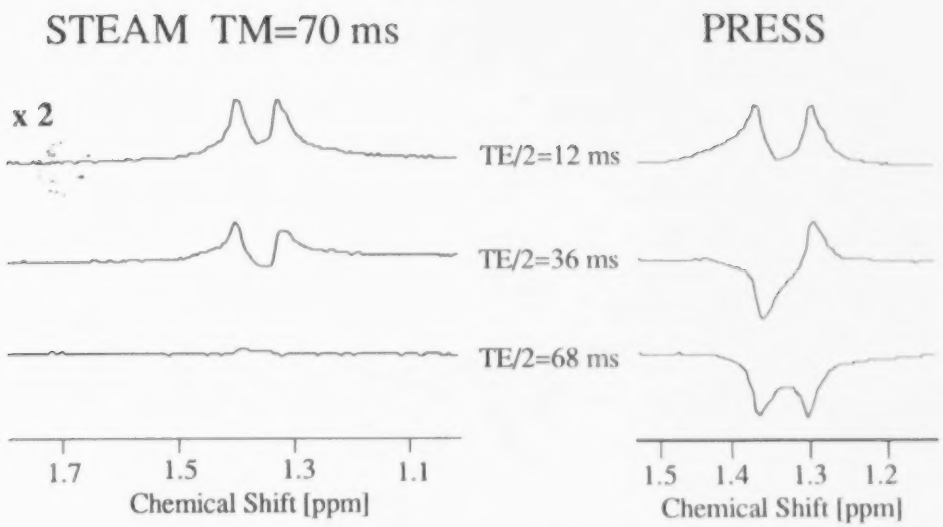

Figure 8.1 100 MHz proton spectra of the lactate doublet acquired with either the PRESS or the STEAM sequences of Fig. 4.1 from a phantom of lithium lactate. The TE/2 times are listed in the figure. Note that the PRESS sequence yields zero area at TE/2=36 ms, and the STEAM sequence yields zero area when TE/2=68 ms.

From the spectra in Fig. 8.1, zero area was measured for the PRESS sequence with TE/2=36 ms (1/4J), and for the STEAM sequence with TE/2=68 ms (1/2J) and TM=70 ms. From the spectral shapes of Fig. 8.1 the STEAM result is in fact a complete null, while the PRESS result is an antiphase doublet. In this case, one would like to maximize inphase magnetization and therefore minimize cancellation, so a timing that produces zero area should be avoided. Occasionally however, the measurement of zero area may correspond to the existence of well-separated antiphase peaks, such as the two-spin antiphase doublet of GABA in Chapter 3. Therefore, the calculations of the complete spectral response would also be valuable.

One may calculate the complete spectral response analytically by using the product approach, however, all of the antiphase coherences that exist at the start of the detection period must then be considered since they may evolve into detectable antiphase magnetization. Including all of these terms would greatly complicate the theoretical treatment, especially in the strong coupling cases, and lead to a series of extra terms in the analytical equations that contribute zero to the net area of the

multiplet. The additional complexity of the equations would serve little value for the *in vivo* audience who are concerned with maximizing the area of the multiplet of interest. The best compromise, may be to use the analytical equations presented here for the majority of cases where the inphase magnetization is to be maximized, and occasionally, when precise evaluation of spectral shape is required make use of numerical simulations using either the density matrix or operator approach.

8.2 Spectral Editing of GABA

GABA is one of the few metabolites in the *in vivo* proton spectrum of brain that cannot be observed at *in vivo* field strengths without spectral editing. In Chapter 2, results are reported on the evaluation of a series of single scan editing techniques in relation to the editing of the GABA 3.0 ppm triplet which lies beneath the 3.0 ppm creatine (Cr) singlet. It was found that provided the filtered coherence pathways did not select single quantum or gradient insensitive coherences, the Cr resonance could be suppressed by greater than a factor of 1600 while retaining up to 25% of the GABA triplet signal, thus giving rise to an apparent improvement in the GABA/Cr ratio of 450. The method which achieved this level of effectiveness was a triple quantum filter with TE~1/J or 136 ms. However, while this sequence performed the editing effectively, its long duration leads to significant relaxation losses *in vivo*.

Chapter 3 addresses the twin challenges of inherent filter yield improvement and relaxation time loss reduction. In this chapter, two additional GABA editing techniques are introduced which exploit the τ dependence of different terms in the product operator expansion of the density operator. The new techniques rely on double quantum filtering (DQF), and yield at least 50% more signal than the best GABA filtering method introduced in Chapter 2, and at the same time reduce the sequence duration by factors of 2 and 4 respectively. The two new methods also performed favourably when compared to difference spectroscopy (see Figs. 3.5 and 3.6). However, unlike difference spectroscopy, the DQF editing was performed in a single scan by using gradient dephasing of unwanted coherences, so sensitivity to motion was all but eliminated

8.3 Localization Sequence Effects

The effects of localization sequences on the coupled spin response are illustrated in Chapter 4, 5, and 7. The localization sequences produce coherences which can have marked effects on the signal observed.

8.3.1 Lactate

In Chapter 4, the response of the lactate doublet to the STEAM sequence was derived. The resulting equation which describes the net in phase magnetization signal is shown in Eq. (4.10). As is evident from this equation, four periodicities, each involving a sequence parameter, appear. As a result, an inappropriate choice of either TE or TM can lead to unnecessary signal loss. The choice of TM=70 ms (~1/2J), will eliminate any zero quantum coherence effects in the TM period and lead to a smooth TE dependence as illustrated in Fig. 4.2. When TM is less than 1/2J, the TE dependence also depends in a periodic way on the chemical shift difference $\delta\omega$ between the lactate doublet and quartet (see Fig. 4.3). A particularly poor choice of TE/2 is 70 ms (~1/2J), which leads to a large zero quantum coherence contribution in the TM period that oscillates rapidly (see Fig. 4).

8.3.2 Citrate and N-Acetylaspartate

When the scalar coupling regime is strong rather than weak, the oscillations in the signal response are no longer periodic in the sequence timing parameters. To evaluate this regime, the strong coupling product operator formalism of Kay and McClung (1) proved to be effective in the cases of the the strongly coupled citrate (AB system) and N-acetylaspartate multiplets (AB part of an ABX system), where the response to both the STEAM and the PRESS sequences was addressed. An illustration of the non-periodic oscillations at 2.35 T is given in Figs. 5.3 and 7.3 for the PRESS sequence and Figs. 5.5 and 7.5 for the STEAM sequence. In both cases, the strongly coupled spin response also exhibited a significant dependence on the chosen static magnetic field strength. This field strength dependence arises form the fact that, unlike weakly coupled systems, the chemical shift evolution cannot be treated separately from the J coupling evolution. A dramatic illustration of the field strength dependence is shown in Fig. (7.8) where the NAA aspartyl multiplet

response to the PRESS sequence is shown. In the weak coupling limit, the curves at different field strengths would be similar in each case.

The appropriate sequence timing parameters for either of the PRESS or the STEAM localization sequences for any strongly coupled AB system, or AB part of an ABX system, at any field strength, are now given a quantitative basis by means of Eqs. (5.13), (5.19) and Eqs. (7.17) and (7.24). By making use of the formulae developed here, it will be possible to optimize both the citrate and the 2.6 ppm aspartyl resonance of NAA subject to any individual constraint.

8.4 The Value of the Analytical Product Operator Approach

Through use of the product operator description, we have been able to shed light on the complex modulations of four J-coupled metabolites that play important roles in the human body. The product operator approach has allowed us to visualize easily the state of the system at any given time. Moreover, the effects of radiofrequency (r.f.) pulses or J-coupling interactions were calculated by merely performing a rotation in the product operator space where each axis represented a physical (but not necessarily directly observable) variable such as transverse magnetization or double quantum coherence. This product operator approach has allowed us to return to a vector model, not with the classical three axes, but with 4^N axes, where N is the number of coupled spins in the system.

In contrast to the density matrix approach, the product operator method is much easier to work with analytically and provides results which are more easily interpreted. For example, the six spin system of GABA would have required a 64 by 64 entry matrix to describe properly any achievable state. Instead of using such a large matrix, we were able to represent the matrix by a few product operators, and by keeping only the terms of interest, the calculations were performed relatively easily by hand, leading to analytical expressions.

As hinted at by the complexity of the results for the ABX system of NAA, an analytical product operator approach for more complex strongly coupled spin systems may not be worthwhile. For example, transformation equations under J-

coupling have yet to be derived for strongly coupled spin systems with more than three spins. The derivation alone would be very time consuming, and when combined with the time to determine product operator evolutions due to even simple pulse sequences, this method of approach becomes very unattractive. Thus for more complicated pulse sequences and spin systems, it may be better to dispense with the product operator approach for that of a computer-implemented density matrix approach (2). In addition, by making use of computer methods, many of the analytical simplifications made in this thesis become unnecessary. For example, there are at present, no analytical product operator transformational equations available to describe the simultaneous evolution under both J-coupling, Larmor precession and a time-dependent r.f. pulse. Even though the losses from such an evolution are generally small when J~7 Hz and when pulse lengths are less than 5 ms, the effects can easily be accounted for by using a numerical approach. While the product operator approach has proven itself to be immensely valuable for providing physical insight and for determining the analytical response in relatively simple cases, the introduction of further complicating factors such as larger spin systems with strong coupling, variable r.f. pulse angles and pulse shapes, or consideration of simultaneous r.f. pulse, Larmor precession and J coupling effects, may lead to the demise of this approach.

8.5 Future Directions

From an experimental point of view, the techniques introduced here for editing GABA can be implemented for *in vivo* testing on human brain. The use of appropriately chosen slice selective r.f. pulses may enhance the editing ability of these sequences. Once successful editing is achieved, studies on various GABA-related disorders should take place. For example, time course studies of the effects of antiepileptic or antidepressive drug therapy on brain GABA levels could be performed. In addition, *in vivo* proton spectroscopy should be used to monitor other amino acid neurotransmitters such as aspartic acid, glutamate and N-acetylaspartylglutamate. In each case, it will be important to evaluate the coupled spin response to the chosen localization sequence in order to maximize the signals of interest.

As outlined in Section 8.4, one clear direction of future research is to use numerical density matrix calculations to study the response of more complicated J-coupled metabolites such as glutamine, glutamate and inositol. By using this approach, the exact *in vivo* pulse sequence can be analyzed. In particular, the effects of simultaneous evolution under a time-dependent r.f. pulse, J-coupling, and Larmor precession can be investigated, and the r.f. pulses can then be optimized for the J-coupled metabolite of interest.

8.6 References

1. L.E. Kay and R.E.D. McClung, *J. Magn. Reson.* **77**, 502 (1988).
2. R.R. Ernst, G. Bodenhausen, and A. Wokaun, "Principles of Nuclear Magnetic Resonance in One and Two Dimensions," Clarendon Press, New York,1987.

Appendix A

Product Operator Transformation Equations for a Weakly Coupled Two Spin System

A.1 Cartesian Product Operator Representation

A.1.1 Transformation Under a Radiofrequency Pulse

$$I_z \xrightarrow{\theta I_x} I_z \cos\theta - I_y \sin\theta$$
$$I_y \xrightarrow{\theta I_x} I_y \cos\theta + I_z \sin\theta$$
$$I_x \xrightarrow{\theta I_x} I_x . \qquad \text{(A.1a)}$$

$$I_z \xrightarrow{\theta I_y} I_z \cos\theta + I_x \sin\theta$$
$$I_x \xrightarrow{\theta I_y} I_x \cos\theta - I_z \sin\theta$$
$$I_y \xrightarrow{\theta I_y} I_y . \qquad \text{(A.1b)}$$

A.1.2 Transformation Under Chemical Shift

$$I_x \xrightarrow{\omega_I I_z t} I_x \cos(\omega_I t) + I_y \sin(\omega_I t)$$
$$I_y \xrightarrow{\omega_I I_z t} I_y \cos(\omega_I t) - I_x \sin(\omega_I t)$$
$$I_z \xrightarrow{\omega_I I_z t} I_z . \qquad \text{(A.2)}$$

A.1.3 Transformation Under Weak J Coupling

$$I_x \xrightarrow{2\pi J I_z S_z t} I_x \cos(\pi J t) + 2 I_y S_z \sin(\pi J t)$$
$$I_y \xrightarrow{2\pi J I_z S_z t} I_y \cos(\pi J t) - 2 I_x S_z \sin(\pi J t)$$

$$
\begin{aligned}
I_z &\xrightarrow{2\pi J I_z S_z t} I_z \\
2I_xS_z &\xrightarrow{2\pi J I_z S_z t} 2I_xS_z\cos(\pi Jt) + I_y\sin(\pi Jt) \\
2I_yS_z &\xrightarrow{2\pi J I_z S_z t} 2I_yS_z\cos(\pi Jt) - I_x\sin(\pi Jt) \\
2I_zS_z &\xrightarrow{2\pi J I_z S_z t} 2I_zS_z \\
2I_xS_x &\xrightarrow{2\pi J I_z S_z t} 2I_xS_x \\
2I_xS_y &\xrightarrow{2\pi J I_z S_z t} 2I_xS_y \\
2I_yS_y &\xrightarrow{2\pi J I_z S_z t} 2I_yS_y
\end{aligned}
\qquad \text{(A.3)}
$$

A.2 Raising and Lowering Product Operator Representation

The raising and lowering operators are defined in terms of the Cartesian spin angular momentum operators by

$$I_+ = I_x + iI_y \quad \text{and} \quad I_- = I_x - iI_y\,, \qquad \text{(A.4a)}$$

and hence

$$I_x = (1/2)(I_+ + I_-) \quad \text{and} \quad I_y = (1/2i)(I_+ - I_-) \qquad \text{(A.4b)}$$

A.2.1 Transformation Under a Radiofrequency Pulse

$$
\begin{aligned}
I_z &\xrightarrow{\theta I_x} I_z\cos\theta + (i/2)(I_+ - I_-)\sin\theta \\
I_+ &\xrightarrow{\theta I_x} (1/2)[I_+(1+\cos\theta) + I_-(1+\cos\theta)] - iI_z\sin\theta \\
I_- &\xrightarrow{\theta I_x} (1/2)[I_-(1+\cos\theta) + I_+(1+\cos\theta)] - iI_z\sin\theta
\end{aligned}
\qquad \text{(A.5a)}
$$

$$
\begin{aligned}
I_z &\xrightarrow{\theta I_y} I_z\cos\theta + (1/2)(I_+ + I_-)\sin\theta \\
I_+ &\xrightarrow{\theta I_y} (1/2)[I_+(1+\cos\theta) - I_-(1+\cos\theta)] - I_z\sin\theta \\
I_- &\xrightarrow{\theta I_y} (1/2)[I_-(1+\cos\theta) - I_+(1+\cos\theta)] - I_z\sin\theta
\end{aligned}
\qquad \text{(A.5b)}
$$

A.2.2 Transformation Under Chemical Shift

$$
\begin{aligned}
I_+ &\xrightarrow{\omega_I I_z t} I_+ \exp(-i\omega_I t) \\
I_- &\xrightarrow{\omega_I I_z t} I_- \exp(i\omega_I t) \\
I_z &\xrightarrow{\omega_I I_z t} I_z
\end{aligned}
\qquad \text{(A.6)}
$$

A.2.2 Transformation Under Weak J Coupling

$$
\begin{aligned}
I_+ &\xrightarrow{2\pi J I_z S_z t} I_+ \cos(\pi J t) - 2i\, I_+ S_z \sin(\pi J t) \\
I_- &\xrightarrow{2\pi J I_z S_z t} I_- \cos(\pi J t) + 2i\, I_- S_z \sin(\pi J t) \\
I_z &\xrightarrow{2\pi J I_z S_z t} I_z \\
2I_+ S_z &\xrightarrow{2\pi J I_z S_z t} 2I_+ S_z \cos(\pi J t) - iI_+ \sin(\pi J t) \\
2I_- S_z &\xrightarrow{2\pi J I_z S_z t} 2I_- S_z \cos(\pi J t) + iI_- \sin(\pi J t) \\
2I_z S_z &\xrightarrow{2\pi J I_z S_z t} 2I_z S_z \\
2I_+ S_+ &\xrightarrow{2\pi J I_z S_z t} 2I_+ S_+ \\
2I_+ S_- &\xrightarrow{2\pi J I_z S_z t} 2I_+ S_- \\
2I_- S_- &\xrightarrow{2\pi J I_z S_z t} 2I_- S_-
\end{aligned}
\qquad \text{(A.7)}
$$

A.3 Spherical Product Operator Representation

The spherical spin angular momentum operators, $I_{\pm}$, differ slightly from the raising and lowering operators $I_{\pm}$ and are defined as follows,

$$I_{+} = -(1/\sqrt{2})\, I_{+} \quad \text{and} \quad I_{-} = (1/\sqrt{2})\, I_{-} \quad . \tag{A.8}$$

The transformations under chemical shift and J coupling are exactly the same as the raising and lowering operator transformations in Section A.2, however, the transformations under a radiofrequency pulse differ.

A.3.1 Transformation Under a Radiofrequency Pulse

$$\begin{aligned}
I_z &\xrightarrow{\theta I_x} I_z \cos\theta - (i/\sqrt{2})(I_{+} + I_{-})\sin\theta \\
I_{+} &\xrightarrow{\theta I_x} (1/2)[I_{+}(1+\cos\theta) - I_{-}(1+\cos\theta)] - (i/\sqrt{2}) I_z \sin\theta \\
I_{-} &\xrightarrow{\theta I_x} (1/2)[I_{-}(1+\cos\theta) - I_{+}(1+\cos\theta)] - (i/\sqrt{2}) I_z \sin\theta
\end{aligned} \tag{A.9a}$$

$$\begin{aligned}
I_z &\xrightarrow{\theta I_y} I_z \cos\theta + (1/\sqrt{2})(-I_{+} + I_{-})\sin\theta \\
I_{+} &\xrightarrow{\theta I_y} (1/2)[I_{+}(1+\cos\theta) + I_{-}(1+\cos\theta)] + (1/\sqrt{2}) I_z \sin\theta \\
I_{-} &\xrightarrow{\theta I_y} (1/2)[I_{-}(1+\cos\theta) + I_{+}(1+\cos\theta)] - (1/\sqrt{2}) I_z \sin\theta
\end{aligned} \tag{A.9b}$$

Appendix B

Product Operator Transformation Equations for a Strongly Coupled Two Spin System

Using the spherical product operator notation, Kay and McClung (Ref. 1, Chapter 8) derived the transformations for an AB spin system. A summary of some of their results is included below. We shall represent the two spin operators by A and B. The Hamiltonian is divided into two commuting parts, $\mathcal{H}_0$ and $\mathcal{H}_1$,

$$\mathcal{H}_0=\bar{\omega}\,(A_Z+B_Z)+2\pi J A_Z B_Z$$
$$\mathcal{H}_1=\delta\omega(A_Z-B_Z)+2\pi J(A_X B_X+A_Y B_Y) \quad , \qquad \text{(B.1)}$$

where A and B are the spin angular momentum operators, where $\delta\omega=(\omega_A-\omega_B)/2$, $\bar{\omega}=(\omega_A+\omega_B)/2$ with $\omega_{A,B}$ representing the respective chemical shift frequencies of the spins A and B.

$$A_+ \xrightarrow{\mathcal{H}_0 t} A_+\{\cos(\pi Jt) - i2A_+B_Z\sin(\pi Jt)\}\exp(-i\bar{\omega}t)$$
$$2A_+B_Z \xrightarrow{\mathcal{H}_0 t} 2A_+B_Z\{\cos(\pi Jt) + iB_+\sin(\pi Jt)\}\exp(-i\bar{\omega}t)$$
$$B_+ \xrightarrow{\mathcal{H}_0 t} B_+\{\cos(\pi Jt) + i2B_+A_Z\sin(\pi Jt)\}\exp(-i\bar{\omega}t)$$
$$2B_+A_Z \xrightarrow{\mathcal{H}_0 t} 2B_+A_Z\{\cos(\pi Jt) + iB_+\sin(\pi Jt)\}\exp(-i\bar{\omega}t)$$
$$A_Z \xrightarrow{\mathcal{H}_0 t} A_Z \qquad \text{(B.2)}$$

$$A_+ \xrightarrow{\mathcal{H}_1 t} A_+\{\cos(\Lambda t) - i(\delta\omega/\Lambda)\sin(\Lambda t)\} + i2A_ZB_+(\pi J/\Lambda)\sin(\Lambda t)$$
$$2A_+B_Z \xrightarrow{\mathcal{H}_1 t} 2A_+B_Z\{\cos(\Lambda t) - i(\delta\omega/\Lambda)\sin(\Lambda t)\} + iB_+(\pi J/\Lambda)\sin(\Lambda t)$$
$$B_+ \xrightarrow{\mathcal{H}_1 t} B_+\{\cos(\Lambda t) + i(\delta\omega/\Lambda)\sin(\Lambda t)\} + i2B_ZA_+(\pi J/\Lambda)\sin(\Lambda t)$$
$$2B_+A_Z \xrightarrow{\mathcal{H}_1 t} 2B_+A_Z\{\cos(\Lambda t) + i(\delta\omega/\Lambda)\sin(\Lambda t)\} + iA_+(\pi J/\Lambda)\sin(\Lambda t)$$
$$A_Z+B_Z \xrightarrow{\mathcal{H}_1 t} A_Z+B_Z \quad (A_Z \text{ or } B_Z \text{ alone is not invariant under } \mathcal{H}_1) \qquad \text{(B.3)}$$

where $\Lambda=\{(\delta\omega)^2+(\pi J)^2\}^{1/2}$.